

Alma Mater Studiorum – Università di Bologna

DOTTORATO DI RICERCA IN

CHIMICA

Ciclo XXX

Settore Concorsuale: 03/B1

Settore Scientifico Disciplinare: CHIM/03

NOVEL INSIGHTS INTO GOLD(I) CHEMISTRY:  
FROM ANTICANCER ACTIVITY TO NEW  
SYNTHETIC METHODOLOGIES

**Presentata da:** Assunta De Nisi

Coordinatore Dottorato

Prof. Aldo Roda

Supervisore

Prof. Magda Monari

Co-supervisore

Prof. Marco Bandini

Esame finale anno 2018





## ABSTRACT

Gold is a unique metal for its peculiar properties and for its role in society, where it is used as a coinage metal, for jewellery, and in industrial application. The interest in the science, technology, and applications of gold has grown considerably over recent years, as evidenced by the huge increase in scientific publications. Traditional industrial applications have been centered mainly on its metallic properties. The discovery, in recent years, of gold (0, I, III) catalytic and biological properties and the studies of its nanoproperties are leading to some new exciting applications. In the twentieth-century, gold(I) complexes were introduced for the treatment of rheumatoid arthritis, culminating in the introduction of the oral drug Auranofin in 1985. Among the new non-platinum anticancer drugs, especially gold species have gained more and more attention due to their generally strong tumor cell growth inhibiting effects. Unfortunately, in modern organic chemistry gold was the victim of several misconceptions, being considered rare, expensive and also chemically inert. All changed at the end of the 1980's with the discovery of its activity in two fundamental reactions - the oxidation of CO to CO<sub>2</sub> (Haruta) and the hydrochlorination of ethylene (Hutchings), from that moment on heterogeneous gold catalysis underwent an exceptional development. Nevertheless, a very interesting area of application of gold is the homogeneous catalysis and, in the last 15 years, there was a real “gold rush” in the chemistry world.

The work herein presented, embraces various aspects of gold chemistry:

- the documentation of novel [alkynyl(triphenylphosphine)gold(I)] complexes carrying differently substituted propargylic amines and their pharmacological investigation on a series of cancer cell lines with particular emphasis on HT29, IGROV1, HL60 and I407 (Figure Ia);

- the investigation of the dearomative cycloaddition reaction of indoles with electron-rich allenes catalysed by commercially available gold(I) complexes that show competence in performing the chemo-, regio- and diastereoselective formal [2+2]-cycloaddition between a wide range of substrates under mild conditions (Figure Ib).

Since gold complexes are highly carbophilic Lewis acids that activate C–C multiple bonds towards nucleophilic attack, they have been applied as catalysts for a number of selective organic transformations including the intramolecular hydroamination of inactivated unsaturated C–C bonds. It should be pointed out that also soft quaternary ammonium salts are known to act as synthetic equivalents of late-transition metal species in activating unsaturated hydrocarbons towards nucleophilic attack. In this field, a work on the possibility to replace second and third row transition metals with catalytic amounts of readily accessible and cheaper ammonium salts to obtain synthetically useful highly functionalized indoles is presented. The metal-free approach exploits the combined efficiency of  $\text{Bu}_4\text{N}^+$  and  $\text{F}^-$  ions in performing a cascade sequence involving intramolecular hydroamination of the C–C triple bond, cleavage of silyl-protecting groups and site-selective sigmatropic aza-Cope-type [3,3]-rearrangement (Figure Ic).

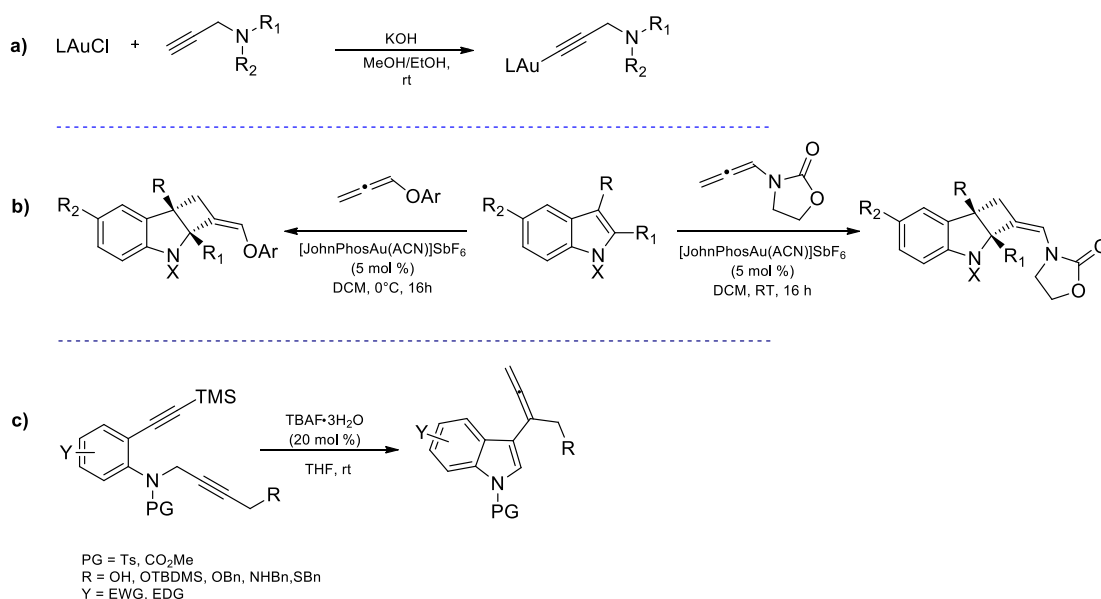


**Figure I**

## RIASSUNTO

L'oro è un metallo unico per le sue proprietà chimico-fisiche e per il ruolo che ha svolto e che tuttora svolge nella società, infatti è usato come metallo da conio, in gioielleria e in varie applicazioni industriali. Negli ultimi anni l'interesse nella scienza, tecnologia e applicazioni dell'oro è cresciuto considerevolmente come dimostrato dall'aumento di pubblicazioni scientifiche in questa tematica. Le applicazioni industriali dell'oro tradizionalmente erano incentrate sulle sue proprietà metalliche ma la scoperta delle proprietà catalitiche e biologiche dell'oro(0), (I) e (III) hanno portato allo sviluppo di nuove e interessanti applicazioni. Nel ventesimo secolo, complessi di oro(I) sono stati testati come farmaci per il trattamento dell'artrite reumatoide e, nel 1985, l'Auranofin, un complesso di oro(I), è stato approvato come farmaco a somministrazione orale proprio per il trattamento di tale patologia. Successivamente se ne studiarono i meccanismi d'azione e si comprese che i complessi di oro potevano essere una promettente classe di farmaci antitumorali grazie al loro effetto inibente della crescita delle cellule tumorali. Nella moderna chimica organometallica, l'oro è sempre stato vittima di pregiudizi poiché era considerato raro, costoso e chimicamente inerte. Alla fine degli anni 80 ci fu una rinascita della chimica dell'oro dovuta alla scoperta della sua attività in due reazioni: l'ossidazione del monossido di carbonio ad anidride carbonica (Haruta) e l'idroclorurazione dell'etilene (Hutchings). Da quel momento in poi lo sviluppo della catalisi eterogenea con oro ebbe un incredibile sviluppo e non da meno sono stati gli sviluppi della catalisi omogenea.

Il lavoro qui presentato abbraccia vari aspetti della chimica dell'oro. Nella prima parte è documentata la sintesi e la caratterizzazione di nuovi complessi alchilici di oro(I) variamente sostituiti e lo studio della loro attività biologica su una serie di linee cellulari tumorali quali HT29,

IGROV1, HL60 e I407 (Figura Ia). Nella seconda parte invece è descritto lo sviluppo di una reazione di cicloadizione di indoli con alleni elettron-ricchi con conseguente dearomatizzazione, catalizzata da complessi commerciali di oro i quali sono efficaci nel catalizzare una formale cicloadizione [2+2] in modo chemo-, regio-, e diastereoselettivo su un 'ampia gamma di substrati in condizioni blande (Figura Ib). I complessi di oro sono acidi di Lewis altamente carbofilici capaci di attivare i legami multipli C-C per attacchi nucleofili, infatti tali complessi sono stati utilizzati come catalizzatori per numerose trasformazioni organiche e in particolare per l'idroamminazione di legami insaturi C-C. I sali di ammonio quaternari in molti casi possono essere considerati degli equivalenti sintetici dei metalli di transizione "late" nell'agire da attivatori dei legami insaturi C-C nel subire attacco nucleofilo. Nella terza parte è riportato uno studio che esplora la possibilità di rimpiazzare i metalli di transizione con quantità catalitiche di sali di ammonio per la sintesi di indoli altamente funzionalizzati, in particolare, è stata verificata l'efficienza degli ioni  $\text{Bu}_4\text{N}^+$  e  $\text{F}^-$  nel catalizzare una sequenza di reazioni, nello specifico, una idroamminazione intramolecolare di un triplo legame C-C, la rimozione dei gruppi protettori silicei e un riarrangiamento sigmatropico del tipo aza-Cope [3,3] (Figura Ic).

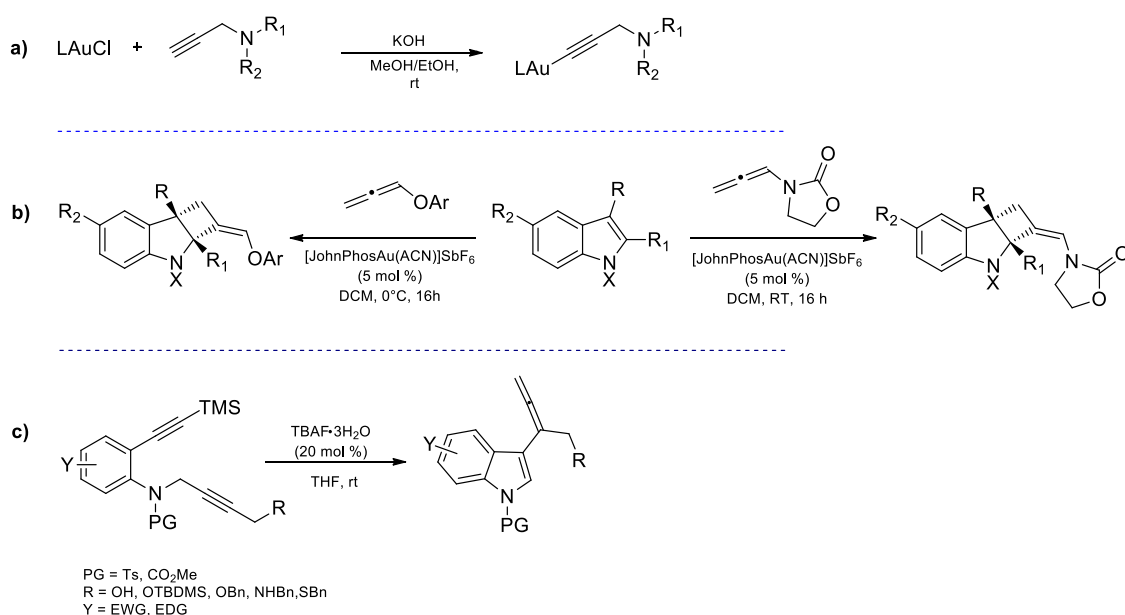


**Figura I**

## TABLE OF CONTENTS

<b>1 GOLD CHEMISTRY: GENERAL INTRODUCTION .....</b>	<b>1</b>
1.1 GOLD: “KING OF METALS” .....	1
1.1.1 <i>History of gold</i> .....	1
1.1.2 <i>General physical and chemical properties</i> .....	3
1.1.3 <i>Applications</i> .....	3
1.2 THEORETICAL CONSIDERATION AND RELATIVISTIC EFFECT .....	4
1.3 COORDINATION CHEMISTRY OF GOLD <sup>[22]</sup> .....	8
1.3.1 <i>Gold(I) coordination chemistry: an overview</i> .....	8
1.4 HOMOGENEOUS GOLD CATALYSIS .....	11
1.5 AIM OF THE PROJECT .....	15
1.6 BIBLIOGRAPHY .....	16
<b>2 ALKYNYL-GOLD(I) COMPLEXES FEATURING ANTICANCER ACTIVITY .....</b>	<b>21</b>
2.1 INTRODUCTION .....	22
2.1.1 <i>Metals in medicine: an overview</i> .....	22
2.1.2 <i>Metal complexes in cancer therapy</i> .....	24
2.1.3 <i>Gold complexes as anticancer drugs</i> .....	29
2.2 RESULTS AND DISCUSSION.....	42
2.2.1 <i>Synthesis and characterization</i> .....	42
2.2.2 <i>Single crystal X-ray diffraction of complexes 3ab and 3ac</i> .....	44
2.2.3 <i>Biology</i> .....	47
2.2.4 <i>UV-Vis absorption titration analysis</i> .....	55
2.3 CONCLUSIONS .....	59
2.4 EXPERIMENTAL PART .....	61
2.4.1 <i>General methods</i> .....	61
2.4.2 <i>Synthesis of the propargyl amino derivative 2a-2e</i> .....	62



2.4.3	<i>Synthesis of 2f</i> .....	64
2.4.4	<i>Synthesis of the [alkynylAu(I)] complexes 3</i> .....	64
2.4.5	<i>Cell culture and cytotoxicity</i> .....	67
2.4.6	<i>Cell cycle analysis</i> .....	68
2.4.7	<i>TrxR inhibition assay</i> .....	68
2.4.8	<i>DNA-compound interaction assay</i> .....	69
2.4.9	<i>Competitive binding fluorescence studies</i> .....	70
2.4.10	<i>Liquid chromatography and mass spectra analysis</i> .....	70
2.4.11	<i>Crystallographic Data Collection and Structure Determination for 3ab and 3ac</i> .....	71
2.5	BIBLIOGRAPHY.....	74
<b>3</b>	<b>GOLD(I)-CATALYSED DEAROMATIVE [2+2]-CYCLOADDITION OF INDOLES WITH ACTIVATED ALLENES</b>	<b>83</b>
3.1	INTRODUCTION.....	84
3.2	RESULTS AND DISCUSSION .....	86
3.2.1	<i>Gold catalysed dearomatization reaction: the racemic version (allenamides)</i> .....	86
3.2.2	<i>Gold catalysed dearomatization reaction: the racemic version (aryloxyallene)</i> .....	92
3.2.3	<i>Gold catalysed dearomatization reaction: mechanistic study</i> ....	96
3.2.4	<i>Enantioselective gold catalysed [2+2]-cycloaddition between indoles and electron-rich allenes</i> .....	104
3.3	CONCLUSIONS .....	109
3.4	EXPERIMENTAL PART .....	111
3.4.1	<i>General methods</i> .....	111
3.4.2	<i>General Procedure for the synthesis of Propargyl-Phenol Ethers 3'</i> .....	112
3.4.3	<i>General Procedure for the synthesis of Alkoxyallenes 3</i> .....	113
3.4.4	<i>General procedure for the [2+2] cycloaddition reaction between indoles and allenamide/ aryloxyallenes (2/3): racemic variant</i> .....	114

3.4.5 General procedure for the enantioselective [2+2] cycloaddition reaction.....	122
3.4.6 Computational details .....	123
3.4.7 Crystallographic Data Collection and Structure Determination for 4b', 4r and 7hd .....	127
3.5 BIBLIOGRAPHY .....	132
<b>4 I THOUGHT IT WAS GOLD INSTEAD...TBAF CATALYSED ONE-POT SYNTHESIS OF ALLENYL-INDOLES.....</b>	<b>136</b>
4.1 INTRODUCTION.....	137
4.1.1 Intramolecular hydroamination reaction.....	137
4.2 RESULTS AND DISCUSSION.....	139
4.2.1 Synthesis of ortho-alkynyl aniline .....	139
4.2.2 Study of the catalytic system.....	140
4.2.3 Proving the synthetic flexibility of allenyl-indoles.....	148
4.3 CONCLUSIONS .....	151
4.4 EXPERIMENTAL PART .....	151
4.4.1 General methods.....	151
4.4.2 General procedure for the synthesis of 7 .....	152
4.4.3 Procedure for the synthesis of 7h.....	155
4.4.4 Procedure for the synthesis of 7i.....	156
4.4.5 General procedure for the synthesis of 7j:.....	156
4.4.6 Procedure for the synthesis of 7m .....	157
4.4.7 Procedure for the synthesis of 7n.....	158
4.4.8 General procedure for the synthesis of 1 .....	158
4.4.9 General procedure for the synthesis of 1k .....	162
4.4.10 General procedure for the synthesis of 1a' .....	163
4.4.11 General procedure for the synthesis of 1a''.....	164
4.4.12 General procedure for the one-pot synthesis of allenyl-indoles 2 .....	165
4.4.13 <sup>1</sup> H-NMR experiment.....	169

<i>4.4.14 Procedure for the scrambling reaction.....</i>	<i>174</i>
<i>4.4.15 Optimization of the catalytic cyclization of 2a to dihydrofuran 4a .....</i>	<i>175</i>
<i>4.4.16 Gold-catalyzed synthesis of the tetrahydrocarbazole 6aa through intermolecular cycloaddition of allenyl indoles and N-allenyl amides. .....</i>	<i>176</i>
<i>4.4.17 Single Crystal X-ray crystallography .....</i>	<i>177</i>
<b>4.5 BIBLIOGRAPHY.....</b>	<b>181</b>



# 1 GOLD CHEMISTRY: GENERAL INTRODUCTION

## 1.1 Gold: “King of metals”

### 1.1.1 History of gold

Gold is a unique metal. It was probably one of the first metals, along with copper, to be discovered by man. The chemical symbol, Au, derives from the Latin word *aurum*, which is associated with the dawn goddess, Aurora and the English word “gold” comes from ancient English/Germanic word *gulth, ghol* that means “to shine, to gleam, to be yellow or green”.

From the beginning of civilization, man attributed great value to this brilliant and rare metal by associating it with power, beauty and wealth. In fact, it was used to make jewellery and the oldest finds were found in the tombs of Egyptian pharaohs. The discovery of the tomb of Tutankhamun in 1920, one of the few not to be plundered over the centuries, brought to light his great treasure and his funeral mask in gold, a masterpiece of rare beauty. There are sources that attest that the Egyptians in 3600 B.C. were able to separate gold from ores by melting.

Throughout human history, there have been religious references to gold: the Greek myth of King Midas, which transformed everything into gold, as well as the adoration of the golden calf reported in the book of the Exodus, or to the Magi gifts to Jesus (gold, incense and myrrh) and also in the Buddhist religion, gold is one of the seven treasures, the treasure of conviction.<sup>[1,2]</sup>

The first gold coins were minted by King Croesus, sovereign of Lydia, in Western Asia Minor, from 560 B.C. to 546 B.C.. For a long time the monetary system was based on silver coins; in the thirteenth and fourteenth centuries the gold coins were reintroduced. At the beginning of the nineteenth century the golden standard, a link between the national currency and a certain quantity of gold, which allowed to have fixed exchange rates between the nations, was introduced. The gold system was finally abandoned in 1971, when the US abolished the convertibility of the dollar into gold, decreeing the birth of the floating system. Gold is currently a safe haven for investments.

As a consequence, gold has become one of the most influential commodities in human history and remains the subject of intense aspirations, in fact in all competitions the first prizes are gold medals.

The proximity of atomic numbers led thinking the twentieth century scientists to obtain gold by bombarding mercury with neutrons via transmutation of chemical elements.

The main purpose of the alchemists was to produce gold from other substances, such as iron or lead, by means of the philosopher's stone. The alchemical symbol of gold was a circle with a dot in the centre,  $\odot$ , which is also the Egyptian hieroglyphic symbol and the Chinese pictogram of the Sun.

In more recent times, there were several attempts at transmutation, among them the attempt to transform the silver in gold by Stephan H. Emmens in 1897.<sup>[3]</sup>

### 1.1.2 General physical and chemical properties

Despite its discovery since the dawn of civilization, gold chemistry was overshadowed since it was used only in the metallic state, and all the knowledge was related exclusively to its physical properties and its recovery and purification.

Gold is widespread on the earth's crust and is found in alluvial deposits as free metal for its chemical inertness, and in tellurides associated with pyrite and quartz. It is estimated that the earth's crust contains about 0.03 ppm and up to today about 160000 tons have been extracted. It can also be extracted from seawater in which the concentrations range is 0.1 - 2 mg ton<sup>-1</sup>.<sup>[4]</sup> Among its physical properties, we recall the high melting temperatures of 1060 °C and the boiling point, 2860 °C. Gold possesses a highly positive standard potential, it is not sensitive to corrosion or oxidation under mild conditions, in fact it only dissolves in aqua regia or in solution of cyanide salts. It has high energies of first and second ionization (889.3 kJ mol<sup>-1</sup> and 1980.0 kJ mol<sup>-1</sup>, respectively), and an electronegativity value of 2.54, the highest among metals and similar to that of carbon (2.55). It is extremely malleable and ductile: one gram of gold can be reduced to a sheet of about 1 m<sup>2</sup> of surface with a thickness of only 230 atoms, or profiled to give a 165 m long wire with a diameter of 20 μm. The electrical and thermal conductivity are exceptional (respectively 317 W m<sup>-1</sup> K<sup>-1</sup> and 45.2 x 10<sup>6</sup> S m<sup>-1</sup>) as well. All these properties can be directly related to the electronic configuration  $d^{10}s^1$ , as its air stability and inertia to the attack of other substances that make it particularly suitable for use in various fields such as jewellery, electronics and dentistry.<sup>[5]</sup>

### 1.1.3 Applications

Nowadays gold is mainly used in jewellery for about 60%, for investments (about 30%), the rest is used for industrial purposes.<sup>[6]</sup>

Traditional industrial applications have based mainly on its metallic properties: in fact, for its excellent conductivity and insensitivity to corrosion and oxidation, it is used in electronic applications to produce connectors, switches and relay contacts, bonding wires and connection strips.

Another important application is its use as protective coating against radiation in the aeronautical and spatial industry due to its capability of reflect infrared radiation. It has been used in medicine throughout the history of civilisation (see section 2.1.3). Metallic gold is biocompatible and it is used in dentistry for fillings, bridges and orthodontic appliances, but gold in ionic form is toxic. Although the major uses and applications of gold are restricted to its metallic state, new developments have emerged in the modern era.

## 1.2 Theoretical consideration and relativistic effect

Electronic configuration of [Au(0)] is [Xe]  $4f^{14}5d^{10}6s^1$  in the ground state, while cation [Au(I)] and anion [Au(-I)] have respectively  $5d^{10}6s^0$  and  $5d^{10}6s^2$  configurations. These configurations explain the relative stability of the compounds [Au(I)] and [Au(-I)] both with full orbitals, the first with 10 electrons in the  $5d$  orbitals and the second with 2 electrons filling the more external  $6s$  orbital. However, this does not justify the high chemical inertness of metallic gold.

All the post-lanthanide elements contain a large number of protons in their nuclei, so the electrons are subject to a high field that leads them to move at speeds close to that of light. The only classical treatment of electrons, by itself, does not guarantee a sufficient description of this phenomenon, but it is necessary a further treatment, the relativistic one. The “relativistic effect” refers to any phenomenon resulting from the need to consider velocity as significant relative to the speed of light. The relativistic effect become



apparent for the electrons in the  $s$  orbitals, which have wave functions to which corresponds an electronic density on the nucleus, but it is less important for the electrons in the orbitals  $p$  and  $d$ . The relativistic treatment predicts the assignment of a relativistic mass that is greater than the mass of the electron at rest. The result is the reduction of the Bohr radius, which is inversely proportional to the mass of the electron orbiting a nucleus.<sup>[7]</sup> Figure 1.1 shows the relation between the relativistic and non-relativistic radius of the 6s orbital according to the atomic number.

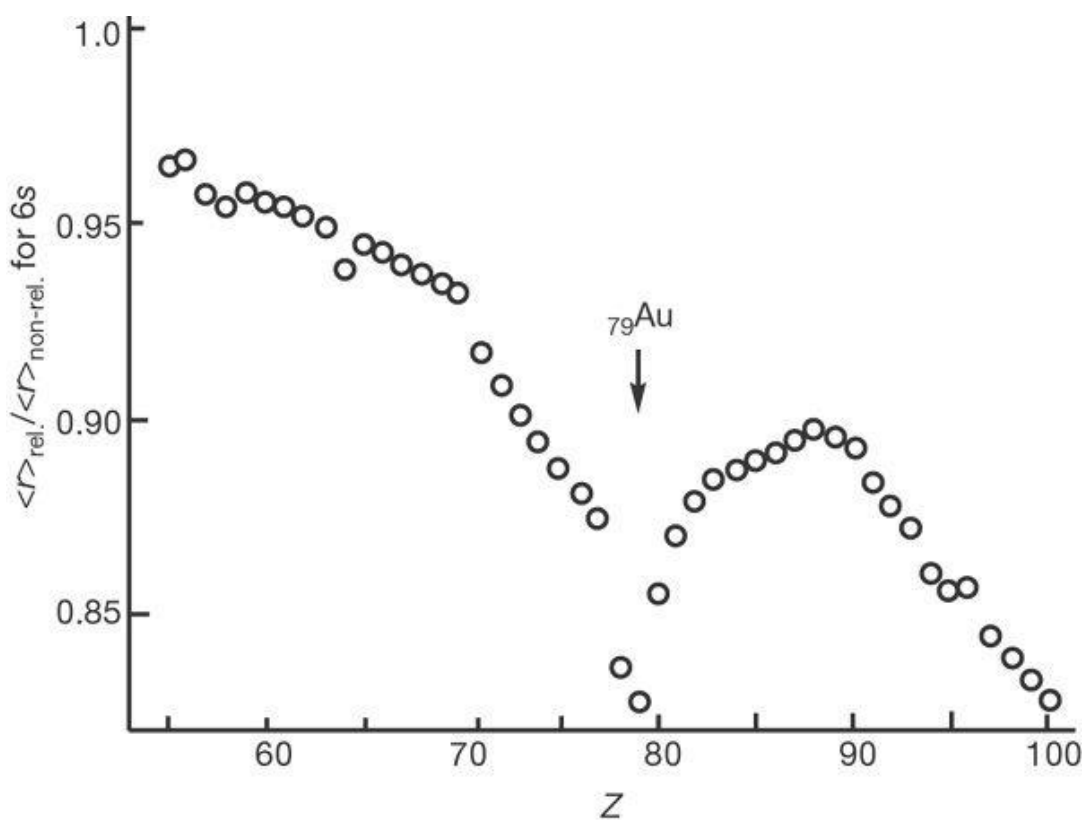


**Figure 1.1** Calculated relativistic contraction of the 6s orbital. The relativistic and non-relativistic atomic radii were determined computationally.<sup>[8]</sup> Reproduced from ref [7].

It is possible to observe how this relationship differs strongly as the atomic number increases, and reaches a minimum value in the case of gold.<sup>[9]</sup>

This involves different effects in the chemistry of gold.

The most visible one is the colour of gold. Since the  $s$  and  $p$  orbitals are contracted, the electrons in the  $5d$  and  $4f$  orbitals are better shielded by the attraction of the nucleus and therefore the  $d$  orbitals expand. The

consequence is a substantial decrease of the  $5d/6s$  band gap. The golden colour is due to this band gap reduction ( $h\nu = 2.38$  eV, 521 nm) which is the transition from the  $5d$  band to the Fermi level (the vacant  $6s$  band). For this reason, gold absorbs in the blue-green region of the visible spectrum and reflects red and yellow. For silver the  $s$  and  $p$  orbital contraction is less and the band gap is larger ( $h\nu = 3.7$  eV, 335 nm) and it absorbs in the UV region leading to its peculiar metallic shine.

The destabilization of the  $5d$  orbitals makes it possible to explain the presence of +3 oxidation state, almost absent for silver, and the stabilization of the  $6s$  orbital explains the formation of [Au(-I)] compounds, unknown for silver.

The higher energy gap between  $6s$  and  $6p$  orbitals justifies the preference for the formation of coordinate complexes with linear geometry for [Au(I)] and the reluctance of [Au(I)] to accept more than two ligands. In fact, Molecular Orbital (MO) calculations suggest that the bonding involves mostly the  $5d_z^2$  and  $6s$  orbitals.<sup>[10]</sup> The reluctance of [Au(I)] to accept more than two ligands is indicative of the special situation of gold valence orbitals when compared to [Cu(I)] and [Ag(I)] behaviour.<sup>[11,12]</sup>

Another peculiar property of gold is the so-called “aurophilicity” and this phenomenon is also governed by relativistic effect. Atoms of gold tend to approach an equilibrium distance ranging between 2.7 and 3.6 Å (the Van Der Waals distance is 3.60 Å), with a bond strength of 20 - 50 kJ mol<sup>-1</sup>, that is similar to hydrogen bond energy. Aurophilicity is the result of the orbital mixing of molecular orbitals between two gold centres in their respective complexes with the creation of a new set of bonding and antibonding molecular orbitals and this led to the formation of a new kind of interaction between the two gold atoms that stabilizes the complexes.<sup>[9,13,14]</sup>

Theoretical calculations have made possible to understand the origin of these differences between gold and silver. The introduction of relativistic effects

in the calculation leads to an increase of the aurophilicity effect between two atoms of gold with close-shell. The aurophilic bond is considered as an effect based on the correlation of electrons between the closed-shell components, very similar to the attractive forces of Van der Waals but unusually stronger. All these studies have consistently shown that calculations can reproduce the attractive forces between gold atoms only if the relativistic effect is included.

The relativistic contraction of the valence  $s$  and  $p$  orbitals is also responsible of the high Lewis  $\pi$ -acidity of gold cations which is the basis for the use of gold in catalysis, in fact that contraction corresponds to a relative low-lying lowest unoccupied molecular orbital (LUMO), this makes gold(I) a better Lewis acid than that other Group 11 metals.<sup>[7]</sup> Gold(I) and gold(III) activate the alkynes to undergo nucleophilic addition, in fact alkyne reacts as basic Lewis donors, donating electrons to the metal and behaving as a  $\pi$ -ligand.<sup>[15]</sup>

The Dewar-Chatt-Duncanson model can explain this type of coordination.

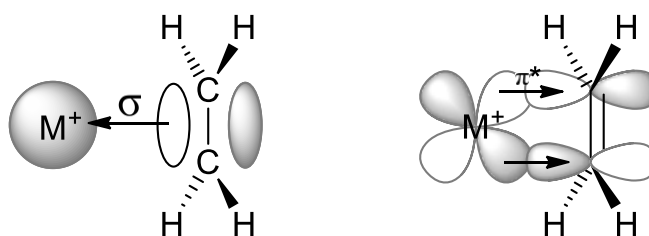


**Figure 1.2** The schematic representation of a group 11 metal-ethylene bonding model.

As depicted in Figure 1.2, the interaction between the metal cation and the alkene takes place in two different ways. On the left of the Figure 1.2 is shown the donation to the empty  $s$  orbital of the metal from the filled  $\pi$ -orbital of ethylene and on the right the back donation of the electron density from a metal filled  $d$  orbital to the vacant antibonding  $\pi^*$ -orbital.

In addition, the alkyne has a second occupied  $\pi$ -orbital perpendicular to the previous one that can form another M-L bond. Based on this model it is possible to understand how the unsaturated  $C\equiv C$  bond is elongated so it is

weakened and the alkyne becomes more electrophilic and more prone to nucleophilic attack. Due to the contraction of the orbital  $6s$ , the orbital  $5d$  is shielded and it is affected by a lower attraction of the nucleus. The result is an expansion of the  $5d$  orbital whose electrons are more likely to be delocalized, so gold(I) does not act only as a Lewis acid but also as an electron donor and can contribute to the stabilization of carbocation intermediates.<sup>[16,17]</sup> The chemistry of gold can be better understood in light of these important theoretical considerations.<sup>[18–21]</sup>

### 1.3 Coordination chemistry of gold<sup>[22]</sup>

The possible oxidation states of gold are - I, + I, + III and + IV.

Actually, there are very rare cases of compounds in which the Au atom presents an oxidation state higher than +3, such as fluorine complexes of [Au(IV)]. Even the complexes that have gold in a +2 oxidation state are few. The difficulty in synthesising these complexes lies not so much in the high energy needed to reach the oxidation state +2 from atomic gold, but resides in the lack of stability of [Au(II)]. In fact, they show a high tendency to disproportion to generate [Au(I)] and [Au(III)] due to the unpaired electron in the orbital  $d^9$  that can be easily ionized. Gold(III) gives stable complexes with C, N, P, S or even O-donor ligands, but its chemistry is less developed than that of gold(I).<sup>[22]</sup>

#### 1.3.1 Gold(I) coordination chemistry: an overview

The [Au(I)] complexes are undoubtedly the most studied. The external configuration of gold in these complexes is [Xe]  $4f^{14}5d^{10}$ , many of which are extremely stable but they easily undergo a ligand exchange reaction. They can have variable coordination numbers between 1 and 4 even if the coordination number 2 is the most widespread.

The chemistry of [Au(I)] is dominated by complexes with linear geometry commonly represented in the form [AuXL]. In these complexes the neutral ligand is generally a phosphine, an isocyanate or an amine, while the anionic portions can be a halogen, aryl, or alkyne. Generally, these species aggregate in the solid state thanks to the aforementioned aurophilicity. In some complexes, however, it is possible to observe the formation of aggregates that exploit secondary bonds, in addition to aurophilicity, such as hydrogen bonds and / or gold-sulfur interactions. [Au{SSi(O<sup>i</sup> Pr)<sub>3</sub>}(PPh<sub>3</sub>)] is an example of thiolated compounds that aggregates into dimers via gold-sulfur interactions,<sup>[23]</sup> or complexes such as [Au(O<sub>2</sub>CCF<sub>3</sub>)(4-PPh<sub>2</sub>C<sub>6</sub>H<sub>4</sub>CO<sub>2</sub>H)], which crystallize like a polymer chain.<sup>[24]</sup>

Another important effect of aurophilicity in the [Au(I)] compounds is the luminescence observed under UV excitation in the solid state. This is evident in complexes with a short Au...Au interaction: in the complex [AuCl(TPA)] (TPA = 1,3,5-triaza-7-phosphaadamantane) the ligand has a small cone angle that lets the compound to shorter intermolecular Au...Au distance and the protonated complex [AuCl(TPA·HCl)], which presents different emission spectra due to a change in the gold-gold interaction.<sup>[25]</sup>

Among the polydentate ligands, the most important are the diphosphines, which allow the achievement of different structural models according to the presence or not of the Au-Au interaction. The complexes derived from 1,4-bis (diphenylphosphino)butane (n = 4) or hexane (n = 6) have a crystalline structure in which the molecules are completely independent. In contrast, complexes derived from diphosphines with shorter or longer bridges tend to form intermolecular or intramolecular Au-Au interactions with consequent formation of dimers or polymeric chains.<sup>[26-29]</sup> Another important class of bidentate ligands is represented by sulfur ligands as dithiocarbamates, dithiolates, etc. These complexes have the same structural characteristics and same aurophilic interactions already encountered in complexes with

diphosphine ligands. What differentiates these bidentate ligands from the diphosphines is the possibility of establishing a further Au-S interaction in addition to Au-Au one. The soft behaviour of [Au(I)] cation manifests itself in its marked carbophilicity (preference in forming Au-C bonds). Organometallic gold(I) complexes are a very important part of the chemistry of this element.

A relevant class of [Au(I)] complexes consists of organometallic complexes of the [RAuL] type where R represents a variety of organic residues, such as aryls, vinyls, etc.... The neutral ligand L is often a tertiary phosphine, a carbene or an isocyanide. The Au-C bond is covalent and its stability strongly depends on the type of ligand. In fact, gold(I) complexes with carbonyls are among the most unstable and only a few examples are known; the order of stability, from the least stable, is the following: alkyls, aryls and allyl.

Gold(I) complexes with N-heterocyclic carbenes, based on imidazoles or benzimidazoles, [AuCl(carbene)], have been intensively used in catalytic organic reactions.<sup>[30]</sup> Carbenes are species with divalent carbon atoms with various substituents and a lone pair of electrons. An important carbene complex is [AuF(carbene)], which represents the first example of an isolable gold(I) fluoride complex.<sup>[31]</sup> An important property of some carbene complexes is their luminescence. Cationic bis(carbene) complexes such as [Au{C(NHMe)<sub>2</sub>}<sub>2</sub>]PF<sub>6</sub> show structures in which the cations have aurophilic interactions and hydrogen bonds and are emissive.<sup>[32]</sup>

The chemistry of the alkynyl complexes of [Au(I)] has been particularly developed in recent years. The preference of gold(I) for linear coordination, together with the linearity of the triple bond allowed the gold alkynyl complexes to become attractive building blocks for molecular wires and polymeric materials, which may have important properties in non-linear optics or luminescence.<sup>[33]</sup>

The luminescence of gold(I)-alkynyl complexes, firstly reported in 1993 by Che,<sup>[34]</sup> is one of the most studied properties of this class of complexes and many examples are present in literature with different kind of second ligands in particular isocyanide,<sup>[35,36]</sup> alkynyl,<sup>[37,38]</sup> phosphane<sup>[39]</sup> and carbene.<sup>[40,41]</sup>

Due to the well-known ability of gold to interact with other metals, Wolf and coworkers synthesized a series of thiophene ligands derivatised with alkynyl group in order to prepare gold complexes featuring important electronic properties for applications in photoinduced electron transfer (PET) and electropolymerization processes.<sup>[42,43]</sup>

Because of the linear shape of gold-alkynyl moiety and the absence of  $\beta$ -hydrogen, the alkynyl compounds are precursors for thermally stable species with liquid-crystal behavior.<sup>[44,45]</sup> Another important emerging application of gold-alkynyl complexes is their use as anticancer metallodrugs, this aspect is discussed in chapter 2.

## 1.4 Homogeneous gold catalysis

For a long time gold has been considered too expensive, an inert and inactive metal. Today it is known that gold(0), (I) and (III) species are able to act as catalysts or pre-catalyst in homogeneous and heterogeneous catalysis.<sup>[46]</sup> From the economical point of view, gold is not so expensive and rare compared to rhodium, palladium and platinum. In addition, gold can be easily recycled and the price of the catalyst is often determined by the ligand rather than by the metal.<sup>[47,48]</sup>

The industrial catalytic applications are dominated by heterogeneous catalysis. The first example of heterogeneous catalysis dates back to 1973, when Bond and co-workers reported the hydrogenation of olefins catalysed by gold particles.<sup>[49]</sup> Later, in the 80s, Haruta and co-workers reported a study on the oxidation of carbon monoxide at low temperature<sup>[50]</sup> and, almost

simultaneously, Hutchings obtained excellent results in the hydrochlorination reaction of acetylene to vinyl chloride.<sup>[51]</sup>

The homogeneous catalysis based on gold was developed more recently. A large and varied quantity of reactions can be catalysed both by simple salts, usually halides, and by various complexes of [Au(I)] and [Au(III)].

The first important example was reported in 1986 by Ito, Sawamura and Hayashi which demonstrated that a gold(I) complex with a chiral ferrocenyl diphosphine ligand was an efficient catalytic system for the asymmetric addition of isocyanate onto aldehydes to produce oxazolines.<sup>[52]</sup>

Among the many some important breakthroughs deserve mentioning:

- the gold(III) catalysed nucleophilic addition of water, alcohols and amines;<sup>[53]</sup>
- the intramolecular addition of oxygen-based nucleophiles to alkynes and the intermolecular addition of arenes onto allenes and alkenes catalysed by AuCl<sub>3</sub>;<sup>[54]</sup>
- the cyclization of  $\alpha$ -hydroxyallenes into 2,5-dihydrofurans.<sup>[55]</sup>

At the beginning of 2000, with the excitement for these important results, the field of homogeneous gold catalysis has grown exponentially leading to the so-called “gold rush”.<sup>[56]</sup> Gold catalysis is also entered in the field of polymerization. In fact, in 2008, it was reported the first example of olefin polymerization catalysed by complexes of [Au(III)] in which the catalytic precursor has a carbene ligand.<sup>[57,58]</sup>

The main advantages of homogeneous gold catalysis are: the use of milder reaction conditions, the compatibility of gold-based catalysts with a wide range of functional groups and, the wide portfolio of chemical reactivities accessible due to its unique properties.

Many investigations on the catalytic reactivity of gold exploited the propensity of the [Au(III)] and [Au(I)] complexes to activate alkynes



towards nucleophilic addition. The multiple C-C bond of alkynes, alkenes, allenes coordinates the gold complex, which effectively activates the multiple bond for the attack of a nucleophile, but also the activation of carbonyl functionalities is possible with gold(III) catalysts.<sup>[59]</sup>

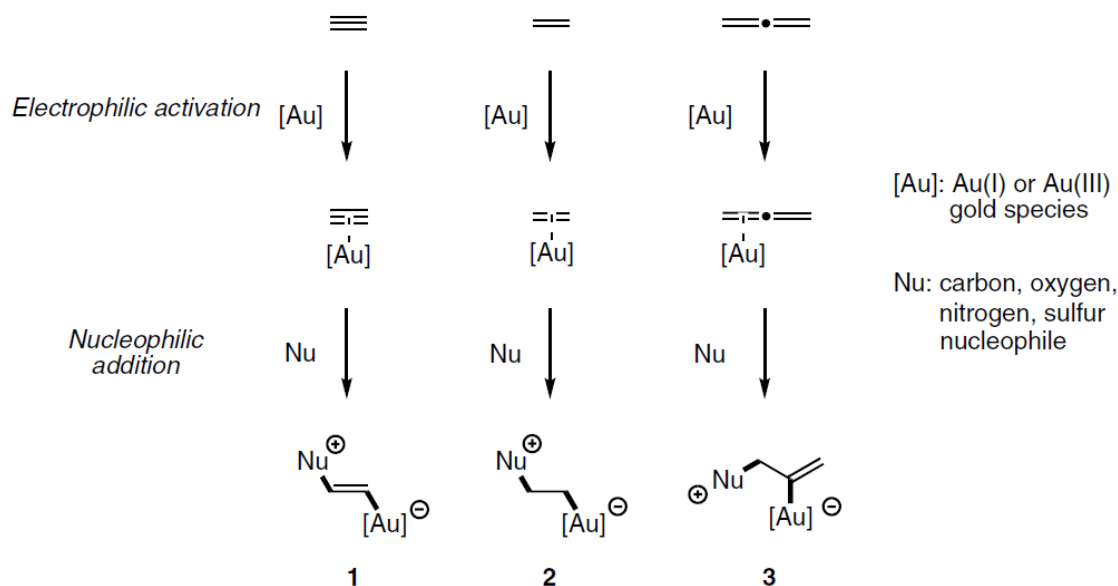


**Figure 1.3** General reactivity of alkynes, alkenes and allenes towards the addition of a nucleophile. Reproduced from ref. [48].

This kind of reactivity is based on the Lewis acid properties of gold species. The simplest example of nucleophilic addition to a  $\pi$ -system is shown in Figure 1.3. The first step involves the interaction of the gold species with the  $\pi$ -system making the nucleophilic attack to alkene/alkynes/allenes possible. After the nucleophilic attack, the simplest pathway is that the **1-3** intermediates release the addition product and regenerate the gold catalyst for simple protodemetalation.

As just mentioned in section 1.2, gold can also act as an electron donor and stabilizing the carbocationic species.<sup>[16,60]</sup>

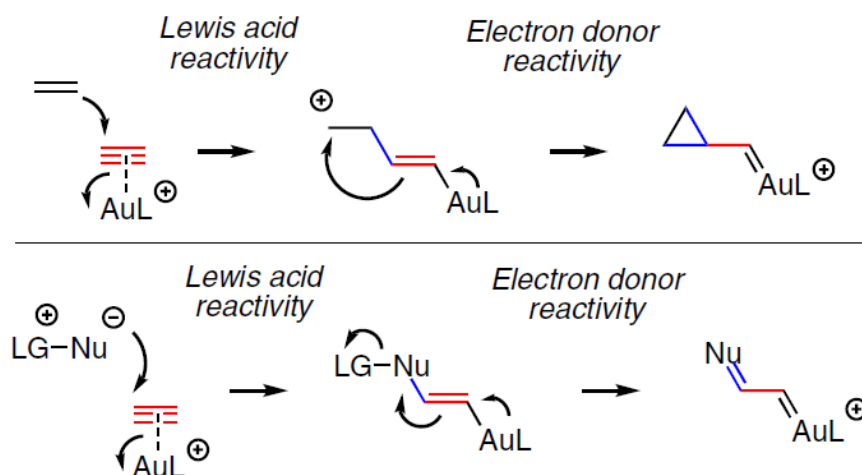


**Figure 1.4** Schematic representation of Lewis acid/electron donor reactivity. Adapted from ref. [48].

In the schematic pathway, reported in Figure 1.4, is represented the activation of the alkyne moiety and the subsequent electron donor behavior that produces a gold-carbene species.<sup>[61,62]</sup> The organogold species can act in both ways and the prevalence of the carbocationic or carbenoid character depends mainly on gold oxidation state and on the type of ligand as well as on the functional groups on the substrate. In a study by Toste and coworkers it was documented how the nature of the ligand strongly influences the reactivity of the organogold species.  $\Pi$ -acid ligands, such as phosphites, favor a carbocationic-type reactivity because they decrease the  $\pi$ -donation from the metal to the substrate; instead in the opposite way  $\sigma$ -donating ligands such as N-heterocyclic carbenes, favor a carbene-type reactivity because they let the  $\sigma$ -donation from the substrate to gold disfavored.<sup>[17]</sup>

In the last twenty years an incredible number of publications in the field of gold catalysis has been published, this is also evidenced by the numerous reviews organized on sub-categories as a complete treatment of all the homogeneous gold catalysis would be a huge undertaking.<sup>[63–67]</sup>

The homogeneous gold catalysis is today an important and consolidated instrument in organic synthesis thanks to its oxygen tolerance, mild reaction

conditions and its excellent chemoselectivity. In chapters 3 and 4 of this dissertation, some examples of applications of gold reactivity will be described.

## 1.5 Aim of the project

The work, presented here, embraces various aspects of gold chemistry.

Chapter 2 is focused on the use of gold(I) compounds as antitumour drugs, where the documentation of novel [alkynyl(triphenylphosphine)gold(I)] complexes carrying variously substituted propargylic amines and their pharmacological investigation on a series of cancer cell lines is described.

In chapter 3 the use of commercially available gold(I) complexes as catalyst for the dearomative [2+2]-cycloaddition of indoles with electron-rich allenes is documented.

Because gold complexes are highly carbophilic Lewis acids that activate C–C multiple bonds towards nucleophilic attack, they have been applied as catalyst for a number of selective organic transformations, including the intramolecular hydroamination of inactivated unsaturated C–C bonds, but soft quaternary ammonium salts are known to act as synthetic equivalents of late-transition metal species in activating unsaturated hydrocarbons towards nucleophilic attack. In this field, in chapter 4, a work on the possibility to replace second and third row transition metals with catalytic amounts of readily accessible and cheap ammonium salts for obtaining synthetically useful highly functionalized indoles is presented. The metal-free approach exploits the combined efficiency of  $\text{Bu}_4\text{N}^+$  and  $\text{F}^-$  ions in performing a cascade sequence involving intramolecular hydroamination of the C–C triple bond, cleavage of silyl-protecting groups and site-selective sigmatropic aza-Cope-type [3,3]-rearrangement. The last work is the result of an unexpected serendipitous discovery.

## 1.6 Bibliography

- [1] R. W. Hesse, *Jewelrymaking through History: An Encyclopedia*, Greenwood Press, **2007**.
- [2] A. Gopher, T. Tsuk, S. Shalev, R. Gophna, *Curr. Anthropol.* **1990**, *31*, 436–443.
- [3] “Adept Alchemy. Part II. Chapter 1. Transmutations of Silver to Gold,” can be found under [http://www.levity.com/alchemy/nelson2\\_1.html](http://www.levity.com/alchemy/nelson2_1.html), **n.d.**
- [4] J. H. Crocket, in *Gold Metallog. Explor.*, Springer US, Boston, MA, **1991**, pp. 1–36.
- [5] H. Schmidbaur, *Gold: Progress in Chemistry, Biochemistry, and Technology*, Wiley, **1999**.
- [6] J. N. Pelton, *The New Gold Rush: The Riches of Space Beckon!*, Springer International Publishing, Cham, **2016**.
- [7] D. J. Gorin, F. D. Toste, *Nature* **2007**, *446*, 395–403.
- [8] J. P. Desclaux, *At. Data Nucl. Data Tables* **1973**, *12*, 311–406.
- [9] P. Pyykkö, *Chem. Rev.* **1988**, *88*, 563–594.
- [10] J. J. Vittal, R. J. Puddephatt, *Encycl. Inorg. Bioinorg. Chem.* **2011**, 1–15.
- [11] H. Schmidbaur, S. Cronje, B. Djordjevic, O. Schuster, *Chem. Phys.* **2005**, *311*, 151–161.
- [12] M. A. Carvajal, J. J. Novoa, S. Alvarez, *J. Am. Chem. Soc.* **2004**, *126*, 1465–1477.
- [13] H. Schmidbaur, A. Schier, *Chem. Soc. Rev.* **2008**, *37*, 1931.
- [14] H. Schmidbaur, A. Schier, *Chem. Soc. Rev.* **2012**, *41*, 370–412.
- [15] A. S. K. Hashmi, G. J. Hutchings, *Angew. Chem. Int. Ed. Engl.* **2006**,

45, 7896–936.

- [16] A. M. Echavarren, *Nat. Chem.* **2009**, *1*, 431–432.
- [17] D. Benitez, N. D. Shapiro, E. Tkatchouk, Y. Wang, W. A. Goddard, F. D. Toste, *Nat. Chem.* **2009**, *1*, 482–486.
- [18] A. S. K. Hashmi, *Top. Organomet. Chem.* **2013**, *44*, 143–164.
- [19] A. S. Hashmi, F. D. Toste, Wiley InterScience (Online service), *Modern Gold Catalyzed Synthesis*, Wiley-VCH, **2012**.
- [20] A. S. K. Hashmi, *Gold Bull.* **2003**, *36*, 3–9.
- [21] F. D. Toste, V. Michelet, *Gold Catalysis: An Homogeneous Approach*, **2014**.
- [22] C. M. Gimeno, in *Mod. Supramol. Gold Chem. Gold-Metal Interact. Appl.*, **2009**, pp. 1–63.
- [23] J. Chojnacki, B. Becker, A. Konitz, W. Wojnowski, *Z. Anorg. Allg. Chem.* **2000**, *626*, 2173–2177.
- [24] F. Mohr, M. C. Jennings, R. J. Puddephatt, *Angew. Chemie - Int. Ed.* **2004**, *43*, 969–971.
- [25] Z. Assefa, B. G. McBurnett, R. J. Staples, J. P. Fackler, B. Assmann, K. Angermaier, H. Schmidbaur, *Inorg. Chem.* **1995**, *34*, 75–83.
- [26] P. M. Van Calcar, M. M. Olmstead, A. L. Balch, *J. Chem. Soc., Chem. Commun.* **1995**, *0*, 1773–1774.
- [27] D. S. Eggleston, D. F. Chodosh, G. R. Girard, D. T. Hill, *Inorganica Chim. Acta* **1985**, *108*, 221–226.
- [28] P. A. Bates, J. M. Waters, *Inorganica Chim. Acta* **1985**, *98*, 125–129.
- [29] H. Schmidbaur, P. Bissinger, J. Lachm, O. Steigeimann, *Z. Naturforsch. B* **1992**, *47*, 1711–1716.
- [30] N. Marion, S. P. Nolan, *Chem. Soc. Rev.* **2008**, *37*, 1776–82.

- [31] D. S. Laitar, P. Müller, T. G. Gray, J. P. Sadighi, *Organometallics* **2005**, *24*, 4503–4505.
- [32] R. L. White-Morris, M. M. Olmstead, F. Jiang, D. S. Tinti, A. L. Balch, *J. Am. Chem. Soc.* **2002**, *124*, 2327–2336.
- [33] J. Carlos Lima, L. Rodríguez, *Chem. Soc. Rev.* **2011**, *40*, 5442.
- [34] D. Li, X. Hong, C.-M. Che, W.-C. Lo, S.-M. Peng, *J. Chem. Soc. Dalton Trans.* **1993**, *0*, 2929–2932.
- [35] H. Xiao, K.-K. Cheung, C.-M. Che, *J. Chem. Soc. Dalton Trans.* **1996**, *0*, 3699.
- [36] M. J. Irwin, J. J. Vittal, R. J. Puddephatt, *Organometallics* **1997**, *16*, 3541–3547.
- [37] M. Ferrer, L. Rodríguez, O. Rossell, F. Pina, J. C. Lima, M. F. Bardia, X. Solans, *J. Organomet. Chem.* **2003**, *678*, 82–89.
- [38] S. K. Yip, E. C. C. Cheng, L. H. Yuan, N. Zhu, V. W. W. Yam, *Angew. Chemie - Int. Ed.* **2004**, *43*, 4954–4957.
- [39] V. W. W. Yam, K. M. C. Wong, *Top. Curr. Chem.* **2005**, *257*, 1–32.
- [40] J. Gil-Rubio, V. Cámara, D. Bautista, J. Vicente, *Organometallics* **2012**, *31*, 5414–5426.
- [41] A. A. Penney, G. L. Starova, E. V. Grachova, V. V. Sizov, M. A. Kinzhalov, S. P. Tunik, *Inorg. Chem.*, **2017**, *56*, 14771–14787.
- [42] O. Clot, Y. Akahori, C. Moorlag, D. B. Leznoff, M. O. Wolf, R. J. Batchelor, B. O. Patrick, M. Ishii, in *Inorg. Chem.*, American Chemical Society, **2003**, 2704–2713.
- [43] A. M. Kuchison, M. O. Wolf, B. O. Patrick, *Inorg. Chem.* **2010**, *49*, 8802–8812.
- [44] M. Benouazzane, S. Coco, P. Espinet, J. M. Martín-alvarez, *J. Mater.*

*Chem.* **1995**, *5*, 441–445.

- [45] S. Coco, C. Cordovilla, C. Domínguez, P. Espinet, *Dalt. Trans.* **2008**, *0*, 6894.
- [46] G. C. Bond, C. Louis, D. T. Thompson, *Catalytic Science Series*, **2006**.
- [47] W. A. Herrmann, B. Cornils, *Angew. Chemie (International Ed. English)* **1997**, *36*, 1048–1067.
- [48] S. Kramer, F. Gagosz, **2014**, 1–49.
- [49] G. C. Bond, P. A. Sermon, G. Webb, D. A. Buchanan, P. B. Wells, *J. Chem. Soc. Chem. Commun.* **1973**, *0*, 444b–445.
- [50] M. Haruta, T. Kobayashi, H. Sano, N. Yamada, *Chem. Lett.* **1987**, *16*, 405–408.
- [51] G. J. Hutchings, *J. Catal.* **1985**, *96*, 292–295.
- [52] Y. Ito, M. Sawamura, T. Hayashi, *J. Am. Chem. Soc.* **1986**, *108*, 6405–6406.
- [53] Y. Fukuda, K. Utimoto, *J. Org. Chem.* **1991**, *56*, 3729–3731.
- [54] A. Hashmi, L. Schwarz, J. Choi, T. Frost, *Angew. Chem. Int. Ed. Engl.* **2000**, *39*, 2285–2288.
- [55] A. Hoffmann-Roder, N. Krause, *Org. Lett.*, **2001**, *3*, 2537–2538.
- [56] A. S. K. Hashmi, *Angew. Chemie - Int. Ed.* **2005**, *44*, 6990–6993.
- [57] J. Urbano, A. J. Hormigo, P. de Frémont, S. P. Nolan, M. M. Díaz-Requejo, P. J. Pérez, *Chem. Commun. (Camb)*. **2008**, *4*, 759–761.
- [58] F. Nzulu, A. Bontemps, J. Robert, M. Barbazanges, L. Fensterbank, J. P. Goddard, M. Malacria, C. Ollivier, M. Petit, J. Rieger, et al., *Macromolecules* **2014**, *47*, 6652–6656.
- [59] A. W. Sromek, M. Rubina, V. Gevorgyan, *J. Am. Chem. Soc.* **2005**, *127*, 10500–10501.

- [60] A. S. K. Hashmi, *Angew. Chemie - Int. Ed.* **2008**, *47*, 6754–6756.
- [61] C. Nieto-Oberhuber, S. López, M. P. Muñoz, E. Jiménez-Núñez, E. Buñuel, D. J. Cárdenas, A. M. Echavarren, *Chem. - A Eur. J.* **2006**, *12*, 1694–1702.
- [62] L. Ye, L. Cui, G. Zhang, L. Zhang, *J. Am. Chem. Soc.* **2010**, *132*, 3258–3259.
- [63] M. Bandini, Ed. , *Au-Catalyzed Synthesis and Functionalization of Heterocycles*, Springer International Publishing, Cham, **2016**.
- [64] S. A. Shahzad, M. A. Sajid, Z. A. Khan, D. Canseco-Gonzalez, *Synth. Commun.* **2017**, *47*, 735–755.
- [65] A. M. Asiri, A. S. K. Hashmi, *Chem. Soc. Rev.* **2016**, *45*, 4471–4503.
- [66] A. Quintavalla, M. Bandini, *ChemCatChem* **2016**, *8*, 1437–1453.
- [67] S. Kramer, *Chem. - A Eur. J.* **2016**, *22*, 15584–15598.



## 2 ALKYNYL-GOLD(I) COMPLEXES FEATURING ANTICANCER ACTIVITY

The class of metallodrugs based on gold complexes continues to gain credit within the scientific community and in this chapter, the application of gold(I) complexes as anticancer agent is discussed.

Assorted alkynyl-gold(I) complexes, carrying variously substituted propargylic amines, were synthesized, characterized and tested on a series of cancer cell lines in collaboration the group of Prof. Natalia Calonghi of the Department of Pharmacy and Biotechnology of the University of Bologna. For some of them, high levels of toxicity were found and these preliminary results represent an interesting possibility for future. Part of this chapter has been published on *Dalton Transaction*<sup>[1]</sup> and reproduced from ref. [1] with permission from The Royal Society of Chemistry.

## 2.1 Introduction

### 2.1.1 Metals in medicine: an overview

The important role of metals in biological systems is well known. Several biomolecules show, in their structure, the presence of different metal ions. For instance, iron is fundamental in the respiratory process as it is present in haemoglobin, a globular protein responsible for the oxygen transport from lungs (or gills in aquatic organisms) to the rest of the body; it is also present, in high quantity, in ferritin, a protein involved in the iron storage and in many other proteins and enzymes;<sup>[2]</sup> traces of cobalt are vital to life because it is the centre of vitamin B<sub>12</sub> that is involved in the formation of red blood cells and has key roles in the proper functioning of brain and nervous system;<sup>[3]</sup> the correct function of many enzymes is based on the crucial role of copper and zinc ions as in the case of the superoxide dismutase (SOD) an important antioxidant defence in the living cells.<sup>[4-6]</sup> These are few examples of the importance of metal ions in the maintenance of the dynamic equilibrium of the biological systems and their key role in the structure of the so-called metalloproteins. In humans, fourteen metals (Na, K, Mg, Ca, V, Cr, Mn, Fe, Co, Ni, Cu, Zn, Mo and Cd) are required for crucial biological functions and insufficient amounts of these metals is the cause of many diseases as neurological disorders, in the case of scarcity of copper and cobalt. On the other hand metal ions can be very toxic if present in excess in the precarious biological system or if the latter is exposed to nonessential metals as mercury and lead.<sup>[7]</sup>

Understanding the modulability of physical and chemical properties of the metal ions is a key point in the development of new metal drugs and, to this end, the principle of coordination and organometallic chemistry are fundamental.

Although the use of metal-based drugs is known since very ancient time, it was only in 1965, with the serendipitous discovery of the property of cisplatin to inhibit cell division by Barnett Rosenberg and Loretta VanCamp<sup>[8]</sup>, that the new era of medicinal inorganic chemistry started. Nowadays various metal-based drugs and diagnostic agents are in use in the therapy and in the diagnosis of human diseases (Figure 2.1).<sup>[9]</sup>

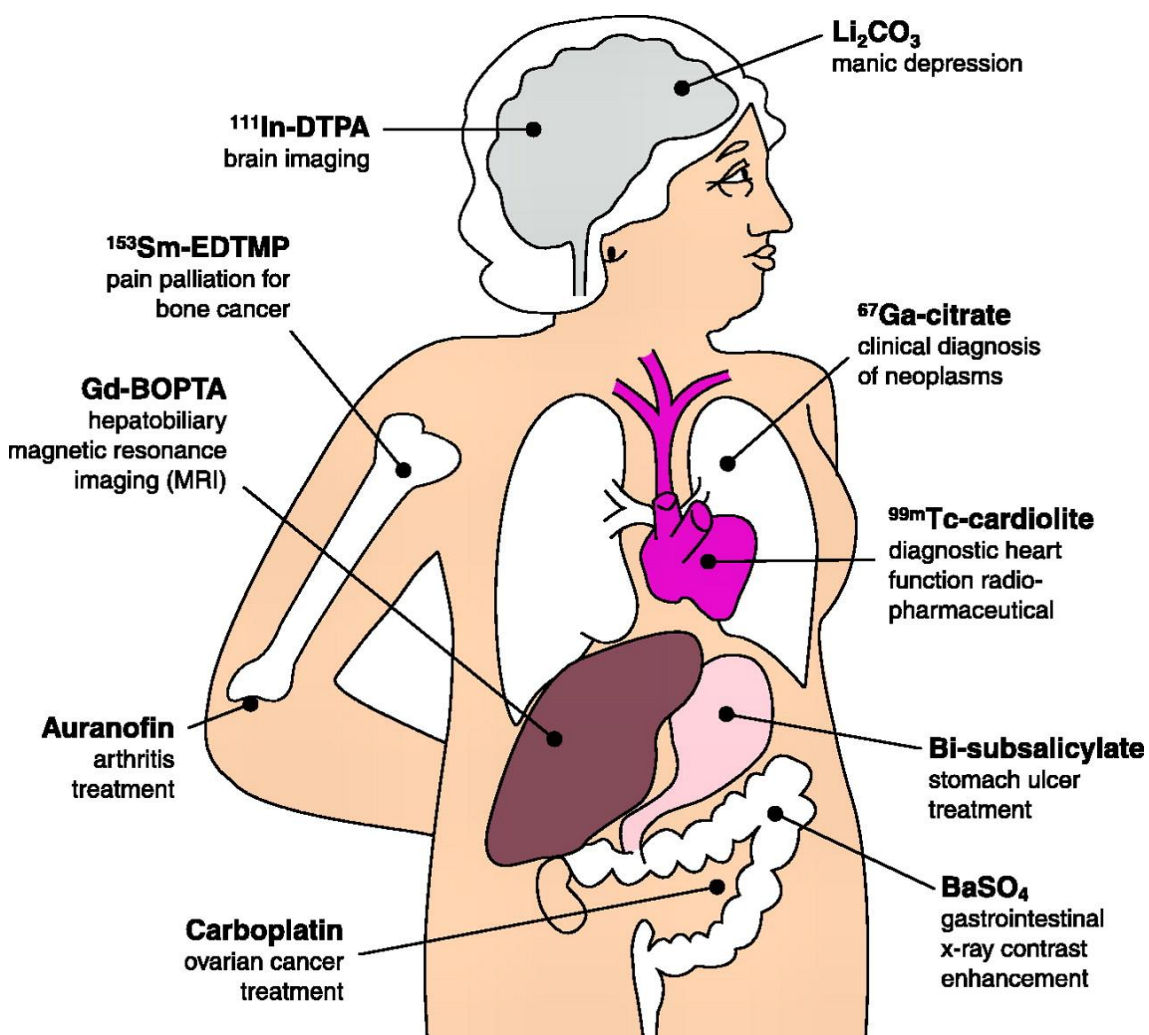


**Figure 2.1** Metal-based drugs and diagnostic agents currently in use. Reproduced from ref. [8].

In 1970 FDA (Food and Drug Administration) approved the use of lithium carbonate in the treatment of mental disease, in particular bipolar disorder and manic depression;<sup>[10]</sup> more recently the bismuth subsalicylate was found

to be an antidiarrheal agent and, as a derivative of salicylic acid, it shows also anti-inflammatory and antibacterial properties.<sup>[11–13]</sup> Many metal ions play also an important role as diagnostic agents: in fact <sup>111</sup>In-DTPA, <sup>67</sup>Ga-citrate and <sup>99m</sup>Tc-cardiolite are important  $\gamma$ -emitting radiopharmaceuticals used for single-photon emission computed tomography<sup>[14]</sup> and Gd(III)-BOPTA is a very used contrast medium in Magnetic Resonance Imaging (MRI).<sup>[15]</sup>

The use of metals in medicine is well established as witnessed by the reported examples and nowadays the effort of scientific community is to find new and less toxic metal drugs and to predict their structure-activity relationships.<sup>[16]</sup>

### 2.1.2 Metal complexes in cancer therapy

Although cancer has been known since ancient times, with the oldest written evidence found in an Egyptians papyrus, dating back to 3000 B.C., in which a description of a breast cancer is reported<sup>[17]</sup>, this pathology is still one of the principle cause of death worldwide. It was estimated that 1 out of 6 deaths is due to cancer and this number is expected to rise in the next twenty years.<sup>[18]</sup> Tremendous efforts in the research of new drugs and therapy have been made to reduce mortality and increase the survival rate of patients.

The development of chemotherapy, i.e. active molecules capable of reaching neoplastic cells and destroy them, can be traced back to 1865 with the use of Fowler's solution, containing 1% of potassium arsenide (KAsO<sub>2</sub>), in the treatment of leukaemia.<sup>[19]</sup> It was after the World War I that new important advances were made. Studies on the effects of mustard gas on the population showed a reduction in the proliferation of tumour cells and, after several studies of the effects of mustard gas and analogues on animal models, in 1942, the first clinical trial of nitrogen mustard, shown in Figure 2.2, on a man with lymphosarcoma at terminal stage, occurred. Goodman, Gilman

and Lindskog made this first important step in the development of new anticancer drugs,<sup>[20]</sup> but in the end they found that the malignant tumour regressions were temporary.<sup>[21]</sup> In the same period, during his studies on leukemia, Sidney Farber discovered that folic acid stimulated the hematopoietic stem cells of red bone marrow and he hypothesized that some folic acid antagonist, such as aminopterin and amethopterin, could inhibit tumour cells growth.<sup>[22]</sup> Amethopterin, shown in Figure 2.2, is still used for chemotherapy in the treatment of different tumours.

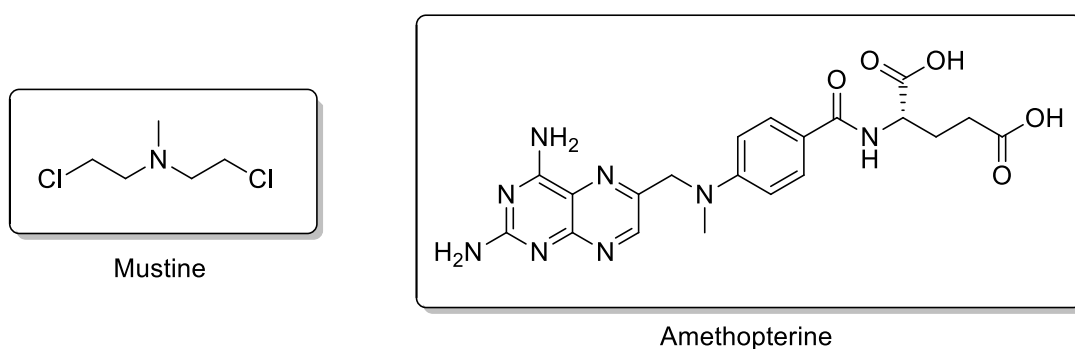


**Figure 2.2** Chemical structures of Mustine and Amethopterin.

The real breakthrough in the anticancer therapy was the serendipitous discovery of tumour-inhibiting quality of *cis*-diamminedichloroplatinum(II), cisplatin, in 1965, that has opened up the door of the metal-based drugs new era.

In 1961, Rosenberg decided to study the effect of electric current on the replication process of the *Escherichia Coli* bacterium. The experimental setup required the use of platinum electrodes immersed in an ammonium chloride solution. The first experiments showed an extension of the bacterium without any cell division. After several tests, it was understood that this effect was not due to the electrical current but to the cisplatin that was formed in situ. These results opened up the hypothesis that these compounds could be able to inhibit the tumour growth.<sup>[8]</sup> After the synthesis of different platinum complexes, showed in Figure 2.3 and the study of their effect on sarcoma 180 and on L 1210 leukemia in mice, in 1969, Rosenberg

and his co-workers published the first paper on the tumour-inhibiting effect of platinum compounds.<sup>[23]</sup>

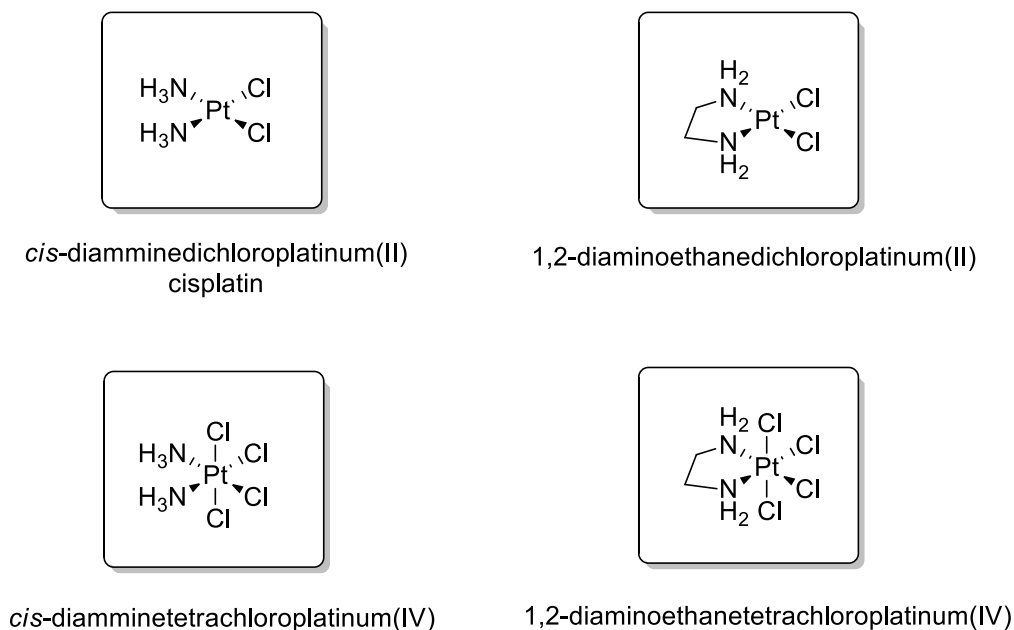


**Figure 2.3** The most efficacious compound tested by Rosenberg.

Although with some doubts around the use of heavy metals in medicine, clinical studies showed excellent results of cisplatin on various advanced stage tumors and, in 1979, the use of cisplatin was approved by the FDA for treating testicular and ovarian cancers. Nowadays cisplatin is still in use, in combination with other antitumor agents as therapy for lung, bladder, brain, cervical and esophageal cancers.<sup>[24]</sup>

The efficacy of cisplatin is related to its ability to interact with the DNA contained in the nucleus cells by inducing apoptosis, i.e. the programmed cell death. Apoptosis occurs when the cell reaches the natural end of its life cycle or when it is irreversibly damaged. When the cisplatin is inside the cell, the two *cis*-chloride ligands are replaced by two water molecules because of the lower chloride concentration in the intracellular medium (3-20 mM) compared to the extracellular fluid (~100 mM).<sup>[25]</sup> The aqua complex is the activated form and is able to enter the nucleus and interact with the DNA, as

shown in Figure 2.4, binding the nucleophilic centers of the purine bases of DNA, especially the N<sup>7</sup> atom of guanosine residue.

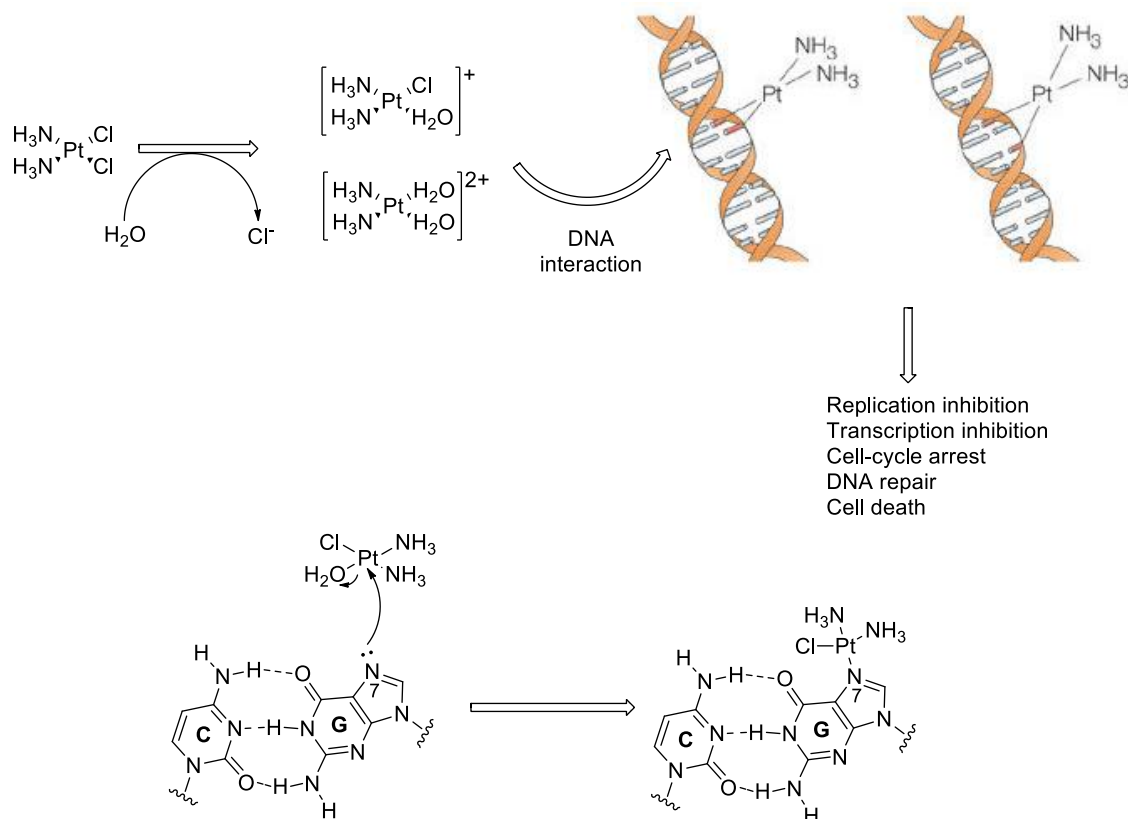


**Figure 2.4** Cisplatin interaction with DNA. Adapted from ref. 25.

Various types of adducts can be formed and they generally involve a second donor atom. Depending on the origin of the second donor atom, it is possible to have:

- a link with a protein or an interstrand crosslink (i.e. between two filaments) with another guanine;
- an intrastrand crosslink (i.e. within the same filament) between two adjacent guanine;
- an intrastrand crosslink by two guanine divided from a third nucleotide;
- an intrastrand crosslink between a guanine and an adenine.<sup>[26]</sup>

These crosslinks cause significant distortions in the DNA geometry, bending the double helix and hindering replication and transcription processes

inducing apoptotic cell death. Despite its enormous benefits, cisplatin also has considerable nephrotoxic effects and side effects for the nervous system and, moreover, many types of cancers develop mechanisms of resistance to it: this is a huge limitation of cisplatin-based chemotherapy.<sup>[27,28]</sup>

Although cisplatin treatment has had an ultimate impact on modern chemotherapy and is still the basis for the treatment of many solid tumours, scientific research scope is to find new active molecules that have null or minor side effects and that do not give rise to resistance problems.

In these 50 years, thousands of platinum complexes have been synthesized and tested as antitumor, and few of these, such as carboplatin,<sup>[29]</sup> oxaliplatin<sup>[30]</sup> and nedaplatin<sup>[31]</sup> are commercially available (Figure 2.5). Many of them were discontinued from clinical trials because of their lack of advantage over cisplatin.<sup>[32]</sup>

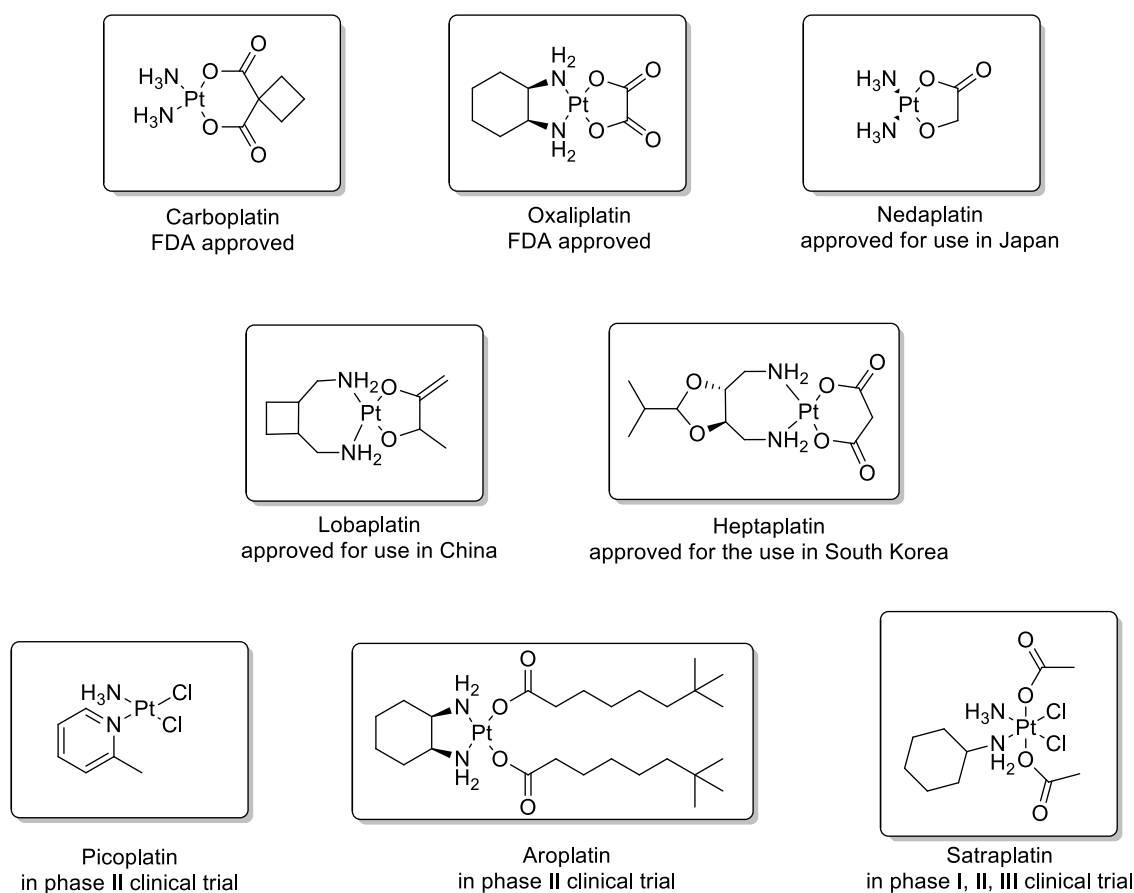


**Figure 2.5** Examples of platinum(II) and (IV) complexes commercially available or employed in clinical trials.



Research in the field of anticancer metal drugs is growing and is not only focused on platinum complexes. Many other complexes based on “d” block metals have been screened as anti-cancer. The transition metal complexes possess peculiar properties, mainly due to the metal core. They usually have more stable oxidation states; can give various ligand exchange reactions that allow the metal to interact with biological molecules and can also adopt various coordination geometries that give different shapes to the complexes. This modulability and the excellent performances of platinum complexes have led to the development of new metal drugs, many of which based on ruthenium. In fact, actually there are two compounds in clinical trials: NAMI-A<sup>[33]</sup> in phase I and KP1019<sup>[34]</sup> in phase II.

A large number of new metal complexes with good cytotoxic properties and very promising as anticancer agents were discovered and many of them are showing various modes of action.<sup>[35–38]</sup> Among the new non-platinum drugs especially gold compounds have received increased attention in recent years.

### 2.1.3 Gold complexes as anticancer drugs

#### 2.1.3.1 History of gold in medicine

The history of medical use of gold is not recent. Its pharmacological properties have been known since ancient times and the first uses in medical applications seem to date back to 2500 BC in China. In the Middle Ages, a colloidal gold solution, known *aurum potabile*, was considered a panacea and alchemists assured that its intake prevented aging.<sup>[39]</sup> It is striking how today, expensive anti-age creams, containing gold particles, are being sold, whose effectiveness is very controversial.<sup>[40,41]</sup> In 17<sup>th</sup> century, Nicholas Culpepper proposed the use of gold as an antidepressant and as a treatment for mental illness and, about two hundred years later, a mixture of gold chloride and sodium chloride, Na[AuCl<sub>4</sub>], was used in the treatment of syphilis.

The modern era of medical uses of gold started in 1890 with the discovery of the German scientist, Robert Koch, that potassium dicyanoaurate(I) was bacteriostatic to tuberculosis bacillus. As it was assumed that this bacillus was responsible for rheumatoid arthritis, in the 1960s it was thought to use gold therapy against various rheumatic diseases, such as psoriatic and juvenile arthritis, and also inflammatory skin diseases as urticarial and psoriasis.<sup>[39,42]</sup> It was soon discovered that gold therapy was ineffective against tuberculosis, but excellent results were obtained against rheumatoid arthritis and this gave birth to Chrysotherapy (from Greek *chrysos* = gold) in modern medicine. In 1972 there was a great discovery made by Sutton and Waltz who experimented the use of gold(I) phosphine complexes, orally bioavailable, for the treatment of rheumatoid arthritis.<sup>[43]</sup> The drug Auranofin was approved in 1985 by the Food and Drug Administration and is still used in the treatment of the most severe cases of rheumatoid arthritis, along with a series of similar derivatives shown in Figure 2.6, given by injection but with high nephrotoxicity and various side effects (Allochromin, Myochromin, Sanochromin, Solganol).<sup>[44]</sup>

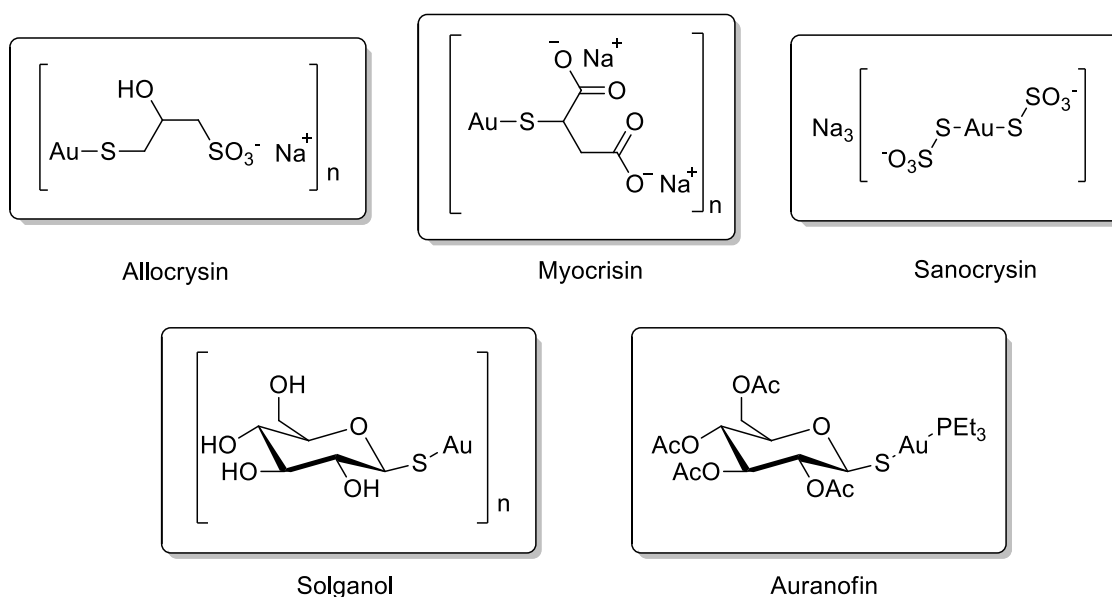


**Figure 2.6** Gold complexes used in rheumatoid arthritis therapy.

Studies on the mechanism of action of Auranofin have shown that the thiolate ligand is more labile than the phosphine ligand. The leading hypothesis is that the metabolism of the drug provides exchange reactions of thiolate ligand with carrier proteins that only carry the fragment Au-PR<sub>3</sub>.<sup>[45]</sup> Over the years, in patients treated with Auranofin therapy, it was possible to observe other drug properties, such as antihistamines. This discovery opened the way to new applications for this drug. Currently, Auranofin is no longer the drug of choice for rheumatoid arthritis because of its long-term side effects but tests are ongoing for its potential use in the treatment of HIV,<sup>[46,47]</sup> parasitic infections,<sup>[48,49]</sup> bacterial infections,<sup>[50,51]</sup> neurodegenerative disorders such as Parkinson's disease and Alzheimer's<sup>[52,53]</sup> and some cancers.<sup>[54-56]</sup>

With the discovery of Auranofin, and its many potential uses, the golden era in medicinal chemistry began.

#### 2.1.3.2 Biological targets of Auranofin and related gold complexes

Unlike platinum complexes, which interact primarily with DNA, gold complexes, due to the affinity of gold with thiols, seem to target some enzymes especially those rich in cysteine. Many thiol-rich proteins, such as Thioredoxin reductases (TrxR), glutathione reductase (GR) and cysteine proteases, are overexpressed in tumour cells and this may be the reason for the efficacy of such complexes.<sup>[49,57]</sup>

TrxR and GR, which are responsible for the reduction of thioredoxin (Trx) and glutathione disulfide respectively, are enzymes belonging to the family of flavoproteins. The TrxR are homodimers, each monomer contains a flavin adenine dinucleotide (FAD), that is a redox cofactor, a NADPH (the reduced form of nicotinamide adenine dinucleotide phosphate) binding domain, and an active site containing a redox-active disulfide bond.<sup>[58]</sup> The main isoforms of these proteins in human cells are TrxR1 present in cytosol and TrxR2 in mitochondria and all the thioredoxin system, that consists of thioredoxin,

NADPH and TrxR, plays a key role in the redox regulation of DNA synthesis, transcription, cell growth, etc...<sup>[59]</sup> Thioredoxin acts as an electron donor species for a large number of enzymes, including ribonucleotide reductase, which plays an important role in DNA synthesis. Many transcription factors have been identified, whose activity requires thioredoxin to be reduced, so that they can bind DNA effectively. A high expression of thioredoxin is associated with the aggressive growth of tumour cells, the inhibition of apoptosis, and the decrease in the probability of survival of cancer patients. In addition, high concentrations of thioredoxin reductase can increase cisplatin resistance by tumour cells.<sup>[60,61]</sup> TrxR inhibition significantly increases the concentration of ROS (reactive oxygenated species) within mitochondria, resulting in cell death, which can explain, at least partially, the cytotoxic action of some gold complexes.<sup>[62]</sup> TrxR is a selenoenzyme because a selenocysteine is present in the active site Gly-Cys-Sec-Gly responsible for the redox mode of action of the enzyme. It is well known that gold, in particular gold(I), is a “soft” Lewis acid and it has an affinity for “soft” donors such as the selenolate groups. The formation of a covalent bond between the electrophilic gold centre and the nucleophilic cysteine or selenocysteine residue of the active site of the enzyme lead to its inhibition. Certain crystal structures of gold-enzyme adducts support this thesis. In particular, Becker and co-workers reported the crystal structure of an Au(I)-hGR adduct where the gold source is a gold phosphole, in particular GoPI ([1-phenyl-2,5-di(2-pyridyl)phosphole]AuCl) and human disulfide reductase (hGR), an enzyme containing cysteines in its active site. The crystalline structure shows a gold ion coordinated in a linear way to Cys58 and Cys63 and the Cys284 acting as a GoPi ligand instead of chloride (Figure 2.7a).<sup>[57]</sup> From the crystals obtained after the reaction of the Auranofin with thioredoxin-glutathione reductase (TGR), a parasite enzyme similar to TrxR, triethylphosphine and thioglucose ligands were not found but it was possible to observe two Au<sup>+</sup> ions linearly coordinated to two cysteines, in particular

their position are between Cys154 and Cys159 and Cys520 and Cys574 (Figure 2.7b).<sup>[63]</sup> Instead, in the adduct Auranofin-TR (trypanothione reductase, an enzyme belonging to the family of disulphide oxidoreductase) the Au<sup>+</sup> ion coordinate two cysteines and a chloride.<sup>[49]</sup> These crystal structures confirm that gold manages to coordinate the cysteines of the active sites of such enzymes inhibiting their activity.<sup>[64]</sup>

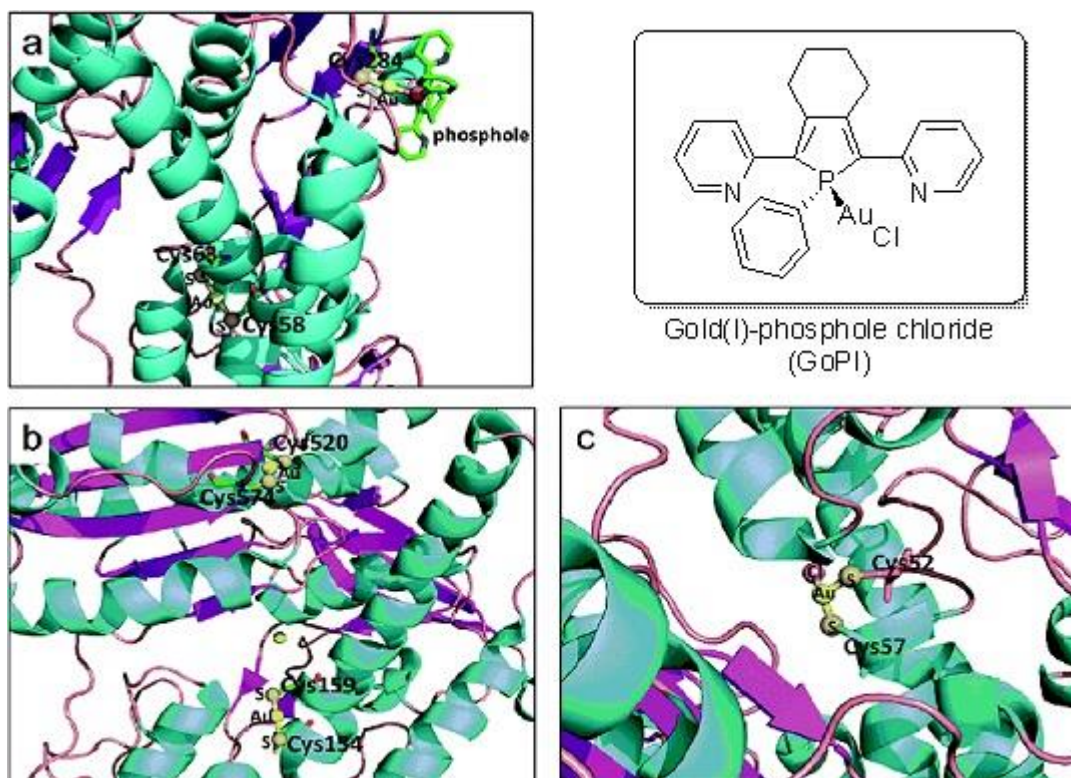


**Figure 2.7** Gold(I)-protein adducts: a) Interactions between GoPI, molecular structure on the right, and glutathione reductase active site; b) Au(I)-TGR adduct; c) Au(I)-TR adduct. Adapted from ref. [64].

The inhibition of mitochondrial TrxR prevents Trx reduction and hydrogen peroxidase, formed during the respiration chain, accumulates in mitochondria. Oxidized Trx and H<sub>2</sub>O<sub>2</sub> act on many factors within the mitochondria and, in particular, increase the permeability of the membrane, this causes the release of apoptotic factors that leads to cell death.<sup>[65]</sup>

The interaction of gold with TrxR, and its analogues, does not seem to be the only mechanism of action. It is reported in literature that Auranofin can

inhibit the activity of cathepsin K and S, which are cysteine proteases, always by coordinating the sulfur of a cysteine in the active site.<sup>[66]</sup> It can be thought that, given the high affinity of gold for sulfur and selenium, it can interact with other proteins rich in thiols and selenols, in fact it has been reported that gold(I) complexes inhibit the action of glutathione peroxidase (GPx)<sup>[67]</sup> and iodothyronine deiodinase (ID).<sup>[68]</sup>

In some cases adducts in which gold does not bind cysteines have been observed but the gold(I) ion is coordinated by the histidine nitrogen as in the structure, reported by Sadler, Au(I)-Cyp3 (Cyclophilin 3, a protein having four cysteine residues). In this structure gold is not bound to any of the four cysteines, but there is an N<sub>His</sub>-Au-PEt bond and this, however, leads to the inhibition of the enzyme.<sup>[69]</sup> At present, it has not been possible to isolate any adduct between gold in oxidation state +3 and proteins already mentioned above, probably because Au(III) is unstable in the reaction environment and is reduced to Au(I).<sup>[70,71]</sup> In any case, the cytotoxicity of the gold(III) complexes is known and, recently, some targets have been identified: Aquaporin3,<sup>[72]</sup> a membrane protein, and a deubiquitase,<sup>[73]</sup> being the interaction always due to the binding of the metal ion with the cysteinyl thiols.

A unique mode of action for gold complexes is not plausible, it can change depending on the complex properties (redox properties, ligands, geometry, lipophilicity, etc ...).

In general, from the results obtained, the following structure/toxicity correlations can be drawn: oxidation state, nature of ligands, and coordination geometry are of primary importance in determining the tendency to participate in the ligand exchange reactions with biological substrates and in solubility, stability and toxicity. The activities and toxicity of complexes depend strongly on their hydrophilic/lipophilic character that can be adequately balanced, so as to have sufficient solubility in a

physiological environment and lipophilicity such as to allow the molecule to enter the inside cells (up-take).<sup>[74]</sup>

The “fine-tuning” of the properties, just mentioned, is extremely important in order to improve biological activity and reduce side effects.

#### 2.1.3.3 Gold(I) and gold(III) as anticancer drugs: state of the art

At present, the antitumour properties of gold complexes continue to rise great interest, since the first studies on their properties dating back to the '80s. Initially, tests were carried out on Auranofin and its analogues that showed a potent *in vitro* activity with the half maximal inhibitory concentration ( $IC_{50}$ ) values in the range of 1-10 $\mu$ M, but the low *in vivo* activity precluded development as antineoplastic agents.

The  $IC_{50}$  is a measure of the inhibition power of a substance on a specific biological or biochemical function. According to the FDA, it represents the concentration of a drug that is required for 50% inhibition *in vitro*. The values are typically expressed as molar concentration.

The high toxicity that some gold(I) and gold(III) complexes have shown against several tumour cell lines inspired the development of a number of structurally different organometallic species with chemical permutations both at the metal oxidation state and at the organic counterpart.

Having a coordination geometry similar to that of platinum(II), gold(III) complexes aroused much interest as possible antitumour, but because of their oxidizing potential and their high hydrolysis speed, usually they are more toxic and less stable under physiological conditions than gold(I) complexes. This is why their potential pharmacological activity was initially neglected until the second half of the 1990s. Gold(III) is coordinated preferentially by ligands with nitrogen donors. Using appropriate ligands such as nitrogen chelating species including  $N^{\wedge}N$ ,  $N^{\wedge}N^{\wedge}N$ ,  $C^{\wedge}N$ ,  $C^{\wedge}N^{\wedge}N$ ,  $C^{\wedge}N^{\wedge}C$ , porphyrin and dithiocarbamate, it is possible to decrease the reduction potential and

stabilize the metal center, thus avoiding its reduction to [Au(I)] or [Au(0)] before reaching the desired site and express all its toxicity.

The antitumor properties of some of these complexes, of which representative examples are shown in Figure 2.8, are very encouraging in fact a gold(III) porphyrin complex (gold-1a in Figure 2.8) has shown to be very stable in the reducing environment and to have *in vitro* cytotoxicity at micromolar or nanomolar level in some cell lines. The tetrarylporphyrin complex is effective also in cisplatin-resistant cancer cell lines this means that the mechanism of action is different from that of the cisplatin.<sup>[75]</sup>

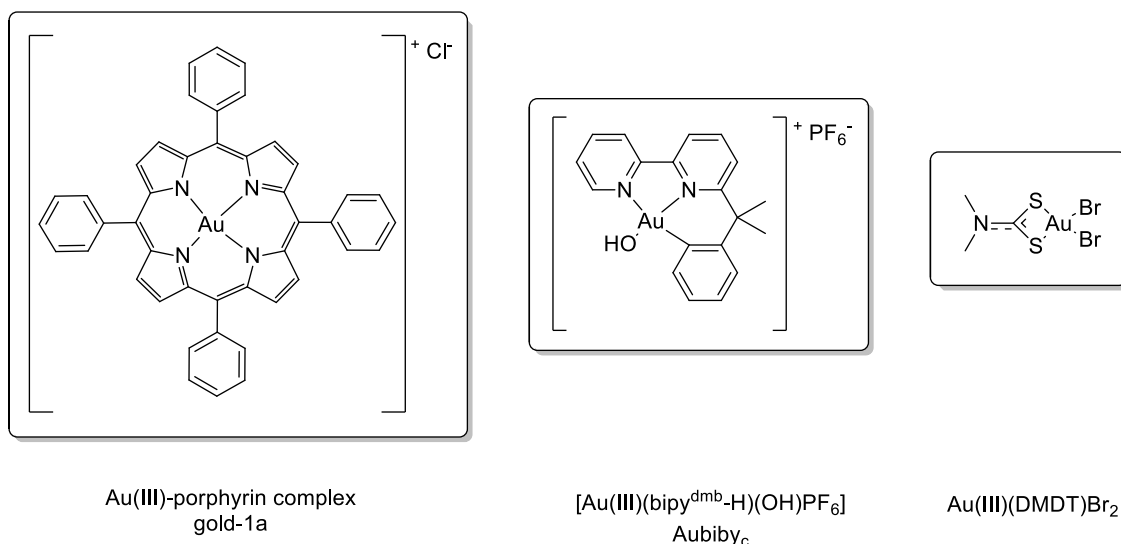


**Figure 2.8** Representative examples of gold(III)-complexes as anticancer agents.

Aubipy<sub>c</sub> ([Au(bipy<sup>dmb</sup>-H)(OH)PF<sub>6</sub>]) is also a promising anticancer drug, in fact it is stable in the physiological condition and the hydroxyl group is the preferred site for the ligand exchange reaction and for protein binding. Aubipy<sub>c</sub> was found to be cytotoxic towards the human ovarian cancer cell line A2780 and proteomic study demonstrates that it can disrupt mitochondrial function having, among its targets, several glycolytic enzymes.<sup>[76]</sup>

Various dithiocarbamate gold(III) complexes were developed because the Au-S bonds can stabilize the Au<sup>3+</sup> ion; particularly, Au(III)(DMDT)Br<sub>2</sub> and



its analogues are able to trigger cell death, to induce ROS generation and to irreversibly inhibit TrxR activity.<sup>[77]</sup>

Due to the development of chrysotherapy, mainly based on gold(I), and also to their thermodynamic stability, the research on gold complexes as anticancer drugs has focused largely on complexes with gold(I).

In particular, the organic frameworks constituting the prodrug system proved to be actively involved in determining the overall activity of the species also because by modulating the substituents it is possible to confer greater hydrophilicity or lipophilicity on the whole, thereby improving the potentialities as a carrier for the metallic center.<sup>[78]</sup> Ligand exchange is the most important reaction for gold(I) complexes in a biological environment, for which such drugs are better defined as pro-drugs: the active species is formed in situ and the originally coordinated ligand has the only function to enhance reactivity and selectivity in drug action. In this direction, soft ligands such as phosphine, thiols, or  $\sigma$ -donating nitrogen heterocyclic carbenes (NHCs) have been employed in the synthesis of new gold complexes with the aim of enhance their cytotoxicity. In Figure 2.9 some leading examples of this class of compounds are shown.

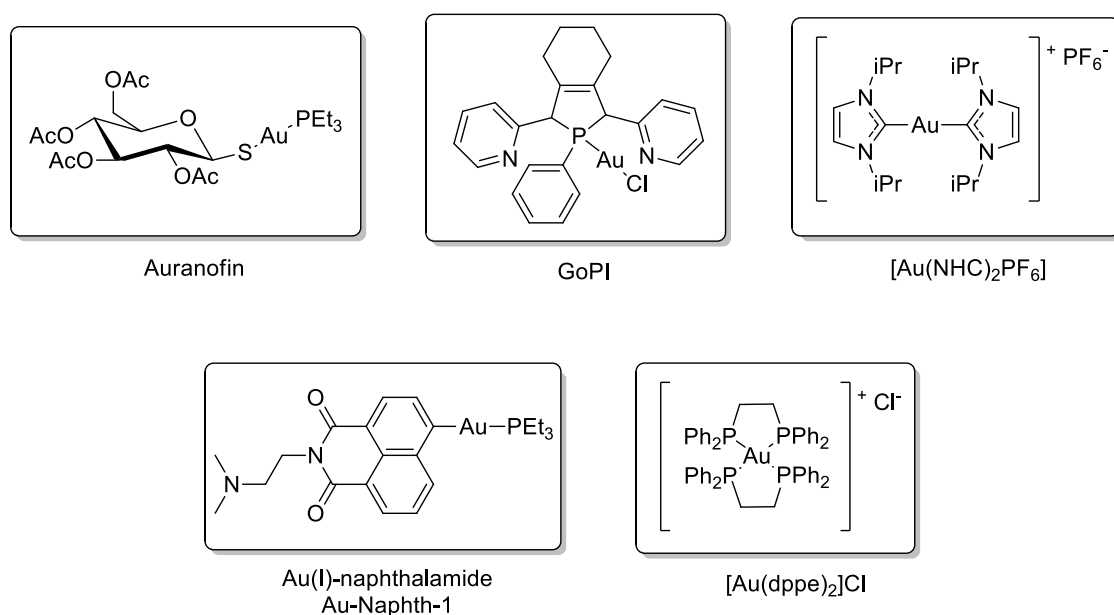


**Figure 2.9** Representative examples of gold(I)-complexes as anticancer agents.

As mentioned above Auranofin is the precursor of this family of compounds and it has long been known to interact with TrxR leading to cancer cell death as well as GoPI that is a potent inhibitors of TrxR and glutathione reductase (Figure 2.7). GoPI is a phosphole complex and its strong TrxR inhibitory potential is proven by  $IC_{50}$  values in the micromolar range in glioblastoma, an aggressive cancer.<sup>[79]</sup> Because the carbohydrate moiety of Auranofin was supposedly more relevant for the biodistribution of the compound than for its cytotoxic properties, Ott *et al.* replaced the thiocarbohydrate with a thionaphthalimide ligand which was proved to be bioactive, in fact it displayed significant cell growth inhibiting properties.<sup>[80]</sup> The studies on the complex Au-Naphth-1 showed a strong antiproliferative effects in MCF-7 breast cancer cells and in HT-29 colon carcinoma cells. The experiments confirmed an elevate uptake in the nuclei compared to non-naphthalimide  $Et_3PAuCl$  and the presence of multiple biological targets, the most relevant are nuclear (DNA) and mitochondrial (TrxR) macromolecules. Then Ott's group synthesized a series of complexes replacing the triethylphosphine moiety with other aliphatic and aromatic phosphine and also with carbene with the aim of enhancing the pharmacological properties of this class of complexes.<sup>[81,82]</sup>

Au(I) complexes with *N*-heterocyclic carbenes (NHCs) ligands are often used in catalytic application because of the strong electron-donating properties of the ligand, but, recently, their biological functions have been extensively investigated.<sup>[83]</sup> NHCs ligands are similar to the phosphine ones and their lipophilicity is easily tunable modifying the functional groups. Berners-Price and coworkers reported the synthesis and the biological activity of a family of homoleptic cationic bis-NHC gold(I) complexes (one member is depicted in Figure 2.9) that showed promising cytotoxic properties accompanied by interesting mitochondrial membrane permeabilization depending on the lipophylicity of the complex.<sup>[84,85]</sup>

Biological studies have shown that the cationic derivative inhibits the growth of tumour cells but not of healthy ones. It has also been observed that they are inhibitors of thioredoxin reductase and tyrosine phosphatase giving ligand exchange reactions with thiol and selenol groups.<sup>[86]</sup>

Together with carbenes, gold(I)-phosphine complexes are one of most studied classes of complex not only for their catalytic properties but also for the biological one. They can be divided into two classes: neutral linear two-coordinated complexes, such as  $\text{PPh}_3\text{AuCl}$ , and cationic tetra-coordinated bis-chelated diphosphine derivatives of  $[\text{Au}(\text{I})]$  as  $[\text{Au}(\text{dppe})_2]\text{Cl}$  (dppe=bis(diphenylphosphinoethane), shown in Figure 2.9.

Although studies suggest that the mechanism of anti-tumour activity of the two classes is different, both cause a mitochondrial disfunction leading to cell death.<sup>[87]</sup> The tetrahedric  $[\text{Au}(\text{dppe})_2]\text{Cl}$  complex was first tested by Mirabelli and coworkers in the 1980s and found to be more stable and less reactive than the two-coordinated phosphinic gold(I) complexes. *In vitro* observed cytotoxicity has been confirmed by good results obtained *in vivo*, especially against a range of solid tumours and leukemia in mice. However, preclinical toxicological studies have shown severe cardiotoxic effects and toxicity to liver and lung in rabbits and dogs.<sup>[88]</sup>

This increased activity is probably due to the greater lipophilicity conferred by the ligand. Studies on  $[\text{Au}(\text{dppe})_2]\text{Cl}$  and some analogues revealed that the counter anion effect is not relevant<sup>[89]</sup> but there is a strong relationship between lipophilicity, cellular uptake and toxicity. The lipophilic cation can pass through the cellular membrane, accumulate into the mitochondria and causing to mitochondrial dysfunction,<sup>[90]</sup> but these complexes can also induce DNA protein cross-links and DNA strand breaks in cells.<sup>[91]</sup> To reduce the toxicity, a less lipophilic 2-pyridyl analogues  $[\text{Au}(\text{d2pype})_2]\text{Cl}$  (d2pype= 1,2bis(di-2-pyridylphosphino)ethane) was developed and was found to be active in colon tumours in mice.<sup>[88]</sup> An analogue complex with

a propyl-bridged phosphine,  $[\text{Au}(\text{d2pypp})_2]\text{Cl}$  (d2pypp=1,2bis(di-2-pyridylphosphino) propane), revealed a strong TrxR inhibition and a high selective cytotoxicity towards breast cancer cell but not to normal cells.<sup>[92]</sup> Tuning the lipophilicity and the length of the alkane bridge is a crucial point in the design of new anticancer metal drugs.

The research on biological properties of gold(I)-alkynyl complexes is quite scarce but in the last years some progress has been made. Mohr and collaborators presented a series of complexes containing derivatives already known to be antimalarial drugs. These complexes showed encouraging antitumor activity on various cell lines. In particular the complex, depicted in Figure 2.10, showed  $\text{IC}_{50}$  values of magnitude similar to those of cisplatin in the broadly chemosensitive ovarian cancer cell line CH1 and in the colon cancer cell line SW480.<sup>[93]</sup>

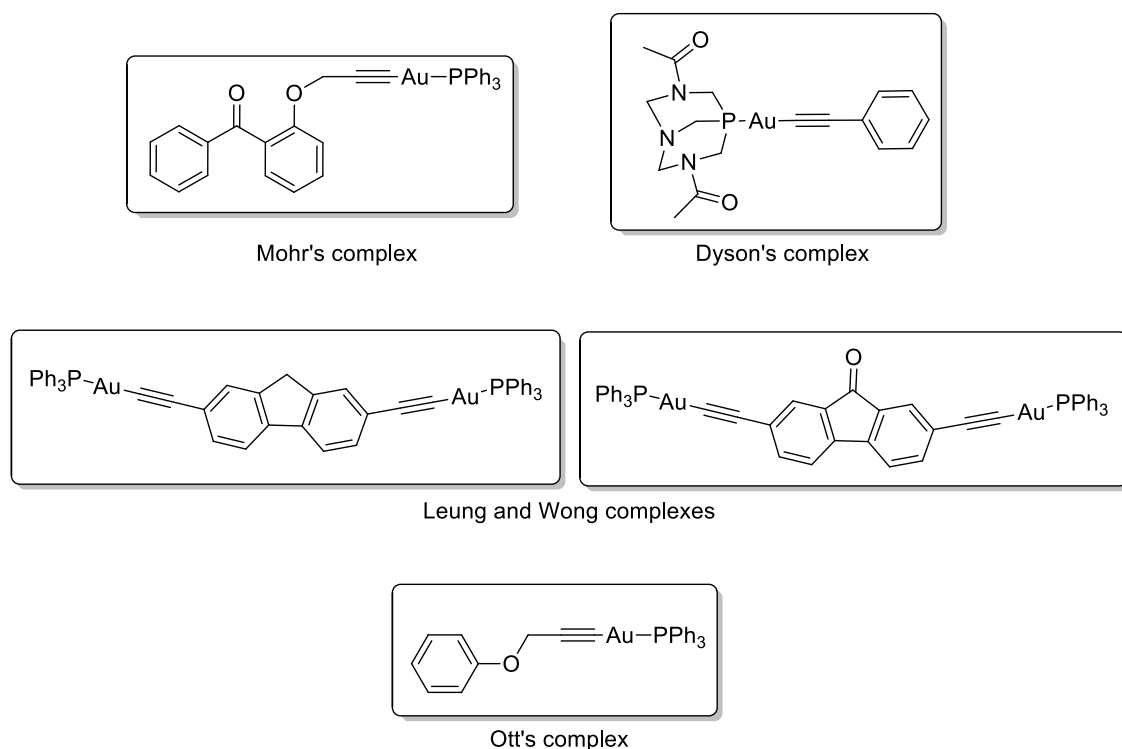


**Figure 2.10** Representative examples of alkynyl gold(I)-complexes as anticancer agents. Another interesting work, published by Dyson, has shown that a series of gold(I) alkynyl complexes containing water-soluble phosphane ligands, one example is depicted in Figure 2.10, have an antiproliferative activity against

a cisplatin sensitive and a cisplatin-resistant ovarian cancer cells. These data suggest a different mechanism of action of this class of complexes respect to cisplatin.<sup>[94]</sup> Encouraging results were also reported with diethynylfluorene derivatives of gold(I), (Figure 2.10) by Leung and Wong. The species containing a fluorenone group was shown to have a good biological activity *in vitro* and *in vivo*. The generation of ROS from the carbonyl group of the central ligand spacer is believed to be essential for its cytotoxicity in fact the change of this carbonyl group with a CH<sub>2</sub> unit is very negative for its toxicity. Very recently, Ott and coworkers documented on the synthesis, characterization and pharmacological investigation of a new family of mononuclear [alkynyl(triphenylphosphine)gold(I)] complexes of general structure PPh<sub>3</sub>Au-C≡CCH<sub>2</sub>XR (X: O, N) with important antiproliferative activity (micromolar range) in breast adenocarcinoma and colon carcinoma cells, one example is shown in Figure 2.10.<sup>[95]</sup> Shortly after, the same team described the remarkable biological properties of binuclear gold(I) alkynyl analogs featuring bidentate phosphines as tethering units.<sup>[96]</sup> These studies emphasized also thioredoxin reductase (TrxR) as a plausible biological target of the pharmacologically active gold(I) species.<sup>[62,97]</sup>

The propargylic sidearm proved to contribute substantially to the overall pharmacological activity of the title species, therefore, careful modulation of this unit could lead to interesting perspectives in developing more selective and potent candidates for anticancer drugs.

In this regard, recent investigation dealing with the documentation of novel [alkynyl(triphenylphosphine)-gold(I)] complexes comprising relatively unexplored propargylic amine derivatives as organic ligands are presented. The possibility to create chemical diversity by means of readily accessible propargylic amine derivatives enabled a survey of several structural aspects such as nitrogen basicity and electronic/steric factors.

## 2.2 Results and discussion

### 2.2.1 Synthesis and characterization

In order to assess the effective role of the alkynyl sidearm on the biological spectrum of the gold species, a range of propargylic mono- and diamine derivatives **2a-f** and mono/binuclear phosphinogold(I) complexes (*i.e.*  $\text{PPh}_3\text{AuCl}$  **1a** and  $[\text{PPh}_2(\text{CH}_2)_2\text{PPh}_2](\text{AuCl})_2$  **1b**), were elected as key building blocks (Figure 2.11).<sup>[98]</sup>

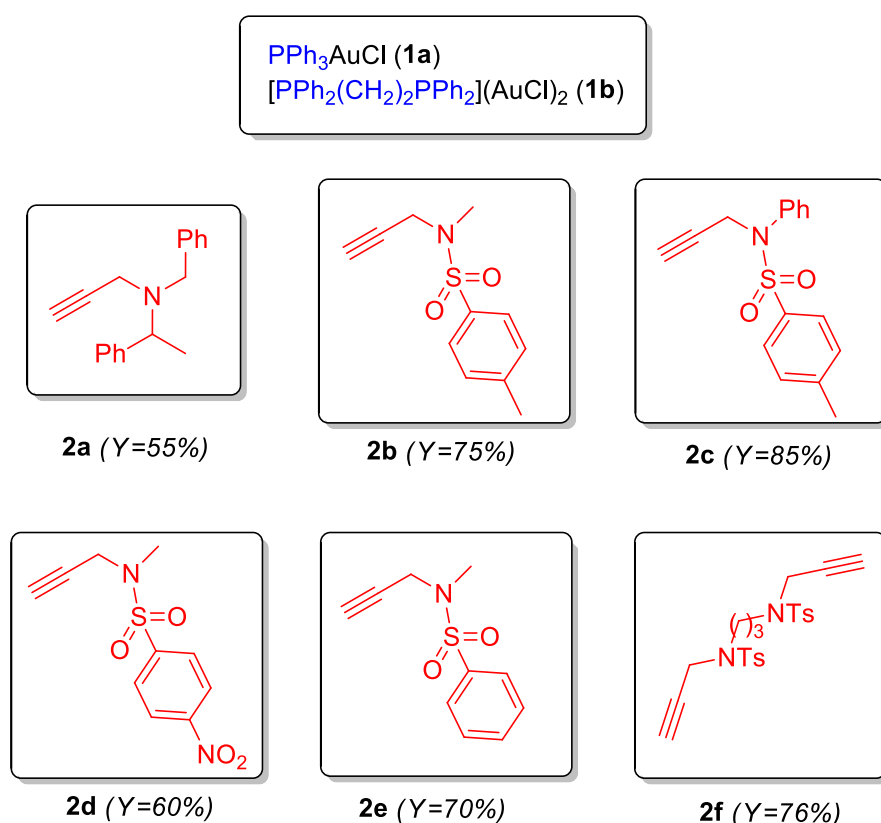


**Figure 2.11** Metal and organic fragments employed in the present investigation. In brackets the isolated yield.

In particular, by reacting an equimolar amount of gold(I)chloride complexes **1a,b** and the desired terminal alkyne under basic conditions (KOH, MeOH/EtOH), the corresponding alkynyl-gold complexes **3** were isolated in moderate to good yields (60-92%). Further purification was mostly carried out either by recrystallization or through flash chromatography on silica gel (Figure 2.12).

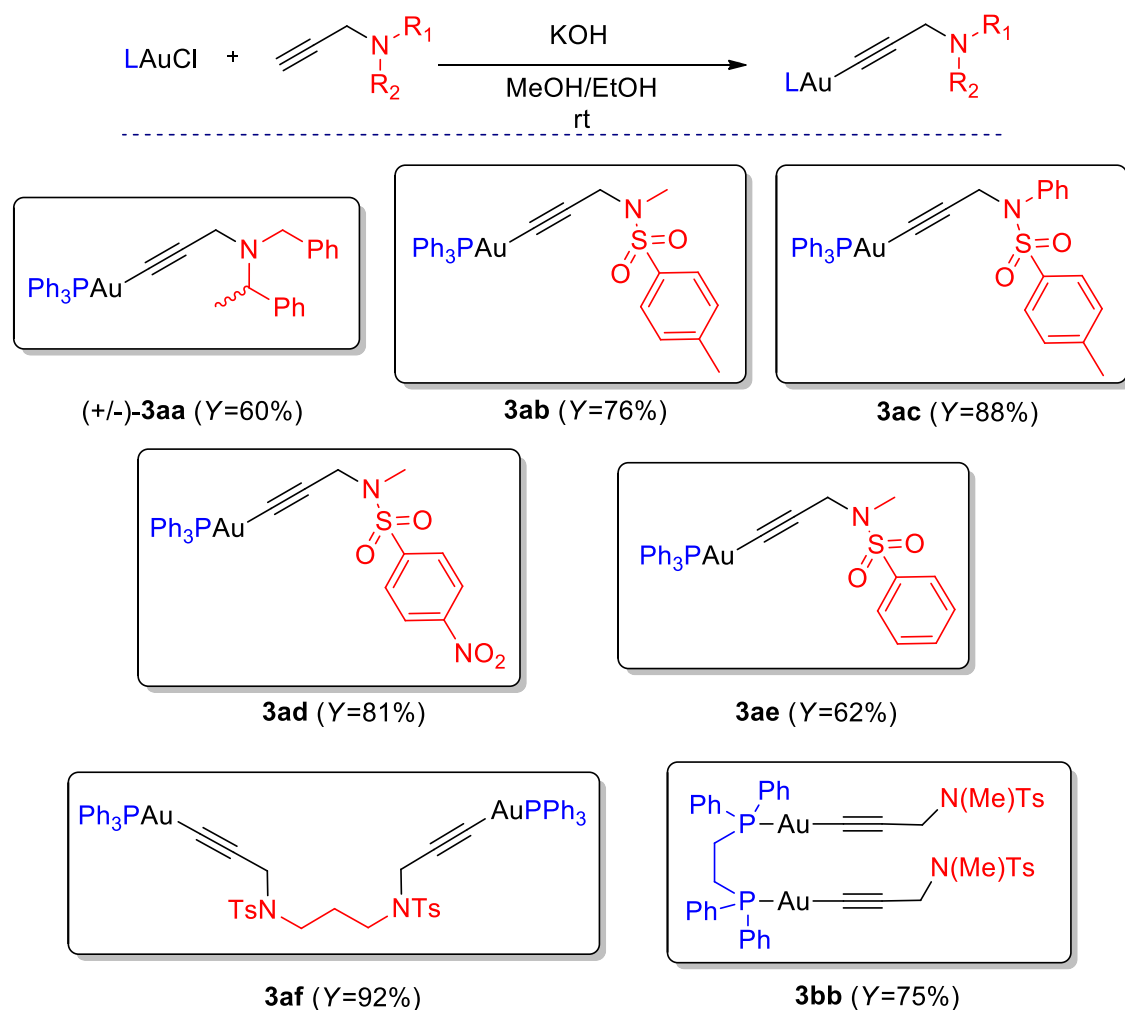


**Figure 2.12** Library of [gold(I)-alkynyl] complexes synthesized and tested in the present work. In brackets the isolated yield.

A ligand exchange mechanism takes place: phosphine-gold(I) chloride loses the  $\text{Cl}^-$  and acquires the alkynic ligand, maintaining a linear geometry. The interaction of the gold centre with the  $\pi$  electrons of the  $\text{C}\equiv\text{C}$  bond is exploited to favour the deprotonation of the acetylenic proton by the base. The acetylide that is formed can then donate electrons to the metal center, building a C-Au covalent bond as shown in Figure 2.13.

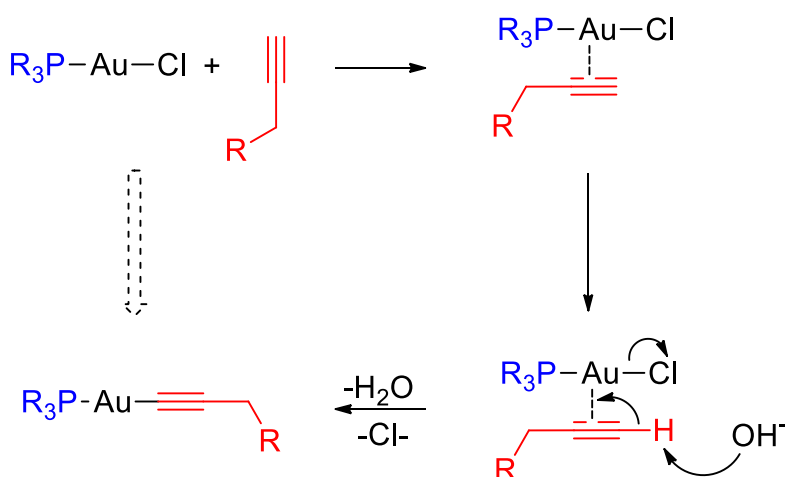


**Figure 2.13** Mechanism of formation of [gold(I)-alkynyl] complexes.

Complexes **3** were obtained as white (pale brown in the case of **3ad**) air stable solids featuring a remarkable solubility in common organic solvents. They were fully characterized both in solution (NMR, IR, LC-MS) and solid state (**3ab** and **3ac**).

In particular, NMR spectroscopy ( $CDCl_3$ , rt) resulted particularly diagnostic in monitoring the reaction course. As a matter of fact, the formation of adducts **3** caused the disappearance of the acetylenic C-H of the alkyne congeners ( $^1H$ -NMR  $\delta = 2.0$ - $2.2$  ppm), with the concomitant deshielding ( $\approx 0.15$  ppm) of the propargylic methylene. Additionally, a marked downshielding of the  $^{31}P$ -NMR signals in the final compounds **3a-f** (39-42 ppm) occurred with respect to the congener **1a** (32.9 ppm). On the contrary, the  $^{31}P$ -NMR spectrum of the binuclear adduct **3bb** displayed a shielded singlet ( $\delta = 21.8$  ppm) if compared with **1b** ( $\delta = 31.5$  ppm). The presence of a single peak accounted for the formation of the  $C_2$ -symmetric adduct depicted in Figure 2.12.

### 2.2.2 Single crystal X-ray diffraction of complexes **3ab** and **3ac**

Solid state structure investigation on complexes **3ab** and **3ac** was also carried out. Crystals suitable for X-ray diffraction were formed through slow



evaporation of AcOEt solutions of the corresponding species, The resulting molecular structures of **3ab** and **3ac** are reported in Figure 2.14.

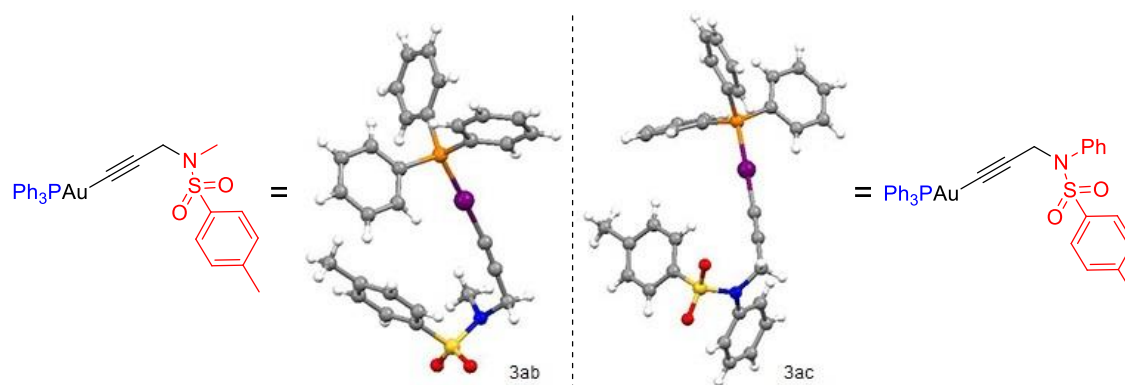


**Figure 2.14** Molecular structure of **3ab** (sx) and **3ac** (dx).

As expected for gold(I) complexes, Au adopts an almost linear coordination and the P-Au-C bond angles are very close to the ideal value of  $180^\circ$  [ $176.5(2)$  and  $178.9(2)^\circ$  for **3ab** and **3ac**, respectively]. The  $C\equiv C$  bond lengths of  $1.183(7)$  and  $1.194(7)$  Å are typical of terminal alkynyl gold(I) complexes.

The crystal packing of **3ab** is dominated by weak non classical intermolecular  $C-H\cdots O$  hydrogen bonds (Figure 2.15) between the oxygen atoms of sulfonamide and the hydrogen atoms of phenyl rings of phosphine, whereas in **3ac** two phosphine phenyl rings in each molecule establish intermolecular  $\pi-\pi$  interactions with their symmetry equivalent adjacent phenyl ligands generating infinite zig-zag chains along the  $c$  axis as shown in Figure 2.16.

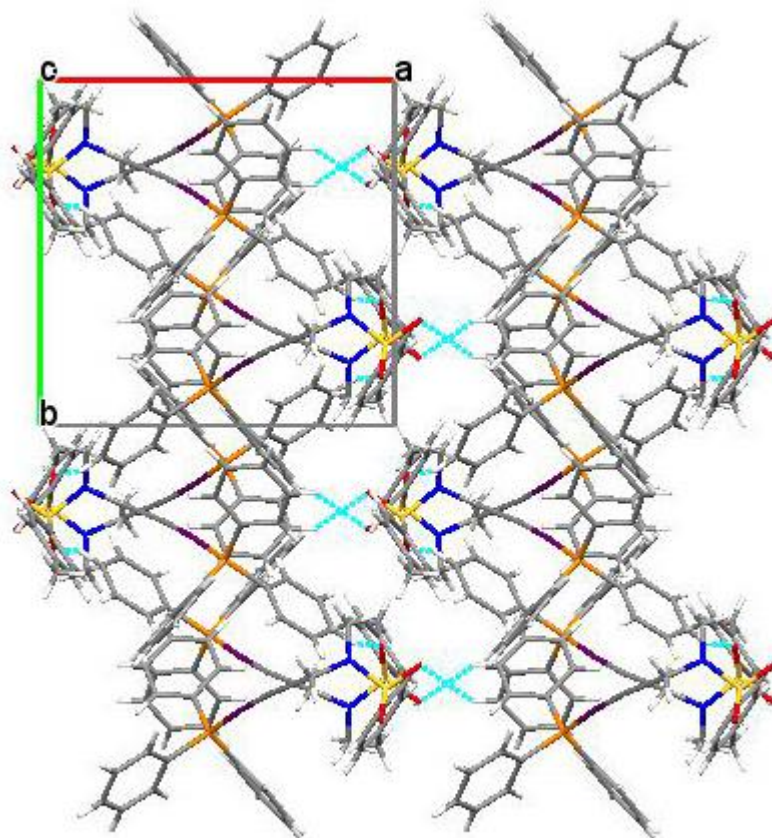


**Figure 2.15** View along the *c* axis of the crystal packing of **3ab** (pale blue dotted lines show non classical intermolecular C-H $\cdots$ O hydrogen bonds).

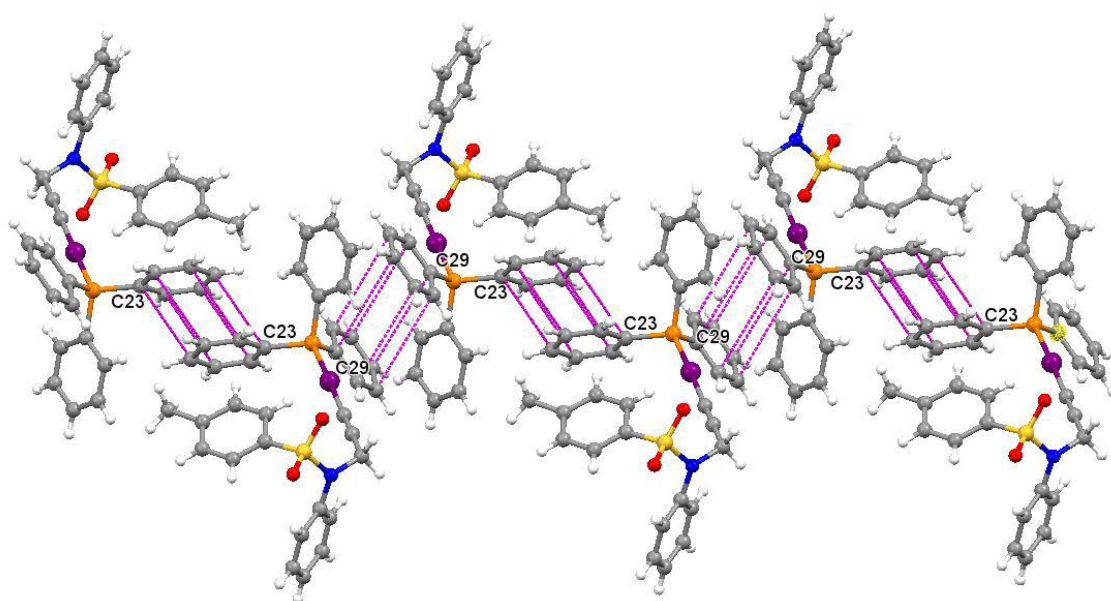


**Figure 2.16** View down the *b* axis of the crystal packing of **3ac**. Violet dotted lines show  $\pi$ - $\pi$  interactions involving two symmetry equivalent phosphine phenyl rings.

### 2.2.3 Biology

In collaboration with the group of Professor Natalia Calonghi from the Department of Pharmacy and Biotechnology of Alma Mater Studiorum – University of Bologna, the biological activity of the alkynyl-gold(I) complexes has been studied. The following experiments were performed by Dr Christian Bergamini.

Cell lines included in the evaluation of toxicity profiles were malignant HT29, IGROV1, and HL60, and a non-malignant human epithelial intestinal cell line I407. HT-29 is a human colorectal adenocarcinoma cell line, colorectal cancer is a cancer originating from the epithelial cells lining the colon or rectum of the gastrointestinal tract.<sup>[99,100]</sup> IGROV1 cell line is another adenocarcinoma, a neoplasia of epithelial tissue, of the human ovary,<sup>[101]</sup> instead the HL-60 are human promyelocytic leukemia cells, promyelocytic leukemia is a cancer of the white blood cells.<sup>[102]</sup>

The determination of the IC<sub>50</sub> was performed with the MTT assay. The MTT assay is a colorimetric assay for measuring the activity of enzymes in reducing MTT (3-(4,5-dimethylthiazol-2-yl)-2,5-diphenyltetrazolium bromide) to formazan ((Z,E)-5-(4,5-dimethylthiazol-2-yl)-1,3-diphenylformazan). The reaction scheme is depicted in Figure 2.17.

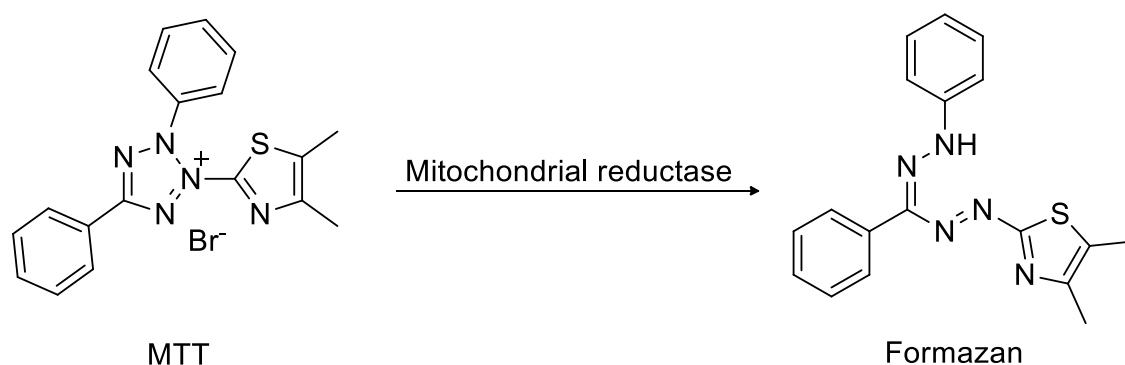


**Figure 2.17** Reaction scheme of MTT reduction.

The test uses water soluble yellow tetrazolium salt MTT which is reduced to formazan, insoluble and blue-violet in color. The reduction process is due to

the mitochondrial succinate dehydrogenase enzyme. This process can only take place if the cells have a metabolic activity. On the contrary, if the cells are dead, they do not show any metabolic activity and consequently the salts are not reduced and the species remains yellow.<sup>[103]</sup>

IC<sub>50</sub> values of the drugs were calculated using Prisma, fitted by means of sigmoidal fit and listed in Table 2.1.

**Table 2.1** IC<sub>50</sub> of gold compounds in different cell lines after 24 hours of treatment (μM)<sup>a</sup>

Compound	HT29	IGROV1	HL60	I407
Auranofin	3.3 (1.8-6)	2.5 (0.4-15)	0.7 (0.3-1.6)	1.6 (0.9-2.8)
(+/-)-3aa	>100	20 (10.06-39.20)	19.0 (7.43-50.69)	15.0 (9.14-24.65)
3ab	7.9 (5.39-11.59)	5.3 (3.87-7.43)	3.3 (1.62-6.88)	1.7 (0.61-4.99)
3ac	>100	5.5 (4.69-6.69)	2.7 (1.19-6.18)	9.6 (7.26-12.63)
3ad	11.0 (8.97-15.01)	6.5 (4.12-10.31)	6.3 (5.05-7.94)	8.0 (6.73-9.66)
3ae	>100	10.0 (6.40-17.84)	9.0 (6.55-12.83)	>100
3af	>100	7.7 (6.26-9.48)	>100	>100
3bb	>100	>100	0.8 (0.28-2.40)	>100

<sup>a</sup> 95% confidence intervals are reported in the brackets

From the data collected in Table 2.1 some preliminary conclusions can be drawn. Within the portfolio of gold complexes in hand, **3ab** was the more effective in inhibiting cell growth in all panel cell lines, in a similar way to Auranofin. Additionally, compound **3ad** showed some levels of cytotoxicity towards all the cell lines but the corresponding IC<sub>50</sub> values were constantly higher than that **3ab**. On the contrary, (+/-)-**3aa**, **3ac**, **3bb**, **3ae** and **3af** proved competent only on a few of the screened cell lines. In this scenario,

some peculiarities were also highlighted. In particular, complexes **3af** and **3bb** showed significant toxicity for IGROV1 and HL60 cells, respectively. Moreover, it is important to stress the lack of toxicity toward non-cancer cell lines showed by the compounds **3bb**, **3ae** and **3af**. PPh<sub>3</sub> and **2b** were tested in the cell lines IGROV1 and HT-29. The results proved that the alkyne is inactive in both cases and the PPh<sub>3</sub> furnished the values of 47  $\mu$ M in IGROV1 cell lines and 39  $\mu$ M on HT-29. These values are higher than the IC<sub>50</sub> values of the complexes, except for **3af** that is inactive on HL60.

These bio-divergences clearly emphasised the role played by the nitrogen substitutions in modulating the overall pharmacological properties of the gold complexes.

As mentioned above, inhibition of the TrxR is considered to be an important mechanism of bioactivity of gold(I) species. In particular Auranofin shows an high inhibitory effect both on cytosolic (Trx1) and mitochondrial (TrxR2) isoforms of the enzyme.<sup>[104]</sup> Therefore, the potential of gold complexes to inhibit TrxR was studied on commercially available TrxR using the 2,6-dichloroindophenol (DCIP) reduction assay.<sup>[105]</sup> DCIP is a redox dye in fact when oxidized, it is blue with a maximal absorption at 600 nm; when reduced it is colorless, Figure 2. 18.

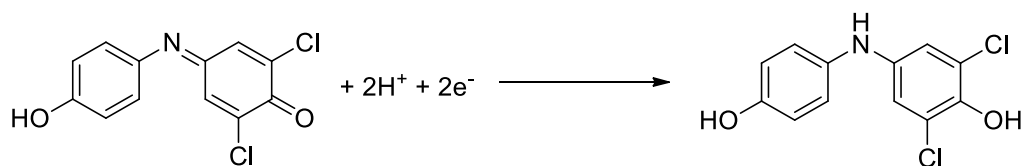


**Figure 2. 18** Reduction reaction of DCIP.

The data are reported in Table 2.2.

**Table 2.2** Inhibition power of gold(I) complexes on TrxR in comparison with Auranofin.<sup>a</sup>

Compound	% of Auranofin inhibition	IC <sub>50</sub> (μM)
Auranofin	100	0.018
3bb	73	0.354
3af	73	0.308
3ae	52	1.555
3ad	55	3.754
(+/-)-3aa	33	0.818
3ab	-	-

<sup>a</sup> First column: the inhibitory effect of different gold(I) complexes on TrxR is expressed as % of inhibition taking as reference the Auranofin maximal inhibition. Second column: IC<sub>50</sub> values of the different gold(I) complexes and Auranofin on TrxR activity.

According to the results given in Table 2.2, complexes **3bb** and **3af** turned out to be effective inhibitors of TrxR inducing a maximal inhibition close to that induced by Auranofin with IC<sub>50</sub> values in the sub-micromolar range. With the exception of **3ab**, the other complexes showed IC<sub>50</sub> values at least two order of magnitude higher than the Auranofin, whereas **3ab** cannot be considered an inhibitor of this class of enzymes.

It can be pointed out that only binuclear compounds are able to inhibit TrxR at sub-micromolar concentration suggesting the presence of strong interaction with the enzyme. To highlight the interaction between compounds and TrxR we have evaluated the LC-MS spectra of the enzyme both in the presence of a binuclear compound (**3bb**) and in the presence of the mononuclear compound **3ab** that does not inhibit the enzyme activity. The mass spectrometric analysis of protein allows the identification of the covalent modification affecting its structure and hence its molecular weight.<sup>[106]</sup> In order to evaluate the possible covalent interaction between TrxR and **3ab** and **3bb**, the LC-MS analyses were performed (Figure 2.19).

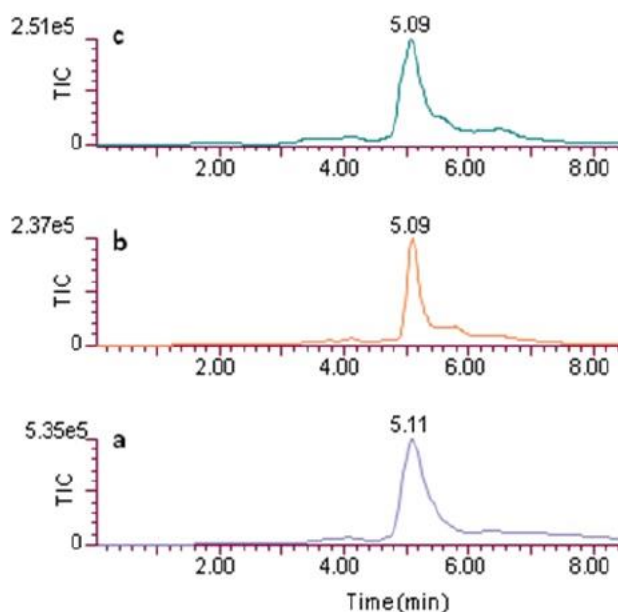


**Figure 2.19** LC-ESI-MS analysis of TrxR alone (a) and in combination with **3ab** (b) and **3bb** (c).

TrxR was previously analysed independently and its multicharged mass spectrum was acquired on its chromatographic peak (5 min retention time). From this spectrum the deconvoluted-ESI mass spectrum was obtained; it reports the molecular weight of the enzyme (Figure 2.20a). Being TrxR a mixture of isoforms three different principal molecular weights were obtained (54342, 58856 and 60885 Da). Analysing the mixtures of the enzyme with **3ab** and **3bb** a second peak appeared in the chromatogram (Figure 2.19b and c) indicating that these moieties have a different chromatographic behavior compared to that of the enzyme. This peak could derive from the molar excess of **3ab** and **3bb**. Concerning the mass spectrometric analysis however no significant changes were detected analysing the enzyme peak. In the presence of a covalent bond the signal corresponding to adduct would have appeared but no new signal was detected thus we can conclude that no covalent bond exists between TrxR and **3ab** or **3bb** (Figure 2.20b and c).

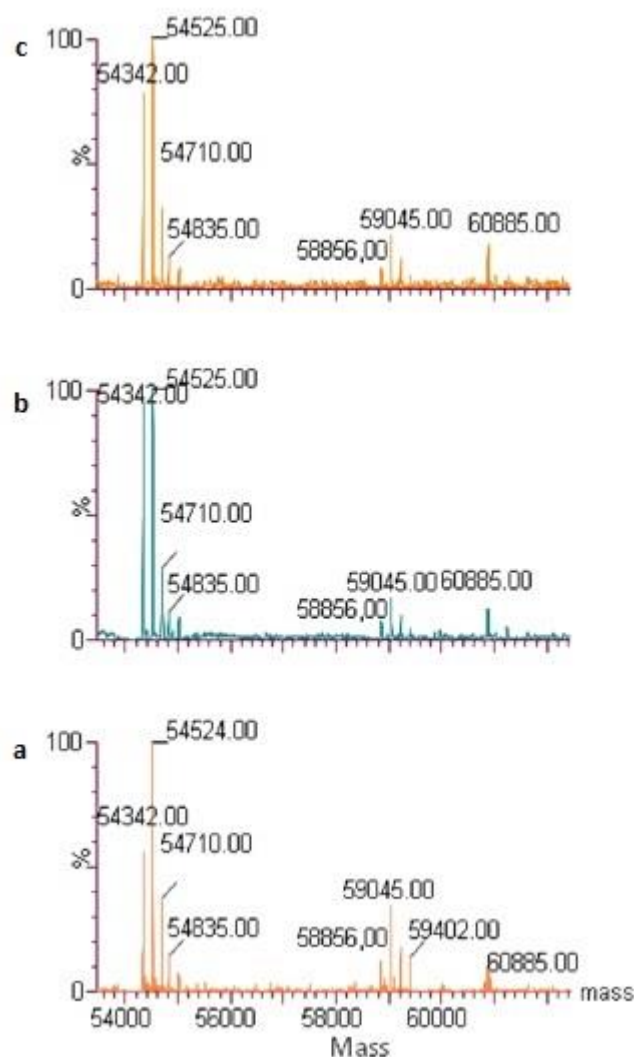


**Figure 2.20** Deconvoluted mass spectra of TrxR alone (a) or after the combination with **3ab** (b) and **3bb** (c).

To gain some insights into the biological effects of these new derivatives, the most active compound towards all cells lines, **3ab** was submitted to additional studies. In order to assess whether the antiproliferative effect of **3ab** was associated with interference with cell cycle progression, DNA profiles of cultured cells were examined by flow cytometry and cell cycle analysis was performed by using the Multicycle Cycle Phoenix Flow system, and Modfit 5.0 software.<sup>[107]</sup>

The cell cycle is a genetically controlled process and a scheme is reproduced in Figure 2. 21. It is characterized by two main phases: interphase and mitosis (phase M). In order to correctly transmit the genetic information from the



mother cell to the daughter cells, the genome must first be duplicated during the interphase and then the chromosomes must be segregated into the two new cells during the phase M. The interphase is divided into three phases: first gap phase  $G_1$ , that is the growing phase during which the cell grows physically larger, and the biosynthetic activity of the cell has a high rate and the molecular building blocks, that the cell need in later steps, are made; the S phase, the cell synthesizes a complete copy of the DNA in its nucleus and the amount of DNA in the cell has effectively doubled; the second gap phase, or  $G_2$  occurs after DNA replication and is a period in which the cell grows more to prepare the cell for mitosis. Phase M is composed of two closely related processes: mitosis, during which the chromosomes of the cell are divided between the two daughter cells and the cytokinesis, which involves the physical division of the cytoplasm of the cell.<sup>[108]</sup>

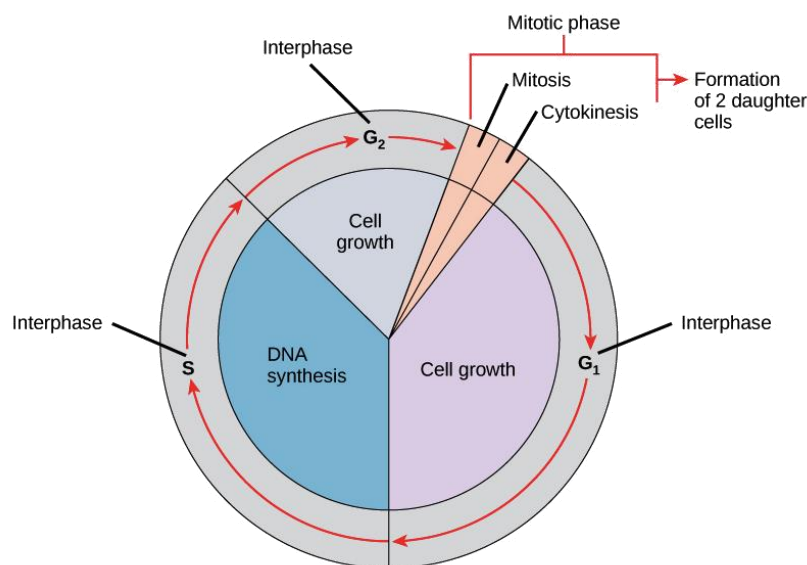


**Figure 2. 21** Schematic image of the cell cycle. Image was reproduced from "The cell cycle: Figure 1" by OpenStax College, Biology (CC BY 3.0).

The analysis of the cell cycle is carried out by measuring the DNA content. The cell is permeabilized so as to introduce a fluorescent dye, in particular the propidium iodide (PI), which colors the DNA quantitatively. The fluorescence intensity of the stained cells correlates with the amount of DNA

they contain in this way the cells that are in S phase will have more DNA than cells in G<sub>1</sub>.<sup>[109]</sup>

The following Table 2.3 shows that the treatment with **3ab** caused a marked accumulation of HT-29, IGROV1 and I407 cells in the S phase, respect to untreated cells.

**Table 2.3** Cell cycle distribution of cell lines treated with 3ab.

	G <sub>0</sub> /G <sub>1</sub> %	S %	G <sub>2</sub> /M %
HT29	49.05	39.58	11.37
HT29 + 3ab (7.9 μM)	45.72	45.25	9.03
IGROV1	55.32	29.57	15.11
IGROV1 + 3ab (5.3 μM)	50.71	37.16	12.13
I407	70.38	23.62	6
I407 + 3ab (1.7 μM)	62.64	28.52	8.84

Contrarily, in HL60 treated cells, the growth arrest was in the G<sub>0</sub>/G<sub>1</sub> phase of the cell cycle and was associated with a well distinguishable pre-G<sub>1</sub> peak in DNA, suggestive of DNA fragmentation, characteristic of apoptosis (Figure 2.22).

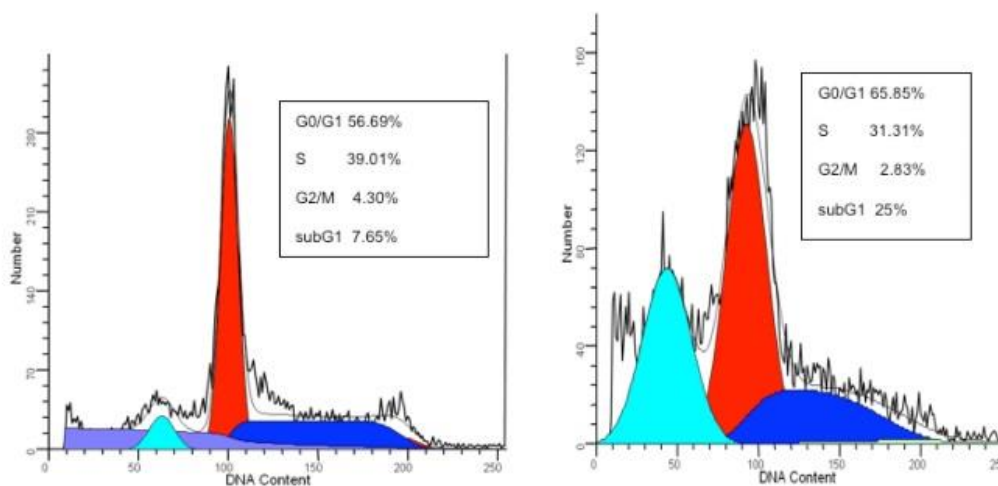


**Figure 2.22** Effect of compound **3ab** on the HL60 cell cycle. Cells were incubated for 24 h, (sx) with the vehicle (Ctrl), or (dx) with compound **3ab** (3,3  $\mu\text{M}$ ), afterward cell cycle distribution was determined by flow cytometry. Following treatment with **3ab**, cells are in the G<sub>0</sub>/G<sub>1</sub> phase and a well detectable fraction of DNA is present as a sub-G<sub>1</sub> peak (light blue peak, dx).

Interestingly, the treatment with the binuclear compounds did not induce any effect on the cell cycle, as reported in Table 2.4, where the cell cycle distribution of IGROV1 and HL60 in the presence of **3af** and **3bb**, respectively is shown.

**Table 2.4** Cell cycle distribution of cell lines treated with **3af** and **3bb**.

	G <sub>0</sub> /G <sub>1</sub> %	S %	G <sub>2</sub> /M %
IGROV1	60	25	15
IGROV1 + 3af (7.7 $\mu\text{M}$ )	64	23	13
HL60	48	14	38
HL60 + 3bb (0.8 $\mu\text{M}$ )	50	17	33

### 2.2.4 UV-Vis absorption titration analysis

Interactions between small molecules and DNA rank among the primary action mechanisms of cytotoxic activity. In order to compare the binding properties of the gold complexes with DNA, dissociation constants ( $K_d$ ) were

determined through inverse titration experiments. Two types of interactions can be devised by these experiments as we can argue by the increase of  $\Delta A$  or a decrease of  $\Delta A$  measured at 260 nm.

The increase of differential absorption of DNA in the presence of **3af**, **3ab**, **3ac**, **3bb**, and **3ac** could be ascribed to a lower base stacking while the decreased differential absorbance observed for (+/-)-**3aa** suggests a higher compactness of DNA. No appreciable effect was observed for **3ad**. In this regard, the differential spectra of **3af** (A), (+/-)-**3aa** (B) and **3ad** (C) are depicted in Figure 2.23.

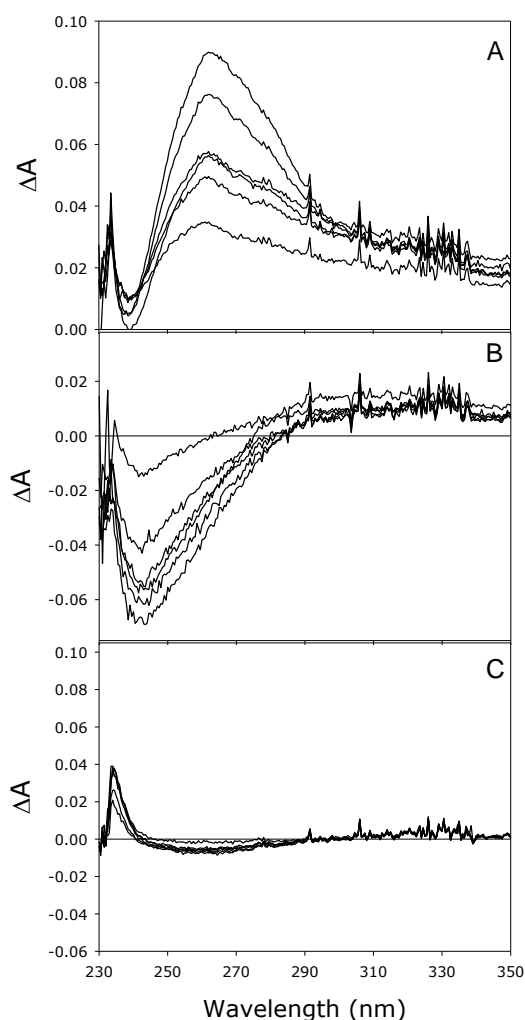


**Figure 2.23** Differential absorption spectra of **3af** (A), (+/-)-**3aa** (B) and **3ad** titrated with DNA.

Then the differential absorbance at 260 nm for each molecule versus DNA concentration was plotted, as reported in Figure 2.24.

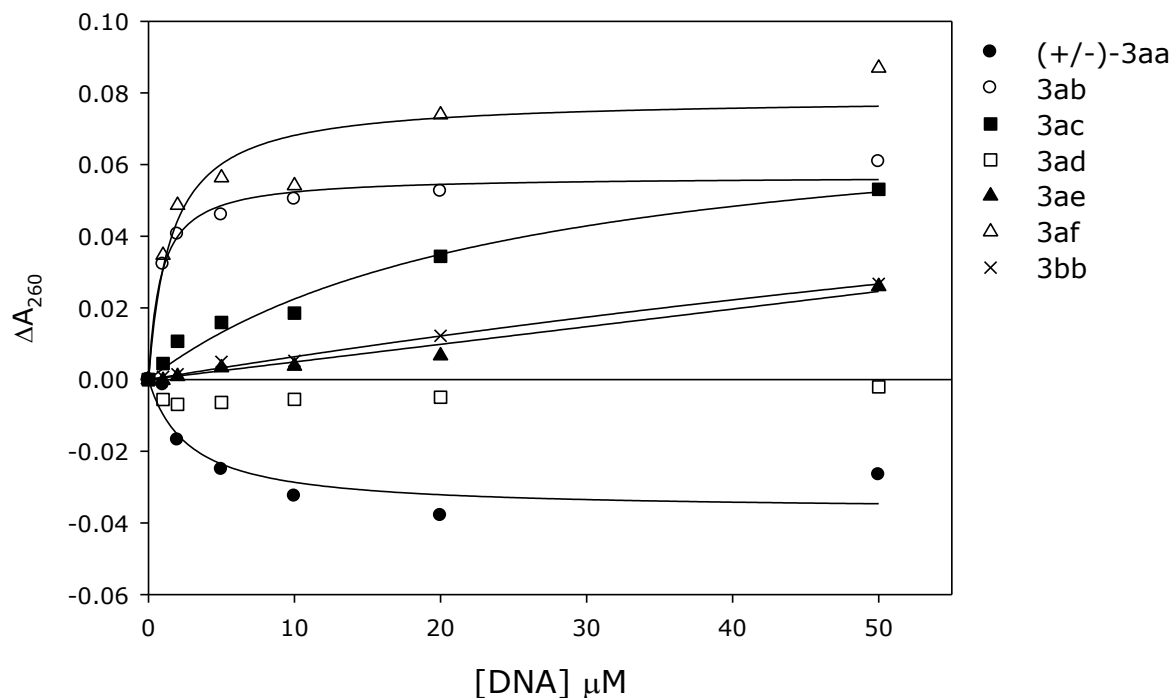


**Figure 2.24** Differential absorbance at 260 nm of DNA – molecules complexes at increasing DNA concentration. Molecule concentration was 10 μM.

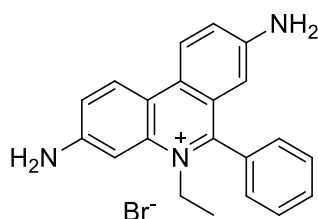
Fitting of these data, the use of a one-site saturation equation, enabled the estimation of the dissociation constant ( $K_d$ ) for the complex formation as well as the limiting value for the  $\Delta A_{260}$  (Table 2.5).

**Table 2.5** Dissociation constant for the complex formation and the limiting value for the  $\Delta A_{260}$  obtained by fitting data in figure 2.19.

	$K_d \pm SE$ ( $\mu\text{M}$ )	$B_{\text{max}} \pm SE$	$r^2$
(+/-)- <b>3aa</b>	$2.78 \pm 1.36$	$-0.0366 \pm 0.0055$	0.8564
<b>3ab</b>	$0.84 \pm 0.17$	$0.0568 \pm 0.0019$	0.9826
<b>3ac</b>	$24.89 \pm 7.12$	$0.0784 \pm 0.0108$	0.9757
<b>3bb</b>	$195.53 \pm 111.89$	$0.1310 \pm 0.0619$	0.9923
<b>3ad</b>	-	-	-
<b>3ac</b>	-	-	-
<b>3af</b>	$1.54 \pm 0.58$	$0.0786 \pm 0.0064$	0.9245

The  $K_d$  analysis confirms that **3ab** interacts with DNA quite strongly ( $K_d = 0.84 \pm 0.17$ ) suggesting a partial explanation for its cellular toxicity. Among the other compounds, only **3af** shows a strong interaction with DNA having a similar value of  $K_d$  ( $1.54 \pm 0.58$ ). On the other hand, a decrease for the differential absorption spectra is observed for (+/-)-**3aa**. While the increase in the absorbance at 260 nm can be ascribed to a partial denaturation of the DNA, the decrease observed in the presence of the compound **3aa**, could be indicative of DNA supercoiling.

A fluorimetric test was performed to evaluate if the **3ad** complex is intercalated in the DNA. The test was carried out using the ETBr (Figure 2.25), which thanks to its unique structure, can easily intercalate in the DNA strand and is used as a fluorescent tag of nucleic acids.

**Figure 2.25** Ethidium bromide structure.

When exposed to ultraviolet light, it gives fluorescence with an orange colour, intensifying almost 20 times after DNA binding. The reason for the intense fluorescence of Ethidium Bromide binding with the DNA is the hydrophobic environment found between the base pairs. The ETBr cation without water molecules, which quench the fluorescence, will emit with greater intensity.<sup>[110]</sup>

Fluorescence titration of 15  $\mu\text{M}$  ETBr bound to DNA with **3ab**, up to 200  $\mu\text{M}$ , does not show any appreciable change of the emission spectra of ETBr, suggesting that no intercalation of **3ab** with DNA takes place (Figure 2.26).

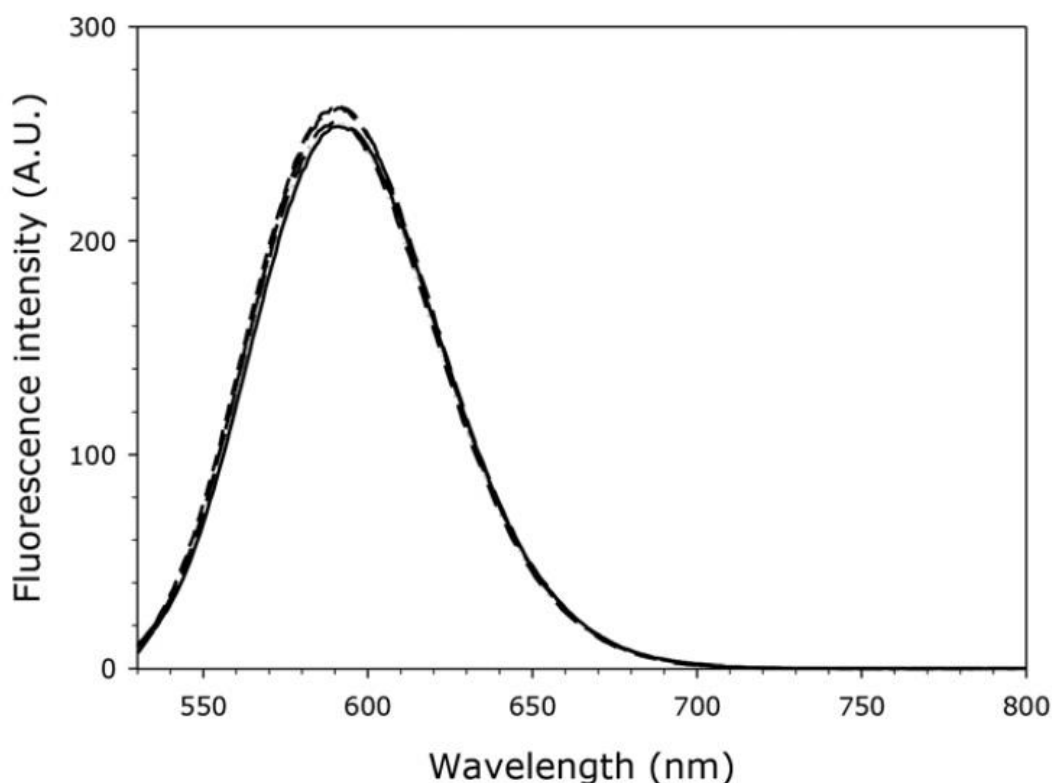


**Figure 2.26** Fluorescence emission spectra of 15  $\mu\text{M}$  ETBr bound to DNA in the presence of increasing concentration of **3ab**. Control: solid line; [**3ab**] 10 $\mu\text{M}$ : long dashed line; [**3ab**] 100 $\mu\text{M}$ : dashed dotted line; [**3ab**] 200 $\mu\text{M}$ : dotted line.

## 2.3 Conclusions

In conclusion, a new class of neutral [Au(I)]-alkynyl complexes based on monodentate or bidentate phosphine ligands has been developed and fully characterized both in the liquid and solid state. The gold(I)–C<sub>sp</sub> linkage was

efficiently realized in high yields (60–92%) by condensing the gold-chloride congener with pre-functionalized terminal alkynes under convenient mild conditions (KOH, MeOH/EtOH).

Additionally, the biological activity of these organometallic species was comprehensively investigated and the data reported suggest that their cellular toxicity could be related to different mechanisms acting on different biological targets.

Compound **3ab** showed a marked cytotoxicity on all cell lines tested, with  $IC_{50}$  values ranging from 1.7  $\mu$ M for I407 to 7.9  $\mu$ M for HT29 and caused cell cycle arrest in the S phase. Only in the HL60 cell line the growth arrest was in the G<sub>0</sub>/G<sub>1</sub> phase of the cell cycle and it was associated with a well distinguishable pre-G<sub>1</sub> peak that indicates DNA fragmentation that is characteristic of apoptosis. These effects on the cell cycle can be associated with an interaction of the molecule with DNA and this hypothesis is supported by the results of DNA titration where the dissociation constant of **3ab** with salmon sperm DNA is in the sub-micromolar range. The real mechanism of **3ab**–DNA interaction has not yet been fully elucidated. However, it cannot be attributed to an intercalation of the molecule into the DNA helix. Additionally, it should be mentioned that **3ab** does not show any inhibitory effect on the thioredoxin reductase enzymatic activity.

On the other hand, the binuclear compounds (**3bb** and **3af**) showed a cytotoxic effect only in HL60 (**3bb**:  $IC_{50}$  = 0.8  $\mu$ M) and in IGROV1 (**3af**:  $IC_{50}$  = 7.7  $\mu$ M) and they do not show any effect on the cell cycle (Table 2.4). This evidence suggests that the biological target of binuclear gold-species is not the DNA and they appear to act through the inhibition of thioredoxin reductase at sub-micromolar concentration (Table 2.2). However the mechanism of interaction of our alkynyl-gold(I) complexes with thioredoxin reductase is different as compared to Auranofin and other gold compounds. In fact, while Auranofin induces a mass shift in the mass spectra of this



enzyme suggestive of protein binding of the gold-containing molecule, in our study no covalent adducts with the enzyme have been detected using LC/ESI-MS. Moreover, inhibition of thioredoxin reductase is responsible for a decrease of the oxidative stress resistance and for alterations in redox signalling that are key factors for cell survival. Cancer cells are more resistant towards oxidative stress, for this reason compounds that are able to interfere with this phenomena, have a good chance to be anticancer drug candidates. Studies addressing the clarification and/or identification of additional biological targets as well as the development of structure–activity relationships are currently ongoing in our laboratories.

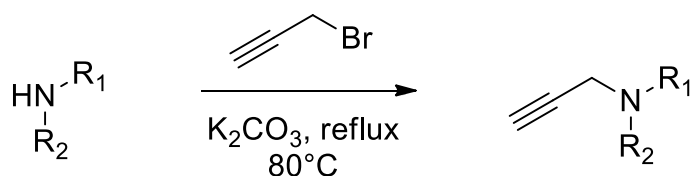
## 2.4 Experimental part

### 2.4.1 General methods

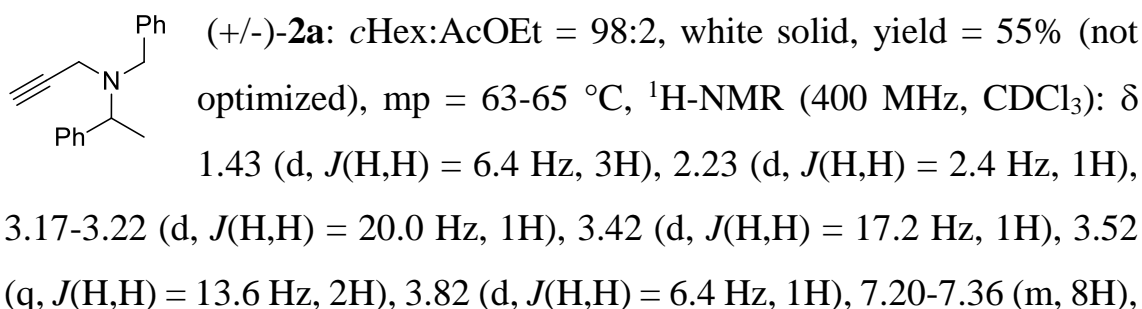
<sup>1</sup>H-NMR spectra were recorded on Varian 200 (200 MHz) or Varian 400 (400 MHz) spectrometers. Chemical shifts are reported in ppm from TMS with the solvent resonance as the internal standard (deuteriochloroform: 7.27 ppm). Data are reported as follows: chemical shift, multiplicity (s = singlet, d = duplet, t = triplet, q = quartet, sext = sextet, sept = septet, p = pseudo, b = broad, m = multiplet), coupling constants (Hz). <sup>13</sup>C-NMR spectra were recorded on a Varian 200 (50 MHz), Varian 400 (100 MHz) spectrometers with complete proton decoupling. Chemical shifts are reported in ppm from TMS with the solvent as the internal standard (deuteriochloroform: 77.0 ppm). <sup>31</sup>P-NMR spectra were recorded on a Varian 400 (162 MHz), spectrometer with complete proton decoupling. Chemical shifts are reported in ppm using H<sub>3</sub>PO<sub>4</sub> (85% H<sub>2</sub>O solution,  $\delta = 0$  ppm) as an external standard. GC-MS spectra were taken by EI ionization at 70 eV on a Hewlett-Packard 5971 with GC injection. They are reported as: *m/z* (rel. intense). LC-electrospray ionization mass spectra were obtained with Agilent Technologies MSD1100 single-quadrupole mass spectrometer. ESI Q-TOF

mass spectrometry was performed on a Xevo™ QToF (Waters MS Technologies, Manchester, UK), a quadrupole and orthogonal acceleration time-of-flight tandem mass spectrometer. IR spectra were performed as Nujol mull or neat on a Bruker Alpha FT-IR Spectrometer. Chromatographic purification was done with 240-400 mesh silica gel. Anhydrous THF and DCM were distilled respectively from sodium-benzophenone and P<sub>2</sub>O<sub>5</sub> prior to use. Elemental analyses were carried out by using an EACE 1110 CHNOS analyzer. Other anhydrous solvents were supplied by Fluka or Sigma Aldrich in Sureseal® bottles and used without any further purification. Commercially available chemicals were purchased from Sigma Aldrich, Stream and TCI and used without any further purification. Melting points were measured using open glass capillaries in a Bibby Stuart Scientific Melting Point Apparatus SMP 3 and are calibrated by comparison with literature values (Aldrich).

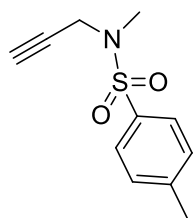
#### 2.4.2 Synthesis of the propargyl amino derivative 2a-2e



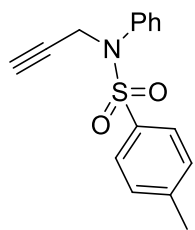
A solution of desired amine/sulfonylamide (2.5 mmol) in reagent grade acetone (8 mL) was treated with K<sub>2</sub>CO<sub>3</sub> (2 eq) and propargyl bromide (80% in toluene, 2.2 eq). The mixture heated under reflux for 8 h. The mixture was quenched with water, the aqueous phase was extracted three times with EtOAc, dried over Na<sub>2</sub>SO<sub>4</sub> and the volatiles removed under reduce pressure.



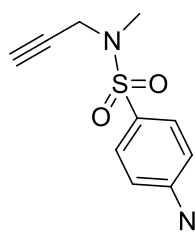
7.46 (d,  $J(\text{H,H}) = 7.2$  Hz, 2H);  $^{13}\text{C}$ -NMR (100 MHz,  $\text{CDCl}_3$ ):  $\delta$  21.2, 38.4, 54.5, 60.9, 73.0, 78.9, 126.9, 127.0, 127.5(2C), 128.3(2C), 128.5(2C), 128.9(2C), 139.5, 145.4; LC/MS-ESI ( $m/z$ ): 250 ( $\text{M}+\text{H}^+$ ); IR ( $\text{cm}^{-1}$ , Nujol mull): 2100  $\text{cm}^{-1}$  ( $\text{C}\equiv\text{C}$ ).



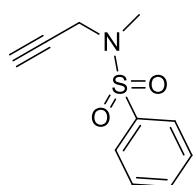
**2b:**  $c\text{Hex}:\text{AcOEt} = 7:3$ , white solid, yield = 75%, mp = 95-97 °C,  $^1\text{H}$ -NMR (400 MHz,  $\text{CDCl}_3$ ):  $\delta$  2.09 (t,  $J(\text{H,H}) = 2$  Hz, 1H), 2.44 (s, 3H), 2.83 (s, 3H), 4.02 (d,  $J(\text{H,H}) = 2.4$  Hz, 2H), 7.31-7.33 (d,  $J(\text{H,H}) = 8.0$  Hz, 2H), 7.72-7.70 (d,  $J(\text{H,H}) = 8.4$  Hz, 2H);  $^{13}\text{C}$ -NMR (100 MHz,  $\text{CDCl}_3$ ):  $\delta$  21.5, 34.3, 39.7, 74.0, 76.3, 127.9, 129.5, 134.1, 143.7; GC/MS( $m/z$ ): 223 ( $\text{M}^+$ ); IR ( $\text{cm}^{-1}$ , Nujol mull): 2120  $\text{cm}^{-1}$  ( $\text{C}\equiv\text{C}$ ).



**2c:**  $c\text{Hex}:\text{AcOEt} = 8:2$ , white solid, yield = 85%, mp = 88-90 °C;  $^1\text{H}$ -NMR (400 MHz,  $\text{CDCl}_3$ ):  $\delta$  2.17 (s, 1H), 2.42 (s, 3H), 4.45 (s, 2H), 7.24-7.32 (m, 7H), 7.54-7.56 (d,  $J(\text{H,H}) = 6.4$  Hz, 2H);  $^{13}\text{C}$ -NMR (100 MHz,  $\text{CDCl}_3$ ):  $\delta$  21.5, 41.0, 73.8, 78.0, 128.0, 128.1, 128.4, 129.0, 129.2, 135.5, 139.3, 143.6; GC/MS( $m/z$ ): 285 ( $\text{M}^+$ ); IR ( $\text{cm}^{-1}$ , Nujol mull): 2129  $\text{cm}^{-1}$  ( $\text{C}\equiv\text{C}$ ).



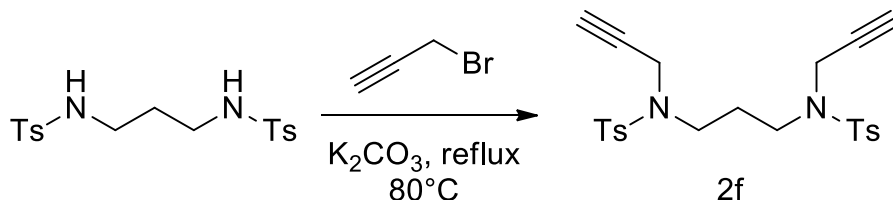
**2d:**  $c\text{Hex}:\text{AcOEt} = 7:3$ , dark yellow solid, yield = 60%, mp = 129-132 °C,  $^1\text{H}$ -NMR (400 MHz,  $\text{CDCl}_3$ ):  $\delta$  2.07 (s, 1H), 2.91 (s, 3H), 4.14 (s, 2H), 8.02-8.05 (d,  $J(\text{H,H}) = 8.4$  Hz, 2H), 8.36-8.38 (d,  $J(\text{H,H}) = 8.0$  Hz, 2H);  $^{13}\text{C}$ -NMR (100 MHz,  $\text{CDCl}_3$ ):  $\delta$  34.3, 39.8, 74.7, 75.4, 124.1, 129.1, 143.4, 150.4; GC/MS ( $m/z$ ): 254 ( $\text{M}^+$ ); IR ( $\text{cm}^{-1}$ , Nujol mull): 2118  $\text{cm}^{-1}$  ( $\text{C}\equiv\text{C}$ ).



**2e:**  $c\text{Hex}:\text{AcOEt} = 7:3$ , light yellow solid, yield = 70%, mp = 55-57 °C,  $^1\text{H}$ -NMR (400 MHz,  $\text{CDCl}_3$ ):  $\delta$  2.06 (t,  $J(\text{H,H}) = 2$  Hz, 1H), 2.85 (s, 3H), 4.04-4.05 (d,  $J(\text{H,H}) = 2.8$  Hz, 1H), 7.51-7.55 (m, 2H), 7.59-7.63 (m, 1H), 7.83-7.85 (m, 2H);  $^{13}\text{C}$ -NMR (100

MHz, CDCl<sub>3</sub>):  $\delta$  34.3, 39.7, 74.0, 76.1, 127.8, 128.9, 132.9, 137.3; LC/MS-ESI (m/z): 209(M<sup>+</sup>); IR (cm<sup>-1</sup>, Nujol mull): 2120 cm<sup>-1</sup> (C $\equiv$ C).

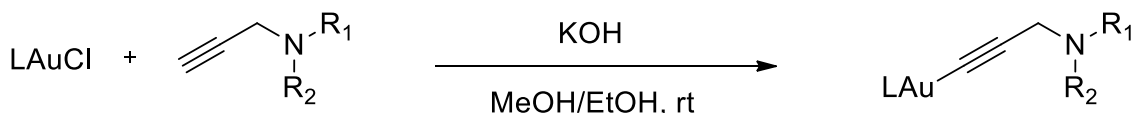
### 2.4.3 Synthesis of 2f



A solution of *N,N'*-(propane-1,3-diyl)bis(4-methylbenzenesulfonamide) (1.12 mmol) in reagent grade acetone (7.5 mL) was treated with K<sub>2</sub>CO<sub>3</sub> (2 eq) and propargyl bromide (80% in toluene, 4 eq). The mixture was refluxed for 8 h, when monitoring by TLC proved the complete consumption of the starting material. The mixture was quenched with water, the aqueous phase extracted three times with DCM, dried over Na<sub>2</sub>SO<sub>4</sub> and the volatiles removed under reduce pressure.

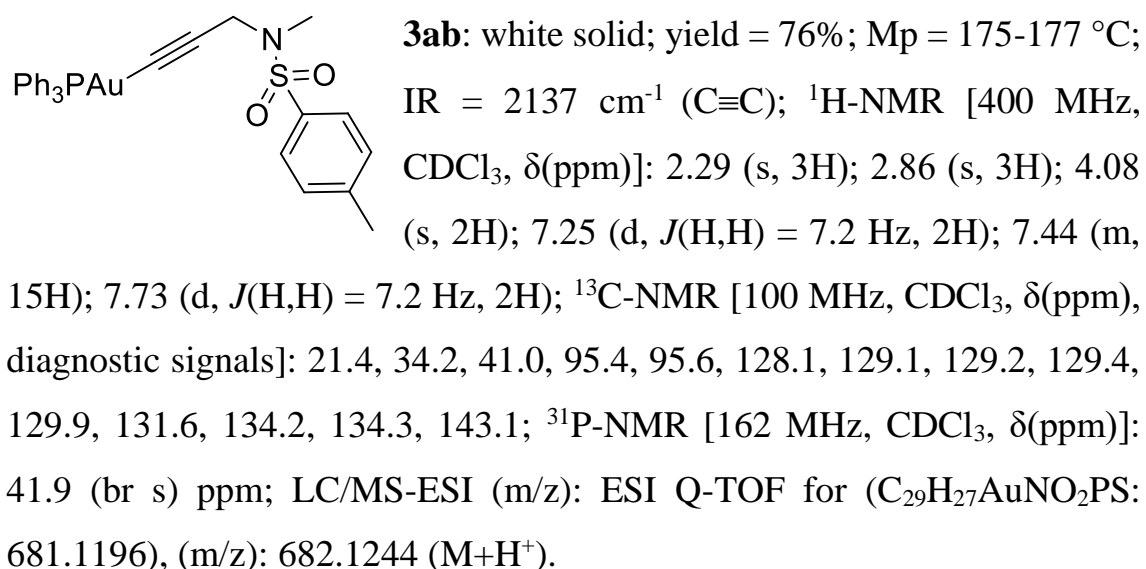
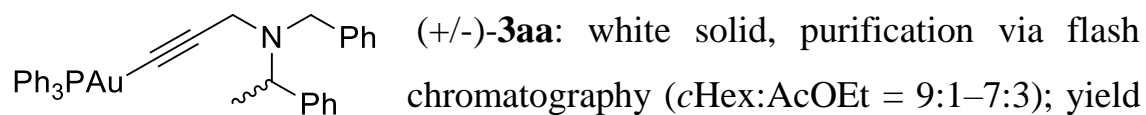
**2f**: *c*Hex:AcOEt = 8:2, white solid, yield = 76%, mp = 110-112 °C, <sup>1</sup>H-NMR (400 MHz, CDCl<sub>3</sub>):  $\delta$  1.92 (qui, *J*(H,H)= 7.2 Hz, 2H), 2.02 (t, *J*(H,H)= 2.4, 2H), 2.41 (s, 6H), 3.24 (t, *J*(H,H)= 7.2 Hz, 4H), 4.12 (d, *J*(H,H)= 2.4 Hz, 4H), 7.28 (d, *J*(H,H)= 8.0 Hz, 4H), 7.69 (d, *J*(H,H)= 8.4 Hz, 4H); <sup>13</sup>C-NMR (100 MHz, CDCl<sub>3</sub>):  $\delta$  143.6, 135.4, 129.5, 127.7, 74.0, 44.1, 36.7, 26.1, 21.5; LC/MS-ESI (m/z): 459 (M+H<sup>+</sup>), 939 (2M+Na<sup>+</sup>); IR (cm<sup>-1</sup>, Nujol mull): 2114 cm<sup>-1</sup> (C $\equiv$ C).

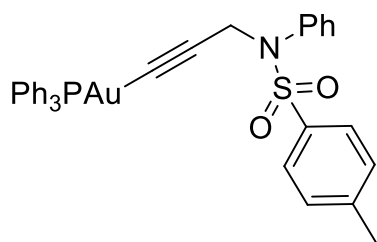
### 2.4.4 Synthesis of the [alkynylAu(I)] complexes 3



A solution of desired alkyne (1.2 or 2.4 eq.) in reagent grade MeOH/EtOH (1:1 ratio, 0.05 M) was treated with the desired gold(I)chloride precursor (**1a,b**, 1 eq.) and a solution of KOH (4 eq., 2 M in MeOH). The mixture was

stirred under dark until complete consumption of the alkyne. The resulting solid was collected by filtration and washed with cooled MeOH. Pure material can be obtained via re-crystallization from a DCM:pentane solution, or flash chromatography.





**3ac:** white solid; yield = 88%; Mp = 139-141 °C;

IR = 2134 cm<sup>-1</sup> (C≡C); <sup>1</sup>H-NMR [400 MHz,

CDCl<sub>3</sub>, δ(ppm)]: 2.32 (br s, 3H); 4.61 (s, 2H);

7.17 (d, *J*(H,H) = 8.4 Hz, 2H); 7.26-7.35 (m, 2H);

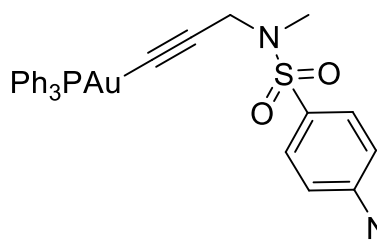
7.37-7.38 (m, 2H), 7.44-7.54 (m, 16H), 7.64 (d, *J*(H,H) = 8.4 Hz, 2H); <sup>13</sup>C-

NMR [100 MHz, CDCl<sub>3</sub>, δ(ppm), diagnostic signals]: 21.5, 42.2, 127.4,

128.2, 128.3, 128.8, 129.0, 129.1, 129.2, 130.0, 131.6, 134.2, 134.3, 136.0,

140.0, 142.9; <sup>31</sup>P-NMR [162 MHz, CDCl<sub>3</sub>, δ(ppm)]: 42.4 (s) ppm; ESI Q-

TOF for (C<sub>34</sub>H<sub>29</sub>AuNO<sub>2</sub>PS: 743.1322), (m/z): 766.1220 (M+Na<sup>+</sup>).



**3ad:** pale yellow solid; yield = 81%; Mp =

208-210 °C; IR = 2137 cm<sup>-1</sup> (C≡C); <sup>1</sup>H-NMR

[400 MHz, CDCl<sub>3</sub>, δ(ppm)]: 2.95 (s, 3H); 4.27

(d, *J*(H,H) = 1.6 Hz, 2H); 7.43-7.53 (m, 15H);

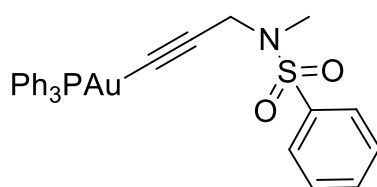
8.13 (d, *J*(H,H) = 8.8 Hz, 2H); 8.34 (d, *J*(H,H) = 8.8 Hz, 2H); <sup>13</sup>C-NMR [100

MHz, CDCl<sub>3</sub>, δ(ppm)]: 34.4, 41.2, 93.7, 94.0, 123.9, 129.2, 129.6, 131.6,

134.0, 134.2, 143.8, 149.9; <sup>31</sup>P-NMR [162 MHz, CDCl<sub>3</sub>, δ(ppm)]: = 39.4 (s)

ppm; ESI Q-TOF for (C<sub>28</sub>H<sub>24</sub>AuN<sub>2</sub>O<sub>2</sub>PS: 712.0860), (m/z): 713.0940

(M+H<sup>+</sup>).



**3ae:** white solid; yield = 62%; Mp = 210-212 °C;

IR = 2136 cm<sup>-1</sup> (C≡C); <sup>1</sup>H-NMR [400 MHz,

CDCl<sub>3</sub>, δ(ppm)]: 2.91 (s, 3H); 4.14 (s, 2H); 7.44-

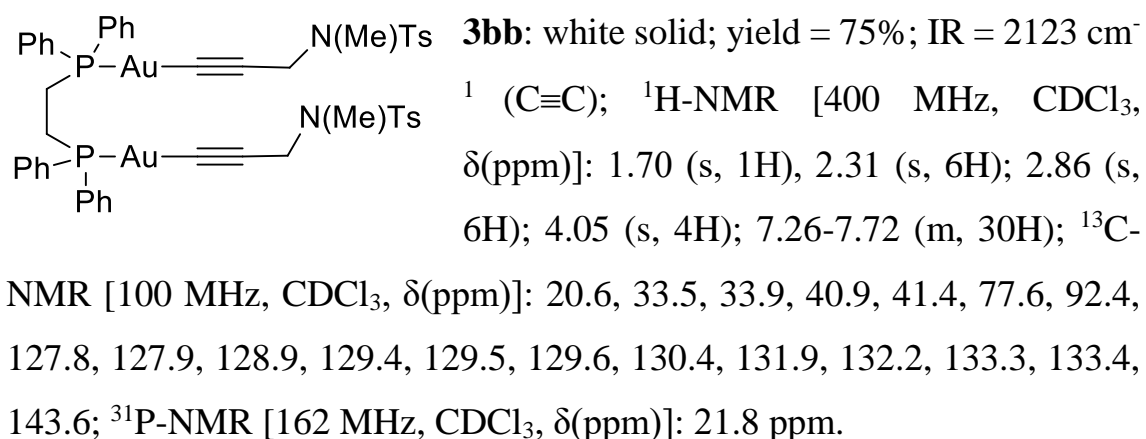
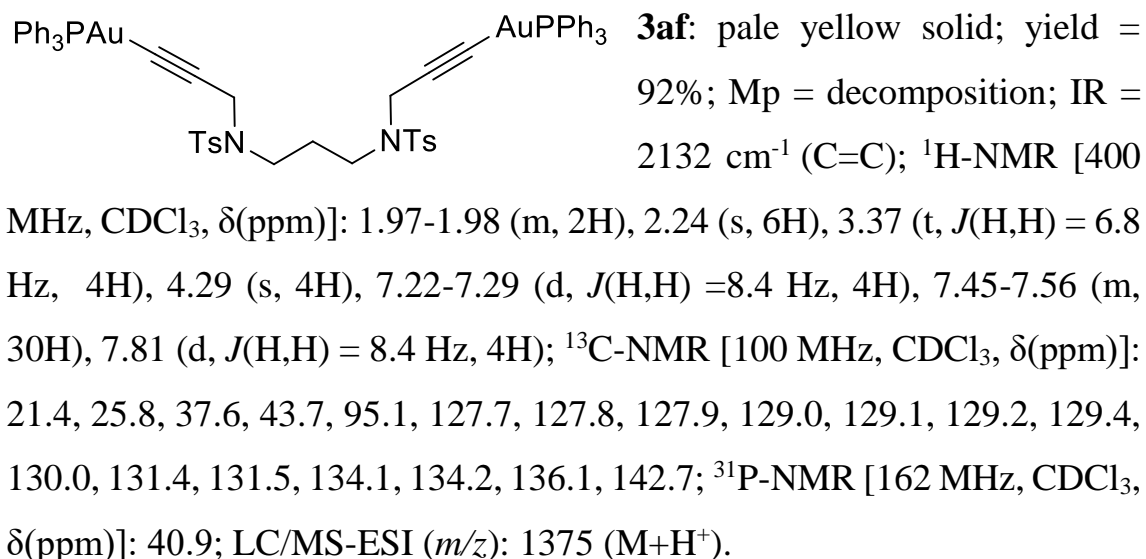
7.48 (m, 18H); 7.88 (d, *J*(H,H) = 6.8 Hz, 2H); <sup>13</sup>C-NMR [100 MHz, CDCl<sub>3</sub>,

δ(ppm)]: 34.3, 41.0, 95.3, 99.0, 127.8, 128.1, 128.7, 129.0, 129.1, 129.2,

129.4, 129.9, 131.6, 131.7, 132.4, 134.1, 134.3, 137.5; <sup>31</sup>P-NMR [162 MHz,

CDCl<sub>3</sub>, δ(ppm)]: 39.2 (s) ppm; ESI Q-TOF for (C<sub>28</sub>H<sub>25</sub>AuNO<sub>2</sub>PS: 667.1009),

(m/z): 668.1088 (M+H<sup>+</sup>).



### 2.4.5 Cell culture and cytotoxicity

Cell lines (HT29, IGROV1, HL60 and I407) were routinely cultured in RPMI 1640 medium supplemented with penicillin (100 U/mL), streptomycin (100  $\mu\text{g/mL}$ ), and 10% fetal bovine serum in an environment of 5%  $\text{CO}_2$ , 37  $^\circ\text{C}$  and sub-cultured using a trypsin 0.25%-EDTA 0.02% solution. The cytotoxicity was determined with the MTT (3-(4,5-dimethylthiazol-2-yl)-2,5-diphenyltetrazolium bromide) dye reduction assay.<sup>[91]</sup> Cells were plated in 96-well flat-bottomed microplates at a density of  $1 \times 10^5$  cells/mL (100  $\mu\text{L}$ /well), and 24 h later the test compounds were added, appropriately diluted with DMSO. Cells were exposed to various concentrations of the compounds (in a range 1nM to 100  $\mu\text{M}$ ) for 24 h. The cytotoxicity was determined with the MTT (3-(4,5-dimethylthiazol-2-yl)-2,5-

diphenyltetrazolium bromide) dye reduction assay with minor modifications. Briefly, after incubation with the test compounds, MTT solution (0,2 mg/mL in PBS) was added (100  $\mu$ L/well). Plates were further incubated for 2 h at 37 °C, and the formazan crystals formed were dissolved by adding 100  $\mu$ L/well of propanol. Optical densitometry was determined with a Wallac 1420 Victor2 Microplate Reader (Perkin Elmer) at 570 nm. One hundred microliters of culture medium supplemented with the same amount of MTT solution and solvent was used as blank solution. The IC<sub>50</sub> value was calculated according to the GraphPad Prism 5 software. All data are expressed as mean  $\pm$  SD.

#### 2.4.6 Cell cycle analysis

Cells were plated at initial density of 10000-20000 cell/cm<sup>2</sup> in dish or flask, depended on the cell line. After 72 h of adhesion, cells were treated with drugs at the concentration correspond to the calculated IC<sub>50</sub>, and after 24 h of treatment the effect was evaluated. Untreated and 24 h treated cells were detached, washed in PBS and the pellet was finally re-suspended in 0.01% Nonidet P-40 (Sigma-Aldrich), 10  $\mu$ g/mL RNase (Sigma-Aldrich), 0.1% sodium citrate (Sigma-Aldrich), 50  $\mu$ g/mL propidium iodide (PI) (Sigma-Aldrich), for 30 min at room temperature in the dark. Propidium iodide (PI) fluorescence was analyzed using a Beckman Coulter Epics XL-MCL flow cytometer and cell analysis was performed using the M cycle (Verity) and MODFIT 5.0 softwares.

#### 2.4.7 TrxR inhibition assay

For this purpose, commercially available rat liver TrxR (Sigma–Aldrich) and baker yeast GR (Sigma–Aldrich) were used and diluted with distilled water to achieve a concentration of 0.05 U mL<sup>-1</sup>. The gold(I) complexes were freshly dissolved as stock solutions in DMSO. The reduction of the DCIP (2,6-dichloroindophenol) was followed spectrophotometrically at 600nm



using  $\epsilon = 19,1\text{mM cm}^{-1}$  using a Jasco V-550 spectrophotometer equipped with stirring device and thermostatic control. To each cuvette was added: 100 $\mu\text{L}$  of enzyme solution, different concentrations of the compounds (ranging from 1 to 100  $\mu\text{M}$ ) or vehicle, 100  $\mu\text{M}$  DCIP, 8 mM EDTA, 0,001% BSA in 20mM potassium phosphate buffer pH 7, 1 ml final volume. The reaction was started by the addition of 2 mM NADPH. The  $\text{IC}_{50}$  values were calculated as the concentration of compound required to decrease enzyme activity of the untreated control by 50%, and are given as the means  $\pm$  SD of 3–6 independent experiments.

#### 2.4.8 DNA-compound interaction assay

Absorption titration experiments were carried out by keeping constant the concentration of compounds (10  $\mu\text{M}$ ) while raising the DNA concentration from 1  $\mu\text{M}$  ([DNA]/[compounds] ratio from 0.1 to 5) in buffer solution (BS; 50 mM NaCl, 5 mM TRIS buffer, pH 7.2) and 4% DMSO. The UV-vis spectra were obtained using a Jasco V-550 spectrophotometer. The absorbance spectra were obtained scanning the solution in 1 cm quartz cuvettes from 230 nm to 400 nm using a 2nm band width. The solubility of different compounds was checked evaluating the lack of scattering. Then additions standard DNA was performed. After each addition of DNA the absorbance spectrum was recorded. The DNA stock solution was prepared with low molecular weight from salmon sperm, Sigma Aldrich in BS. The DNA stock solution concentration was determined spectrophotometrically ( $\lambda$ : 260nm), using an extinction coefficient of  $6600\text{ M}^{-1}\text{ cm}^{-1}$ .

The blank were prepared with standard DNA titration from 1  $\mu\text{M}$  to 50  $\mu\text{M}$  in BS and 4% of DMSO.

The UV-Vis spectra of DNA in the presence of the different compounds were obtained using a Jasco v-550 spectrophotometer. The data analysis was carried out on the subtracted spectrum ( $\Delta A_{\lambda}$ ): the spectra of titration

experiments were subtracted by standard DNA titration and compound lacking DNA.

$$\Delta A_{\lambda} = (\Delta A_{\text{DNA-compound}})_{\lambda} - (\Delta A_{\text{DNA}})_{\lambda} - (\Delta A_{\text{compound}})_{\lambda}$$

The compounds absorbance variations at 260 nm ( $\Delta A_{260}$ ) were plotted *versus* DNA concentration. The calculation of binding parameters was carried out fitting  $\Delta A_{260}$  using following equation:

$$\Delta A_{260} = \frac{B_{\text{max}}[\text{DNA}]}{K_d + [\text{DNA}]}$$

Where  $K_d$  represents the dissociated constant of DNA complex for every compound and  $B_{\text{max}}$  represents the limiting value of  $\Delta A_{260}$ .

#### 2.4.9 Competitive binding fluorescence studies

Aliquots of stock solution of the gold complex **3ab** dissolved in DMSO were added to solutions containing 15  $\mu\text{M}$  ethidium bromide (ETBr) in 15% DMSO 25 mM Tris-HCl buffer (pH 7.0) at 25°C to give the final complex concentration ranging from 0 to 200  $\mu\text{M}$ , according to the literature.<sup>[104,111]</sup>

#### 2.4.10 Liquid chromatography and mass spectra analysis

TrxR alone or in combination with **3ab** or **3bb** was analysed by liquid chromatography tandem mass spectrometry (LC-MS) in order to evaluate the possible covalent interaction between the enzyme and the two moieties. In details, the analyses were performed using a Jasco PU-1585 liquid chromatograph (Jasco Corporation, Tokyo, Japan) equipped with a Reodyne 7281 injection valve (20  $\mu\text{L}$  sample loop). The chromatographic separation was achieved using a monolithic column CIMac C4 Analytical (5.3 mm I.D. X 5 mm), a not commercial prototype provided by BIA Separations (Ljubljana, Slovenia). Mobile phases A [water:acetonitrile:formic acid (99/1/0.1) (v/v/v),] and B [acetonitrile:water:formic acid (98/2/0.1) (v/v/v)] were used to develop a gradient. The optimized mobile phase B gradient program was 0–80 % in 5 min and 80 % of B for 5 min. The column was

equilibrated with the mobile phase composition of the starting conditions for 3 min before the next injection. The flow rate was set at 0.5 mL/min. The injection volume was 20  $\mu$ L. Mass spectrometry analysis was carried out on a Quadrupole-Time of Flight hybrid analyser (QToF Micro, Micromass, Manchester, UK) with Z-spray electrospray ion source (ESI). The ESI-QToF source temperature was set at 120°C, the capillary voltage at 3.2 kV and the cone voltage at 30 V. The scan time was set at 2.0 s and the inter scan time at 0.1 s. The cone gas flow was set at 120 L/h and the desolvation gas at 500 L/h. The mass chromatograms were recorded in total ion current (TIC), within 500 m/z and 2000 m/z. The HSA baseline-subtracted spectrum (m/z 1000–1600) was deconvoluted onto a true mass scale using the maximum entropy (MaxEnt1)-based software supplied with MassLynx 4.1 software. Output parameters were as follows: mass range 20000–70000 Da and resolution 5 Da/channel. The uniform Gaussian model was used, with 0.5 Da width at half height.

#### 2.4.11 Crystallographic Data Collection and Structure Determination for 3ab and 3ac

The X-ray intensity data were measured on a Bruker SMART Apex II CCD area detector diffractometer. Cell dimensions and the orientation matrix were initially determined from a least-squares refinement on reflections measured in three sets of 20 exposures, collected in three different  $\omega$  regions, and eventually refined against all data. A full sphere of reciprocal space was scanned by 0.3°  $\omega$  steps. The software SMART (SMART & SAINT Software Reference Manuals, version 5.051 (Windows NT Version), Bruker Analytical X-ray Instruments Inc.: Madison, WI, 1998) was used for collecting frames of data, indexing reflections, and determination of lattice parameters. The collected frames were then processed for integration by the SAINT program and an empirical absorption correction was applied using SADABS.<sup>[112]</sup> The structures were solved by direct methods (SIR 2004)<sup>[113]</sup>

and subsequent Fourier syntheses and refined by full-matrix least-squares on  $F^2$  (SHELXTL, G. M. Sheldrick, SHELXTLplus (Windows NT Version) Structure Determination Package, Version 5.1. Bruker Analytical X-ray Instruments Inc.: Madison, WI, USA, 1998), using anisotropic thermal parameters for all non-hydrogen atoms. All hydrogen atoms were added in calculated positions, included in the final stage of refinement with isotropic thermal parameters,  $U(H) = 1.2 U_{eq}(C)$  [ $U(H) = 1.5 U_{eq}(C-Me)$ ], and allowed to ride on their carrier carbons. Crystal data and details of the data collection for **3ab** and **3ac** are reported in Table 2. 6.

**Table 2. 6** Crystal data and structure refinement for **3ab** and **3ac**.

	3ab	3ac
Formula	C <sub>29</sub> H <sub>27</sub> AuNO <sub>2</sub> PS	C <sub>34</sub> H <sub>29</sub> AuNO <sub>2</sub> PS
Fw	681.51	743.58
T, K	296 (2)	296 (2)
Crystal symmetry	monoclinic	triclinic
Space group	<i>P 2<sub>1</sub>/c</i>	<i>P -1</i>
<i>a</i> , Å	12.285(5)	8.943(5)
<i>b</i> , Å	11.956(5)	12.762(7)
<i>c</i> , Å	18.281(8)	13.472(7)
$\alpha$ , °	90	90.434(5)
$\beta$ , °	91.473	103.985(5)
$\gamma$ , °	90	90.154(5)
Cell volume, Å <sup>3</sup>	2684(2)	1491.9(14)
<i>Z</i>	4	2
$D_C$ , Mg m <sup>-3</sup>	1.686	1.655
$\mu$ (Mo-K $\alpha$ ), mm <sup>-1</sup>	5.644	5.086
F(000)	1336	732
Crystal size mm	0.15 × 0.20 × 0.25	0.20 × 0.20 × 0.25

$\theta$ limits, °	1.66-26.00	1.56-27.03
Refl. collected, unique ( $R_{int}$ )	23071, 5253 (0.0715)	14559, 6424 (0.0500)
Goodness-of-fit-on $F^2$	0.984	0.973
$R_1(F)^a$ , $wR_2(F^2)$ [ $I > 2\sigma(I)$ ] <sup>b</sup>	0.0395, 0.0533	0.0376, 0.0653
Largest diff. peak and hole, e. Å <sup>-3</sup>	0.545, -0.557	0.838, -1.252

<sup>a</sup>  $R_1 = \Sigma||F_o| - |F_c|| / \Sigma|F_o|$ . <sup>b</sup>  $wR_2 = [\Sigma w(F_o^2 - F_c^2)^2 / \Sigma w(F_o^2)^2]^{1/2}$  where  $w = 1 / [\sigma^2(F_o^2) + (aP)^2 + bP]$  where  $P = (F_o^2 + F_c^2) / 3$ .

## 2.5 Bibliography

- [1] A. De Nisi, C. Bergamini, M. Leonzio, G. Sartor, R. Fato, M. Naldi, M. Monari, N. Calonghi, M. Bandini, *Dalt. Trans.* **2016**, *45*, 1546–1553.
- [2] R. Crichton, in *Inorg. Biochem. Iron Metab.*, John Wiley & Sons, Ltd, Chichester, UK, **2002**, pp. 17–48.
- [3] D. Lindsay, W. Kerr, *Nat. Chem.* **2011**, *3*, 494–494.
- [4] J. Osredkar, *J. Clin. Toxicol.* **2011**, *s3*:001.
- [5] R. A. Festa, D. J. Thiele, *Curr. Biol.* **2011**, *21*, R877-R883.
- [6] M. Hayyan, M. A. Hashim, I. M. Alnashef, *Chem. Rev.* **2016**, *116*, 3029–3085.
- [7] Stephen J. Lippard, in *Bioinorg. Chem.*, **1994**, pp. 505–583.
- [8] B. Rosenberg, L. Van Camp, T. Krigas, *Nature* **1965**, *205*, 698–699.
- [9] K. H. Thompson, C. Orvig, *Science* **2003**, *300*, 936–9.
- [10] A. K. Pachet, A. M. Wisniewski, *Psychopharmacology (Berl)*. **2003**, *170*, 225–234.
- [11] D. W. Bierer, *Rev. Infect. Dis.* **1990**, *12*, S3–S8.
- [12] H. L. DuPont, *Nat. Clin. Pract. Gastroenterol. Hepatol.* **2005**, *2*, 191–198.
- [13] A. Madisch, A. Morgner, M. Stolte, S. Miehle, *Expert Opin. Investig. Drugs* **2008**, *17*, 1829–1837.
- [14] S. Jurisson, D. Berning, W. Jia, D. Ma, *Chem. Rev.* **1993**, *93*, 1137–1156.
- [15] E. Terreno, D. D. Castelli, A. Viale, S. Aime, *Chem. Rev.* **2010**, *110*, 3019–3042.
- [16] M. Varol, *J. Appl. Pharm.* **2016**, *8*, 385–386.

- [17] S. I. Hajdu, *Cancer* **2011**, *117*, 1097–1102.
- [18] W. H. Organization, “WHO, Cancer,” can be found under <http://www.who.int/mediacentre/factsheets/fs297/en/>, **2017**.
- [19] R. J. Papac, *Yale J. Biol. Med.* **2001**, *74*, 391–398.
- [20] A. Gilman, F. S. Philips, C. C. Hunt, F. S. Philips, L. S. Goodman, M. M. Wintrobe, W. Dameshek, M. J. Goodman, A. Gilman, M. T. McLennan, et al., *Am. J. Surg.* **1963**, *105*, 574–8.
- [21] R. CP, *J. Am. Med. Assoc.* **1946**, *131*, 656–658.
- [22] S. Farber, L. K. Diamond, R. D. Mercer, R. F. Sylvester, J. A. Wolff, *N. Engl. J. Med.* **1948**, *238*, 787–793.
- [23] B. Rosenberg, L. Van Camp, J. E. Trosko, V. H. Mansour, *Nature* **1969**, *222*, 385–386.
- [24] M. Rozenzweig, *Ann. Intern. Med.* **1977**, *86*, 803.
- [25] M. S. Davies, S. J. Berners-Price, T. W. Hambley, *J. Inorg. Biochem.* **2000**, *79*, 167–172.
- [26] D. Wang, S. J. Lippard, *Nat. Rev. Drug Discov.* **2005**, *4*, 307–320.
- [27] Z. H. Siddik, *Oncogene* **2003**, *22*, 7265–7279.
- [28] A. Eastman, in *Cisplatin Chem. Biochem. a Lead. Anticancer Drug*, Verlag Helvetica Chimica Acta, Zürich, **2006**, pp. 111–134.
- [29] R. Canetta, M. Rozenzweig, S. K. Carter, *Cancer Treat. Rev.* **1985**, *12*, 125–136.
- [30] T. Alcindor, N. Beauger, *Curr. Oncol.* **2011**, *18*, 18–25.
- [31] M. Shimada, H. Itamochi, J. Kigawa, *Cancer Manag. Res.* **2013**, *5*, 67–76.
- [32] U. Ndagi, N. Mhlongo, M. E. Soliman, *Drug Des. Devel. Ther.* **2017**, *11*, 599–616.

- [33] S. Leijen, S. A. Burgers, P. Baas, D. Pluim, M. Tibben, E. Van Werkhoven, E. Alessio, G. Sava, J. H. Beijnen, J. H. M. Schellens, *Invest. New Drugs* **2015**, *33*, 201–214.
- [34] S. K. Stevens, A. P. Strehle, R. L. Miller, S. H. Gammons, K. J. Hoffman, J. T. McCarty, M. E. Miller, L. K. Stultz, P. K. Hanson, *Mol. Pharmacol.* **2013**, *83*, 225–34.
- [35] J. B. Mangrum, N. P. Farrell, *Chem. Commun. (Camb)*. **2010**, *46*, 6640–6650.
- [36] W. H. Ang, A. Casini, G. Sava, P. J. Dyson, *J. Organomet. Chem.* **2011**, *696*, 989–998.
- [37] T. Gianferrara, I. Bratsos, E. Alessio, *Dalt. Trans.* **2009**, *0*, 7588.
- [38] A. Vessières, S. Top, W. Beck, E. Hillard, G. Jaouen, *Dalt. Trans.* **2006**, *47*, 529–541.
- [39] S. P. Fricker, *Gold Bull.* **1996**, *29*, 53–60.
- [40] “Gold Face Cream: A Costly Leap of Faith - The New York Times,” can be found under <http://www.nytimes.com/2010/05/27/fashion/27skinWEB.html>, **n.d.**
- [41] Jacine Greenwood, “Educated therapists - Gold in cosmetics... Does it really do anything?,” can be found under <http://www.educatedtherapists.com/gold-in-cosmetics-does-it-really-do-anything/>, **n.d.**
- [42] G. D. Champion, G. G. Graham, J. B. Ziegler, *Baillieres. Clin. Rheumatol.* **1990**, *4*, 491–534.
- [43] B. M. Sutton, E. Mcgusty, D. T. Walz, M. J. Dimartino, *J. Med. Chem.* **1972**, *15*, 1095–1098.
- [44] S. L. Best, P. J. Sadler, *Gold Bull.* **1996**, *29*, 87–93.
- [45] S. T. Crooke, R. M. Snyder, T. R. Butt, D. J. Ecker, H. S. Allaudeen,



- B. Monia, C. K. Mirabelli, *Biochem. Pharmacol.* **1986**, *35*, 3423–3431.
- [46] B. Chirullo, R. Sgarbanti, D. Limongi, I. L. Shytaj, D. Alvarez, B. Das, A. Boe, S. DaFonseca, N. Chomont, L. Liotta, et al., *Cell Death Dis.* **2013**, *4*, e944.
- [47] I. Shytaj, B. Chirullo, W. Wagner, M. G. Ferrari, R. Sgarbanti, A. Corte, C. LaBranche, L. Lopalco, A. Palamara, D. Montefiori, et al., *Retrovirology* **2013**, *10*, 71.
- [48] E. R. Sharlow, S. Leimgruber, S. Murray, A. Lira, R. J. Sciotti, M. Hickman, T. Hudson, S. Leed, D. Caridha, A. M. Barrios, et al., *ACS Chem. Biol.* **2014**, *9*, 663–672.
- [49] A. Ilari, P. Baiocco, L. Messori, A. Fiorillo, A. Boffi, M. Gramiccia, T. Di Muccio, G. Colotti, *Amino Acids* **2012**, *42*, 803–811.
- [50] Y. Hokai, B. Jurkowicz, J. Fernández-Gallardo, N. Zakirkhodjaev, M. Sanaú, T. R. Muth, M. Contel, *J. Inorg. Biochem.* **2014**, *138*, 81–88.
- [51] S. Jackson-Rosario, D. Cowart, A. Myers, R. Tarrien, R. L. Levine, R. A. Scott, W. T. Self, *J. Biol. Inorg. Chem.* **2009**, *14*, 507–519.
- [52] J. M. Madeira, E. Bajwa, M. J. Stuart, S. Hashioka, A. Klegeris, *J. Neuroimmunol.* **2014**, *276*, 71–79.
- [53] J. M. Madeira, C. J. Renschler, B. Mueller, S. Hashioka, D. L. Gibson, A. Klegeris, *Life Sci.* **2013**, *92*, 1072–1080.
- [54] C. Fan, W. Zheng, X. Fu, X. Li, Y.-S. Wong, T. Chen, *Cell Death Dis.* **2014**, *5*, e1191.
- [55] W. Fiskus, N. Saba, M. Shen, M. Ghias, J. Liu, S. Das Gupta, L. Chauhan, R. Rao, S. Gunewardena, K. Schorno, et al., *Cancer Res.* **2014**, *74*, 2520–2532.
- [56] C. Marzano, V. Gandin, A. Folda, G. Scutari, A. Bindoli, M. P. Rigobello, *Free Radic. Biol. Med.* **2007**, *42*, 872–881.

- [57] S. Urig, K. Fritz-Wolf, R. Réau, C. Herold-Mende, K. Tóth, E. Davioud-Charvet, K. Becker, *Angew. Chemie - Int. Ed.* **2006**, *45*, 1881–1886.
- [58] R. P. Hirt, S. Müller, T. Martin Embley, G. H. Coombs, *Trends Parasitol.* **2002**, *18*, 302–308.
- [59] J. Lu, A. Holmgren, *Antioxid. Redox Signal.* **2012**, *17*, 1738–1747.
- [60] S. Urig, K. Becker, *Semin. Cancer Biol.* **2006**, *16*, 452–465.
- [61] J. D. Pennington, K. M. Jacobs, L. Sun, G. Bar-Sela, M. Mishra, D. Gius, *Curr. Pharm. Des.* **2007**, *13*, 3368–77.
- [62] A. Bindoli, M. P. Rigobello, G. Scutari, C. Gabbiani, A. Casini, L. Messori, *Coord. Chem. Rev.* **2009**, *253*, 1692–1707.
- [63] F. Angelucci, A. A. Sayed, D. L. Williams, G. Boumis, M. Brunori, D. Dimastrogiovanni, A. E. Miele, F. Pauly, A. Bellelli, *J. Biol. Chem.* **2009**, *284*, 28977–28985.
- [64] T. Zou, C. T. Lum, C.-N. Lok, J.-J. Zhang, C.-M. Che, *Chem. Soc. Rev.* **2015**, *44*, 8786–8801.
- [65] M. P. Rigobello, A. Folda, M. C. Baldoïn, G. Scutari, A. Bindoli, *Free Radic. Res.* **2005**, *39*, 687–695.
- [66] E. Weidauer, Y. Yasuda, B. K. Biswal, M. Cherny, M. N. G. James, D. Brömme, *Biol. Chem.* **2007**, *388*, 331–336.
- [67] K. P. Bhabak, G. Mugesh, *Inorg. Chem.* **2009**, *48*, 2449–2455.
- [68] M. J. Berry, J. David Kieffer, P. Reed Larsen, *Endocrinology* **1991**, *129*, 550–552.
- [69] J. Zou, P. Taylor, J. Dornan, S. P. Robinson, M. D. Walkinshaw, P. J. Sadler, *Angew. Chemie - Int. Ed.* **2000**, *39*, 2931–2934.
- [70] C. F. Shaw, A. A. Isab, M. T. Coffey, C. K. Mirabelli, *Biochem.*

*Pharmacol.* **1990**, *40*, 1227–1234.

- [71] R. M. Snyder, C. K. Mirabelli, S. T. Crooke, *Biochem. Pharmacol.* **1986**, *35*, 923–932.
- [72] A. P. Martins, A. Ciancetta, A. DeAlmeida, A. Marrone, N. Re, G. Soveral, A. Casini, *ChemMedChem* **2013**, *8*, 1086–1092.
- [73] J.-J. Zhang, K.-M. Ng, C.-N. Lok, R. W.-Y. Sun, C.-M. Che, *Chem. Commun.* **2013**, *49*, 5153.
- [74] P. Zhang, P. J. Sadler, *J. Organomet. Chem.* **2017**, *839*, 5–14.
- [75] C.-M. Che, R. W.-Y. Sun, W.-Y. Yu, C.-B. Ko, N. Zhu, H. Sun, *Chem. Commun.* **2003**, *0*, 1718.
- [76] T. Gamberi, L. Massai, F. Magherini, I. Landini, T. Fiaschi, F. Scaletti, C. Gabbiani, L. Bianchi, L. Bini, S. Nobili, et al., *J. Proteomics* **2014**, *103*, 103–120.
- [77] D. Saggioro, M. P. Rigobello, L. Paloschi, A. Folda, S. A. Moggach, S. Parsons, L. Ronconi, D. Fregona, A. Bindoli, *Chem. Biol.* **2007**, *14*, 1128–1139.
- [78] S. J. Berners-Price, P. J. Barnard, in *Ligand Des. Med. Inorg. Chem.*, John Wiley & Sons, Ltd, Chichester, UK, **2014**, pp. 227–256.
- [79] M. Deponte, S. Urig, L. D. Arscott, K. Fritz-Wolf, R. Réau, C. Herold-Mende, S. Koncarevic, M. Meyer, E. Davioud-Charvet, D. P. Ballou, et al., *J. Biol. Chem.* **2005**, *280*, 20628–20637.
- [80] M. F. Braña, A. Ramos, *Curr. Med. Chem. Anticancer. Agents* **2001**, *1*, 237–255.
- [81] A. Meyer, L. Oehninger, Y. Geldmacher, H. Alborzina, S. Wölfl, W. S. Sheldrick, I. Ott, *ChemMedChem* **2014**, *9*, n/a-n/a.
- [82] C. P. Bagowski, Y. You, H. Scheffler, D. H. Vlecken, D. J. Schmitz, I. Ott, *Dalt. Trans.* **2009**, *0*, 10799.

- [83] T. Zou, C.-N. Lok, Pui-Ki Wan, Zhi-Feng Zhang, Sin-Ki Fung, C.-M. Che, *Curr. Opin. Chem. Biol.* **2018**, *43*, 30–36.
- [84] M. V. Baker, P. J. Barnard, S. J. Berners-Price, S. K. Brayshaw, J. L. Hickey, B. W. Skelton, A. H. White, *Dalt. Trans.* **2006**, *0*, 3708.
- [85] P. J. Barnard, M. V. Baker, S. J. Berners-Price, D. A. Day, in *J. Inorg. Biochem.*, Elsevier, **2004**, pp. 1642–1647.
- [86] J. L. Hickey, R. A. Ruhayel, P. J. Barnard, M. V. Baker, S. J. Berners-Price, A. Filipovska, *J. Am. Chem. Soc.* **2008**, *130*, 12570–12571.
- [87] P. J. Barnard, S. J. Berners-Price, *Coord. Chem. Rev.* **2007**, *251*, 1889–1902.
- [88] S. J. Berners-Price, A. Filipovska, *Metallomics* **2011**, *3*, 863.
- [89] S. J. Berners-Price, P. S. Jarrett, P. J. Sadler, G. R. Girard, D. T. Hill, B. M. Sutton, L. F. Faucette, R. K. Johnson, C. K. Mirabelli, *J. Med. Chem.* **1990**, *33*, 1386–1392.
- [90] M. J. McKeage, S. J. Berners-Price, P. Galettis, R. J. Bowen, W. Brouwer, L. Ding, L. Zhuang, B. C. Baguley, *Cancer Chemother. Pharmacol.* **2000**, *46*, 343–350.
- [91] S. J. Berners-Price, C. K. Mirabelli, R. K. Johnson, M. R. Mattern, F. L. McCabe, L. F. Faucette, C. M. Sung, S. M. Mong, P. J. Sadler, S. T. Crooke, *Cancer Res.* **1986**, *46*, 5486–93.
- [92] A. S. Humphreys, A. Filipovska, S. J. Berners-Price, G. A. Koutsantonis, B. W. Skelton, A. H. White, *Dalt. Trans.* **2007**, *0*, 4943.
- [93] E. Schuh, S. M. Valiahdi, M. A. Jakupec, B. K. Keppler, P. Chiba, F. Mohr, *Dalt. Trans.* **2009**, *0*, 10841–10845.
- [94] E. Vergara, E. Cerrada, A. Casini, O. Zava, M. Laguna, P. J. Dyson, *Organometallics* **2010**, *29*, 2596–2603.
- [95] A. Meyer, C. P. Bagowski, M. Kokoschka, M. Stefanopoulou, H.

- Alborzina, S. Can, D. H. Vlecken, W. S. Sheldrick, S. Wölfl, I. Ott, *Angew. Chemie - Int. Ed.* **2012**, *51*, 8895–8899.
- [96] A. Meyer, A. Gutiérrez, I. Ott, L. Rodríguez, *Inorganica Chim. Acta* **2013**, *398*, 72–76.
- [97] A. De Almeida, B. L. Oliveira, J. D. G. Correia, G. Soveral, A. Casini, *Coord. Chem. Rev.* **2013**, *257*, 2689–2704.
- [98] C. K. Mirabelli, D. T. Hill, L. F. Faucette, F. L. McCabe, G. R. Girard, R. K. Johnson, S. T. Crooke, J. O. L. Bartus, B. M. Sutton, D. B. Bryan, *J. Med. Chem.* **1987**, *30*, 2181–2190.
- [99] D. Martínez-Maqueda, B. Miralles, I. Recio, in *Impact Food Bioact. Heal. Vitr. Ex Vivo Model.*, Springer International Publishing, Cham, **2015**, pp. 113–124.
- [100] E. Cohen, I. Ophir, Y. B. Shaul, *J. Cell Sci.* **1999**, *112* ( Pt 1), 2657–66.
- [101] E. Erba, D. Bergamaschi, L. Bassano, S. Ronzoni, G. Di Liberti, I. Muradore, S. Vignati, G. Faircloth, J. M. Jimeno, M. D’Incalci, *Br. J. Cancer* **2000**, *82*, 1732–1739.
- [102] R. Gallagher, S. Collins, J. Trujillo, K. McCredie, M. Ahearn, S. Tsai, R. Metzgar, G. Aulakh, R. Ting, F. Ruscetti, et al., *Blood* **1979**, *54*, 713–733.
- [103] T. Mosmann, *J. Immunol. Methods* **1983**, *65*, 55–63.
- [104] A. Casini, C. Gabbiani, F. Sorrentino, M. P. Rigobello, A. Bindoli, T. J. Geldbach, A. Marrone, N. Re, C. G. Hartinger, P. J. Dyson, et al., *J. Med. Chem.* **2008**, *51*, 6773–6781.
- [105] C. Trampitsch, A. Slavica, W. Riethorst, B. Nidetzky, *J. Mol. Catal. B Enzym.* **2005**, *32*, 271–278.
- [106] M. Naldi, F. A. Giannone, M. Baldassarre, M. Domenicali, P. Caraceni, M. Bernardi, C. Bertucci, *Eur. J. Mass Spectrom.* **2013**, *19*,

491–496.

- [107] P. Pozarowski, Z. Darzynkiewicz, in *Checkp. Control. Cancer*, Humana Press, New Jersey, **2004**, pp. 301–312.
- [108] Cooper GM., *The Cell: A Molecular Approach. Chromosomes and Chromatin.*, **2000**.
- [109] Flow cytometric analysis of cell cycle with propidium iodide DNA staining, [www.abcam.com](http://www.abcam.com), **2009**.
- [110] J. Olmsted, D. R. Kearns, *Biochemistry* **1977**, *16*, 3647–3654.
- [111] A. Albert, C. Brauckmann, F. Blaske, M. Sperling, C. Engelhard, U. Karst, *J. Anal. At. Spectrom.* **2012**, *27*, 975.
- [112] G. M. Sheldrick, *There is no Corresp. Rec. this Ref.* **1996**.
- [113] M. C. Burla, R. Caliendo, M. Camalli, B. Carrozzini, G. L. Cascarano, L. De Caro, C. Giacobazzo, G. Polidori, R. Spagna, *J. Appl. Crystallogr.* **2005**, *38*, 381–388.

# 3 GOLD(I)-CATALYSED DEAROMATIVE [2+2]- CYCLOADDITION OF INDOLES WITH ACTIVATED ALLENES

In this chapter, an investigation on the dearomative formal [2+2]-cycloaddition reaction between 2,3-disubstituted indoles and allenamides, to give densely functionalized 2,3-cyclobutyl-indolines is presented. In particular, the gold-catalysed racemic and enantioselective condensations of allenamide/aryloxyallenes with a range of N-substituted indoles is discussed. Moreover, in collaboration with Professor Gian Piero Miscione's group, a detailed computational investigation at the density functional theory (DFT) level is carried out to obtain a mechanistic insight. This chapter is published on *Chemistry, a European Journal*<sup>[1]</sup> and is reproduced from ref [1] with John Wiley and Sons license number 4193560285611.

### 3.1 Introduction

Achieving chemical complexity in indolyl-based alkaloid chemistry is a current hot topic within the synthetic organic chemistry scenario.<sup>[2,3]</sup> In particular, the intrinsic molecular diversity of synthetic and natural occurring compounds belonging to this family continues to inspire further developments in organic synthesis. To this aim, catalysis is the ultimate forefront in the area with a large portfolio of reliable metal- and metal-free methodologies nowadays available.<sup>[4,5]</sup>

Partially dearomatized C(2),C(3)-polycyclic fused indoline and indolenine motifs are widely diffused molecular architectures in indole alkaloids, featuring stereochemically defined all carbon quaternary stereocenters at the C(3)-position.<sup>[6–10]</sup> A collection of titled compounds is reported in Figure 3.1.

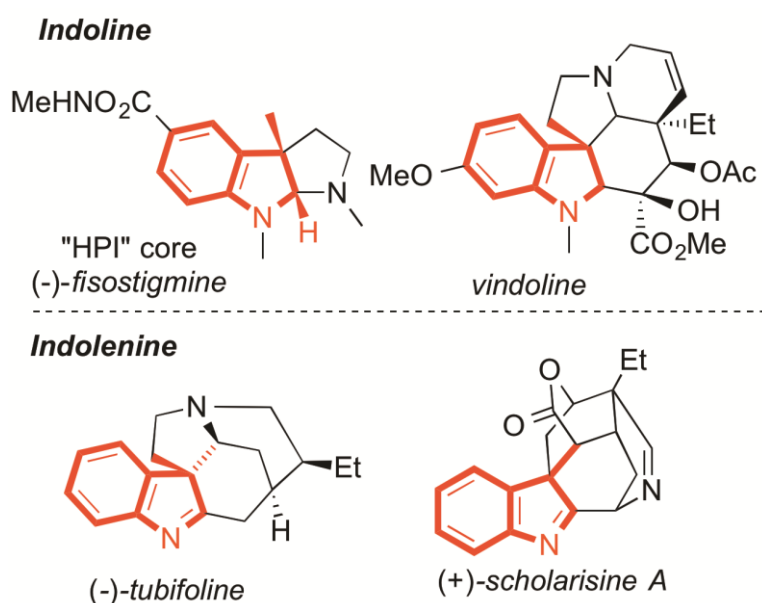


**Figure 3.1** Collection of natural products featuring polycyclic C(2),(3)-fused indoline and indolenine scaffolds.

Among the numerous catalytic methodologies available, the enantioselective C(2),C(3)-annulation of indoles via cycloaddition reactions is gaining growing credit in terms of chemical efficiency. Based on these methodologies, densely functionalized C(2),C(3)-fused cyclopropa-



([2+1]),<sup>[11]</sup> cyclopenta- ([3+2])<sup>[12–15]</sup> and cyclohexa-indoline cores ([3+3])<sup>[16]</sup> have been prepared in stereochemically defined manners.

Intriguingly, C(2),C(3)-indolincyclobutanes<sup>[17,18]</sup> have found less attention in literature. More precisely, besides the elegant intramolecular approach reported by Zhang,<sup>[19]</sup> the cyclobutyl-fused indole species was isolated only in low yields via condensation of allenamides with indoles by Lopéz, and Mascareñas.<sup>[20]</sup> Additionally, Xie and co-workers documented the dearomative [2+2]-cycloaddition between *o*-carboryne and N-silylated indoles under thermal conditions.<sup>[21]</sup>

In this context, as explained in chapter 1, gold catalysis offers unique opportunities due to the peculiar attitude of this coinage metal in promoting cycloaddition transformations via electrophilic activation of  $\pi$ -systems.<sup>[22–24]</sup> Recently, Bandini and co-workers exploited the potentiality of gold-based catalysis and documented the first enantioselective gold catalysed synthesis of C(2),C(3)-indolincyclobutanes via formal [2+2]-cycloaddition reactions between N-protected indoles and allenamides (see Figure 3.2).<sup>[25]</sup>

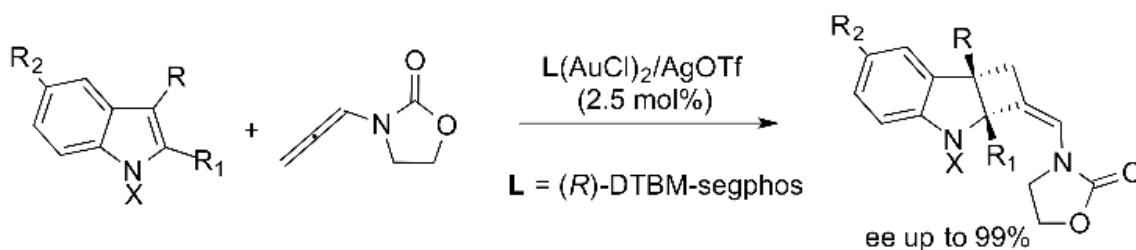


**Figure 3.2** Preliminary results on the gold-catalysed asymmetric condensation of indoles and allenamides.

With the aim of expanding the scope of the previous work, a comprehensive investigation on the dearomative formal [2+2]-cycloaddition reaction between 2,3-disubstituted indoles and allenamides, to give densely functionalized 2,3-cyclobutyl-indolines is presented. In particular, the gold catalysed racemic and enantioselective condensations of allenamide/aryloxyallenes with a range of N-substituted indoles **1** will be discussed. Moreover, a detailed computational investigation at the Density

Functional Theory (DFT) level is carried out in order to obtain a mechanistic insight on the high regioselectivity experimentally observed.

The complete range of indoles (**1**) and allenyl-derivatives (**2** and **3**) herein employed has been collected in Figure 3.3.

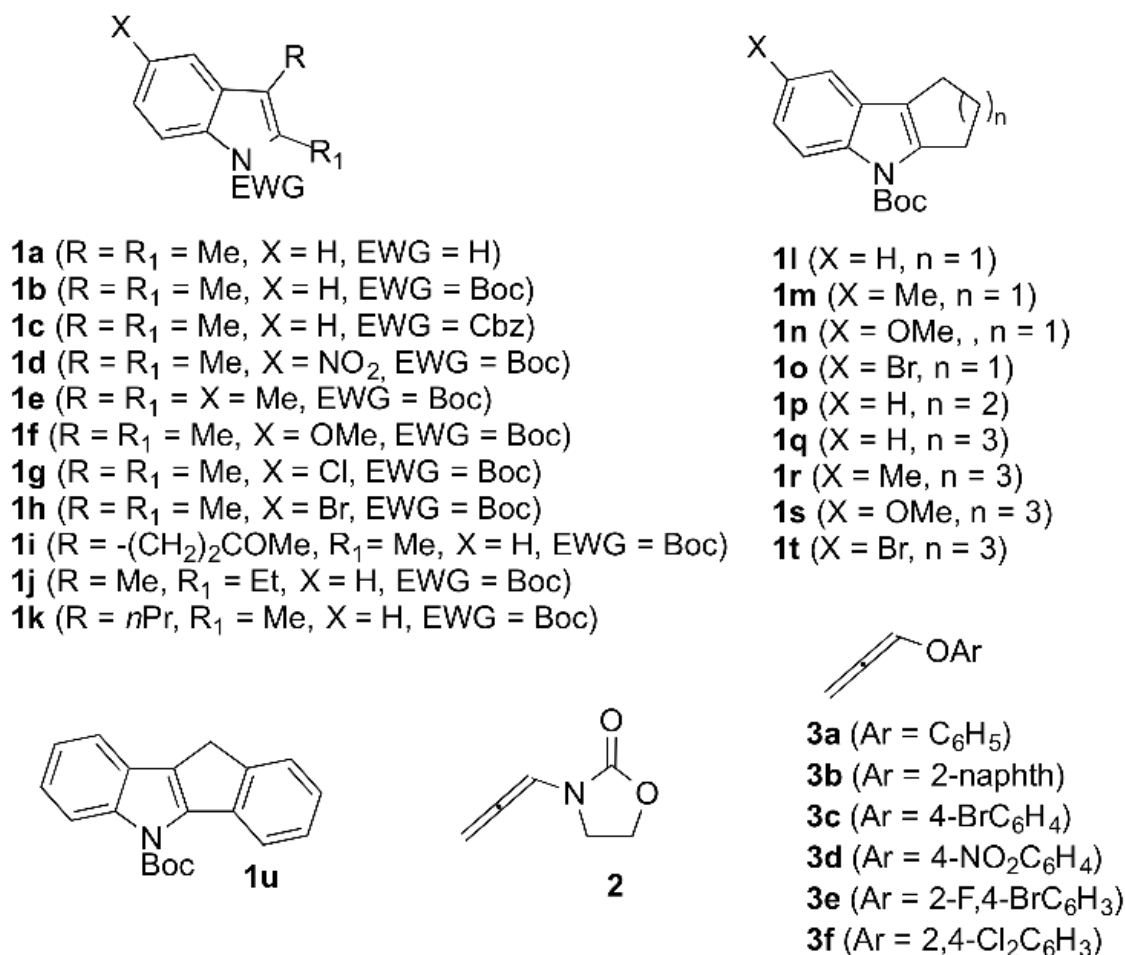


**Figure 3.3** List of all indoles **1**, allemanide **2** and aryloxy allene **3** employed in this work.

## 3.2 Results and discussion

### 3.2.1 Gold catalysed dearomatization reaction: the racemic version (allenamides)

To optimize the synthesis of indolyl-2,3-cyclobutyl derivatives via cycloaddition reaction between electron-rich allenes and indoles, a range of cationic [Au(I)] complexes in the model reaction involving the nitrogen free 2,3(Me)<sub>2</sub>-indole **1a** and the allenamide **2** were initially examined. At the same time, a survey of reaction conditions elected DCM as the best reaction

medium, since other solvents furnished lower isolated yields of **4a** (CH<sub>3</sub>CN=21 %, THF=17 %, toluene=15 %, DCE (80 °C)=22 %). Initial attempts afforded the partially dearomatized indolenine **5a** and the nitrogen-allylated indole **6a** as main by-products of the process as shown in Figure 3.4.

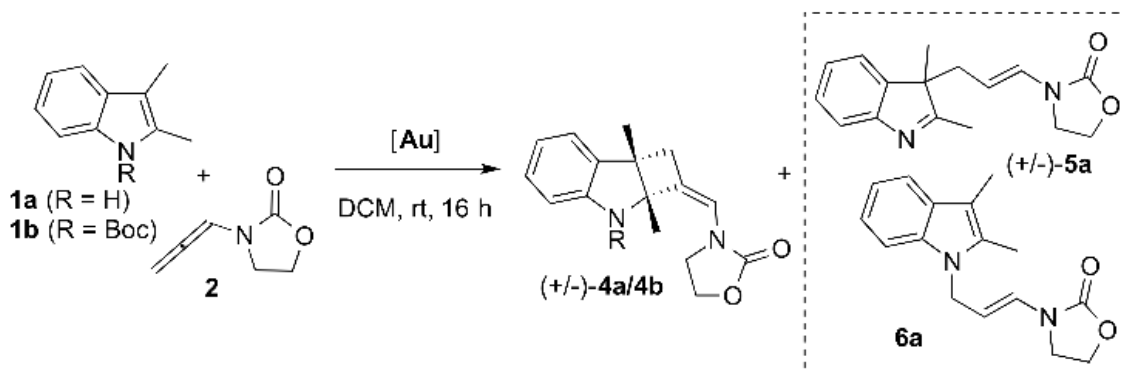


**Figure 3.4** Scheme of reaction of the formal [2+2]-cycloaddition between indole **1** and allenamide **2**.

From the collection of results summarized on Table 3.1, clearly emerged the attitude of [JohnPhosAu(NCMe)]SbF<sub>6</sub><sup>[26,27]</sup> in promoting the cycloaddition, providing the [2+2]-adduct **4a** as the major product (entry 6, yield = 49%) under mild reaction conditions (CH<sub>2</sub>Cl<sub>2</sub>, rt, 16 h).

**Table 3.1** Optimization of the reaction conditions for the racemic variant of the formal [2+2]-cycloaddition reaction.<sup>a</sup>

Run	[Au] (5 mol%)	Yield (%) <sup>b</sup> <b>4</b>	Yield (%) <sup>b</sup> <b>5a/6a</b>
1	JackiePhosAuNTf <sub>2</sub>	< 5 ( <b>4a</b> )	22 / 33
2	Ph <sub>3</sub> PAuNTf <sub>2</sub>	6 ( <b>4a</b> )	18 / 75
3	XPhosAuNTf <sub>2</sub>	19 ( <b>4a</b> )	-- / --
4	JohnPhosAuTFA	< 5 ( <b>4a</b> )	77 / < 5
5	XPhosAuTFA	8 ( <b>4a</b> )	70 / < 5
6	[JohnPhosAu(NCMe)]SbF <sub>6</sub>	49 ( <b>4a</b> )	5 / --
7	[JohnPhosAu(NCMe)]SbF <sub>6</sub>	40 ( <b>4a</b> )	-- / --
8	[JohnPhosAu(NCMe)]SbF <sub>6</sub>	60 ( <b>4b</b> )	-- / --
9 <sup>c</sup>	[JohnPhosAu(NCMe)]SbF <sub>6</sub>	73 ( <b>4b</b> )	-- / --
10 <sup>d</sup>	[JohnPhosAu(NCMe)]SbF <sub>6</sub>	89 ( <b>4b</b> )	-- / --

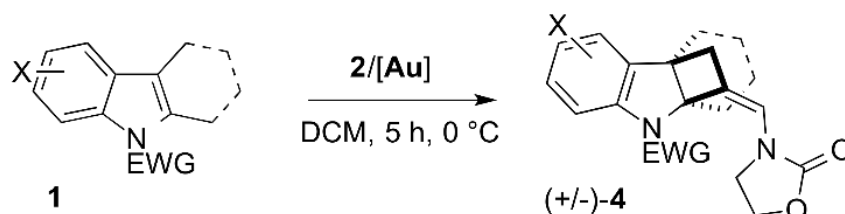
<sup>a</sup> All the reactions were carried out under nitrogen atmosphere (**1**:**2**:**[Au]** = 1.2:1:0.05). <sup>b</sup> Isolated yields after flash chromatography. <sup>c</sup> T = - 20 °C, t = 5 h. <sup>d</sup> T = - 40 °C, t = 16 h.

Based on these promising results, it was supposed that the introduction of an electron-withdrawing group at the N(1)-position of the indole could have significant effects on the reaction mechanism and its energetics by preventing the undesired N-alkylation (**6a**) and by increasing the electrophilic character of the intermediate immonium derivative (vide infra for further mechanistic details).<sup>[28,29]</sup> It was proved that, N(Boc)-2,3-(Me)<sub>2</sub>-indole **1b** is a competent reaction partner providing the desired diastereomerically pure cyclobutyl derivative **4b** in 60%, 73% and 89% yield at room temperature, - 20 °C and - 40 °C, respectively (entries 8-10 of Table 3.1). The increase of isolated yields at lower temperatures can be rationalized in terms of minimization of gold-promoted self-condensation of **2** (dimerization or polymerization).<sup>[30]</sup>

Concerning the stereochemical aspects, optimal conditions provided the *cis*-C(2),C(3)-fused tricyclic compounds in high diastereomeric ratio (d.r. =

20:1). Furthermore, the *exo*-C=C double bond was exclusively obtained in the *Z* configuration.

The scope of the reaction was then examined by reacting a range of *N*-protected-2,3-disubstituted indoles (**1c-u**) under the conditions of election (Figure 3.5).

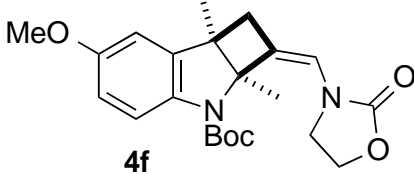
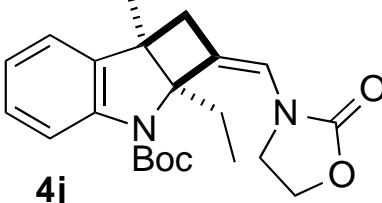
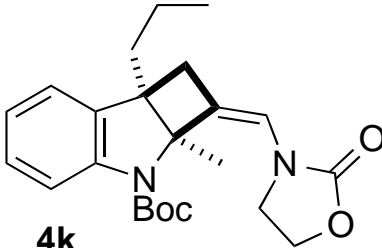
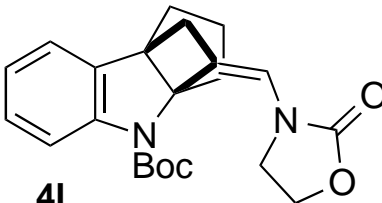
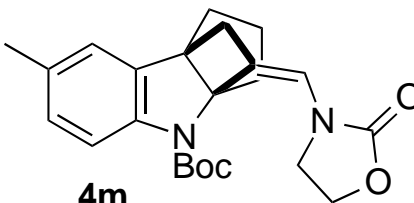
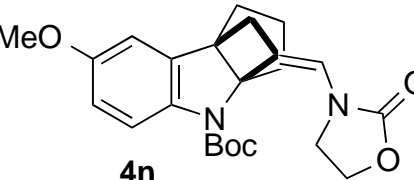
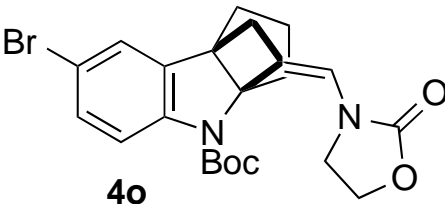


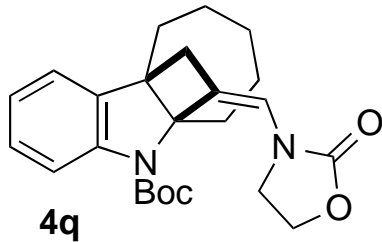
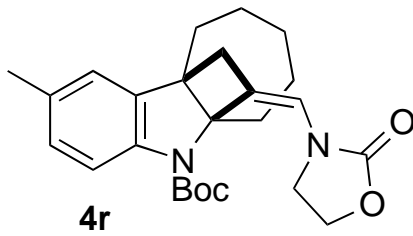
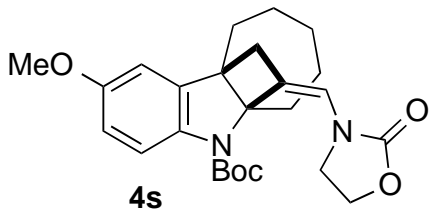
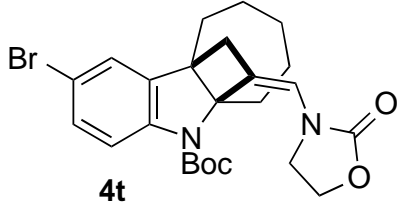
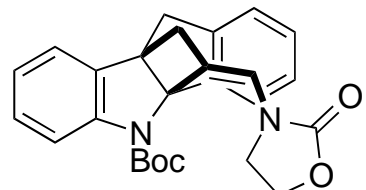
**Figure 3.5** Scheme of reaction for the indole scope of the dearomative [2+2]-cycloaddition.

The obtained results are collected in Table 3.2.

**Table 3.2** Indole scope of the dearomative [2+2]-cycloaddition.<sup>a</sup>

Run	1	Product (3)	Yield (%) <sup>b</sup>
1	<b>1c</b>	 <b>4c</b>	95
2	<b>1d</b>	 <b>4d</b>	NR
3	<b>1e</b>	 <b>4e</b>	76

4	<b>1f</b>	 <p><b>4f</b></p>	85
5	<b>1j</b>	 <p><b>4j</b></p>	64
6	<b>1k</b>	 <p><b>4k</b></p>	62
7	<b>1l</b>	 <p><b>4l</b></p>	78
8	<b>1m</b>	 <p><b>4m</b></p>	75
9	<b>1n</b>	 <p><b>4n</b></p>	80
10	<b>1o</b>	 <p><b>4o</b></p>	60

11	<b>1q</b>		81
		<b>4q</b>	
12	<b>1r</b>		70
		<b>4r</b>	
13	<b>1s</b>		70
		<b>4s</b>	
14	<b>1t</b>		41
		<b>4t</b>	
15	<b>1u</b>		95
		<b>4u</b>	

<sup>a</sup> All the reactions were carried out under nitrogen atmosphere [Au]: [JohnPhosAu(NCMe)]SbF<sub>6</sub> (5 mol%). <sup>b</sup> Isolated yields after flash chromatography. Each compound was isolated as a single diastereoisomer. NR = no reaction.

Interestingly, the presence of C5- and C7-membered cycles fused at the C(2),C(3)-positions of the pyrrolyl ring (**1l-u**) were adequately tolerated providing the corresponding tetra- and pentacyclic compounds **4l-u** from moderate to excellent yields (41-95%). Similarly, the cycloadducts **4c-k** were obtained in high yield from indoles carrying acyclic C(2),C(3) substituents (**1c-k**). This screening significantly addressed also the tolerance towards substituents on the benzene ring. In particular, electron-donating

(i.e. Me, OMe) and moderately electron-withdrawing groups (i.e. Br) were found to be effective in the process. On the contrary, strong electron-withdrawing NO<sub>2</sub> group (C(5), **1d**) completely suppressed the kinetics of the transformation (entry 2 in Table 3.2). Finally, the Boc-protecting group was also successfully replaced by Cbz (**1c**) with an untouched isolated yield (95%).

Also, it is worth mentioning that, the 2,3-disubstitution pattern at the indole core was mandatory for the reaction course. More precisely, while with N-Boc-indole and N-Boc-3-Me-indole the dimerization products of **2** were the main outcomes, N-Boc-2-Me-indole furnished the desired [2+2]-cycloadduct only in 18% yield.

### 3.2.2 Gold catalysed dearomatization reaction: the racemic version (aryloxyallene)

Aryloxyallenes are an important class of electron-rich  $\pi$ -systems that found extensive applications in organic chemistry, with particular concern to cycloaddition reactions and site-selective condensation with nucleophilic agents.<sup>[31]</sup> Analogously to the afore-described allenamides, the nucleophilic addition to the  $\gamma$ -carbon would lead to a formal allylation reaction with the simultaneous insertion of a synthetically versatile enol ether moiety.

Despite their undoubted synthetic interest, to the best of our knowledge, this family of unsaturated compounds has never been employed in dearomative processes up to now.

To assess the possibility of extending this synthetic methodology to aryloxyallenes, a range of allenyl derivatives (**3a-f**) was synthesized via a conventional two-step procedure (i.e. propargylation of the corresponding phenol followed by base-assisted isomerization) and subjected to the dearomative cyclization in the presence of **1b** and [JohnPhosAu(NCMe)]SbF<sub>6</sub> (1-5 mol%).



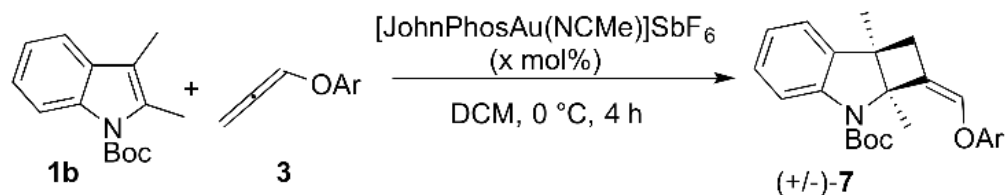


**Figure 3.6** Scheme of reaction between **1b** and aryloxyallenes **3**.

Electron-“neutral” and electron-poor arenes were employed in order to guarantee synthetically acceptable stability of the corresponding allenes. Aryloxyallenes featuring electron-rich arenes proved to self-polymerize rapidly even at low temperatures and turned out to be unsuitable for the present protocol.

**Table 3.3** Gold catalysed dearomative [2+2]-cycloaddition between **1b** and aryloxyallenes **3**.<sup>a</sup>

Run	[Au] (x mol%)	3 (Ar)	Yield <b>7</b> (%) <sup>b</sup>
1	5	<b>3a</b> (Ph)	75 ( <b>7ba</b> )
2	1	<b>3b</b> ( $\beta$ -naphth)	83 ( <b>7bb</b> )
3	5	<b>3c</b> ( <i>p</i> BrC <sub>6</sub> H <sub>5</sub> )	96 ( <b>7bc</b> )
4	5	<b>3d</b> ( <i>p</i> NO <sub>2</sub> C <sub>6</sub> H <sub>5</sub> )	81 ( <b>7bd</b> )
5	5	<b>3e</b> ( <i>p</i> F, <i>o</i> BrC <sub>6</sub> H <sub>4</sub> )	83 ( <b>7be</b> )
6	5	<b>3f</b> ( <i>p</i> , <i>o</i> Cl <sub>2</sub> C <sub>6</sub> H <sub>4</sub> )	95 ( <b>7bf</b> )

<sup>a</sup> All the reactions were carried out under nitrogen atmosphere (**1b**:**3** = 1.2:1). <sup>b</sup> Isolated yields after flash chromatography. *d.r.* > 20 :1.

The synthetic procedure turned out to be extraordinarily adaptable to a variety of aryloxyallenes. Accordingly, a range of racemic methylene cyclobutanes **7** (Table 3.3) was isolated as a single stereoisomer in good to excellent yields (75-96%) under mild reaction conditions ([Au]: 1-5 mol%, DCM, 0 °C, 4 h).

Subsequently, the substrate scope was further investigated by condensing differently substituted N-Boc-indoles and allenes **3b** and **3d**. The results reported in the Figure 3.7 emphasize the efficiency of the above-described gold-catalysed methodology in providing densely functionalized tricyclic fused indolenyl scaffolds **7**.

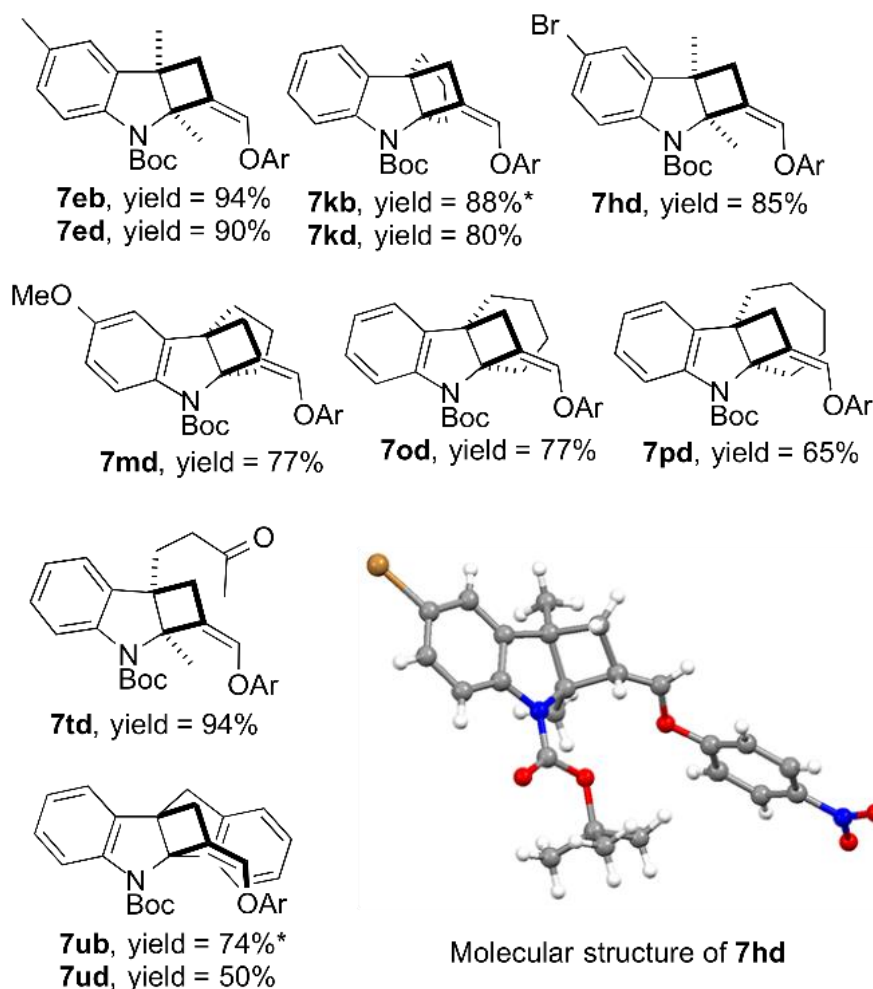


**Figure 3.7** Formal [2+2]-cycloaddition between *N*-Boc-indoles and aryloxyallenes (1:3:([JohnPhosAu(NCMe)]SbF<sub>6</sub>)= 1:2:0.05, DCM, 0 °C, 16 h). \* 1 mol% of catalyst was used. **7xb**: Ar = 2-naphth; **7xd**: Ar = *p*NO<sub>2</sub>C<sub>6</sub>H<sub>4</sub>.

In particular, we found that the reaction course proved to be not significantly affected by the presence of substituents (including either carbon- or heteroatom-based groups) at the indole N(1), C(2), C(3) and C(5) positions. The isolated yields ranged between 50% and 94% and the decrease of the catalyst loading to 1 mol% did not affect at all the chemical outcome. Both molecular skeleton and stereochemical aspects were finally elucidated by obtaining the X-Ray structure of (+/-)-**7hd** from a crystal grown via slow evaporation of a solution of AcOEt.

### 3.2.3 Gold catalysed dearomatization reaction: mechanistic study

Interesting and unexpected experimental evidences were obtained on the classic cycloaddition reaction among allenamide **2** and N-Boc-indole **1b**. In particular, we observed that, when the condensation was carried out at temperatures higher than 0 °C (i.e. room temperature or 40 °C), a second product that became predominant in the latter case (yield = 35%) was present. Crystallographic analysis showed that this product has the structure of the regioisomeric indoline-cyclobutyl ring **4b'**, corresponding to a reverse approaching orientation (with respect to **4b**) of the two reaction partners (Figure 3.8). Furthermore, when **4b** was treated in the presence of the gold complex in hot DCM (40 °C), **4b'** was again isolated along with some decomposition products. This experimental finding suggests the existence of a kinetic (**4b**) and thermodynamic (**4b'**) product that can interconvert.

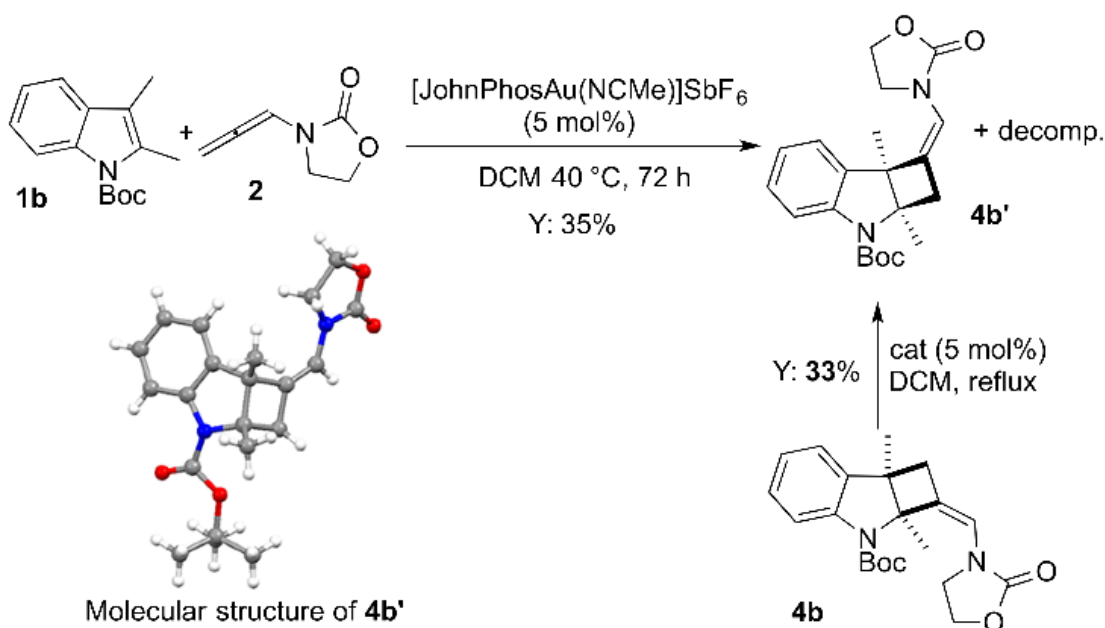


**Figure 3.8** Regiodivergent outcome of the [2+2]-cycloaddition when performed in refluxing DCM. Proving the interconversion of **4b** into **4b'** in hot DCM.

These intriguing experimental results stressed the importance of elucidating the reaction mechanism to answer important and unsolved questions, such

as: 1) What is the coordination/activation mode of the gold catalyst with the allenamides? 2) Is the mechanism concerted or step-wise? 3) What is the rationale for the recorded regio- and stereo-chemistry? In particular, why the ring closing occurs without affecting the stereochemistry of the exocyclic double bond (Figure 3.9)? 4) Are the "kinetic" and "thermodynamic" adducts the results of two separate reaction channels coexisting on the reaction surface?

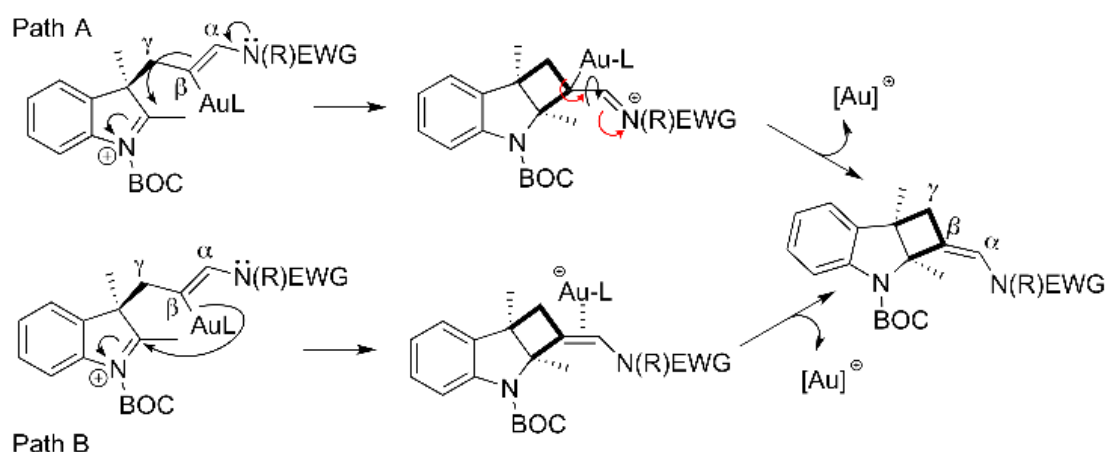


**Figure 3.9** Hypothetical mechanisms for the ring-closing step.

To answer these questions, the group of Professor Gian Piero Miscione from the Department of Chemistry of the Universidad de los Andes Carrera, Bogotá, carried out a computational investigation of the reaction surface. A DFT approach and a model-system formed by **1b** and **2** activated by the [Au(I)] cation bonded to the JohnPhos ligand ([JohnPhosAu<sup>+</sup>]) were used.

First how the cationic gold complex governs the electrophilic activation of allenamide **2** was examined.<sup>[32]</sup> The result was that the interaction of the metal with the cumulated diene involves an equilibrium between three different complexes **M1**( $\pi$ ), **M2**( $\sigma$ ), **M3**( $\pi$ ) showing  $\eta^2$ ,  $\eta^1$  and  $\eta^2$  coordination with [Au(I)], respectively. Both  $\eta^2$  complexes (**M1**( $\pi$ ) and **M3**( $\pi$ )) are more stable than **M2**( $\sigma$ ) (2.9 and 3.4 kcal mol<sup>-1</sup>, respectively). A 3D representation of the three complexes is given in Figure 3.10.

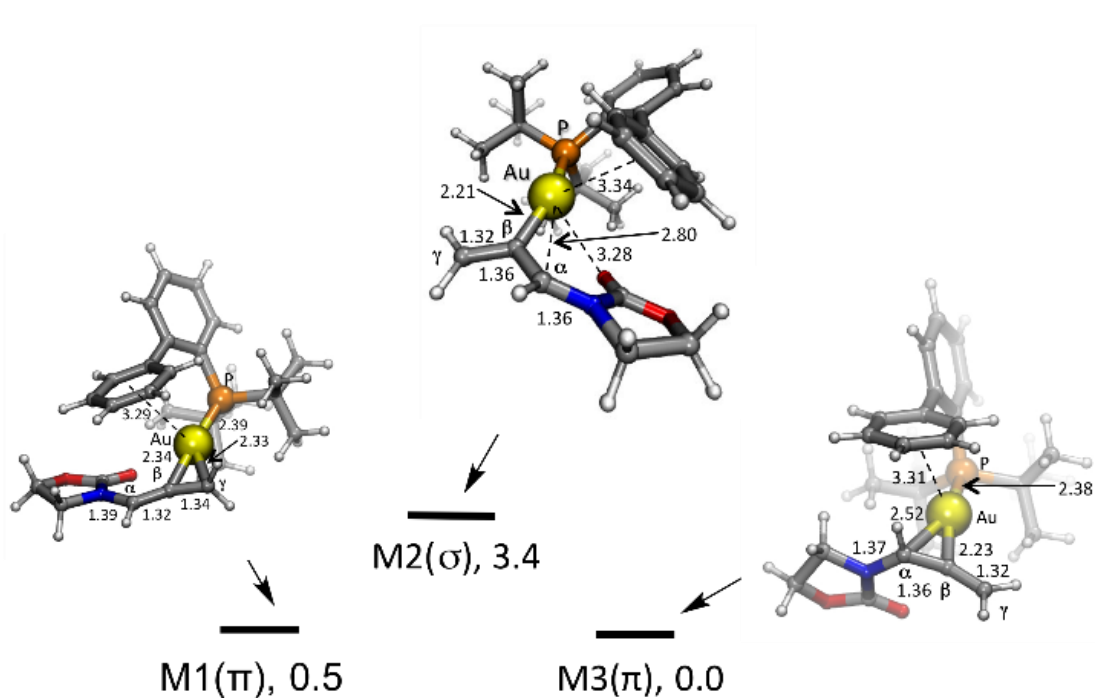


**Figure 3.10** A schematic 3D representation of the allenamide-[Au(I)] complexes. Energy values ( $\text{kcal mol}^{-1}$ ) are relative to **M3( $\pi$ )**. Bond lengths are given in Å.

The perturbation of the  $\pi$ -system caused by the interaction with the gold complex is evidenced by a slight increase of the C-C bond lengths in **M1( $\pi$ )** and **M3( $\pi$ )** and the increase of the corresponding positive charge density on  $\alpha$  and  $\gamma$  carbons.

The reaction surface for the cycloaddition involving indole **1b** and allenamide **2** complexed with [Au(I)] (reactants) is reported in Figure 3.11 where two reaction channels are evidenced.

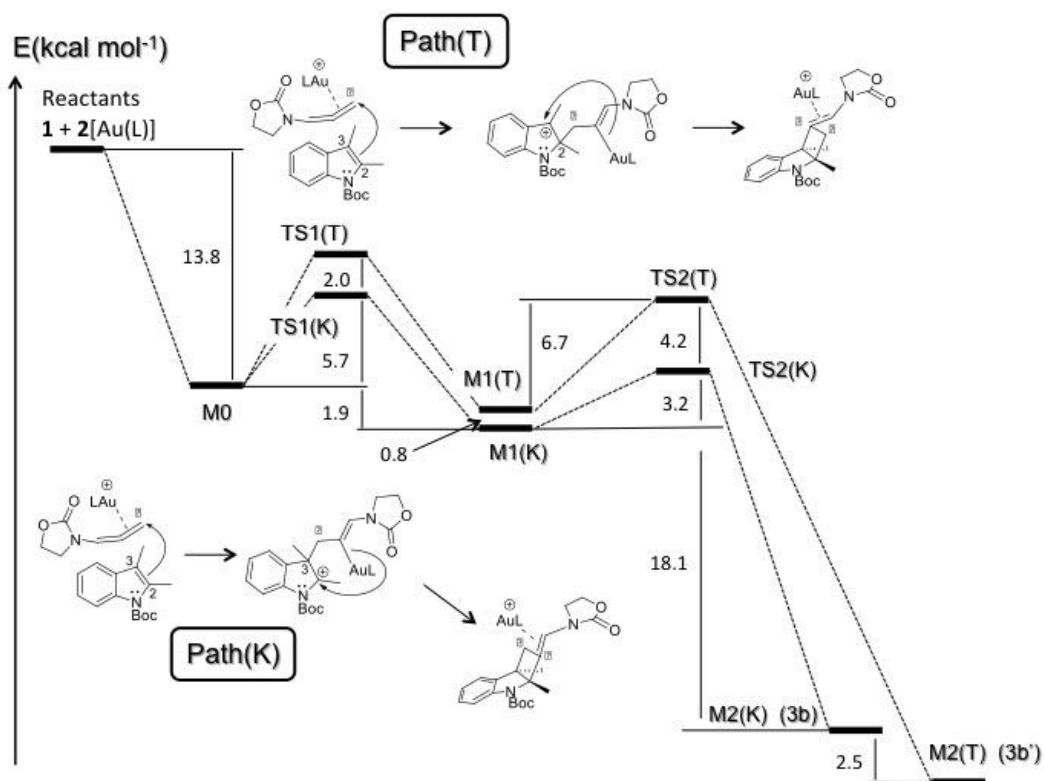


**Figure 3.11** The two computed reaction profiles Path(K) and Path(T). Energies are given in  $\text{kcal mol}^{-1}$ .

In Figure 3.11 a schematic representation of the corresponding reaction patterns is also given. Additionally, two-dimensional pictures of the structure of the various critical points located along the two pathways are given in Figure 3.12. More detailed 3D representations, for each point, are reported in section 3.4.6 of the Experimental part.

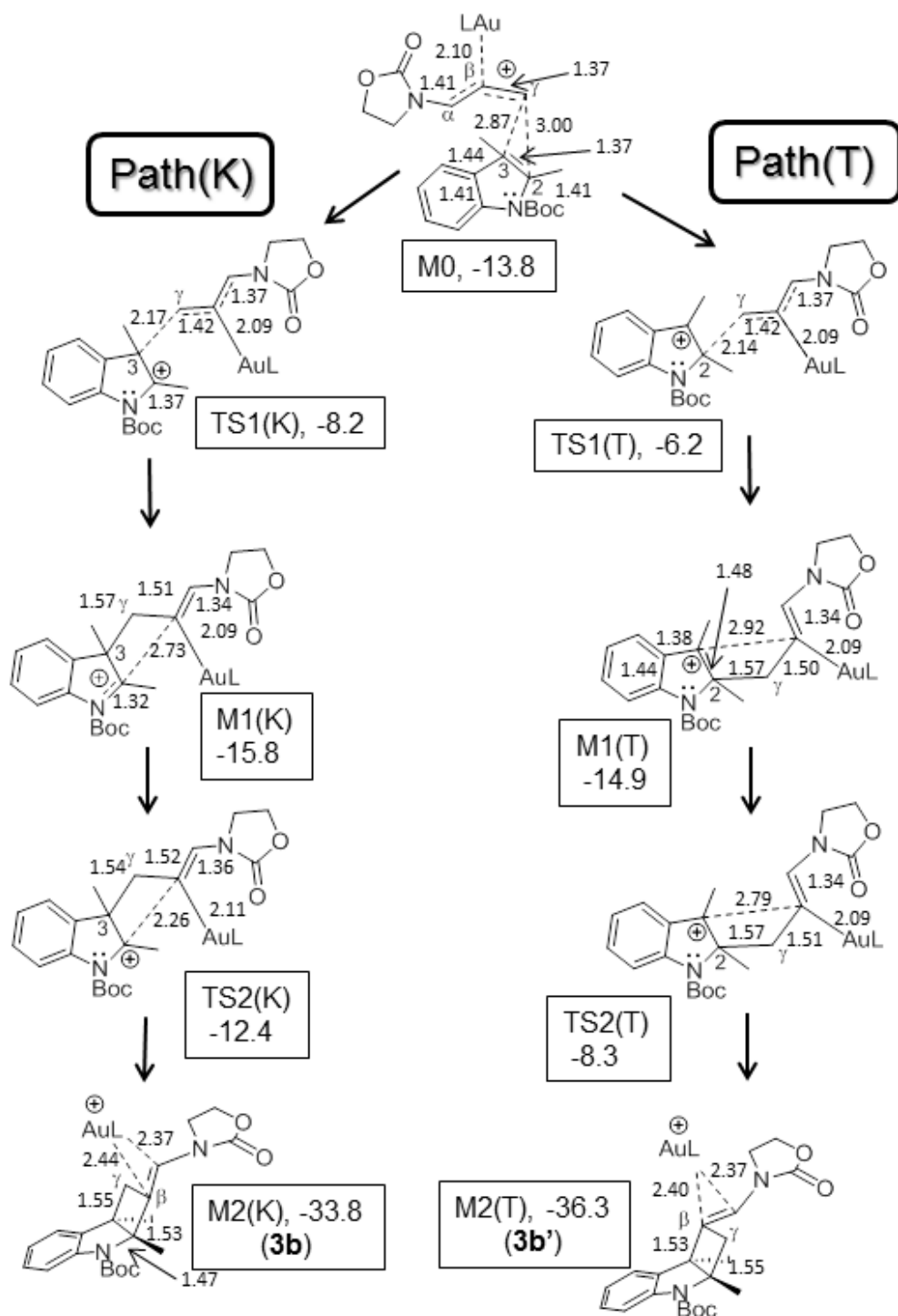


**Figure 3.12** A schematic representation of the structures of the critical points located along Path(K) and Path(T). Energies (kcal mol<sup>-1</sup>) are relative to reactants (Bond lengths are given in Å).

The approach of the two reacting species initially leads to the formation of an encounter complex **M0** (13.8 kcal mol<sup>-1</sup> more stable than reactants), where the indole ring plane and the plane of the metal allyl cation are facing each



other, the C(3)-C $\gamma$  and C(2)-C $\gamma$  distances being 2.87 and 3.00 Å, respectively. Interestingly, in the encounter complex the preferred coordination of the gold cation is  $\eta^1$  and not  $\eta^2$  as found in the isolated allenamide-[JhonPhosAu<sup>+</sup>] species. The higher stability of the  $\sigma$  type complex ( $\eta^1$ ) can be reasonably ascribed to the stabilizing interaction between the electron rich indole  $\pi$ -system and the positive charge localized on the  $\alpha$  allenamide carbon (0.3 is the net computed charge on C $\alpha$ ).

Two reaction paths (both consisting of two steps) originate from **M0** and lead to different regioisomers corresponding to opposite approaching orientations of the reacting species. These regioisomers should correspond to the hypothesized thermodynamic and kinetic products **4b'** and **4b** (the former being 2.5 kcal mol<sup>-1</sup> more stable than the latter). The two paths, leading to **4b'** and **4b**, are denoted as Path(T) and Path(K), respectively.

Along Path(K) (kinetic pathway) the transition state **TS1(K)** (5.6 kcal mol<sup>-1</sup> above **M0**) corresponds to the rate determining step of the process and describes the attack of C(3) on C $\gamma$  and leads to the formation of the indoleninic intermediate **M1(K)**, 15.8 kcal mol<sup>-1</sup> more stable than reactants. The newly forming bond is 2.17 Å in **TS1(K)** and becomes 1.57 Å in **M1(K)** where the bond is completed. Here the distance C(2)-C $\beta$  (that identifies the second bond required to obtain the final product) is 2.73 Å. The  $\sigma$ -coordination of the gold atom as found in **M0** is conserved in **TS1(K)** and **M1(K)**. The variation of the N-C(2) bond length along the transformation **M0**  $\rightarrow$  **TS1(K)**  $\rightarrow$  **M1(K)** (1.41, 1.37, 1.32 Å, respectively) indicates that the formation of the new C(3)-C $\gamma$  bond is brought about by the indole nitrogen lone pair *via* an enaminic-type electronic shift (see **M1(K)** structure in Figure 3.12).

A rather low activation barrier (3.2 kcal mol<sup>-1</sup>) must be overcome (transition state **TS2(K)**) to close the ring. The structure of **TS2(K)** is similar to that of

the previous intermediate **M1(K)**: the most important difference is the decrease of the C(2)-C $\beta$  distance (the incipient C-C bond), which becomes 2.26 Å.

Importantly, the C $\alpha$ -C $\beta$  bond length remains approximately constant on passing from **M1(K)** to **TS2(K)** (1.34 and 1.36 Å, respectively). This suggests that the formation of the C(2)-C $\beta$  bond involves the [Au]-C $\beta$  heterolytic bond breakage (path B in Figure 3.12) rather than the enammidic fragment (N-C $\alpha$ -C $\beta$ ) electrons (path A in Figure 3.12). Thus, the ring closing process does not affect the nature of the C $\alpha$ -C $\beta$  exocyclic double bond, which maintains its *Z*-configuration generated from the initial outer-sphere nucleophilic attack of the indole on the gold-activated allenamide.

The final **M2(K)** product complex (the **4b** regioisomer) is 33.8 kcal mol<sup>-1</sup> more stable than reactants. In this complex the gold atom gets away from C $\beta$  (C $\beta$ -Au distance = 2.44 Å) and becomes much closer to C $\alpha$  (2.37 Å), thus reactivating a  $\eta^2$  coordination with the exocyclic double bond. Notably, the N-C2 distance (indole moiety) increases from 1.32 Å to 1.47 Å along the transformation **M1(K)**  $\rightarrow$  **M2(K)**. This points out the disappearing of the formal charge on the immonium ion (characterizing the indoleninic intermediate **M1(K)**) and the repositioning of the lone-pair on the nitrogen atom in **M2(K)**. In addition, it demonstrates the importance of the protecting group Boc that assists the cycloaddition process by displacing electron density from the N-C(2).

Along Path(T) (thermodynamic pathway) the first transition state **TS1(T)** describes the nucleophilic attack of C2 on C $\gamma$  (the new incipient C2-C $\gamma$  bond is 2.14 Å) and corresponds again to the rate determining step of the process. **TS1(T)** is 7.6 kcal mol<sup>-1</sup> higher than **M0** (2.0 kcal mol<sup>-1</sup> above **TS1(K)**) and leads to **M1(T)**, the indoleninic dearomatized intermediate, where the new C2-C $\gamma$  bond is completed (1.57 Å). The dearomatization process occurring

in the passage **M0** → **M1(T)** and involving the delocalization of the benzene  $\pi$  electrons on indole is evidenced by the gradual increase in the indole moiety of the C2-C3 (from 1.37 to 1.48 Å) and C4-C5 (from 1.41 to 1.44 Å) distances and a simultaneous shortening of C3-C4 bond (from 1.44 to 1.38 Å).

The transition state for the subsequent ring-closing step (transition state **TS2(T)**, 4.2 kcal mol<sup>-1</sup> above **TS2(K)**) has an intrinsic activation energy of 6.7 kcal mol<sup>-1</sup>. The values of the computed bond lengths again indicates that the ring closing process involves the C $\beta$ -[Au] electrons. The stability of the resulting product **M2(T)** (36.3 kcal mol<sup>-1</sup> below reactants) can be reasonably ascribed to the restoring of the aromaticity of the indolinic ring. As observed for **M2(K)** the coordination mode of the gold cation [Au(I)] becomes again  $\eta^2$ . It is reasonable to believe that the energetic gap among these two adducts is due to the steric hindrance between the Boc and the oxazolinonic groups highlighted in Figure 3.13.

In **M2(K)** these two groups are rather close, but this steric hindrance is partially cancelled in the thermodynamic adduct **M2(T)**.

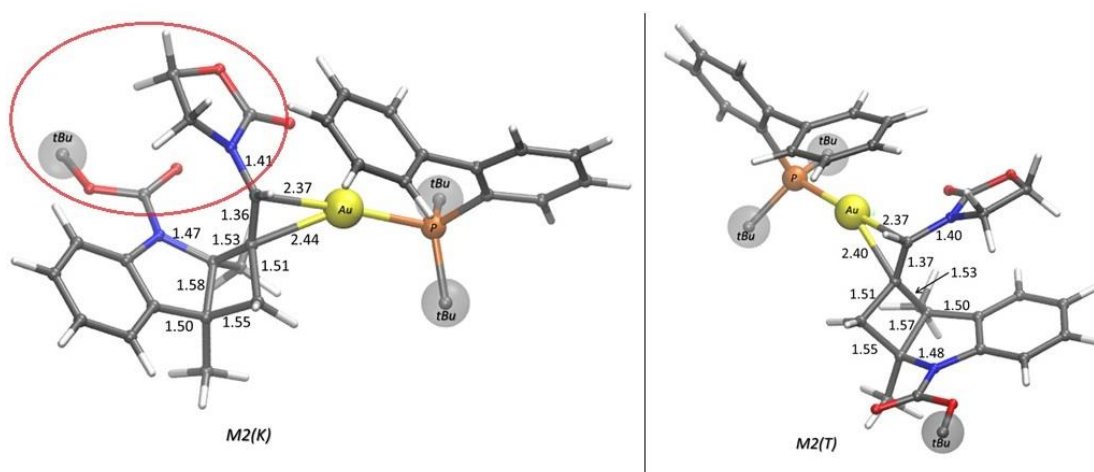


**Figure 3.13** Comparison of the two organogold complexes **M2(K)** on the left and **M2(T)** on the right. The red circle highlights the steric hindrance between BOC and oxazolinonic group.

Comparison of the two reaction profiles clearly indicates that the two transition states for indole dearomatization (rate-determining step in both

cases) are close enough (the two activation barriers differ by 2.0 kcal mol<sup>-1</sup>) to explain why, when the reaction is performed at 0 °C, small amounts of the thermodynamic product are observed and only through a rigid kinetic control (-40° C) it is possible to avoid the formation of the regioisomer **4b'**.

The energy difference between **TS1(K)** and **TS1(T)** can be plausibly ascribed to the different indole dearomatization ability associated with the attack of C(3) and C(2) on the allenamidic carbon C $\gamma$ . The energy cost is higher in the latter case where a loss of aromaticity of the entire system (also involving the benzene ring) occurs. Otherwise, when the attack proceeds from C(3) the loss of aromaticity is confined to the heterocyclic portion.

### 3.2.4 Enantioselective gold catalysed [2+2]-cycloaddition between indoles and electron-rich allenenes

The enantioselective cycloaddition reactions<sup>[33]</sup> involving indoles, represents a powerful tool for a direct access to stereochemically defined dearomatized indolyl-based scaffolds.<sup>[34-42]</sup> As a matter of fact, several metal- and metal-free stereoselective methodologies have been developed with the site-selective functionalization of the C(2)- and C(3)-positions of the indole core.<sup>[7,8,6]</sup>

Interestingly, despite the enormous interest towards the development of efficient catalytic methodologies to polycyclic fused indolines, enantioselective protocols to access C(2)/(3)-cyclobutylindoline compounds were still unreported in literature with the exception of contribution on the stereoselective gold catalyzed formal [2+2]-cycloaddition reaction published by the group of Professor Bandini.<sup>[25]</sup>

In that previous communication, the use of *in situ* formed (*R*)-DTBM-segphos(AuOTf)<sub>2</sub> (2.5-5.0 mol%) enabled the enantioselective preparation of tricyclic indoline scaffolds in straightforward manner by condensing a

range of *N*-Boc-indoles and the allenamide **2** (DCM, -60 °C) as reported in Figure 3.14.

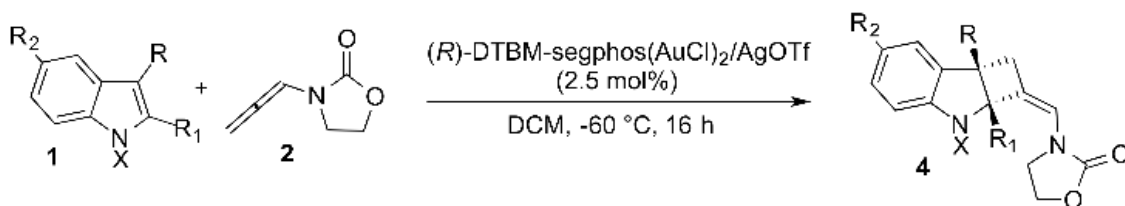


**Figure 3.14** Scheme of reaction of the enantioselective dearomative cycloaddition between indoles and allenamide **2**.

Attempts to synthesize the thermodynamic analogous (**4 b'**) in stereochemical defined manner were carried out in refluxing conditions but substantial decomposition of the starting allenamide was observed.

A collection of results is depicted in the Figure 3.15.

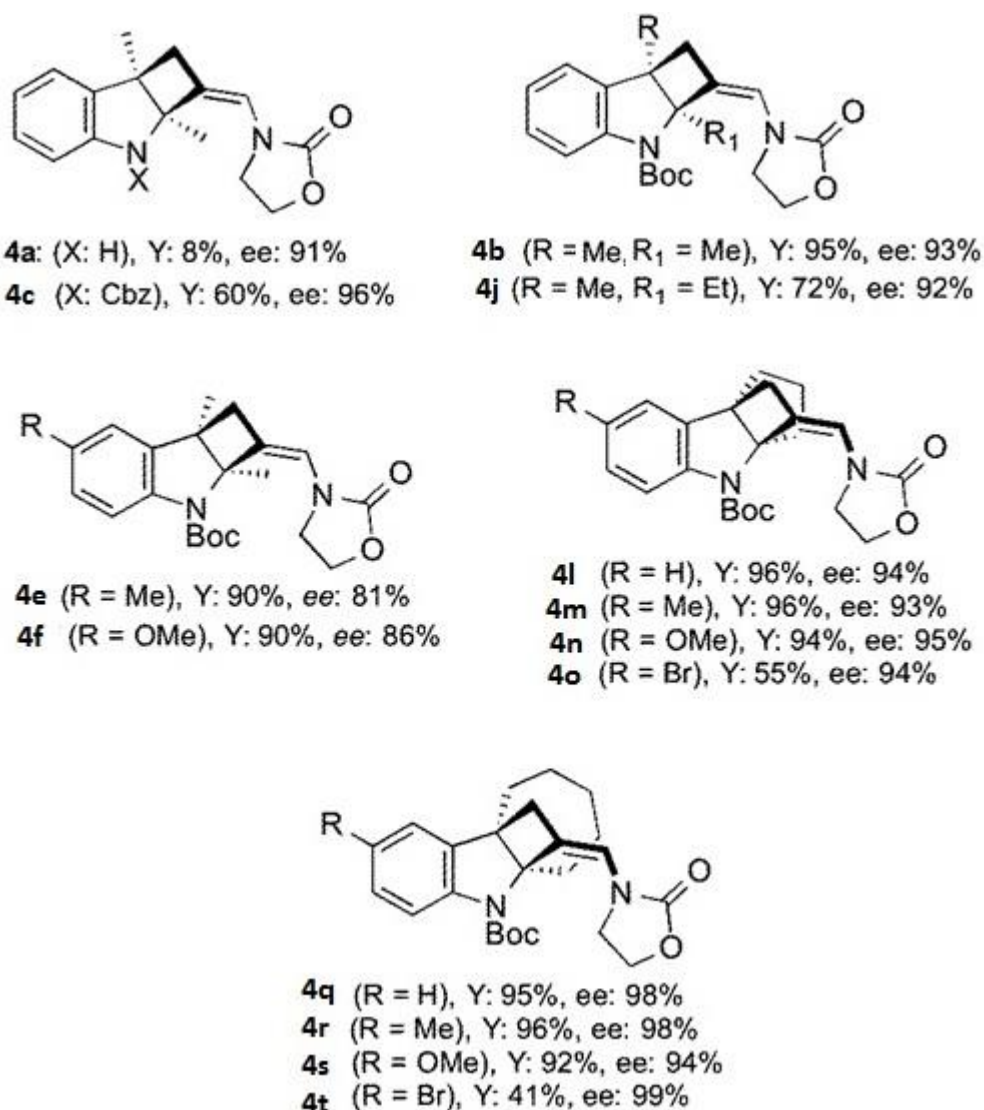


**Figure 3.15** Scope of the reaction for the enantioselective [2+2]-cycloaddition of indoles **1** with allenamide **2**. Adapted from ref [25].

It is possible to notice the excellent levels of regio-, diastereo- (dr > 20:1) and enantioselection (ee up to 98%) obtained for differently substituted indoles. In particular, 2,3-annulated indoles carrying C5 and C7-membered rings worked particularly well providing methylenecyclobuta-indolines **4l-t** in enantiomeric excesses up to 99%. Also, it appears that alkyl substituents were also tolerated at the C(2)/C(3)-sites (**4b-4j**), as well as EDGs and EWGs in the benzene ring C(5)-position. It is worth mentioning, that the removal of the EWG group from the nitrogen causes a marked drop in the isolated yield (**4a**, Y=8%) but with similar enantiocontrol (91%) as shown in Figure 3.15.

On the basis of these former experimental evidences, the efficiency of the stereoselective gold catalysed intermolecular [2+2]-cycloaddition between aryloxyallenes and *N*-Boc indoles was investigated (Figure 3.16).

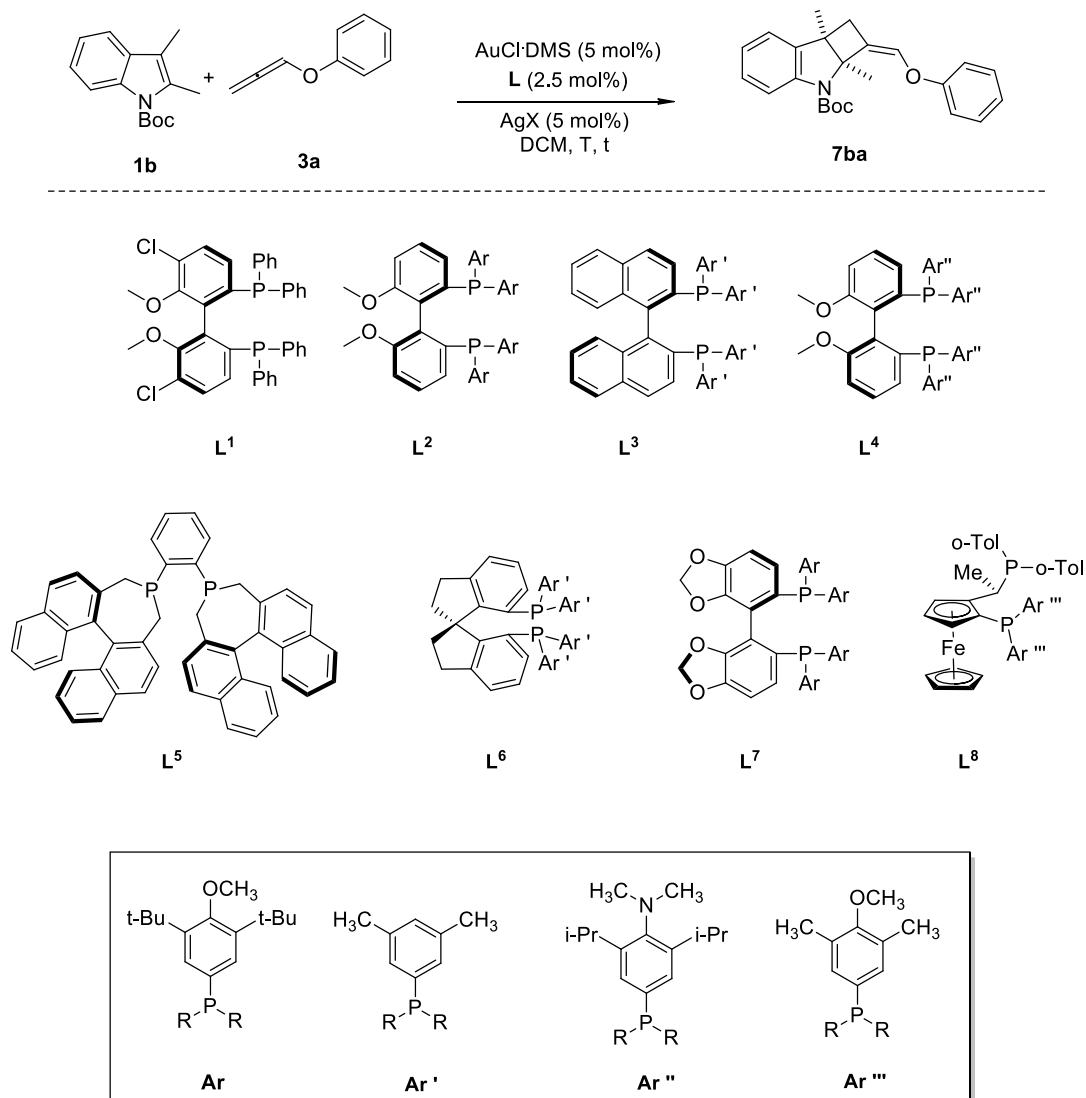


**Figure 3.16** Scheme of reaction and the chiral ligand examined.

Among the screened chiral ligands, (*R*)-DTBM-segphos furnished the highest levels of chemical (61%) and optical (84%) yields ( $\text{CH}_2\text{Cl}_2$ , 0 °C, cat loading = 2.5 mol%) in the model reaction (**3a+1b**) in combination with AgNTf<sub>2</sub> as the gold-activator.<sup>[43–45]</sup> On the contrary, lower performances were recorded with different C1- and C2-symmetric chiral units as shown in Table 3.4.

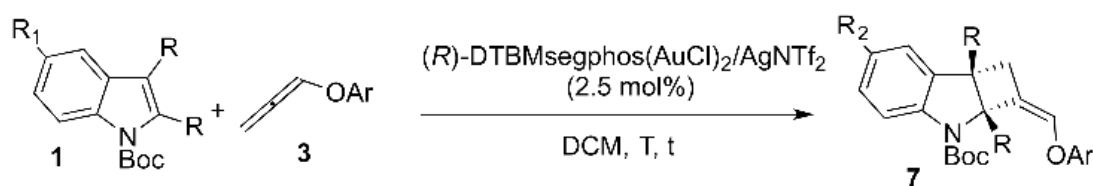
**Table 3.4** Screening of reaction conditions for the enantioselective dearomative cycloaddition of **1b** with **3a**.<sup>[a]</sup>

Entry	L	AgX	T (°C)	Time (h)	Y % <sup>[b]</sup>	ee % <sup>[c]</sup>
1	( <i>R</i> )- <b>L1</b>	AgOTf	0	5	11	11
2	( <i>R</i> )- <b>L2</b>	AgOTf	0	5	26	50
3	( <i>R</i> )- <b>L3</b>	AgOTf	0	5	19	52
4	( <i>R</i> )- <b>L4</b>	AgOTf	0	5	ND	/
5	( <i>R,R</i> )- <b>L5</b>	AgOTf	0	5	ND	/
6	( <i>R</i> )- <b>L6</b>	AgOTf	0	5	ND	/
7	( <i>R</i> )- <b>L7</b>	AgOTf	0	5	60	82
8	( <i>R,S<sub>p</sub></i> )- <b>L8</b>	AgOTf	0	5	30	24
9	( <i>R</i> )- <b>L7</b>	AgOTf	-20	16	72	85
10	( <i>R</i> )- <b>L7</b>	AgN(Tf) <sub>2</sub>	0	5	61	84
11	( <i>R</i> )- <b>L7</b>	AgN(Tf) <sub>2</sub>	-20	16	35	93
12	( <i>R</i> )- <b>L1</b>	AgN(Tf) <sub>2</sub>	0	5	51	11
13	( <i>R</i> )- <b>L2</b>	AgN(Tf) <sub>2</sub>	0	5	26	50
14	( <i>R</i> )- <b>L3</b>	AgN(Tf) <sub>2</sub>	0	5	19	52
15	( <i>R</i> )- <b>L4</b>	AgN(Tf) <sub>2</sub>	0	5	4	/
16	( <i>R,R</i> )- <b>L5</b>	AgN(Tf) <sub>2</sub>	0	5	/	/
17	( <i>R</i> )- <b>L6</b>	AgN(Tf) <sub>2</sub>	0	5	/	/
18	( <i>R,S<sub>p</sub></i> )- <b>L8</b>	AgN(Tf) <sub>2</sub>	0	5	30	24

<sup>a</sup> All reactions were carried out under nitrogen atmosphere in anhydrous solvents (1a:3a:cat = 1:2:0.05). <sup>b</sup> After flash chromatography (cHex:DCM: 8:2). <sup>c</sup> Determined by HPLC with chiral column. ND = not determined.

Finally, the performances of the catalytic system in the case of aryloxyallenes were assessed by condensing several indoles with **3** under optimal conditions.



**Table 3.5** Gold catalysed enantioselective cycloaddition between indoles and **3**.<sup>a</sup>

Run	R/R <sub>1</sub> /R <sub>2</sub> ( <b>1</b> )	<b>3</b>	T (°C)/t (h)	Yield <b>7</b> (%) <sup>b</sup>	ee <b>7</b> (%) <sup>c</sup>
1	Me/Me/H ( <b>1b</b> )	<b>3a</b>	0/4	61	85
2	Me/Me/H ( <b>1a</b> )	<b>3a</b>	-20/6	32	95
3	Me/Me/Me ( <b>1e</b> )	<b>3a</b>	-20/6	56	94
4	-(CH <sub>2</sub> ) <sub>3</sub> -/H ( <b>1l</b> )	<b>3a</b>	0/4	75	95
5	-(CH <sub>2</sub> ) <sub>5</sub> -/H ( <b>1q</b> )	<b>3a</b>	0/4	73	84
6	Me/Me/H ( <b>1a</b> )	<b>3f</b>	0/16	74	64

<sup>a</sup> All the reactions were carried out under nitrogen atmosphere. <sup>b</sup> Isolated yields after flash chromatography. <sup>c</sup> Determined via HPLC analysis with chiral column.

Aryloxyallenes **3** were generally found less reactive than that allenamide **2** in the enantioselective variant and higher reaction temperatures (*i.e.* 0 °C/ -20 °C) were required in order to access synthetically acceptable reaction kinetics.

The enantioselectivity ranges from high (64%) to excellent (95%) with moderate to good yield. Indoles featuring cyclic substituents at the C2/C3 carbon atoms (**1l,q**) and trimethyl-substituted indole **1e** (entry 5) were proved to be particularly competent.

### 3.3 Conclusions

A comprehensive investigation on the gold catalysed dearomative cycloaddition reaction of indoles with electron-rich allenes was documented by means of experimental and computational tools.

Commercially available ( $[\text{JohnPhosAu}(\text{NCMe})]\text{SbF}_6$ ) showed competence in performing the chemo- regio- and diastereoselective formal [2+2]-cycloaddition between a wide range of substrates under mild conditions. A portfolio of densely functionalized C(2),C(3)-fused cyclobutylindolines (**4/7**) was accessible in straightforward manner. Additionally, the use of chiral C(2)-symmetric DTBM-segphos enabled the control of the stereochemical profile of the dearomatization reaction in a convenient manner (ee up to 95% with aryloxyallenes **3**).

The DFT computations have clearly demonstrated that the mechanism for the formal gold-catalyzed cycloaddition among allenamide **2** and *N*Boc-indole **1b** proceeds through a polar non-concerted mechanism involving two kinetic steps. Two different reaction pathways, Path(K) and Path(T), both consisting of two steps, originate from an initial encounter complex and provide the two regioisomers experimentally observed i.e. **4b** obtained under kinetic conditions and **4b'** obtained under thermodynamic conditions. In both cases the first step is rate-determining and corresponds to a dearomatization process. The ring closure occurring in the second step involves the heterolytic rupture of the  $\sigma$  [Au]-C $\beta$  bond and not the electrons of the exocyclic C $\alpha$ =C $\beta$  double bond, which maintains its original *Z*-configuration in agreement with the experiments.

The energy cost for the dearomatization process is higher along the thermodynamic pathway (attack from the C(2)-indole position) where the loss of aromaticity involves the entire system (indole and benzene ring). This cost decreases when the attack proceeds from C(3)- and the dearomatization is confined to the indole moiety.

The energy difference between the two dearomatization transition states is not very large (about 2.0 kcal mol<sup>-1</sup>). This explains why at 0 °C small amounts of the thermodynamic product **4b'** are observed and only under

severe kinetic conditions ( $-40^{\circ}\text{C}$ ) it is possible to avoid the formation of this regioisomer.

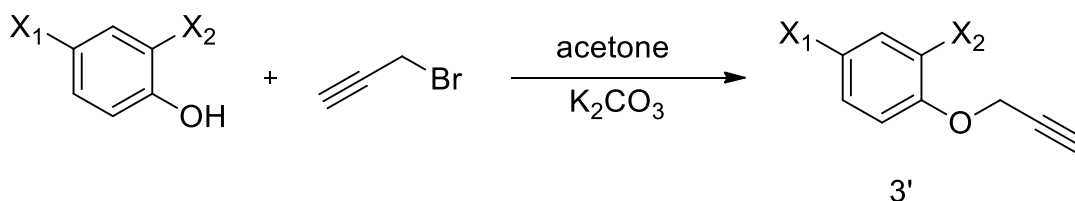
## 3.4 Experimental part

### 3.4.1 General methods

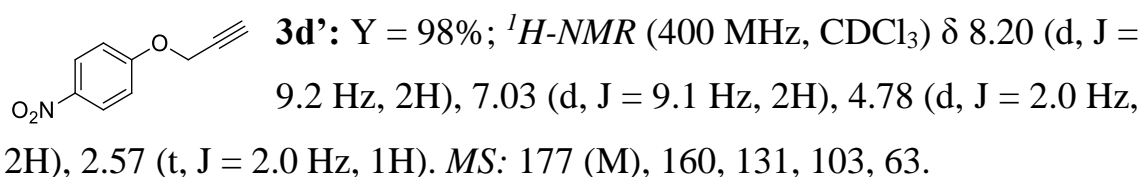
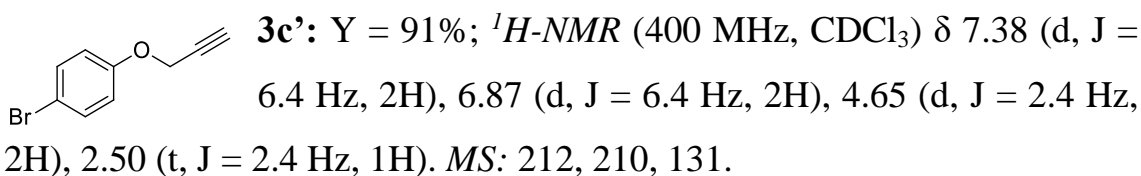
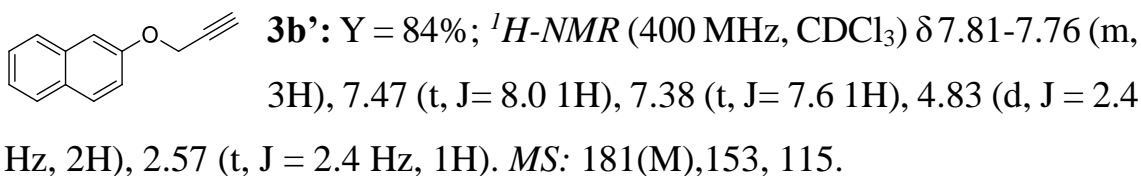
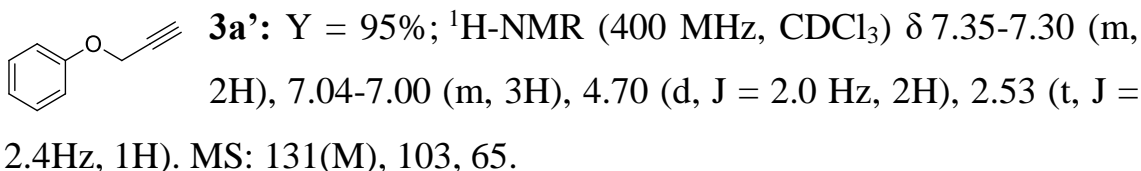
$^1\text{H}$ -NMR spectra were recorded on Varian 200 (200 MHz) or Varian 400 (400 MHz) spectrometers. Chemical shifts are reported in ppm from TMS with the solvent resonance as the internal standard (deuteriochloroform: 7.27 ppm). Data are reported as follows: chemical shift, multiplicity (s = singlet, d = duplet, t = triplet, q = quartet, sext = sextet, sept = septet, p = pseudo, b = broad, m = multiplet), coupling constants (Hz).  $^{13}\text{C}$ -NMR spectra were recorded on a Varian 200 (50 MHz), Varian 400 (100 MHz) spectrometers with complete proton decoupling. Chemical shifts are reported in ppm from TMS with the solvent as the internal standard (deuteriochloroform: 77.0 ppm). GC-MS spectra were taken by EI ionization at 70 eV on a Hewlett-Packard 5971 with GC injection. They are reported as:  $m/z$  (rel. intense). LC-electrospray ionization mass spectra were obtained with Agilent Technologies MSD1100 single-quadrupole mass spectrometer. Elemental analyses were carried out by using an EACE 1110 CHNOS analyser. Optical rotations were measured using a Schmidt+Haensch Unipol L1000 polarimeter. Chromatographic purification was done with 240-400 mesh silica gel. Anhydrous THF and DCM were distilled respectively from sodium-benzophenone and  $\text{P}_2\text{O}_5$  prior to use. Other anhydrous solvents were supplied by Fluka or Sigma Aldrich in Sureseal<sup>®</sup> bottles and used without any further purification. Commercially available chemicals were purchased from Sigma Aldrich, Stream and TCI and used without any further purification. Melting points were measured using open glass capillaries in a Bibby Stuart Scientific Melting Point Apparatus SMP 3 and were calibrated by comparison with literature values (Aldrich). The indoles unavailable in

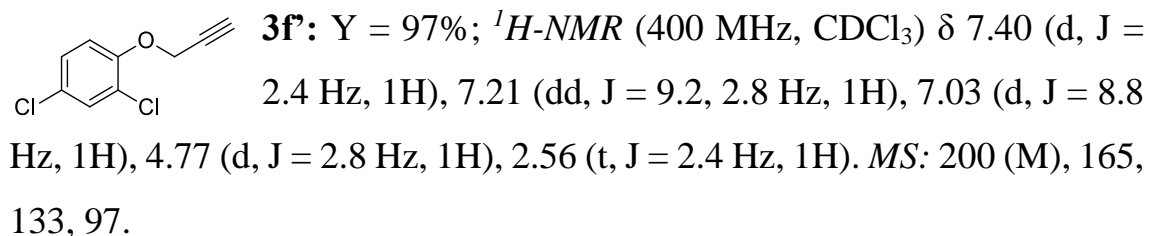
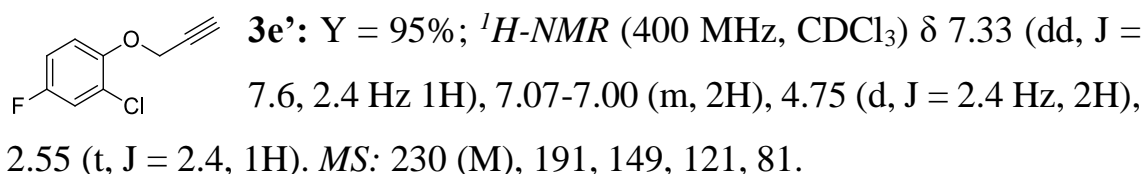
commercial were synthesized according to the general procedure for Fisher indole synthesis.<sup>[46]</sup>

### 3.4.2 General Procedure for the synthesis of Propargyl-Phenol Ethers 3'

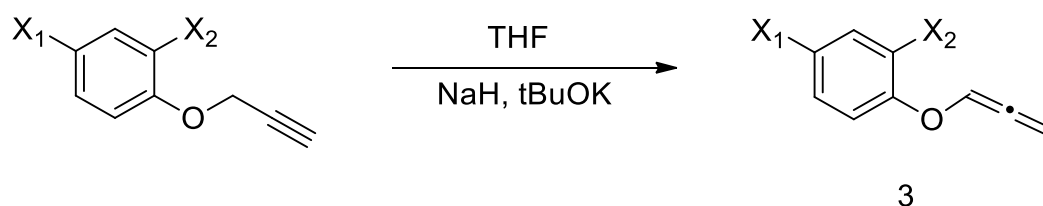


To a stirred solution of phenols (10 mmol) in acetone was added  $\text{K}_2\text{CO}_3$  (21 mmol) at room temperature. After 15 min propargyl bromide (15 mmol, 1.33 ml) was added drop wise and the mixture was heated under reflux for 3h. It was then quenched with  $\text{H}_2\text{O}$  and evaporated under reduced pressure. The resulting aqueous layer was extracted twice with EtOAc and the organic phase was washed with brine, dried over anhydrous  $\text{Na}_2\text{SO}_4$ , and evaporated *in vacuo*. The residue was purified *via* column chromatography (cHex:AcOEt = 2:1) to gain the desired products as yellow solids.

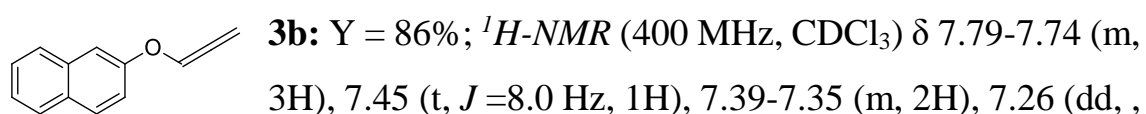
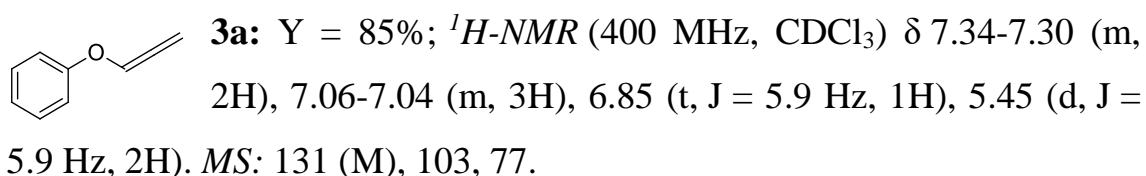




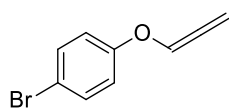
### 3.4.3 General Procedure for the synthesis of Alkoxyallenes 3

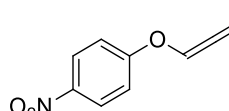


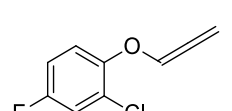
Under a nitrogen atmosphere, NaH (4.2 mmol) was dissolved into an anhydrous THF solution, followed by addition of propargyl-phenol ethers **3'a-f** (2.5 mmol) with stirring. After 15 min anhydrous *t*-BuOK (0.75 mmol) was added and the mixture was allowed to stir at rt for 5 h. The reaction was quenched by addition of H<sub>2</sub>O and evaporated under reduced pressure. The aqueous layer was extracted twice with EtOAc and the resulting organic phase was washed with brine, dried over anhydrous Na<sub>2</sub>SO<sub>4</sub>, filtered and evaporated *in vacuo*. Purification by column chromatography (*c*Hex:AcOEt = 8:2) afforded the desired products **3a-f** as yellow oils.

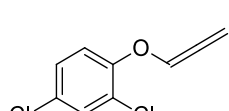


$J = 2.8, 9.2$  Hz, 1H), 6.96 (t,  $J = 6.0$  Hz, 1H), 5.47 (d,  $J = 8.0$  Hz, 2H) *MS*: 181 (M).

 **3c**:  $Y = 90\%$ ;  $^1H$ -NMR (400 MHz,  $CDCl_3$ )  $\delta$  7.41 (d,  $J = 8.4$  Hz, 2H), 6.95 (d,  $J = 8.4$  Hz, 2H), 6.80 (t,  $J = 5.9$  Hz, 1H), 5.46 (d,  $J = 5.9$  Hz, 2H). *MS*: 212 (M), 183.

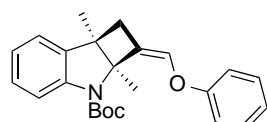
 **3d**:  $Y = 78\%$ ;  $^1H$ -NMR (400 MHz,  $CDCl_3$ )  $\delta$  8.23 (d,  $J = 9.1$  Hz, 2H), 7.15 (d,  $J = 9.1$  Hz, 2H), 6.86 (t,  $J = 5.9$  Hz, 1H), 5.54 (d,  $J = 5.9$  Hz, 2H). *MS*: 176 (M), 160, 131.

 **3e**:  $Y = 73\%$ ;  $^1H$ -NMR (400 MHz,  $CDCl_3$ )  $\delta$  7.30 (dd,  $J = 7.8, 3.0$  Hz, 1H), 7.09 (dd,  $J = 9.0, 5.0$  Hz, 1H), 6.99 (ddd,  $J = 9.0, 7.8, 3.0$  Hz, 1H), 6.83 (t,  $J = 5.9$  Hz, 1H), 5.43 (d,  $J = 5.9$  Hz, 1H). *MS*: 228 (M), 200, 149.

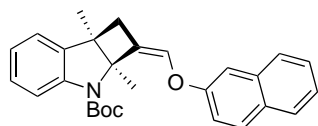
 **3f**:  $Y = 85\%$ ;  $^1H$ -NMR (400 MHz,  $CDCl_3$ )  $\delta$  7.39 (d,  $J = 2.4$  Hz, 1H), 7.19 (dd,  $J = 2.4, 8.7$  Hz, 1H), 7.08 (d,  $J = 8.7$  Hz, 1H), 6.82 (t,  $J = 5.9$  Hz, 1H), 5.46 (d,  $J = 5.9$  Hz, 2H). *MS*: 200 (M), 165, 133.

### 3.4.4 General procedure for the [2+2] cycloaddition reaction between indoles and allenamide/ aryloxyallenes (2/3): racemic variant

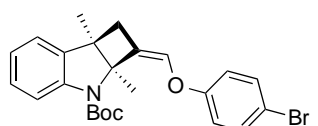
To a stirred solution of anhydrous DCM (1 ml) at 0 °C was added [JohnPhosAu(ACN)]SbF<sub>6</sub> (5% mol, 2 mg). Then, the desired indole (0.05 mmol) and allenamide **2** or aryloxyallenes **3** (0.1 mmol) were added in sequence and the mixture was allowed to stir for 5 hs. Removal of the solvent under reduced pressure and purification by column chromatography afforded the desired products.

 **7ba**. White solid. Yield = 75%, (*c*Hex:DCM = 8:2). *Mp*: 76-78 °C.  $^1H$ -NMR (400 MHz,  $CDCl_3$ )  $\delta$  7.93 (bs, 1H), 7.32 (t,  $J = 7.6$  Hz, 2H) 7.19 (t,  $J = 7.6$  Hz, 1H) 7.11-6.96 (m, 5H), 6.23 (t,  $J$

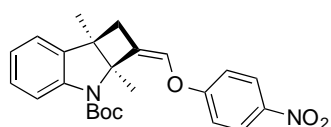
= 1.8 Hz, 1H), 2.80 (dd,  $J = 13.9, 2.2$  Hz, 1H), 2.53 (dd,  $J = 13.9, 1.5$  Hz, 1H), 1.69 (s, 3H), 1.52 (s, 9H), 1.45 (s, 3H).  $^{13}\text{C-NMR}$  (100 MHz,  $\text{CDCl}_3$ )  $\delta$  157.9, 144.0, 137.4, 137.0, 129.5, 127.8, 122.5, 122.3, 122.0, 116.6, 115.9, 80.9, 74.9, 48.1, 40.3, 28.6, 17.7, 17.4. *LC-MS*: 400 ( $\text{M}+\text{Na}$ ), 777 ( $2\text{M}+\text{Na}$ ). *Anal. calcd* for ( $\text{C}_{24}\text{H}_{27}\text{NO}_3$ : 377.48): C, 76.36; H, 7.21, N, 3.71; Found: C, 76.21, H, 7.10, N, 3.60.



**7bb.** Pale yellow liquid. Yield = 83%; (*c*Hex:DCM = 98:2).  $^1\text{H-NMR}$  (400 MHz,  $\text{CDCl}_3$ )  $\delta$  7.91 (bs, 1H), 7.82-7.79 (m, 2H), 7.75 (d,  $J = 8.4$  Hz, 1H), 7.47 (t,  $J = 8.0$  Hz, 1H), 7.40 (t,  $J = 8.0$  Hz, 1H), 7.29- 7.21 (m, 3H), 7.13 (d,  $J = 7.2$  Hz, 1H), 6.99 (t,  $J = 7.2$  Hz, 1H), 6.37 (t,  $J = 2$  Hz, 1H), 2.84 (dd,  $J = 14, 2$  Hz, 1H), 2.60 (dd,  $J = 13.6, 1.6$  Hz, 1H), 1.72 (s, 3H), 1.50 (s, 9H), 1.47 (s, 3H);  $^{13}\text{C-NMR}$  (100 MHz,  $\text{CDCl}_3$ )  $\delta$  155.5, 144.0, 137.3, 136.9, 134.3, 129.8, 129.6, 127.8, 127.7, 126.9, 126.5, 124.3, 122.4, 122.0, 118.8, 116.0, 110.8, 80.9, 74.9, 48.2, 40.3, 28.6, 17.7, 17.4; *LC-MS*: 450( $\text{M}+\text{Na}$ ), 877 ( $2\text{M}+\text{Na}$ ). *Anal. calcd* for ( $\text{C}_{28}\text{H}_{29}\text{BrNO}_3$ : 427.54): C, 78.66; H, 6.84, N, 3.28; Found: C, 78.41, H, 6.71, N, 3.15.

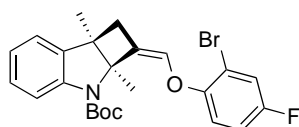


**7bc.** Light yellow oil. Yield = 96%; (*c*Hex:DCM = 95:5).  $^1\text{H-NMR}$  (400 MHz,  $\text{CDCl}_3$ )  $\delta$  7.86 (s, 1H), 7.40-7.38 (m, 2H), 7.17 (t,  $J = 8.8$  Hz, 1H), 7.08 (d,  $J = 7.4$  Hz, 1H), 6.94 (t,  $J = 7.5$  Hz, 1H), 6.87-6.83 (m, 2H), 6.13 (t,  $J = 1.6$  Hz, 1H), 2.77 (dd,  $J = 2.0, 14.1$  Hz, 1H), 2.52 (dd,  $J = 1.6, 14.1$  Hz, 1H), 1.65 (s, 3H), 1.58 (s, 1H), 1.48 (s, 9H), 1.41 (s, 3H).  $^{13}\text{C-NMR}$  (100 MHz,  $\text{CDCl}_3$ )  $\delta$  156.7, 143.90, 137.2, 136.4, 132.5, 132.4, 132.3, 132.3, 127.8, 122.4, 122.1, 118.3, 116.7, 115.96, 114.9, 810, 74.7, 56.0, 48.1, 40.1, 28.6, 17.8, 17.5; *LC-MS*: 478 ( $\text{M}+\text{Na}$ ), 935 ( $2\text{M}+\text{Na}$ ). *Anal. calcd* for ( $\text{C}_{24}\text{H}_{26}\text{BrNO}_3$ : 456.38): C, 63.16; H, 5.74, N, 3.07; Found: C, 63.01, H, 5.61, N, 3.00.

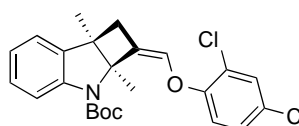


**7bd.** White solid. Yield = 86%; (*c*Hex:DCM = 8:2). *Mp*: 154-157 °C.  $^1\text{H-NMR}$  (400 MHz,  $\text{CDCl}_3$ )  $\delta$  8.20

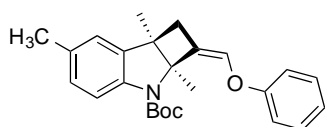
(d,  $J = 9.0$  Hz, 2H), 7.77 (s, 1H), 7.19 (t,  $J = 7.8$  Hz, 1H), 7.12 (d,  $J = 7.4$  Hz, 1H), 7.07 (d,  $J = 9.1$  Hz, 2H), 6.99 (t,  $J = 7.4$  Hz, 1H), 6.24 (t,  $J = 1.6$  Hz, 1H), 2.82 (d,  $J = 14.8$  Hz, 1H), 2.58 (d,  $J = 14.2$  Hz, 1H), 1.66 (s, 3H), 1.46 (s, 9H), 1.41 (s, 3H).  $^{13}\text{C-NMR}$  (100 MHz,  $\text{CDCl}_3$ )  $\delta$  162.3, 142.8, 137.0, 134.8, 127.9, 125.8, 122.6, 122.2, 116.2, 115.9, 81.1, 74.6, 39.9, 28.5, 17.8, 17.1. *LC-MS*: 445 (M+Na), 867 (2M+Na). *Anal. calcd* for ( $\text{C}_{24}\text{H}_{26}\text{N}_2\text{O}_5$ : 422.48): C, 68.23; H, 6.20, N, 6.63; Found: C, 68.06, H, 6.12, N, 6.63.



**7be.** White solid. Yield = 83%. *Mp* = 118-120 °C.  $^1\text{H-NMR}$  (400 MHz,  $\text{CDCl}_3$ )  $\delta$  7.87 (s, 1H), 7.29 (dd,  $J = 7.6, 2.8$  Hz, 1H), 7.19-7.14 (m, 1H), 7.07 (dd,  $J = 7.2, 1.0$  Hz, 1H), 6.98-6.89 (m, 3H), 6.07 (t,  $J = 1.6$  Hz, 1H), 2.75 (dd,  $J = 14.0, 2.0$  Hz, 1H), 2.51 (dd,  $J = 14.0, 1.6$  Hz, 1H), 1.75 (s, 3H), 1.43 (s, 3H), 1.41 (s, 9H).  $^{13}\text{C-NMR}$  (100 MHz,  $\text{CDCl}_3$ ) 159.1, 156.7, 151.0, 143.9, 137.4, 137.2, 127.8, 122.4, 122.0, 120.5, 120.3, 118.3, 118.2, 115.9, 115.1, 114.9, 113.3, 113.1, 80.9, 74.8, 48.1, 40.0, 28.4, 17.7, 17.6; *LC-MS*: 497 (M+Na), 519 (M+K). *Anal. calcd* for ( $\text{C}_{24}\text{H}_{25}\text{BrFNO}_3$ : 474.37): C, 60.77; H, 5.31, N, 2.95; Found: C, 60.61, H, 5.13, N, 2.87.



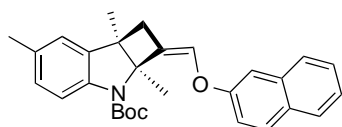
**7bf.** Light yellow oil. Yield = 95% (*cHex*:DCM = 8:2).  $^1\text{H-NMR}$  (400 MHz,  $\text{CDCl}_3$ )  $\delta$  7.84 (s, 1H), 7.38 (d,  $J = 2.8$  Hz, 1H), 7.19 – 7.14 (m, 2H), 7.10 (d,  $J = 7.4$ , 1H), 6.95 (td,  $J = 8.0, 1.6$  Hz, 1H), 6.89 (d,  $J = 8.4$  Hz, 1H), 6.10 (t,  $J = 1.6$ , 1H), 2.80 (dd,  $J = 14.1, 2.1$  Hz, 1H), 2.54 (dd,  $J = 14.1, 1.5$  Hz, 1H), 1.72 (s, 3H), 1.42 (s, 3H), 1.40 (s, 9H).  $^{13}\text{C-NMR}$  (100 MHz,  $\text{CDCl}_3$ ) 152.2, 143.9, 143.6, 140.9, 136.6, 130.1, 127.8, 127.7, 124.6, 122.4, 122.0, 118.1, 115.9, 81.0, 77.3, 77.0, 76.6, 74.8, 40.0, 29.7, 28.4, 17.7, 17.4; *LC-MS*: 470 (M+Na), 445 (M+K). *Anal. calcd* for ( $\text{C}_{24}\text{H}_{25}\text{Cl}_2\text{NO}_3$ : 446.37): C, 64.58; H, 5.65, N, 3.14; Found: C, 64.41, H, 5.51, N, 3.00.



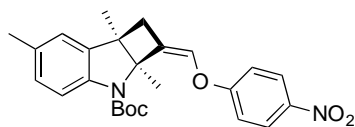
**7ea.** White solid. Yield = 76%; (*cHex*:DCM = 8:2). *Mp*: 102-104 °C.  $^1\text{H-NMR}$  (400 MHz,  $\text{CDCl}_3$ )  $\delta$  7.77



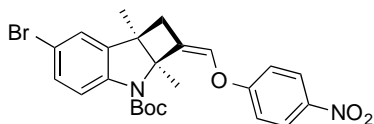
(s, 1H), 7.32-6.90 (m, 7H), 6.21 (t,  $J = 1.8$  Hz, 1H), 2.77 (dd,  $J = 13.6, 2.0$  Hz, 1H), 2.51 (dd,  $J = 13.8, 1.6$  Hz, 1H), 2.29 (s, 3H), 1.65 (s, 3H), 1.48 (s, 9H), 1.40 (d, 3H).  $^{13}\text{C-NMR}$  (100 MHz,  $\text{CDCl}_3$ ) 157.7, 136.8, 131.7, 129.5, 128.2, 122.6, 122.4, 116.6, 115.7, 80.7, 74.9, 40.2, 31.4, 30.2, 29.6, 28.5, 20.8, 17.7, 17.3. *LC-MS* 392 (M+H), 414 (M+Na), 430 (M+K), 805 (2M+Na). *Anal. calcd* for ( $\text{C}_{25}\text{H}_{29}\text{NO}_3$ ; 391.51): C, 76.70; H, 7.47, N, 3.58; Found: C, 76.55, H, 7.31, N, 3.60.



**7eb.** White solid. Yield = 94%; (cHex:EtOAc = 98:2). *Mp*: 112-115 °C.  $^1\text{H-NMR}$  (400 MHz,  $\text{CDCl}_3$ )  $\delta$  7.77-7.71 (m, 4H), 7.45 (t,  $J = 8.4$  Hz, 1H), 7.37 (t,  $J = 8.0$  Hz, 1H), 7.26-7.20 (m, 2H), 6.99 (d,  $J = 8.4$  Hz, 1H), 6.91 (s, 1H), 6.34 (t,  $J=2.0$ Hz, 1H), 2.81 (dd,  $J = 2.0, 14.0$  Hz, 1H), 2.56 (dd,  $J = 1.6, 14.0$  Hz, 1H), 2.31 (s, 3H), 1.69 (s, 3H), 1.47 (s, 9H), 1.43 (s, 1H).  $^{13}\text{C-NMR}$  (100MHz,  $\text{CDCl}_3$ ): $\delta$  155.6, 136.8, 134.3, 131.8, 129.8, 129.6, 128.3, 127.7, 126.9, 126.5, 124.3, 122.7, 118.8, 115.7, 110.7, 80.8, 75.0, 28.6, 20.9, 17.7, 17.4. *LC-MS*: 442 (M+H), 464 (M+Na), 905 (2M+Na). *Anal. calcd* for ( $\text{C}_{29}\text{H}_{31}\text{NO}_3$ ; 441.57): C, 78.88; H, 7.08, N, 3.17; Found: C, 78.62, H, 6.95, N, 3.11.

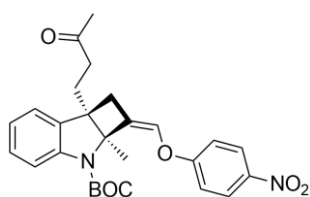


**7ed.** White solid. Yield = 50%. *Mp* = 196-198 °C;  $^1\text{H-NMR}$  (400 MHz,  $\text{CDCl}_3$ ):  $\delta$  8.22 (d,  $J = 9.2$  Hz, 2H), 7.67 (bs, 1H), 7.05 (d,  $J = 9.2$  Hz, 2H), 7.00 (d,  $J = 8.4$  Hz, 1H), 6.93 (s, 1H), 6.25 (t,  $J = 1.6$  Hz, 1H), 2.83 (dd,  $J = 2.0, 14.4$  Hz, 1H), 2.59 (d,  $J = 15.6$  Hz, 1H), 2.32 (s, 3H), 1.67 (s, 3H), 1.47 (s, 9H), 1.43 (s, 1H);  $^{13}\text{C-NMR}$  (100 MHz,  $\text{CDCl}_3$ ): 162.4, 142.6, 141.3, 134.7, 132.1, 128.4, 127.9, 125.8, 122.9, 117.5, 116.2, 115.8, 107.4, 80.9, 74.7, 71.5, 68.8, 39.9, 29.7, 28.6, 20.9, 19.5, 17.8, 17.1, 7.6. *LC-MS*: 459 (M+Na), 895 (2M+Na). *Anal. calcd* for ( $\text{C}_{25}\text{H}_{28}\text{N}_2\text{O}_5$ ; 436.51): C, 68.79; H, 6.47, N, 6.42; Found: C, 68.65, H, 6.29, N, 6.25.

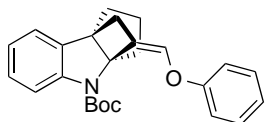


**7hd.** White solid. Yield = 85%. *Mp* = 191-193 °C;  $^1\text{H-NMR}$  (400 MHz,  $\text{CDCl}_3$ ):  $\delta$  8.24 (d,  $J = 9.2$  Hz,

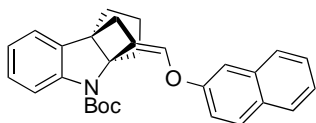
2H), 7.69 (bs, 1H), 7.29 (dd,  $J = 2.0, 8.8$  Hz, 1H), 7.21 (d,  $J = 2.4$  Hz, 1H), 7.06 (d,  $J = 8.0$  Hz, 2H), 6.28 (s, 1H), 2.85 (dd,  $J = 2.0, 14.4$  Hz, 1H), 2.60 (dd,  $J = 1.6, 14.4$  Hz, 1H), 1.67 (s, 3H), 1.45 (s, 9H), 1.43 (s, 3H).  $^{13}\text{C-NMR}$  (100 MHz,  $\text{CDCl}_3$ ): 162.2, 142.7, 139.3, 135.1, 130.7, 125.9, 125.8, 125.4, 117.5, 116.3, 116.2, 114.7, 90.3, 81.5, 75.1, 39.9, 28.5, 17.6, 17.1. *LC-MS*: 525 ( $\text{M}+\text{Na}$ ). *Anal. calcd* for ( $\text{C}_{24}\text{H}_{25}\text{BrN}_2\text{O}_5$ : 501.38): C, 57.49; H, 5.03, N, 5.59; Found: C, 57.31, H, 5.15, N, 5.31.



**7id.** White oil. Yield = 94%.  $^1\text{H-NMR}$  (400 MHz,  $\text{CDCl}_3$ ):  $\delta$  8.16 (d,  $J = 9.2$  Hz, 2H), 7.78 (bs, 1H), 7.21 (t,  $J = 7.2$  Hz, 1H), 7.09 (d,  $J = 6.4$  Hz, 1H), 7.01-6.95 (m, 3H), 6.13 (bs, 1H), 2.75 (dd,  $J = 1.6, 14.4$  Hz, 1H), 2.68 (dd,  $J = 2.0, 14.8$  Hz, 1H), 2.43-2.33 (m, 1H), 2.25-2.13 (m, 3H), 2.04 (s, 3H), 1.83 (s, 3H), 1.44 (s, 9H).  $^{13}\text{C-NMR}$  (100 MHz,  $\text{CDCl}_3$ ): 208.7, 162.1, 162.1, 144.1, 142.7, 134.9, 134.5, 128.3, 126.1, 125.8, 123.3, 123.0, 116.3, 115.6, 81.5, 73.3, 39.46, 38.3, 30.1, 28.4, 26.9, 17.8. *Anal. calcd* for ( $\text{C}_{26}\text{H}_{28}\text{N}_2\text{O}_5$ : 448.52): C, 69.63; H, 6.29, N, 6.25; Found: C, 69.51, H, 6.12, N, 6.05

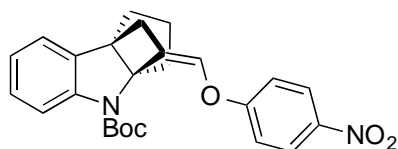


**7la:** White oil. Yield 54%, (*c*Hex:DCM = 8:2).  $^1\text{H-NMR}$  (400 MHz,  $\text{CDCl}_3$ )  $\delta$  7.93 (s, 1H), 7.28 (t,  $J = 7.6$  Hz, 2H), 7.19 (t,  $J = 7.9$  Hz, 2H), 7.14 (d,  $J = 6.4$  Hz, 1H), 7.03 (t,  $J = 7.6$  Hz, 1H), 6.98-6.94 (m, 2H), 6.09 (bs, 1H), 2.77 (dd,  $J = 2.0, 15.2$  Hz, 1H) 2.66 (dd,  $J = 2.4, 15.6$  Hz, 1H) 2.18 – 2.01 (m, 3H), 1.92-1.89 (m, 3H), 1.72-1.63 (m, 1H), 1.57-1.54 (m, 1H), 1.44 (s, 9H);  $^{13}\text{C-NMR}$  157.7, 129.5, 127.9, 123.6, 122.6, 117.4, 115.7, 80.4, 78.8, 38.1, 36.6, 36.6, 28.2, 28.0; *LC-MS*: 412 ( $\text{M}+\text{Na}$ ), 801 ( $2\text{M}+\text{Na}$ ); *Anal. calcd* for ( $\text{C}_{25}\text{H}_{27}\text{NO}_3$ : 389.50): C, 77.09; H, 6.99, N, 3.60; Found: C, 77.15, H, 7.10, N, 3.55.



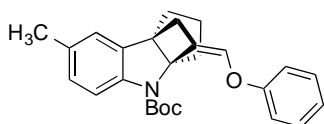
**7lb.** Pale yellow liquid. Yield = 88%; (*c*Hex:EtOAc = 95:5).  $^1\text{H-NMR}$  (400 MHz,  $\text{CDCl}_3$ )  $\delta$  8.00 (bs, 1H), 7.81-7.79 (m, 2H), 7.75 (d,  $J = 8$  Hz, 1H), 7.47 (t,  $J = 7.2$  Hz, 1H), 7.40 (t,  $J = 7.2$  Hz, 1H), 7.29-7.22 (m, 3H), 7.18 (d,  $J = 6.4$  Hz, 1H), 7.01 (t,  $J = 6.4$

Hz, 1H), 6.25 (bs, 1H), 2.88-2.73 (m, 2H), 2.24-2.20 (m, 2H), 2.13-2.06 (m, 1H), 1.99-1.94 (m, 1H), 1.76-1.70 (m, 1H), 1.59 (d,  $J = 14.7$  Hz, 1H), 1.45 (s, 9H).  $^{13}\text{C-NMR}$  (100 MHz,  $\text{CDCl}_3$ )  $\delta$  155.5, 136.1, 134.3, 130.0, 129.6, 128.0, 127.7, 127.0, 126.5, 124.5, 122.7, 119.2, 115.8, 80.5, 78.9, 38.2, 36.7, 36.6, 28.3, 28.1. *LC-MS*: 462 ( $\text{M}+\text{Na}$ ), 901 ( $2\text{M}+\text{Na}$ ); *Anal. calcd* for ( $\text{C}_{29}\text{H}_{29}\text{NO}_3$ : 439.56): C, 79.24; H, 6.65, N, 3.19; Found: C, 79.03, H, 6.51, N, 3.11.



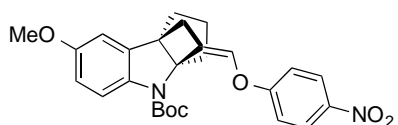
**7ld.** White solid. Yield = 80%; (*c*Hex:DCM = 95:5). *Mp* = 185-187 °C;  $^1\text{H-NMR}$  (400 MHz,  $\text{CDCl}_3$ ):  $\delta$  8.19 (d,  $J = 8.8$  Hz, 2H), 7.91 (bs, 1H)

7.20 (t,  $J = 7.2$  Hz, 1H), 7.17 (d,  $J = 1.8$  Hz, 1H), 7.06 (d,  $J = 9.2$  Hz, 2H), 6.98 (t,  $J = 7.6$  Hz, 1H), 6.16 (bs, 1H), 2.81 (d,  $J = 16.0$  Hz, 1H), 2.72 (d,  $J = 15.6$  Hz, 1H), 2.21-2.50 (m, 3H), 1.98-1.87 (m, 1H), 1.74-1.65 (m, 1H), 1.57-1.52 (m, 4H), 1.42 (s, 9H).  $^{13}\text{C-NMR}$  (100 MHz,  $\text{CDCl}_3$ )  $\delta$  206.8, 162.3, 142.8, 136.2, 136.1, 135.9, 135.7, 128.1, 125.8, 123.8, 122.9, 116.8, 115.8, 80.6, 78.7, 36.6, 36.4, 30.9, 28.2, 28.1; *LC-MS*: 457 ( $\text{M}+\text{Na}$ ). *Anal. calcd* for ( $\text{C}_{25}\text{H}_{26}\text{N}_2\text{O}_5$ : 434.49): C, 69.11; H, 6.03, N, 6.45; Found: C, 69.01, H, 6.66, N, 6.63.



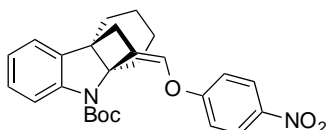
**7ma:** White oil. Yield = 72% (*c*Hex:DCM = 8:2).  $^1\text{H-NMR}$  (400 MHz,  $\text{CDCl}_3$ )  $\delta$  7.83 (bs, 1H), 7.28 (t,  $J =$

8.0 Hz, 2H), 7.04-6.93 (m, 5H), 6.08 (bs, 1H), 2.76 (dd,  $J=2.4, 15.6$  Hz, 1H), 2.65 (dd,  $J=1.6, 15.2$  Hz, 1H), 2.29 (s, 3H), 2.22-1.88 (m, 4H), 1.71-1.51 (m, 2H), 1.43 (s, 9H).  $^{13}\text{C-NMR}$  (100 MHz,  $\text{CDCl}_3$ ) 157.7, 138.4, 136.1, 132.1, 129.5, 128.4, 124.2, 122.8, 117.4, 115.5, 80.2, 78.9, 65.8, 38.1, 36.6, 36.5, 28.2, 28.1, 20.8, 15.2; *LC-MS*: 426 ( $\text{M}+\text{Na}$ ), 442 ( $\text{M}+\text{K}$ ), 829 ( $2\text{M}+\text{Na}$ ). *Anal. calcd* for ( $\text{C}_{26}\text{H}_{29}\text{NO}_3$ : 403.52): C, 77.39; H, 7.24, N, 3.47; Found: C, 77.50, H, 7.11, N, 3.40.



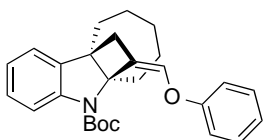
**7nd.** White oil. Yield = 77%. (*c*Hex:DCM = 95:5);  $^1\text{H-NMR}$  (400 MHz,  $\text{CDCl}_3$ ):  $\delta$  8.19 (d,  $J$

= 8.8 Hz, 2H), 7.84 (bs, 1H), 7.04 (d,  $J = 8.8$  Hz, 2H), 6.75-6.70 (m, 2H), 6.12 (bs, 1H), 3.77 (s, 3H), 2.82 (d,  $J = 16.0$  Hz, 1H), 2.70 (d,  $J = 16.8$  Hz, 1H), 2.19-2.03 (m, 3H), 1.93 (bs, 1H), 1.74-1.67 (m, 1H), 1.55 (s, 1H), 1.38 (s, 9H).  $^{13}\text{C-NMR}$  (100 MHz,  $\text{CDCl}_3$ )  $\delta$  162.3, 155.9, 136.9, 136.3, 125.8, 117.0, 116.3, 112.6, 109.9, 78.9, 55.7, 36.4, 36.2, 31.9, 31.5, 30.2, 29.7, 28.3, 28.1, 26.9, 22.7. *LC-MS*: 487 ( $\text{M}+\text{Na}$ ). *Anal. calcd* for ( $\text{C}_{26}\text{H}_{28}\text{N}_2\text{O}_6$ : 464.52): C, 67.23; H, 6.08, N, 6.03; Found: C, 67.02, H, 6.00, N, 6.21.



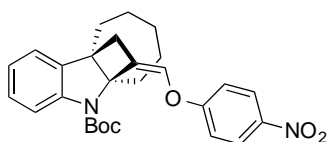
**7pd.** White solid. Yield = 77%. *Mp* = 171-174 °C;

$^1\text{H-NMR}$  (400 MHz,  $\text{CDCl}_3$ ):  $\delta$  8.22 (d,  $J=9.2$  Hz, 2H), 7.84 (bs, 1H), 7.18 (t,  $J = 8.0$  Hz, 1H), 7.07 (d,  $J = 8.8$  Hz, 3H), 6.96 (t,  $J = 7.2$  Hz, 1H), 6.37 (s, 1H), 2.86-2.78 (m, 2H), 2.50 (d,  $J = 13.2$  Hz, 1H), 2.38 (d,  $J = 13.2$  Hz, 1H), 1.75-1.53 (m, 5H), 1.46 (s, 9H), 1.24-1.35 (m, 1H), 1.05 (t,  $J = 12.8$  Hz, 1H), 0.87-0.84 (m, 1H).  $^{13}\text{C-NMR}$  (100 MHz,  $\text{CDCl}_3$ ) 142.5, 134.6, 128.0, 125.9, 122.4, 116.3, 115.8, 81.0, 30.0, 29.7, 29.3, 28.6, 20.9, 20.7. *LC-MS*: 471 ( $\text{M}+\text{Na}$ ). *Anal. calcd* for ( $\text{C}_{26}\text{H}_{28}\text{N}_2\text{O}_5$ : 448.52): C, 69.63; H, 6.29, N, 6.25; Found: C, 69.51, H, 6.12, N, 6.05.



**7qa.** White oil. Yield = 71% (*c*Hex:DCM = 8:2).  $^1\text{H-NMR}$

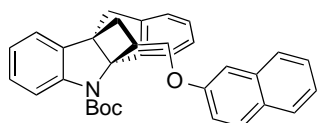
(400 MHz,  $\text{CDCl}_3$ )  $\delta$  7.97 (d,  $J = 7.6$  Hz, 1H), 7.30 (t,  $J = 7.2$  Hz, 2H), 7.19 (t,  $J = 8.4$  Hz, 1H), 7.07-6.92 (m, 5H), 6.08 (t,  $J = 2.0$ , 1H), 3.16 (m, 1H), 2.69 (dd,  $J = 2.0, 14.8$ , 1H), 2.61 (dd,  $J = 2.0, 14.8$ , 1H), 2.21-2.16 (m, 1H), 1.93 (t,  $J = 12.8$  Hz, 2H), 1.71-1.51 (m, 4H), 1.42 (s, 9H), 1.35-1.24 (m, 2H), 0.98-0.84 (m, 1H).  $^{13}\text{C-NMR}$  (100 MHz,  $\text{CDCl}_3$ ): 157.7, 145.3, 137.3, 136.5, 129.4, 127.7, 122.6, 122.5, 122.4, 117.1, 116.0, 80.7, 39.1, 36.3, 32.4, 31.5, 29.6, 28.3, 25.6, 24.5; *LC-MS*: 440 ( $\text{M}+\text{Na}$ ), 857 ( $2\text{M}+\text{Na}$ ); *Anal. calcd* for ( $\text{C}_{27}\text{H}_{31}\text{NO}_3$ : 417.55): C, 77.67; H, 7.48, N, 3.35; Found: C, 77.86, H, 7.22, N, 3.41.



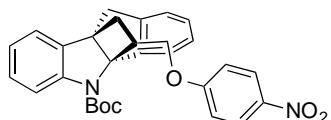
**7qd.** White solid. Yield = 87%. (*c*Hex:DCM = 95:5)

*Mp* = 73-75 °C;  $^1\text{H-NMR}$  (400 MHz,  $\text{CDCl}_3$ ):  $\delta$  8.16 (d,  $J = 9.2$  Hz, 2H), 7.81(1H, bs), 7.18 (t,  $J = 7.2$  Hz,

1H), 7.08 (d,  $J = 7.2$  Hz, 1H), 7.00 (d,  $J = 8.8$  Hz, 3H), 6.10 (bs, 1H), 3.12-3.07 (m, 1H), 2.70 (dd,  $J = 14.0, 15.2$  Hz, 1H), 2.23-2.18 (m, 1H), 1.95-1.89 (m, 2H), 1.68-1.59 (m, 3H), 1.40 (s, 9H), 1.31-1.16 (m, 3H), 0.97-0.89 (m, 1H).  $^{13}\text{C-NMR}$  (100 MHz,  $\text{CDCl}_3$ )  $\delta$  162.4, 144.8, 142.6, 136.12, 134.91, 127.9, 126.7, 125.7, 122.7, 122.7, 116.4, 116.1, 80.9, 53.5, 52.8, 38.9, 36.4, 32.0, 31.5, 30.9, 28.3, 26.9, 25.5, 24.5; *LC-MS*: 485 (M+Na), 947 (2M+Na). *Anal. calcd* for ( $\text{C}_{27}\text{H}_{30}\text{N}_2\text{O}_5$ : 462.55): C, 70.11; H, 6.54, N, 6.06; Found: C, 70.31, H, 6.76, N, 6.20.



**7ub.** Pale yellow solid. Yield = 74%; (*c*Hex:EtOAc = 95:5). *Mp* = 84-86 °C  $^1\text{H-NMR}$  (400 MHz,  $\text{CDCl}_3$ )  $\delta$  8.27 (bs, 1H), 7.75 (t,  $J = 9.2$  Hz, 3H), 7.66 (d,  $J = 8.4$  Hz, 1H), 7.44-7.33 (m, 3H), 7.23-7.16 (m, 4H), 7.01 (t,  $J = 7.2$  Hz, 1H), 6.30 (t,  $J=2.0$  Hz, 1H), 3.41 (s, 2H), 3.11 (dd,  $J = 2.0, 14.8$  Hz, 1H), 2.90 (dd,  $J = 1.6, 14.4$  Hz, 1H), 1.50 (s, 9H).  $^{13}\text{C-NMR}$  (100MHz,  $\text{CDCl}_3$ ): 155.4, 145.7, 141.19, 136.0, 134.2, 129.9, 129.4, 128.6, 128.1, 127.6, 127.0, 126.7, 126.4, 125.14, 124.3, 122.9, 119.1, 116.6, 81.6, 43.4, 38.4, 28.6. *LC-MS*: 510 (M+Na), 997 (2M+Na). *Anal. calcd* for ( $\text{C}_{33}\text{H}_{29}\text{NO}_3$ : 487.60): C, 81.29; H, 6.00, N, 2.87; Found: C, 81.13, H, 6.21, N, 2.71.



**7ud.** White oil. Yield = 50%.  $^1\text{H-NMR}$  (400 MHz,  $\text{CDCl}_3$ ):  $\delta$  8.09 (d,  $J = 9.2$  Hz, 3H), 7.58(bs, 1H), 7.18-7.09 (m, 5H), 6.96-6.89 (m, 3H), 6.14 (t,  $J= 2.0$  Hz, 1H), 3.34 (s, 2H), 3.05 (dd,  $J = 2.0, 15.2$  Hz, 1H), 2.85 (dd,  $J = 2.0, 15.2$  Hz, 1H), 1.50 (s, 9H).  $^{13}\text{C-NMR}$  (100 MHz,  $\text{CDCl}_3$ ): 162.3, 145.6, 140.6, 135.7, 135.1, 128.8, 128.2, 126.9, 125.7, 125.2, 123.9, 123.0, 116.4, 116.2, 81.6, 43.4, 38.3, 29.7, 28.5, 14.2. *LC-MS*: 505 (M+Na), 987 (2M+Na). *Anal. calcd* for ( $\text{C}_{29}\text{H}_{26}\text{N}_2\text{O}_5$ : 482.54): C, 72.19; H, 5.43, N, 5.81; Found: C, 72.01, H, 5.26, N, 5.61.

### 3.4.5 General procedure for the enantioselective [2+2] cycloaddition reaction

Under nitrogen atmosphere, AuCl·DMS (1.5 mg, 5 mol%) and (*R*)-DTBM-Segphos (3.0 mg, 2.5 mol%) were dissolved in CH<sub>2</sub>Cl<sub>2</sub> (0.5 mL), the solution was stirred at room temperature for 20 min. Then the CH<sub>2</sub>Cl<sub>2</sub> was evaporated under reduced pressure, and leave the complex under high vacuum for 20 min. Then, CH<sub>2</sub>Cl<sub>2</sub> (1.0 mL) was added and the solution was protected from light by aluminium foil. AgNTf<sub>2</sub> (1.9 mg, 5 mol%) was added and the solution was stirred at room temperature for 20 min. Then the mixture was cooled to -20 °C, then substrate **1** (0.1 mmol), and **3** (0.2 mmol) were added in sequence and the mixture stirred at the same temperature for 16 h. Removed the solvent under reduced pressure and the crude was purified by flash column chromatography to give the desired product.

**7ba:** Yield = 35%, Ee = 93%, [ $\alpha$ ]<sub>D</sub>=+107 °, (c = 2.1, CHCl<sub>3</sub>). **HPLC:** AMY-2 98:2 Hex:iPrOH 0.5 mL/min, 40 °C: 9.40 min, 10.31 min.

**7bf:** Yield = 65%, Ee = 81%, [ $\alpha$ ]<sub>D</sub>=+100 °, (c = 1.4, CHCl<sub>3</sub>). **HPLC:** AD, 97.5:2.5 Hex:iPrOH 0.5 mL/min, rt: 7.99 min, 9.27 min.

**7ea:** Yield = 56%, Ee = 92%, [ $\alpha$ ]<sub>D</sub>=+141°, (c = 1.8, CHCl<sub>3</sub>). **HPLC:** AD, 97:3 Hex:iPrOH 0.5 mL/min 40 °C: 8.25 min, 12.21 min.

**7la:** Yield = 57%, Ee = 87%, [ $\alpha$ ]<sub>D</sub>=+107 °, (c = 1.1, CHCl<sub>3</sub>). **HPLC:** Amy-2, 95:5 Hex:iPrOH 0.5 mL/min, 40 °C: 9.61 min, 10.79 min.

**7qa:** Yield = 73%, Ee = 84%, [ $\alpha$ ]<sub>D</sub>=+110 °, (c = 2.9, CHCl<sub>3</sub>). **HPLC:** AD, 90:10 Hex:iPrOH 0.5 mL/min, 40 °C: 6.89 min, 7.62 min.

## 3.4.6 Computational details

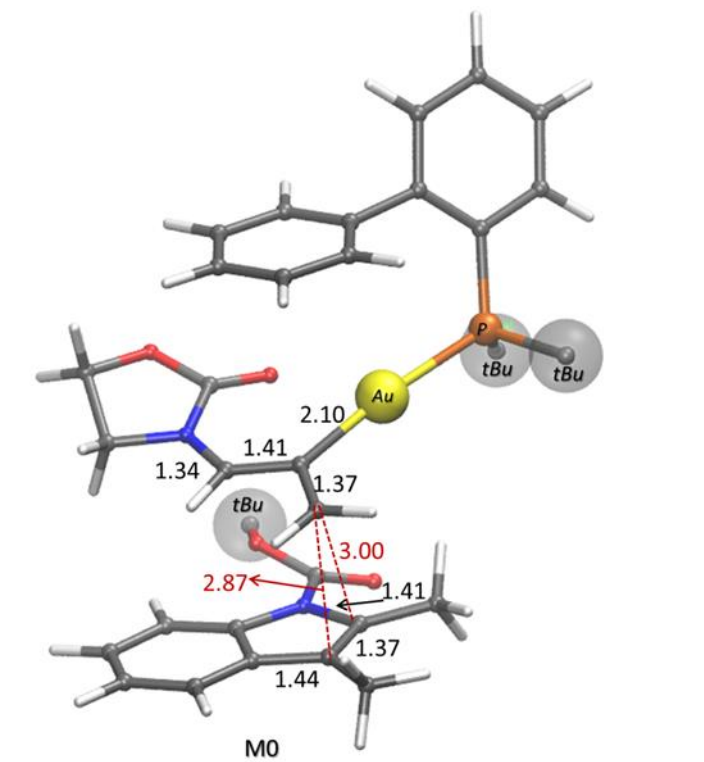


**Figure 3.17** A 3D representation of the encounter complex **M0**. Bond lengths are given in Å.

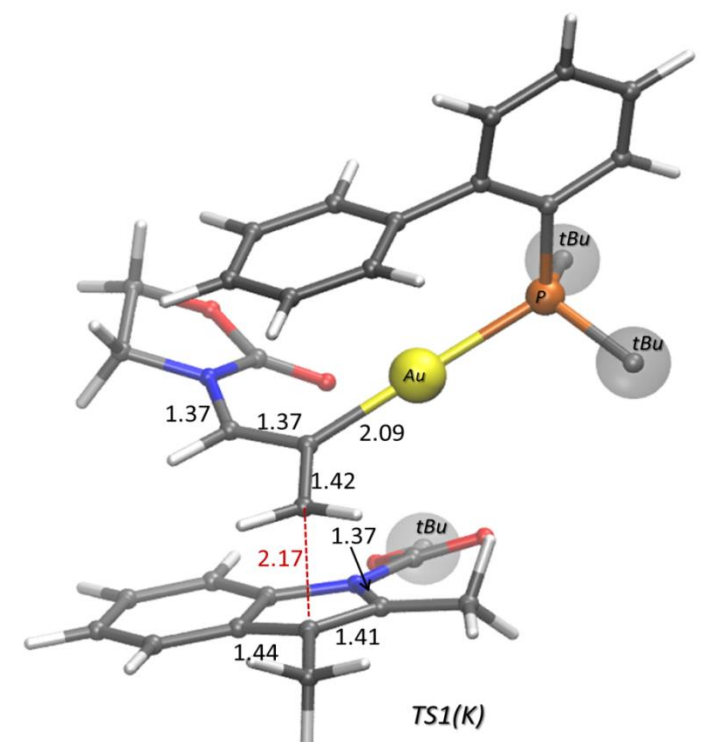


**Figure 3.18** A 3D representation of transition state **TS1(K)**. Bond lengths are given in Å.

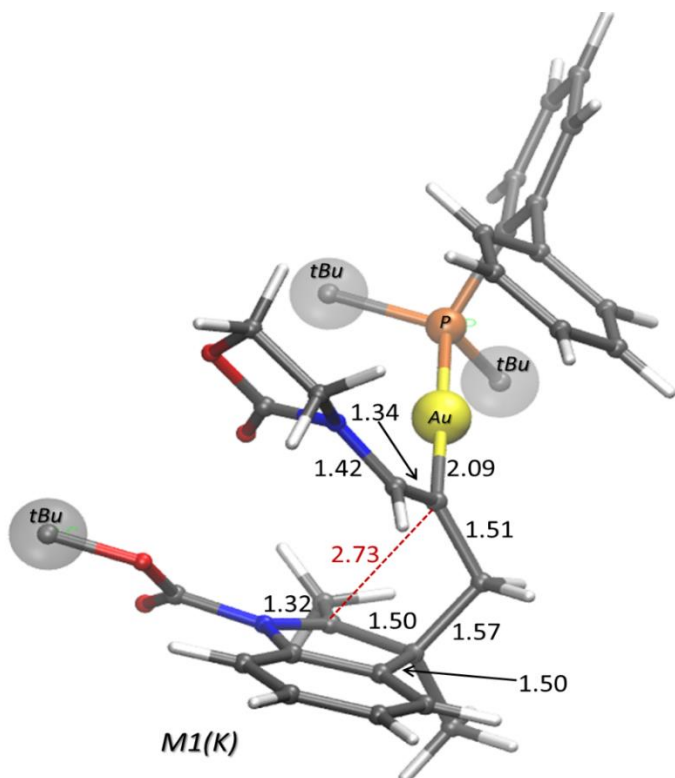


**Figure 3.19** A 3D representation of the intermediate **M1(K)**. Bond lengths are given in Å.

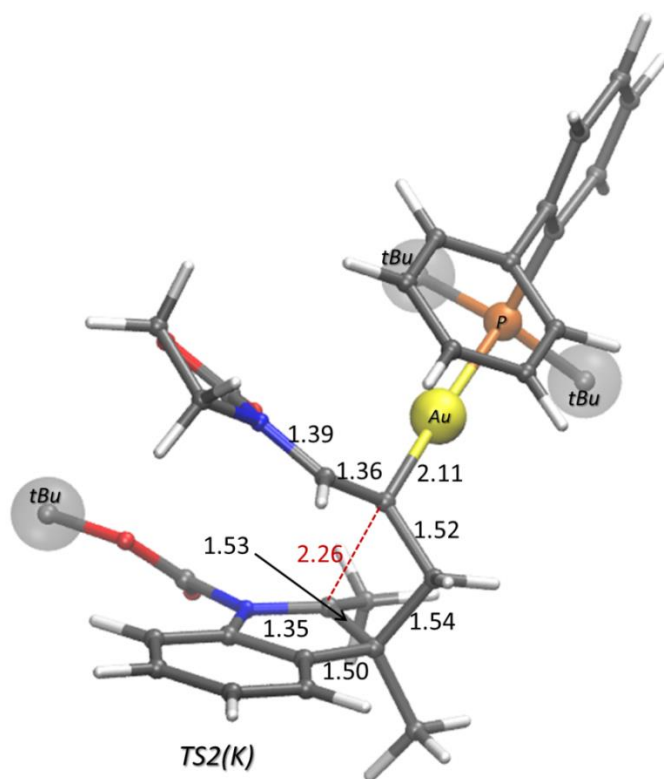


**Figure 3.20** A 3D representation of transition state **TS2(K)**. Bond lengths are given in Å.



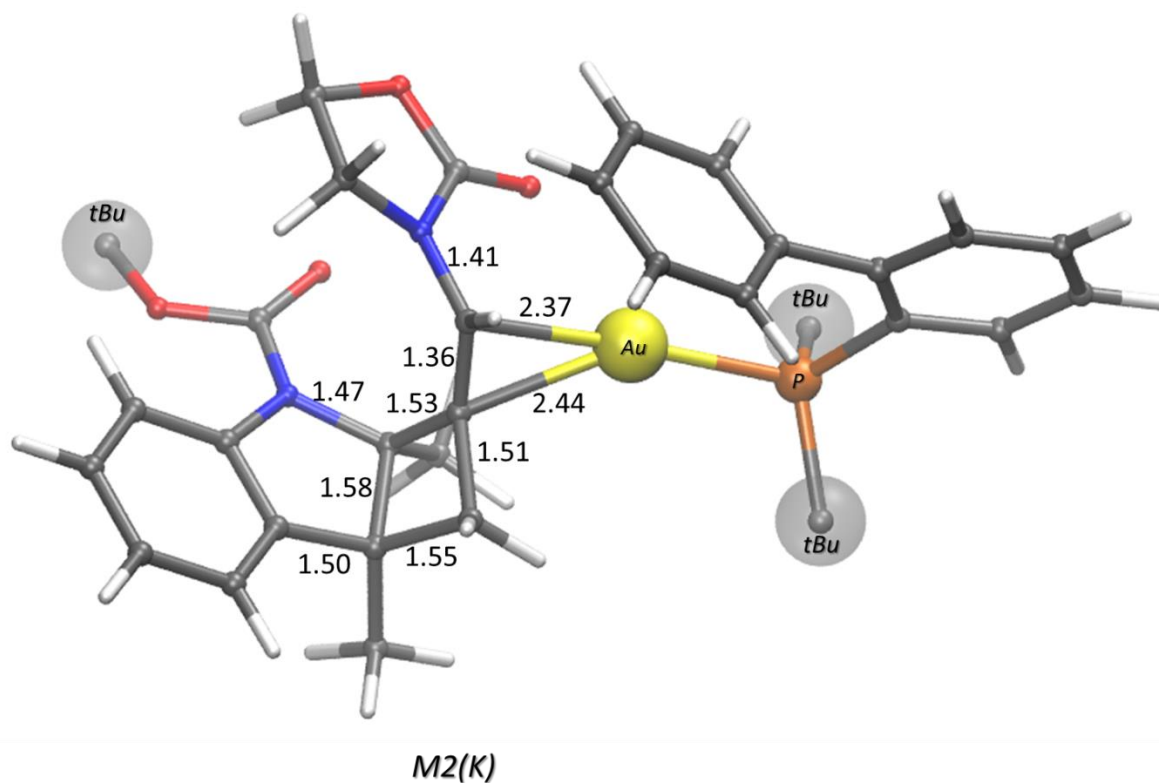


**Figure 3.21** A 3D representation of the final adduct **M2(K)**. Bond lengths are given in Å.

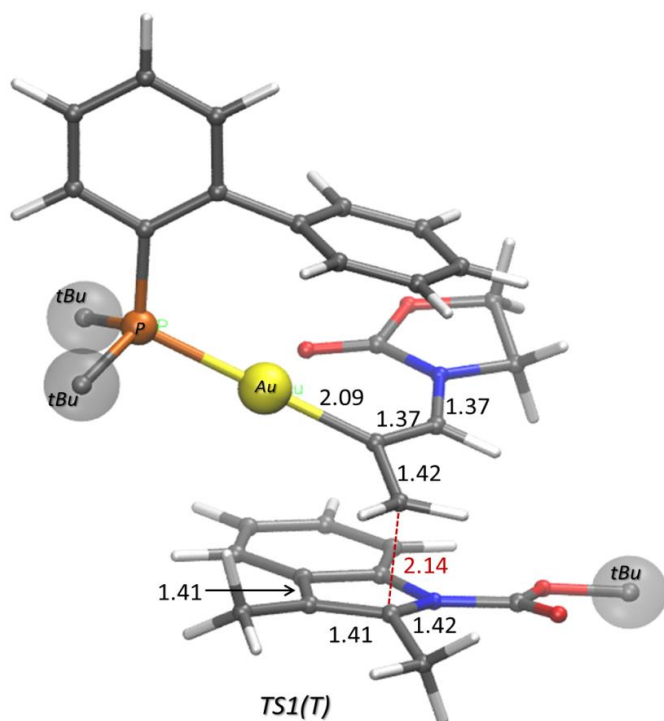


**Figure 3.22** A 3D representation of transition state **TS1(T)**. Bond lengths are given in Å.

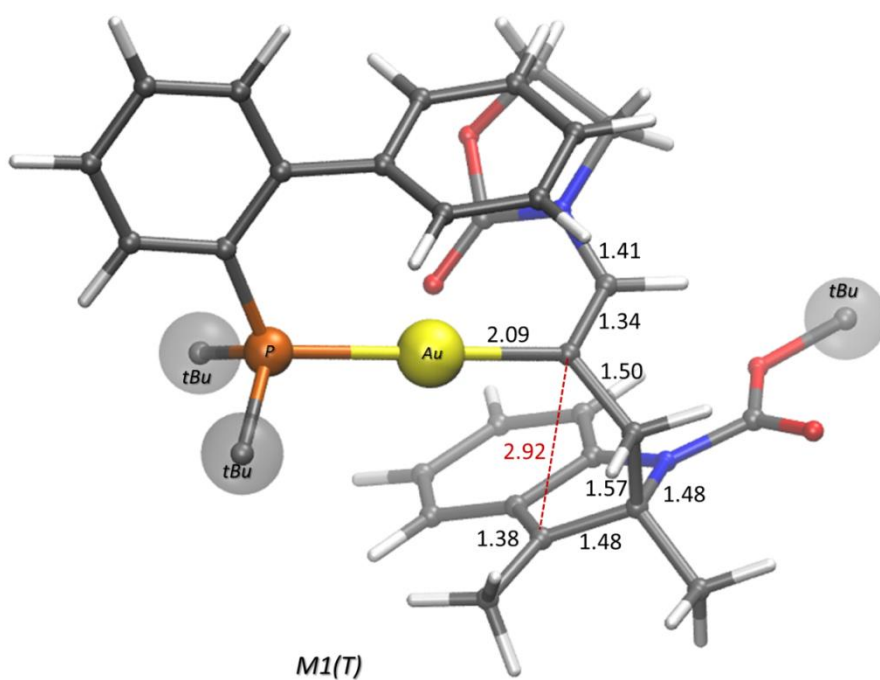


**Figure 3.23** A 3D representation of the intermediate **M1(T)**. Bond lengths are given in Å.

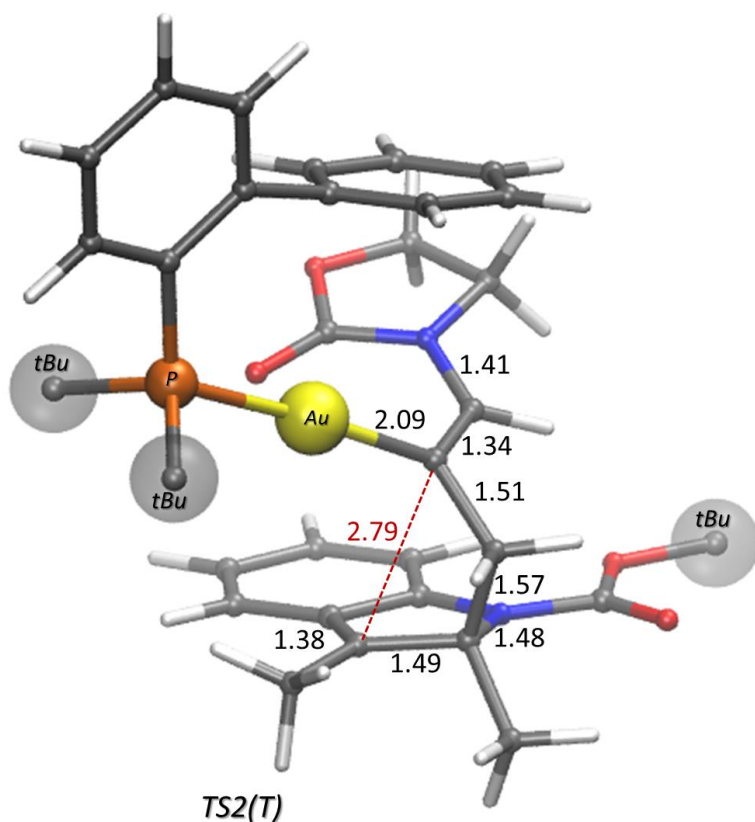


**Figure 3.24** A 3D representation of transition state **TS2(T)**. Bond lengths are given in Å.

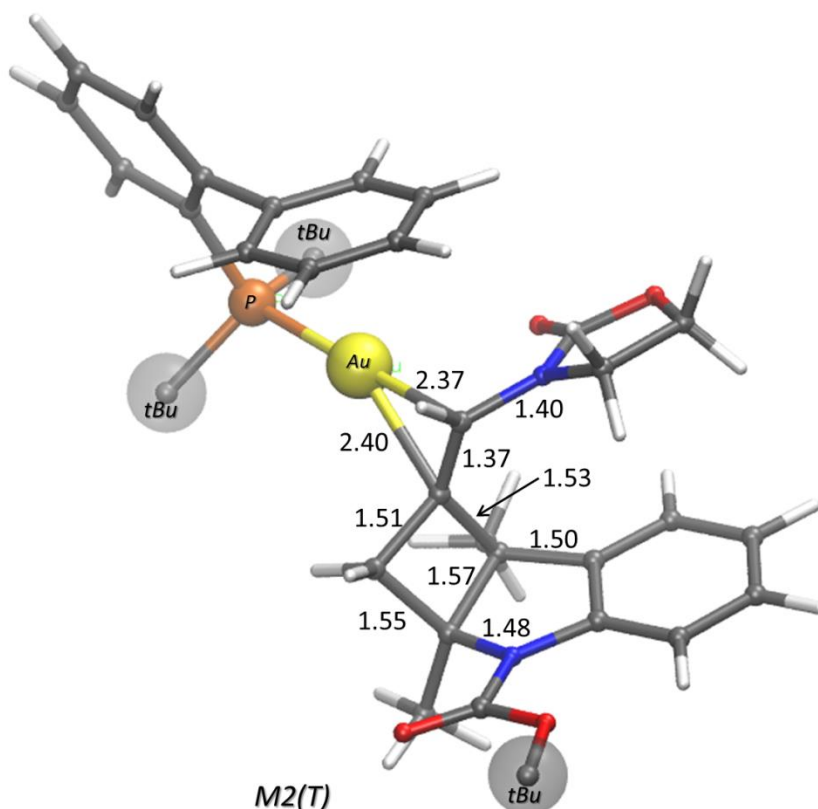


**Figure 3.25** A 3D representation of the final adduct **M2(T)**. Bond lengths are given in Å.

### 3.4.7 Crystallographic Data Collection and Structure Determination for **4b'**, **4r** and **7hd**

The X-ray intensity data of **4b'** and **7hd** were measured on a Bruker SMART Apex II CCD area detector diffractometer whereas the intensity data for compound **4r** were recorded on a four-circle Bruker X8APEX diffractometer (Mo-K $\alpha$  generator,  $\lambda = 0.71073$  Å) equipped with an area detector and controlled by the Bruker-Nonius X8APEX software, that was used also for data reduction. Cell dimensions and the orientation matrix were initially determined from a least-squares refinement on reflections measured in three sets of 20 exposures, collected in three different  $\omega$  regions, and eventually refined against all data. A full sphere of reciprocal space was scanned by  $0.3^\circ$   $\omega$  steps. The software SMART (SMART & SAINT Software Reference Manuals, version 5.051 (Windows NT Version) Bruker Analytical X-ray

Instruments Inc.: Madison, WI, 1998), was used for collecting frames of data, indexing reflections, and determination of lattice parameters. The collected frames were then processed for integration by the SAINT program and an empirical absorption correction was applied using SADABS. The structures were solved by direct methods (SIR 2004)<sup>[47]</sup> and subsequent Fourier syntheses and refined by full-matrix least-squares on  $F^2$  (SHELXTL, G. M. Sheldrick, SHELXTLplus (Windows NT Version) Structure Determination Package, Version 5.1. Bruker Analytical X-ray Instruments Inc.: Madison, WI, USA, 1998), using anisotropic thermal parameters for all non-hydrogen atoms. All hydrogen atoms were added in calculated positions, included in the final stage of refinement with isotropic thermal parameters,  $U(\text{H}) = 1.2 U_{\text{eq}}(\text{C})$  [ $U(\text{H}) = 1.5 U_{\text{eq}}(\text{C-Me})$ ], and allowed to ride on their carrier carbons. Crystal data and details of the data collection for **4b'**, **4r** and **7hd** are reported in **Table 3.6** Crystal data and structure refinement for **3b'** and **4r** and **7hd**. CCDC 1416318 (**4b'**), 1416343 (**4r**) and 1416344 (**7hd**) contain the supplementary crystallographic data for this paper. These data can be obtained free of charge from the Cambridge Crystallographic Data Centre via [www.ccdc.cam.ac.uk/data\\_request/cif](http://www.ccdc.cam.ac.uk/data_request/cif).

### 3.4.7.1 X-ray crystal structure of 4b', 4r and 7hd

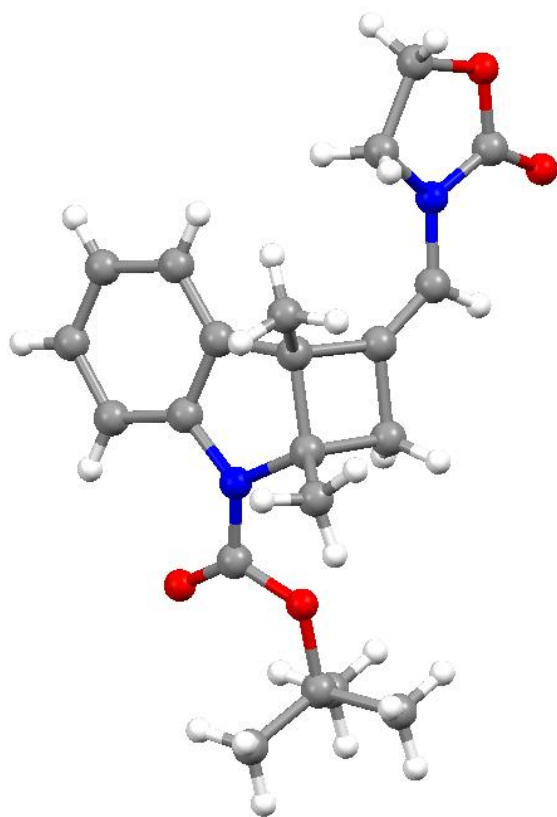


**Figure 3.26** Molecular structure of 4b'.

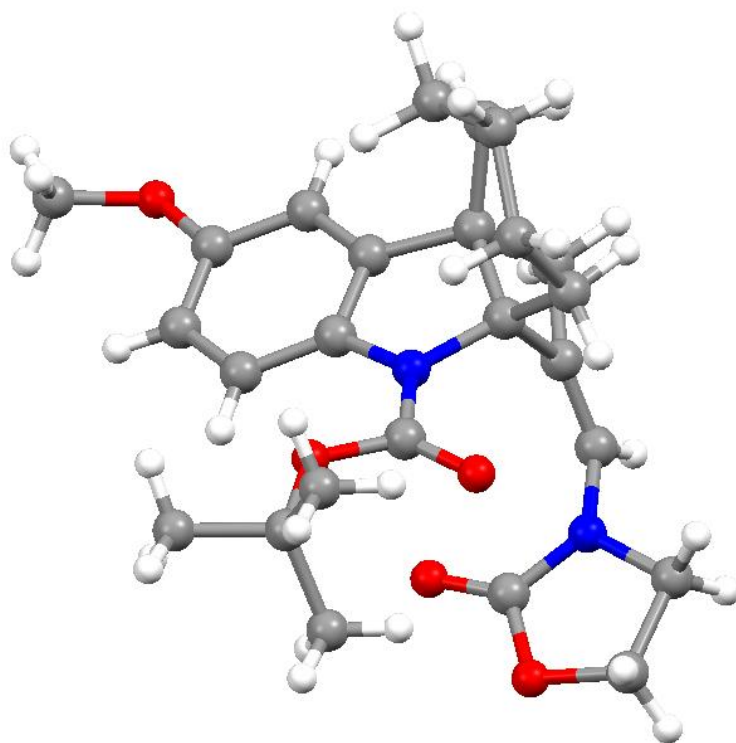


**Figure 3.27** Molecular structure of 4r.

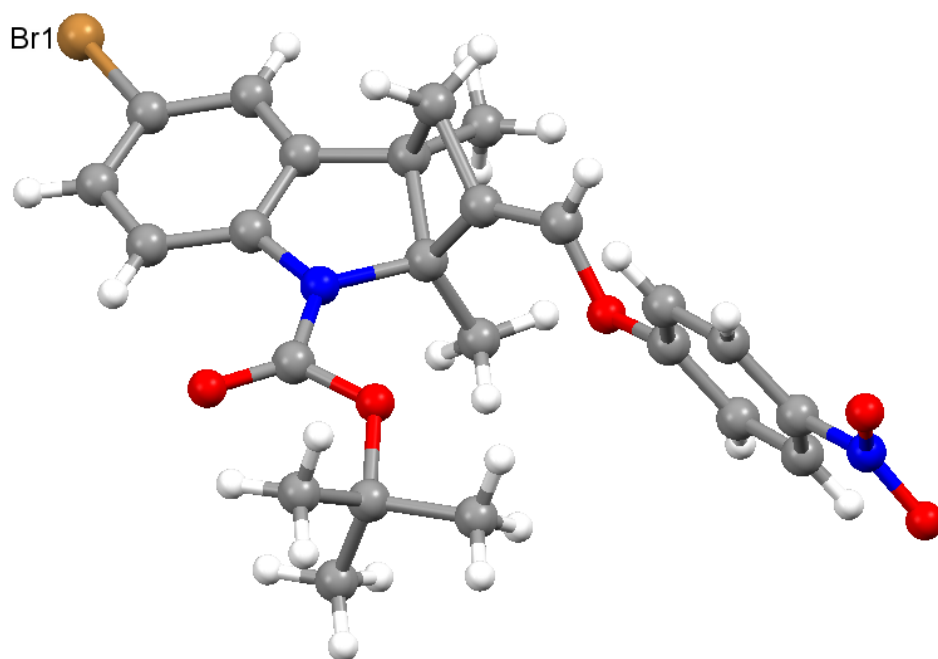


**Figure 3.28** Molecular structure of **7hd**.

**Table 3.6** Crystal data and structure refinement for **3b'** and **4r** and **7hd**.

	4b'	4r	7hd
Formula	C <sub>21</sub> H <sub>26</sub> N <sub>2</sub> O <sub>4</sub>	C <sub>25</sub> H <sub>32</sub> N <sub>2</sub> O <sub>5</sub>	C <sub>24</sub> H <sub>25</sub> BrN <sub>2</sub> O <sub>5</sub>
Fw	370.44	440.53	501.36
T, K	296 (2)	293(2)	296 (2)
Crystal symmetry	orthorhombic	triclinic	monoclinic
Space group	P ca2 <sub>1</sub>	P -1	P 2 <sub>1</sub> /n
a, Å	9.887(1)	9.9946(9)	10.315(3)
b, Å	22.511(3)	11.648(1)	16.082(5)
c, Å	8.827(1)	20.470(2)	14.351(5)
α, °	90	87.347(4)	90
β, °	90	81.681(4)	102.518(4)
γ, °	90	89.034(4)	90
Cell volume, Å <sup>3</sup>	1965(5)	2355.3(4)	2324(13)

Z	4	4	4
$D_C$ , $Mg\ m^{-3}$	1.252	1.242	1.433
$\mu(Mo-K\alpha)$ , $mm^{-1}$	0.087	0.086	1.806
F(000)	792	944	1032
Crystal size mm	0.35x0.20x0.10	0.35x0.15x0.10	0.30x0.15x0.10
$\theta$ limits, $^\circ$	1.81 - 28.73	1.75 - 27.98	1.93 - 24.74
Refl. collected, unique ( $R_{int}$ )	12932, (0.0194)	4363	46979, 11227 (0.0369)
Goodness-of-fit-on $F^2$	1.242	1.020	1.064
$R_1(F)^a$ , $wR_2$	0.0507, 0.0940	0.0634, 0.2105	0.0862, 0.2368
$(F^2) [I > 2\sigma(I)]^b$			
Largest diff. peak and hole, $e. \text{ \AA}^{-3}$	0.134 and -0.157	0.303 and -0.389	1.529 and -0.446

<sup>a</sup> $R_1 = \sum||F_o|-|F_c||/\sum|F_o|$ . <sup>b</sup> $wR_2 = [\sum w(F_o^2 - F_c^2)^2/\sum w(F_o^2)^2]^{1/2}$  where  $w = 1/[\sigma^2(F_o^2) + (aP)^2 + bP]$  where  $P = (F_o^2 + F_c^2)/3$ .

### 3.5 Bibliography

- [1] R. Ocello, A. De Nisi, M. Jia, Q. Q. Yang, M. Monari, P. Giacinto, A. Bottoni, G. Pietro Miscione, M. Bandini, *Chem. - A Eur. J.* **2015**, *21*, 18445–18453.
- [2] N. Gupta, D. Goyal, *Chem. Heterocycl. Compd.* **2015**, *51*, 4–16.
- [3] P. J. Praveen, P. S. Parameswaran, M. S. Majik, *Synth.* **2015**, *47*, 1827–1837.
- [4] S. P. Roche, J. J. Youte Tendoung, B. Tréguier, *Tetrahedron* **2015**, *71*, 3549–3591.
- [5] R. Dalpozzo, *Chem. Soc. Rev.* **2015**, *44*, 742–778.
- [6] W. Zi, Z. Zuo, D. Ma, *Acc. Chem. Res.* **2015**, *48*, 702–711.
- [7] Q. Ding, X. Zhou, R. Fan, *Org. Biomol. Chem.* **2014**, *12*, 4807–4815.
- [8] C. X. Zhuo, C. Zheng, S. L. You, *Acc. Chem. Res.* **2014**, *47*, 2558–2573.
- [9] Q. Ni, H. Zhang, A. Grossmann, C. C. J. Loh, C. Merckens, D. Enders, *Asymmetrische Synthese von Pyrroloindolonen Über Eine Durch N-Heterocyclische Carbene Katalysierte [2+3]-Anellierung von  $\alpha$ -Chloraldehyden Mit Nitrovinylindolen*, **2013**.
- [10] C. C. J. Loh, D. Enders, *Angew. Chemie - Int. Ed.* **2012**, *51*, 46–48.
- [11] J. Barluenga, E. Tudela, A. Ballesteros, M. Tomás, *J. Am. Chem. Soc.* **2009**, *131*, 2096–2097.
- [12] L. M. Repka, J. Ni, S. E. Reisman, *J. Am. Chem. Soc.* **2010**, *132*, 14418–14420.
- [13] Y. Lian, H. M. L. Davies, *J. Am. Chem. Soc.* **2010**, *132*, 440–441.
- [14] J. E. Spangler, H. M. L. Davies, *J. Am. Chem. Soc.* **2013**, *135*, 6802–6805.



- [15] H. Xiong, H. Xu, S. Liao, Z. Xie, Y. Tang, *J. Am. Chem. Soc.* **2013**, *135*, 7851–7854.
- [16] J. Huang, L. Zhao, Y. Liu, W. Cao, X. Wu, *Org. Lett.* **2013**, *15*, 4338–4341.
- [17] G.-J. Duan, J.-B. Ling, W.-P. Wang, Y.-C. Luo, P.-F. Xu, *Chem. Commun.* **2013**, *49*, 4625.
- [18] W. R. Gutekunst, P. S. Baran, *J. Org. Chem.* **2014**, *79*, 2430–2452.
- [19] L. Zhang, *J. Am. Chem. Soc.* **2005**, *127*, 16804–16805.
- [20] H. Faustino, P. Bernal, L. Castedo, F. López, J. L. Mascareñas, *Adv. Synth. Catal.* **2012**, *354*, 1658–1664.
- [21] D. Zhao, J. Zhang, Z. Xie, *J. Am. Chem. Soc.* **2015**, *137*, 9423–9428.
- [22] B. Alcaide, P. Almendros, C. Aragoncillo, *Chem. Soc. Rev.* **2010**, *39*, 783–816.
- [23] F. López, J. L. Mascareñas, *Beilstein J. Org. Chem.* **2011**, *7*, 1075–1094.
- [24] F. López, J. L. Mascareñas, *Beilstein J. Org. Chem.* **2013**, *9*, 2250–2264.
- [25] M. Jia, M. Monari, Q.-Q. Yang, M. Bandini, *Chem. Commun.* **2015**, *51*, 2320–2323.
- [26] C. Nieto-Oberhuber, S. López, A. M. Echavarren, *J. Am. Chem. Soc.* **2005**, *127*, 6178–6179.
- [27] E. Herrero-Gómez, C. Nieto-Oberhuber, S. López, J. Benet-Buchholz, A. M. Echavarren, *Angew. Chemie - Int. Ed.* **2006**, *45*, 5455–5459.
- [28] V. Pirovano, L. Decataldo, E. Rossi, R. Vicente, *Chem. Commun.* **2013**, *49*, 3594.
- [29] Y. Wang, P. Zhang, Y. Liu, F. Xia, J. Zhang, *Chem. Sci.* **2015**, *6*, 5564–

5570.

- [30] S. Suárez-Pantiga, C. Hernández-Díaz, M. Piedrafita, E. Rubio, J. M. González, *Adv. Synth. Catal.* **2012**, *354*, 1651–1657.
- [31] R. Zimmer, H.-U. Reissig, *Chem. Soc. Rev.* **2014**, *43*, 2888–2903.
- [32] S. Montserrat, H. Faustino, A. Lledós, J. L. Mascareñas, F. López, G. Ujaque, *Chem. - A Eur. J.* **2013**, *19*, 15248–15260.
- [33] Y. Xu, M. L. Conner, M. K. Brown, *Angew. Chemie - Int. Ed.* **2015**, *54*, 11918–11928.
- [34] E. Manoni, A. De Nisi, M. Bandini, *Pure Appl. Chem.* **2016**, *88*, 207–214.
- [35] K. Liu, G. Xu, J. Sun, *Chem. Sci.* **2018**, *9*, 634–639.
- [36] Q. Cai, C. Liu, X. W. Liang, S. L. You, *Org. Lett.* **2012**, *14*, 4588–4590.
- [37] Q. Cai, S. L. You, *Org. Lett.* **2012**, *14*, 3040–3043.
- [38] Q. Cai, C. Zheng, J. W. Zhang, S. L. You, *Angew. Chemie - Int. Ed.* **2011**, *50*, 8665–8669.
- [39] W. Zi, H. Wu, F. D. Toste, *J. Am. Chem. Soc.* **2015**, *137*, 3225–3228.
- [40] K. Douki, H. Ono, T. Taniguchi, J. Shimokawa, M. Kitamura, T. Fukuyama, *J. Am. Chem. Soc.* **2016**, *138*, 14578–14581.
- [41] Y. Li, W. Li, J. Zhang, *Chem. - A Eur. J.* **2017**, *23*, 467–512.
- [42] S. Peng, S. Cao, J. Sun, *Org. Lett.* **2017**, *19*, 524–527.
- [43] M. Jia, M. Bandini, *ACS Catal.* **2015**, *5*, 1638–1652.
- [44] B. Ranieri, I. Escofet, A. M. Echavarren, *Org. Biomol. Chem.* **2015**, *13*, 7103–7118.
- [45] L. Rocchigiani, M. Jia, M. Bandini, A. Macchioni, *ACS Catal.* **2015**, *5*, 3911–3915.

- [46] K. S. MacMillan, J. Naidoo, J. Liang, L. Melito, N. S. Williams, L. Morlock, P. J. Huntington, S. J. Estill, J. Longgood, G. L. Becker, et al., *J. Am. Chem. Soc.* **2011**, *133*, 1428–1437.
- [47] M. C. Burla, R. Caliandro, M. Camalli, B. Carrozzini, G. L. Cascarano, L. De Caro, C. Giacovazzo, G. Polidori, R. Spagna, *J. Appl. Crystallogr.* **2005**, *38*, 381–388.

# 4 I THOUGHT IT WAS GOLD INSTEAD...TBAF CATALYSED ONE-POT SYNTHESIS OF ALLENYL- INDOLES

The present work is the result of a serendipitous discovery.<sup>[1]</sup> I was working on the synthesis of a new substrate for a gold-catalysed reaction. The last step of the synthesis was supposed to be the cleavage of the two silyl-protecting group, performed by tetrabutylammonium fluoride (TBAF) but the result was unexpected. I found that  $\text{Bu}_4\text{N}^+$  and  $\text{F}^-$  ions were effective in performing a cascade sequence involving intramolecular hydroamination of the C-C triple bond, cleavage of silyl-protecting groups and site-selective sigmatropic aza-Cope-type [3,3]-rearrangement. Part of this chapter has been published on *Organic Chemistry Frontiers*<sup>[2]</sup> and reproduced from ref. [2] with permission from The Royal Society of Chemistry.

## 4.1 Introduction

### 4.1.1 Intramolecular hydroamination reaction

Intramolecular hydroamination is among the most powerful and employed synthetic approaches to the synthesis of benzofused aza-heterocycles.<sup>[3-5]</sup> The process cannot be spontaneously performed due to lack of reactivity complementarity in the acyclic precursors, therefore an electrophilic activation becomes mandatory. In this regard, soft metal catalysis has gained important credits over the past few years, triggering the efficient activation of the C-C triple bond towards the regioselective inter- as well as intramolecular condensation with heteroatom-based nucleophiles. Among the others, electrophilic metal species based on Pd, In, Au, Pt, Ag... have found efficient applications in catalytic variants showing good chemical performances and substrate scope.<sup>[6-13]</sup> However, the use of noble metals leads to important issues in terms of methodology sustainability and the replacement of coinage metals with cheaper metal-free catalytic agents is still highly desirable.

In this direction, the employment of strong Brønsted acids as well as bases such as pTsOH, TfOH, KOH and Cs<sub>2</sub>CO<sub>3</sub> was found very efficient in the functionalization of alkynes with hetero-nucleophiles even if the protocols suffered by the requirements of harsh reaction conditions and large and even superstoichiometric amounts of additives.<sup>[14-19]</sup> Alternatively, soft quaternary ammonium salts are known to act as synthetic equivalents of late-transition metal species in activating unsaturated hydrocarbons towards nucleophilic attack and the spontaneous replacement of the ammonium fragment by the isoelectronic proton, make catalytic variants potentially amenable. In this direction, Jacobi and coworkers in the 90's demonstrated the efficiency of large amounts of tetrabutylammonium fluoride (TBAF) in promoting the intramolecular hydroamination of acetylenic amides to give cyclic enamides (Figure 4.1a).<sup>[20,21]</sup>

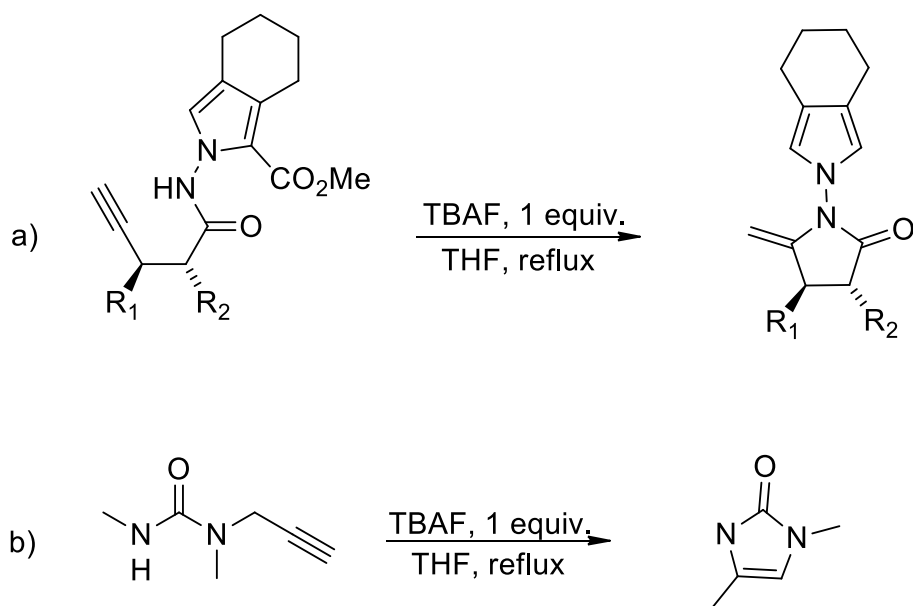


**Figure 4.1** Seminal works on the electrophilic activation of isolated alkynes by means of TBAF: a) Synthesis of cyclic enamides reported by Jacobi;<sup>[20]</sup> b) cyclization of propargyl urea reported by Huguenot.<sup>[22]</sup>

After these seminal works, the methodology found numerous applications in the synthesis of heterocycles through X-H addition to unsaturated hydrocarbons, one example reported by Huguenot is shown in Figure 4.1.<sup>[23,24,22,25,26]</sup>

However the use of ammonium salts in catalytic transformations was sporadically documented and never fully and systematically investigated in organic processes.<sup>[27]</sup>

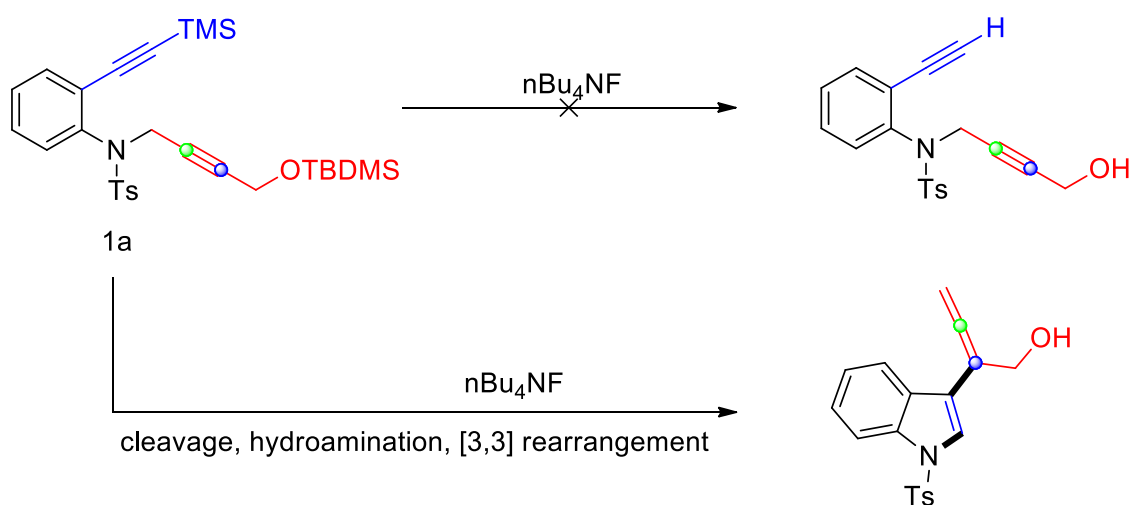


**Figure 4.2** Plan vs cascade sequence discovered.

TBAF is one of the most used reagents for silyl ether deprotection, in fact it is a source of fluoride that can be used in organic solvents since the ammonium cation is lipophilic and this makes it preferable to inorganic bases. Having to deprotect both a terminal alkyne and a silyl ether, the choice fell on the TBAF itself. Serendipitously we obtained not only the two cleavages but also the hydroamination, despite having a tosylated nitrogen, and an aza-Cope-type [3,3] rearrangement (Figure 4.2).

We decided to deepen this discovery trying to optimize the reaction conditions. After having verified that the process is catalytic, we also tried to understand the mechanism and test the synthetic usefulness of 3-allenyl-indoles using it as a substrate for gold catalysis to obtain a tetrahydrocarbazole.

## 4.2 Results and discussion

### 4.2.1 Synthesis of ortho-alkynyl aniline

At the outset of the investigation, ortho-alkynyl aniline **1a** was elected as the model acyclic precursor and the choice for **1a** was dictated by its ready availability and high chemical functionality.

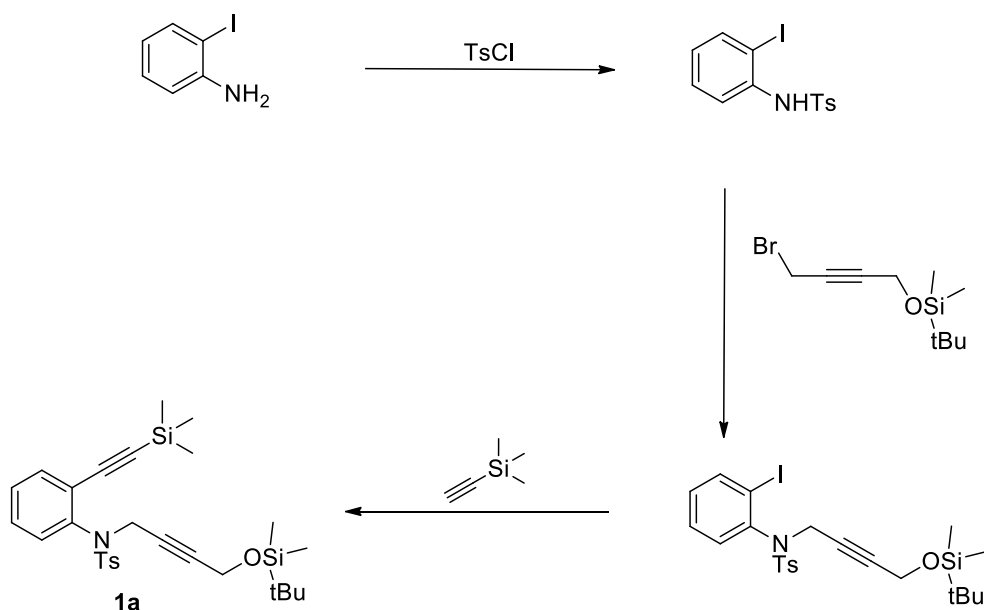
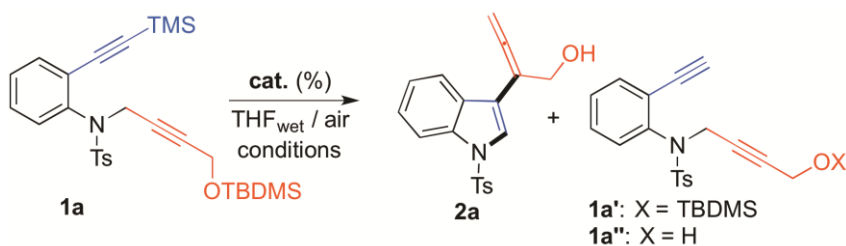


**Figure 4.3** Schematic synthetic route for the obtainment of **1a**.

The synthesis of **1a** started with the tosylation of 2-iodoaniline, then the 2-iodo tosylation was alkylated with a functionalized propargyl bromide. The last step was the Sonogashira coupling with the trimethylsilylacetylene. All the synthetic procedures are reported in the Experimental part.

#### 4.2.2 Study of the catalytic system



We envisioned that the use of fluoride-based catalysts could enable also the concomitant cleavage of the silyl protecting group of **1** during the catalysis, with a positive impact on the overall step economy of process. A survey of reaction conditions involving ammonium salts as catalysts was performed and a collection of results is reported in the Table 4.1.



**Table 4.1** Optimization of the catalytic system.<sup>a</sup>

Run	cat. (%)	T / t (h)	yield (%) <sup>b</sup> 2a/1a'/1a''
1 <sup>c</sup>	TBAF·3H <sub>2</sub> O (200)	0 °C/1	67/-/33
2	TBAF·3H <sub>2</sub> O (100)	rt/16	97/-/-
3	TBAF·3H <sub>2</sub> O (50)	rt/16	97/-/-
4	TBAF·3H <sub>2</sub> O (10)	rt/16	78/10/5
5 <sup>d</sup>	TBAF·3H <sub>2</sub> O (10)	rt/2	70/-/-
6 <sup>e</sup>	TBAF·3H <sub>2</sub> O (10)	rt/16	55/-/-
7	TBACl/KF·2H <sub>2</sub> O (300)	rt/16	-/42/-
8	TBAOH·30H <sub>2</sub> O (300)	rt/16	NR
9	CsF (100)	rt/16	-/88/-

<sup>a</sup> All the reactions were carried out in reagent grade THF without moisture prevention, unless otherwise specified (0.045 M). <sup>b</sup> Isolated yield. <sup>c</sup> Conversion by NMR. <sup>d</sup> Concentration = 0.1 M. <sup>e</sup> Dry THF was employed. Compound **2a'** (*vide infra*) was also observed in the reaction crude. TBAF: tetrabutylammonium fluoride. TBACl: tetrabutylammonium chloride. TBAOH: tetrabutylammonium hydroxide. TMS: trimethylsilyl. TBDMS: tertbutyldimethylsilyl. NR = no reaction.

Initial attempts were carried out in the presence of hydrate tetra-*n*(butyl)ammonium fluoride (TBAF) as the promoter in reagent grade THF and open-air vial. Interestingly, beside the incomplete reaction at 0 °C with 200 mol% of TBAF·3H<sub>2</sub>O (1 h), the desired product **2a** was generally isolated in very high yields (67-97%).<sup>12</sup> Gratifyingly, catalytic amount of ammonium salt (10 mol%, entry 4 in Table 4.1) proved also competence in providing **2a** in satisfactory 78% yield, accompanied by the presence of minor components such as the mono- or bis-desilylated acyclic compounds **1a'** and **1a''**. It is worth noting that tetrabutylammonium fluoride exerts a multiple role during the reaction course. As a matter of fact, besides the assistance in the hydroaminative event (*vide infra* for mechanistic interpretation), the double cleavage of silyl-units was also operated.

In terms of reaction machinery, some experimental evidences enabled preliminary conclusions to be drawn. First: inertness or partial/complete desilylation of **1a** occurred with different fluorinating agents or bases (e.g. TBACl/KF, CsF and TBAOH, entries 7-9); second, the use of wet THF<sup>13</sup> proved mandatory for a complete consumption of **1a** the success of the cascade methodology. As a matter of fact, dry THF performed less efficiently (yield **2a** = 55%), providing also **2a'** as the major by-product (entry 6). All at once, only the synergistic action of both ions  $n\text{Bu}_4\text{N}^+$  and  $\text{F}^-$  in TBAF seemed guaranteeing the correct chemical environment to provide **2a** in synthetically acceptable extents (*vide infra*).

Having established the optimal reaction conditions, the scope of the method was ascertained by subjecting a series of differently substituted *ortho*-alkynyl anilines (**1b-k**) to TBAF·3H<sub>2</sub>O catalysis and the results are reported in Figure 4.4.

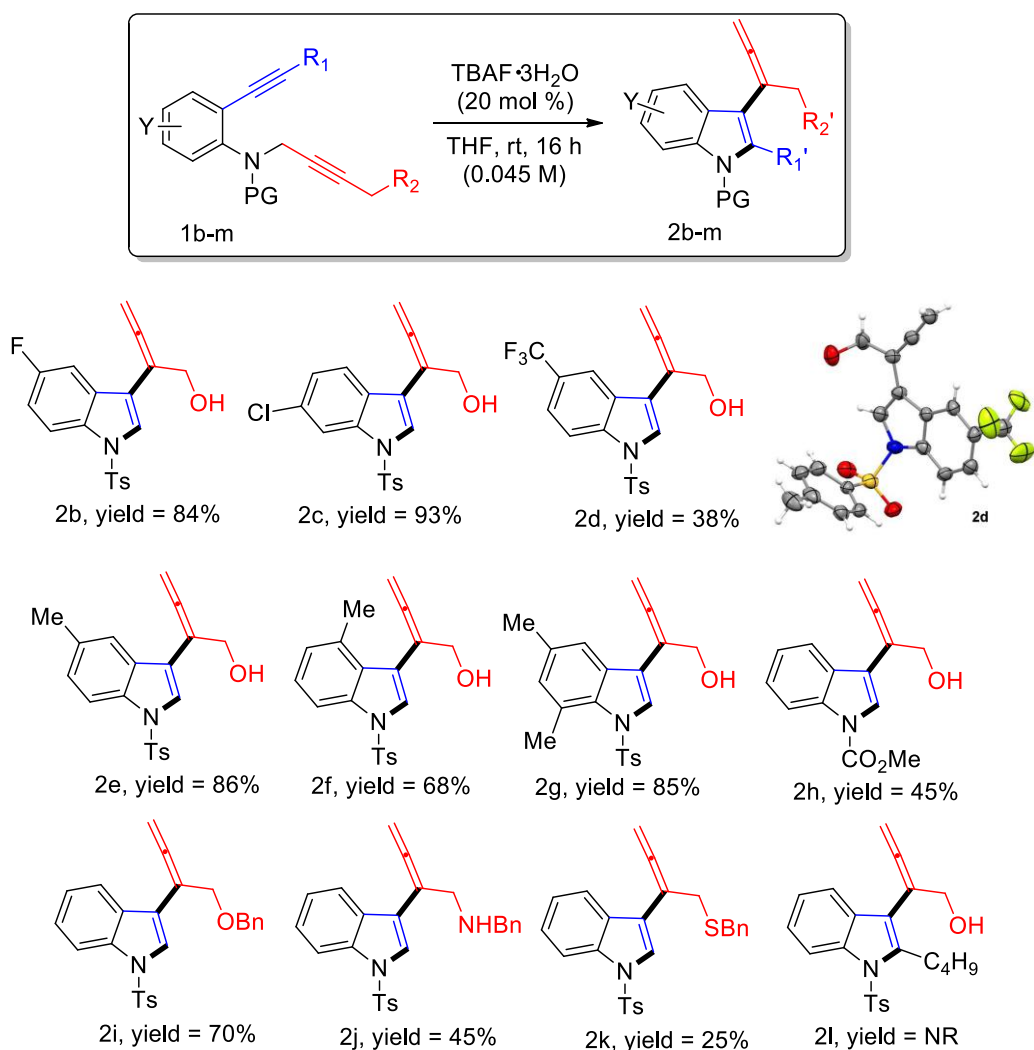


**Figure 4.4** Scope and limitations of the catalytic protocol (NR = no reaction).

From the results collected in Figure 4.4, it emerged that anilines carrying both electron-withdrawing (F, Cl, CF<sub>3</sub>) as well as electron-donating group (e.g. Me) at different positions were suitable candidates for the present transformation, delivering the corresponding cyclized and deprotected allenyl-indoles **2** in high yields (up to 93%). Interestingly, the methodology was not restricted to silyloxy-ether precursors but also -OBn and NHBn derivatives (**1i-j**) performed in moderate to good extents. We also showed that the easily removable *N*-methyl formate group is tolerated in the process, delivering the *N*-CO<sub>2</sub>Me **2h** adduct in 45% yield. However, the replacement of TMS group in **1** with an alkyl chain (*i.e.* *n*C<sub>4</sub>H<sub>9</sub>, **1l**) led to the formation of a complex mixture of unknown compounds.

Despite the undoubted synthetic utility of the protocol, several interrogatives concerning mechanistic aspects were still open.

In this direction, experimental as well as spectroscopic experiments have been performed. With the purpose of ascertaining the order of chemical events in the cascade process and the role of the trialkylsilyl functions on the overall reaction machinery, compounds **1a'** and **1m** were subjected to best catalytic conditions (Figure 4.5). Interestingly, while **1l** reacted smoothly giving **2a** in 82% yield, the employment of the terminal alkyne **1a'** caused the failure of the process in fact unreacted **1a'** was fully recovered at the end of the process. The latter evidence suggests that the initial hydroaminative step, triggered by the synergistic action of the ammonium cation and the fluoride anion, is crucial for the overall reaction profile. Differently, the positive result obtained with **1l** suggests that the TBDMS group is not directly involved in the crucial bond forming steps of the process, as also testified by the promising results obtained with compounds **1i-j** of Figure 4.4.

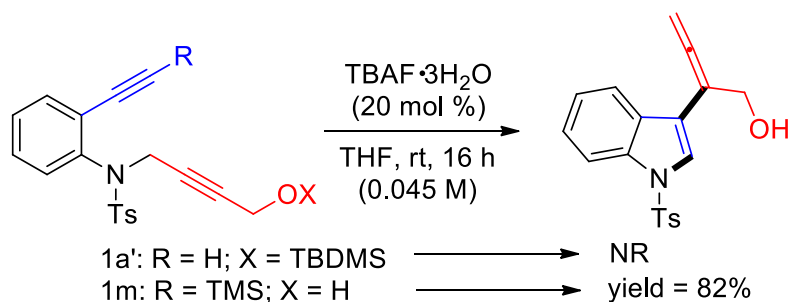


**Figure 4.5** Proving the role of the silyl groups in the cascade process (NR: no reaction).

Additionally, the  $^1\text{H-NMR}$  spectroscopic investigation (THF- $d_8$  dry, rt) of the reaction showed a very fast reaction profile.

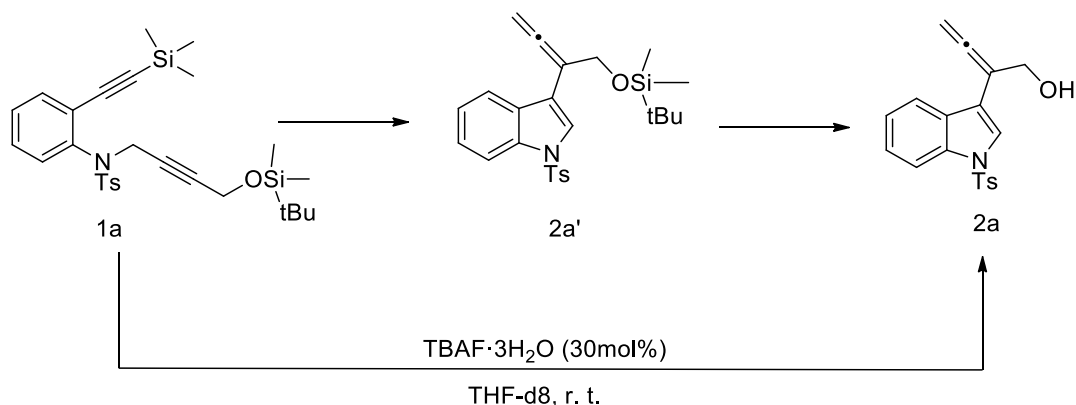


**Figure 4.6** Reaction scheme with the intermediate **2a'**.

Recording the <sup>1</sup>H-NMR of **1a** (Figure 4.7) in the presence of 30% mol of TBAF·3H<sub>2</sub>O, after 2 min reaction time, **2a** was formed in 49.5% conversion along with two new compounds, the magnification of the region between 4 and 5.6 ppm of the <sup>1</sup>H-NMR recorded is shown in Figure 4.8. Although we failed in assigning one of them, the still *O*-silylated indole **2a'** was identified as a reaction intermediate (Figure 4.6). Full conversion into **2a** was reached in 3 hours (Figure 4.9), all the <sup>1</sup>H-NMR recorded are collected in section 4.4.13 of Experimental part.

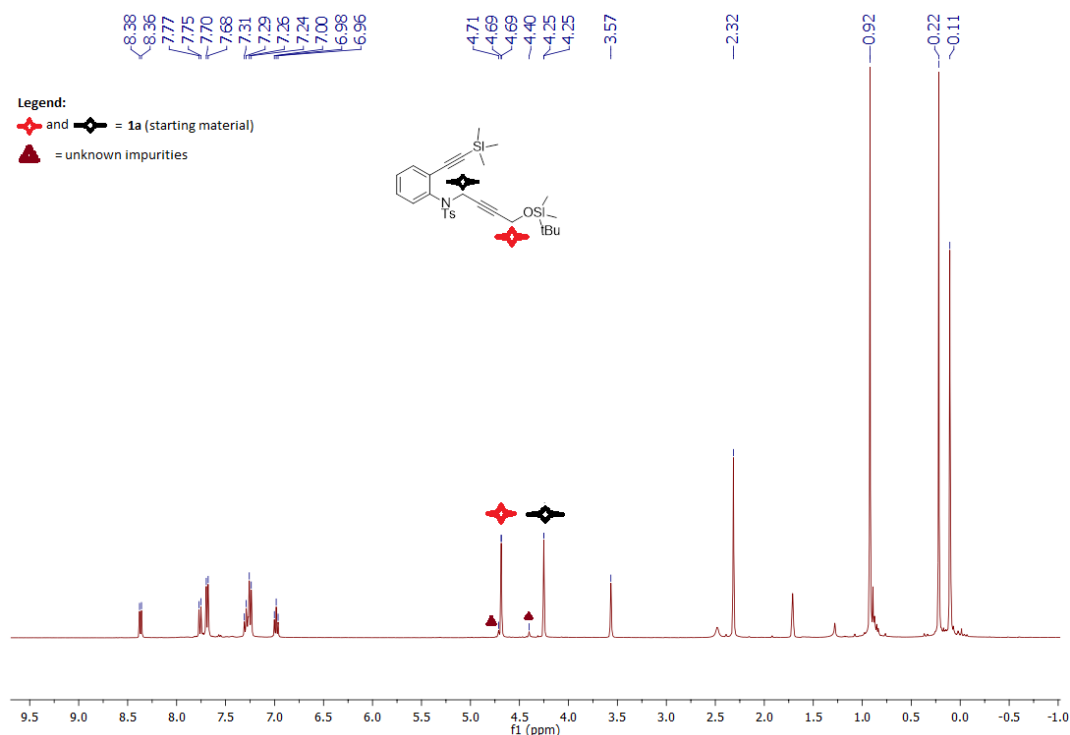


**Figure 4.7** <sup>1</sup>H-NMR of **1a** in THF-d<sub>8</sub>.

Chapter 4: I thought it was gold instead... TBAF catalysed one-pot synthesis of allenyl-indoles

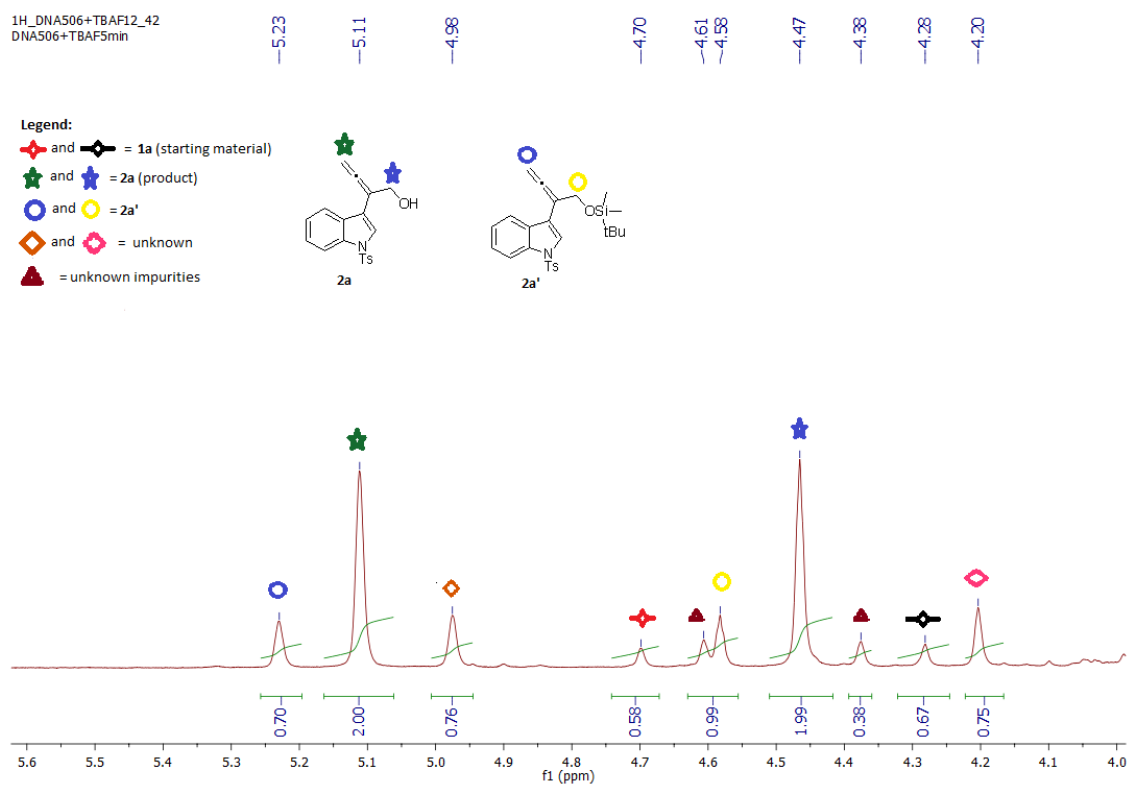


Figure 4.8  $^1\text{H-NMR}$  of reaction in THF- $d_8$  2 minutes after the addition of TBAF solution.

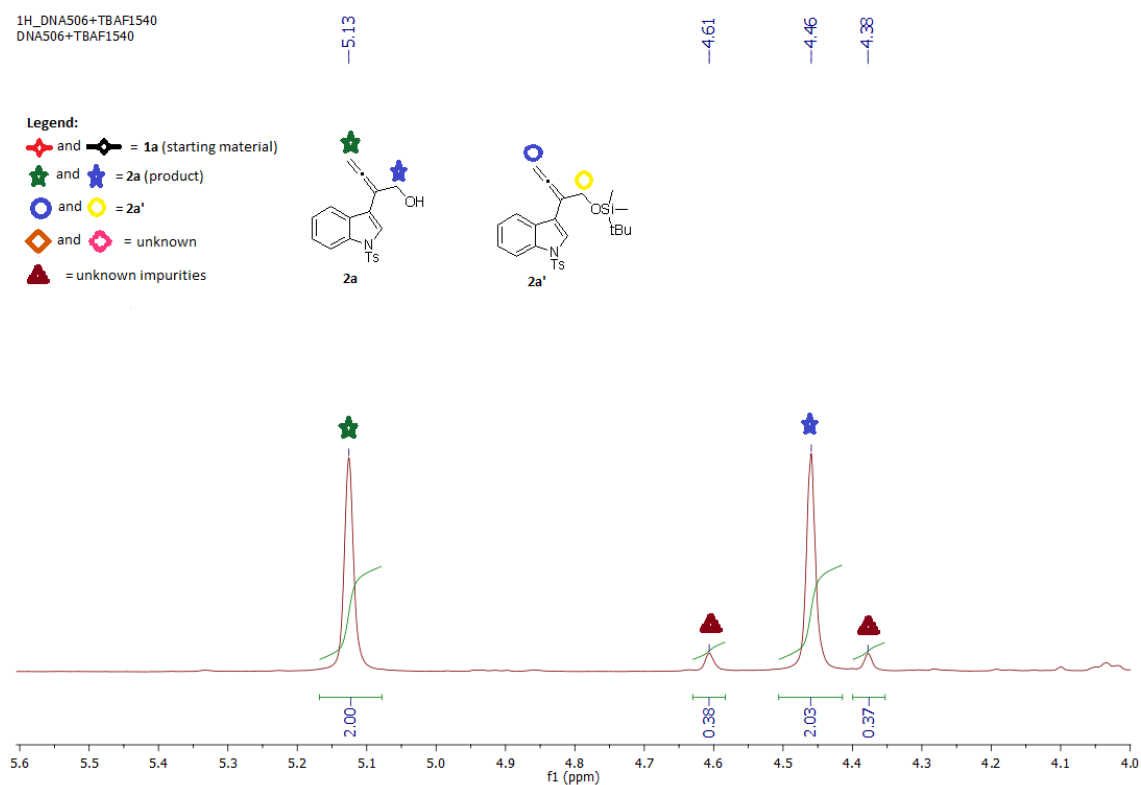
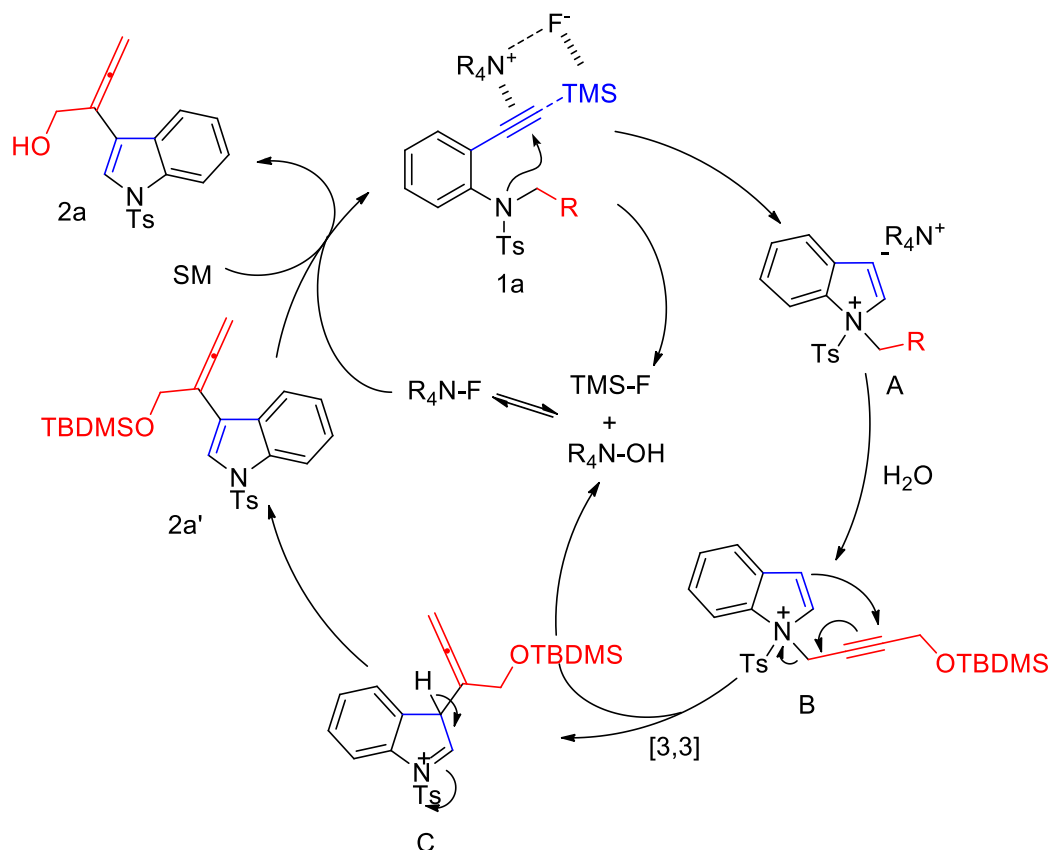


Figure 4.9  $^1\text{H-NMR}$  of reaction in THF- $d_8$  3 hours after the addition of TBAF solution.

Although a univocal mechanistic picture is not available at the present, the following reaction profile can be proposed (Figure 4.10).



**Figure 4.10** Hypothesis of reaction mechanism.

Initially, TBAF is invoked in triggering the hydroamination with simultaneous cleavage of the TMS group ( $\text{Bu}_4\text{N}^+$  can stabilize the incipient acetylenic carbanion), leading, upon C(3)-protonation to the partially indolynium species **B**. The latter intermediate can undergo intramolecular [3,3]-aza-Cope sigmatropic rearrangement resulting into the partially dearomatized adduct **C**. Fast rearomatization would lead to the detected *O*-silylated species **2a'** that can finally deliver the indolyl-alcohol **2a** via cleavage of the OTBDMS group. A certain content of water is therefore requested for both the protonation of the intermediate **A** and transformation of **2a'** into **2a**. The incomplete consumption of **1a** with dry THF (Table 4.1, entry 6) can be consequently addressed. The content of water present in the

commercially available hydrate-TBAF can account for the 55% isolated yield in **2a** via dry THF.

Additionally, a scrambled control experiment with 2-methyl-*N*-tosyl indole (1.5:1 ratio with respect to **1a**) was carried out in order to assess the possible cleavage of the propargylic chain with consequent intermolecular condensation with concomitantly delivered indole core (Figure 4.11).

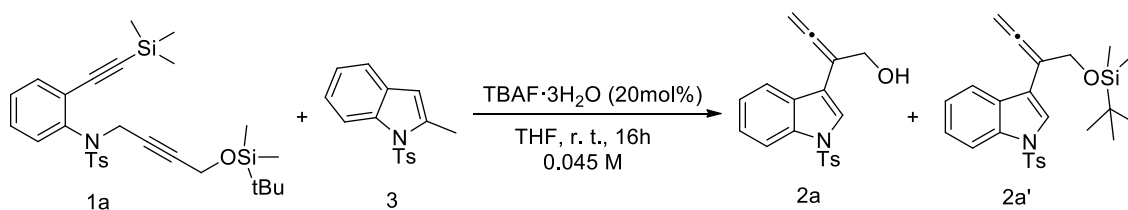
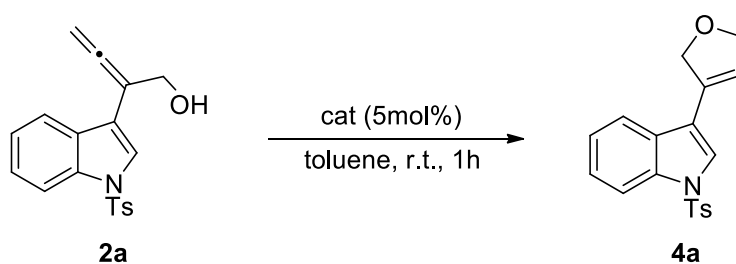


**Figure 4.11** Scrambled-control experiment.

Here, the isolation of a **2a:2a'** mixture (2:1) without any significant incorporation of 2Me-indole in the final product, ruled out this possibility.

#### 4.2.3 Proving the synthetic flexibility of allenyl-indoles

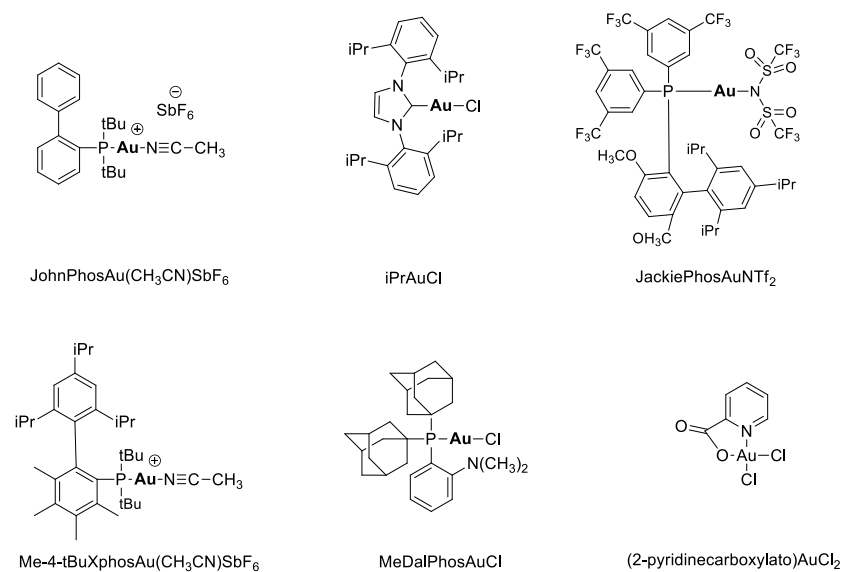
Finally, the synthetic utility of the 3-allenyl-indoles **2** was demonstrated by subjecting allenol **2a** to gold catalyzed ring-closing protocol (Figure 4.12).



**Figure 4.12** Ring closing reaction catalyzed by gold

Upon a screening of [Au(I)] species the carbonyl complex  $iPrAuCl$  (5 mol%), cationized with  $AgSbF_6$  was elected as the catalyst of choice delivering the corresponding dihydrofuran **4a** in 91% yield and mild reaction conditions (1 h, toluene, rt.) as shown in Table 4.2.<sup>[28,29]</sup>



**Table 4.2** Optimization of the reaction conditions.<sup>a</sup>

Entry	Catalyst (5 mol %)	Yield <sup>b</sup> 4a (%)
1	JohnPhos <b>Au</b> (CH <sub>3</sub> CN)SbF <sub>6</sub>	80%
2	IPr <b>AuCl</b> / AgNTf <sub>2</sub>	59%
3	IPr <b>AuCl</b> / AgOTf	83%
4	IPr <b>AuCl</b> / AgSbF <sub>6</sub>	91%
5	AgSbF <sub>6</sub>	20%
6	<b>AuCl</b> ·DMS	28%
7	PPh <sub>3</sub> <b>AuCl</b> /AgSbF <sub>6</sub>	63%
8	JackiePhos <b>Au</b> NTf <sub>2</sub>	40%
9	Me-4-tBuXphos <b>Au</b> (CH <sub>3</sub> CN)SbF <sub>6</sub>	75%
10	MeDalPhos <b>AuCl</b> /AgSbF <sub>6</sub>	53%
11	(2-Pyridinecarboxylato) <b>AuCl</b> <sub>2</sub> /2AgSbF <sub>6</sub>	70%

<sup>a</sup>All the reaction were carried out under nitrogen atmosphere    <sup>b</sup>Isolated yield after flash chromatography.

The compound was fully characterized also by single crystal X-ray diffraction and the molecular structure is depicted in Figure 4.13.

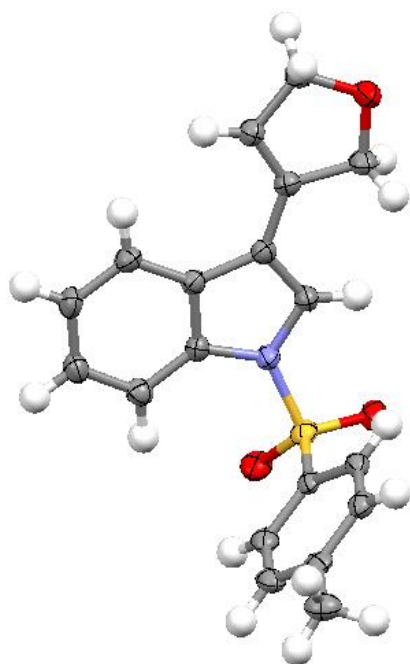


**Figure 4.13** Molecular structure of compound **4a**.

Interestingly, as reported in some paper of Rossi and coworkers for similar substrates, compound **4a** proved to be a reliable dienophile in a formal [4+2]-cycloaddition type reaction when condensed with allenamide **5a** (-20 °C, 4 h) as shown in Figure 4.14.<sup>[30–32]</sup>

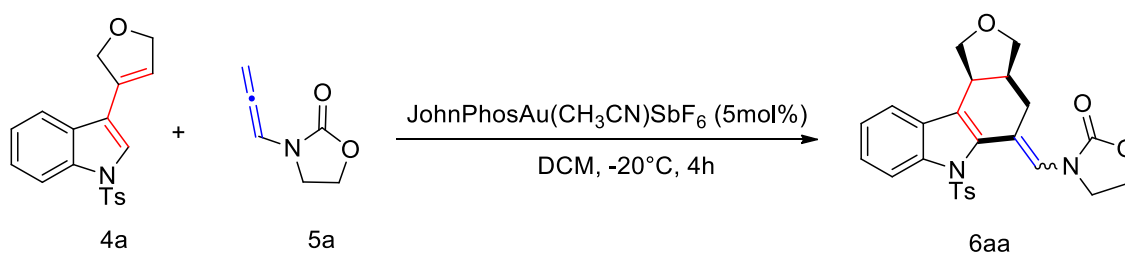


**Figure 4.14** Synthesis of tetrahydrocarbazole **6aa**

In this case, the electrophilic activation of the latter  $\pi$ -system promoted by gold, as depicted in Figure 4.15, was crucial in order to isolate the tetrahydrocarbazole **6aa** in 55% yield and high regioselectivity manner.

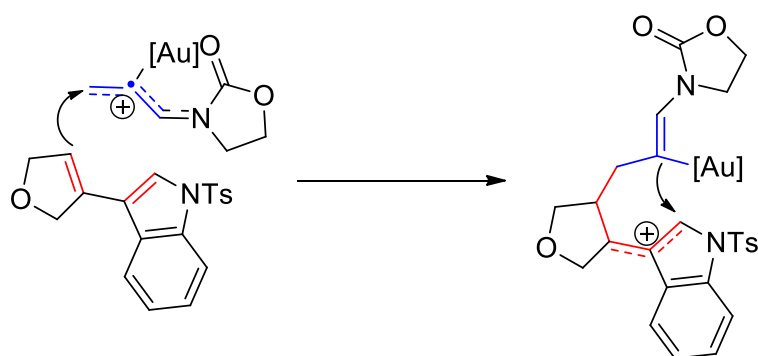


**Figure 4.15** Electrophilic activation of the allenamide  $\pi$ -system promoted by gold.

## 4.3 Conclusions

In conclusion, a new efficient and environmentally acceptable metal free-catalytic protocol for the one-pot synthesis of densely functionalized C(3)-allenyl-indoles is documented. The use of economically acceptable TBAF·3H<sub>2</sub>O as catalyst (20 mol%), in reagent-grade solvent and open-air flask, make the present methodology a desirable synthetic alternative to classic noble-metal based synthesis of heterocyclic scaffolds. The synthetic flexibility of the obtained allenyl-indoles was finally proved in the synthesis of densely functionalized polycyclic fused tetrahydrocarbazoles.

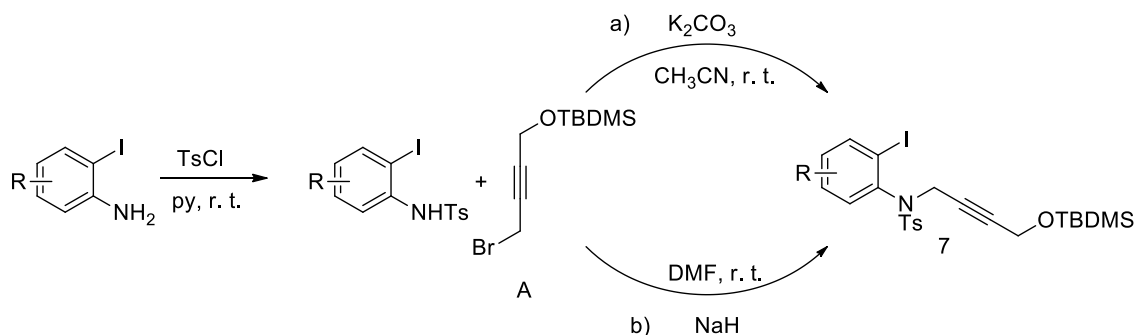
## 4.4 Experimental part

### 4.4.1 General methods

<sup>1</sup>H-NMR spectra were recorded on Varian 400 (400 MHz) spectrometer. Chemical shifts are reported in ppm from TMS with the solvent resonance as the internal standard (deuteriochloroform: 7.27 ppm). Data are reported as follows: chemical shift, multiplicity (s = singlet, d = duplet, t = triplet, q = quartet, sext = sextet, sept = septet, p = pseudo, b = broad, m = multiplet), coupling constants (Hz). <sup>13</sup>C-NMR spectra were recorded on a Varian 400 (100 MHz) spectrometer with complete proton decoupling. Chemical shifts are reported in ppm from TMS with the solvent as the internal standard (deuteriochloroform: 77.0 ppm). GC-MS spectra were taken by EI ionization

at 70 eV on a Hewlett-Packard 5971 with GC injection. They are reported as:  $m/z$  (rel. intense). LC-electrospray ionization mass spectra were obtained with Agilent Technologies MSD1100 single-quadrupole mass spectrometer. Chromatographic purification was done with 240-400 mesh silica gel. Elemental analyses were carried out by using an EACE 1110 CHNOS analyzer. All anhydrous solvents were supplied by Sigma Aldrich in Sureseal® bottles and used without any further purification. Commercially available chemicals were purchased from Sigma Aldrich, Stream and TCI and used without any further purification. Melting points were measured using open glass capillaries in a Bibby Stuart Scientific Melting Point Apparatus SMP 3 and are calibrated by comparison with literature values (Aldrich).

#### 4.4.2 General procedure for the synthesis of 7

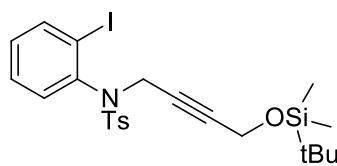


Substituted N-tosyl-2-iodoaniline and [(4-bromo-2-butyne-1-yl)oxy](tert-butyl)dimethylsilane (A) were prepared following reported procedures.<sup>[33,34]</sup>

**Method a)** for compounds **7a,e-g**. To a solution of substituted N-tosyl-2-iodoaniline (1 mmol) in dry acetonitrile (5 mL) under nitrogen atmosphere,  $K_2CO_3$  (2 eq) followed by the propargyl bromide A (1.2 eq) was added. The mixture was stirred at room temperature until TLC analysis indicates complete consumption of starting material. Subsequently, water (10 mL) was added and the aqueous layer was extracted with AcOEt (3 x 10 mL). The combined organic layers were dried with  $Na_2SO_4$ , filtered and concentrated

under reduced pressure. The crude product was purified by column chromatography on silica gel to give the desired product.

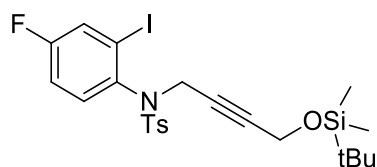
**Method b)** for compounds **7b** and **7c**. To a solution of substituted N-tosyl-2-iodoaniline (1 mmol) in dry DMF (5 mL) under nitrogen atmosphere, NaH (2.0 eq) and the solution was stirred at rt for 15. Then propargyl bromide A (1.2 eq) was added and the mixture stirred at room temperature until the TLC analysis indicates complete consumption of starting material. Subsequently, water (10 mL) was added and the aqueous layer was extracted with AcOEt (1 x 10 mL). The organic phase was washed with water (3 x 5 mL) in order to remove traces of DMF and subsequently dried over Na<sub>2</sub>SO<sub>4</sub>. The crude product was purified by column chromatography on silica gel to give the desired product.



**7a.** Yellow oil. Yield = 62%, (cHex:EtOAc = 9:1).

<sup>1</sup>H-NMR (400 MHz, CDCl<sub>3</sub>) δ 7.92 (d, J = 6.6 Hz, 1H), 7.72 (d, J = 8.3 Hz, 2H), 7.31 – 7.25 (m, 3H),

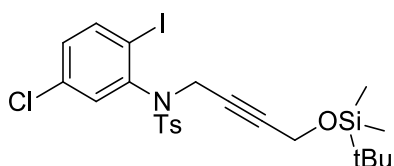
7.11 (d, J = 7.9 Hz, 1H), 7.06 (t, J = 7.7 Hz, 1H), 4.76 (d, J = 16.7 Hz, 1H), 4.18 (d+s, J = 16.6 Hz, 3H), 2.45 (s, 3H), 0.86 (s, 9H), 0.02 (d, J = 4.2 Hz, 6H). <sup>13</sup>C-NMR (100 MHz, CDCl<sub>3</sub>) 143.72, 140.74, 140.12, 136.62, 130.96, 130.26, 129.30, 128.61, 128.21, 102.68, 84.40, 78.32, 51.43, 41.02, 25.67, 21.53, 18.12, -5.36. GC-MS: 498 (M-tBu).



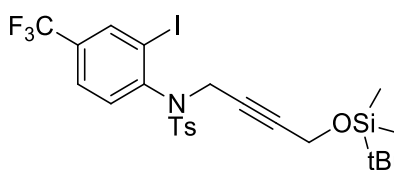
**7b.** Colorless oil. Yield = 76%, (cHex:EtOAc =

95:5). <sup>1</sup>H-NMR (400 MHz, CDCl<sub>3</sub>) δ 7.70 (d, J = 8.3 Hz, 2H), 7.61 (dd, J = 7.8, 2.8 Hz, 1H), 7.30

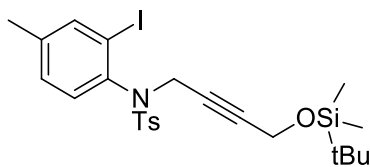
(d, J = 8.5 Hz, 2H), 7.06 (dd, J = 8.8, 5.5 Hz, 1H), 7.01 – 6.95 (m, 1H), 4.75 (d, J = 18.4 Hz, 1H), 4.14 (d+s, J = 13.2 Hz, 3H), 2.45 (s, 3H), 0.86 (d, J = 2.8 Hz, 9H), 0.03 (d, J = 4.4 Hz, 6H). <sup>13</sup>C-NMR (100 MHz, CDCl<sub>3</sub>) δ 162.91, 160.39, 143.95, 137.10, 137.07, 136.40, 131.70, 131.61, 129.44, 128.25, 127.17, 126.92, 115.74, 115.52, 102.97, 102.89, 84.70, 78.18, 51.46, 41.09, 25.69, 21.59, 18.18, -5.33. LC-MS: 574.2 (M<sup>+</sup>), 591.2 (M<sup>+</sup>+H<sub>2</sub>O).



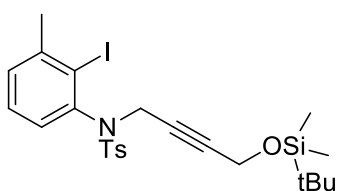
**7c.** Pale yellow oil. Yield = 89%, (cHex:EtOAc = 9:1).  $^1\text{H-NMR}$  (400 MHz,  $\text{CDCl}_3$ ) 7.81 (d,  $J = 9.1$  Hz, 1H), 7.71 (d,  $J = 8.3$  Hz, 2H), 7.32 (d,  $J = 8.1$  Hz, 2H), 7.08-7.05 (m, 2H), 4.70 (d,  $J = 18.3$  Hz, 1H), 4.23 – 4.12 (m, 3H), 2.45 (s, 3H), 0.85 (s, 9H), -0.02 (s, 6H).  $^{13}\text{C-NMR}$  (100 MHz,  $\text{CDCl}_3$ )  $\delta$  144.16, 141.97, 140.64, 134.36, 131.27, 130.55, 129.49, 128.26, 100.12, 84.97, 77.83, 51.43, 40.99, 30.87, 25.72, 21.60, 18.19, -5.31. *LC-MS*: 607.2 ( $\text{M}+\text{H}_2\text{O}$ ), 612.2 ( $\text{M}+\text{Na}^+$ ), 628.2 ( $\text{M}+\text{K}^+$ ).



**7d.** Yellow oil. Yield = 52% (not optimized), (cHex:EtOAc = 9:1).  $^1\text{H-NMR}$  (400 MHz,  $\text{CDCl}_3$ )  $\delta$  8.16 (s, 1H), 7.71 (d,  $J = 8.3$  Hz, 2H), 7.54 (d,  $J = 8.3$ , 1H), 7.32 (d,  $J = 8.0$  Hz, 2H), 7.21 (d,  $J = 8.2$  Hz, 1H), 4.74 (d,  $J = 18.0$  Hz, 1H), 4.21 (d,  $J = 18.0$  Hz, 1H), 4.15 (s, 2H), 2.46 (s, 3H), 0.85 (s, 9H), 0.01 (s, 6H).  $^{13}\text{C-NMR}$  (100 MHz,  $\text{CDCl}_3$ )  $\delta$  144.24, 137.16, 137.12, 136.22, 131.23, 129.58, 128.24, 125.73, 125.69, 102.88, 85.02, 77.78, 51.43, 40.92, 26.88, 25.66, 21.61, 18.16, -5.37. *LC-MS*: 646 ( $\text{M}+\text{Na}^+$ ).

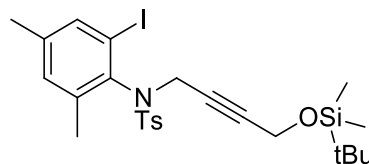


**7e.** Yellow oil. Yield = 62% (not optimized), (cHex:EtOAc = 95:5).  $^1\text{H-NMR}$  (400 MHz,  $\text{CDCl}_3$ )  $\delta$  7.73 – 7.69 (m, 3H), 7.29 – 7.26 (m, 2H), 7.04 (d,  $J = 8.0$  Hz, 1H), 6.94 (d,  $J = 8.0$  Hz, 1H), 4.74 (d,  $J = 18.3$  Hz, 1H), 4.17- 4.13 (m, 3H), 2.44 (s, 3H), 2.30 (s, 3H), 0.85 (s, 9H), 0.02 (d,  $J = 4.4$  Hz, 6H).  $^{13}\text{C-NMR}$  (100 MHz,  $\text{CDCl}_3$ )  $\delta$  143.65, 140.71, 140.60, 138.09, 136.79, 130.42, 129.45, 129.32, 128.27, 102.46, 84.31, 78.51, 65.81, 51.51, 41.11, 25.72, 21.58, 20.57, 18.19, 15.25, -5.31. *LC-MS*: 570.0 ( $\text{M}+\text{H}^+$ ) 587 ( $\text{M}^++\text{H}_2\text{O}$ ).



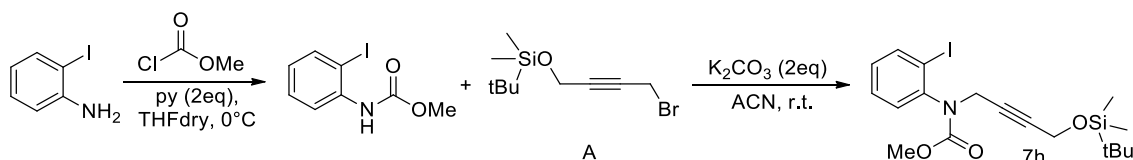
**7f.** Yellow oil. Yield = 55% (not optimized), (cHex:EtOAc = 95:5).  $^1\text{H-NMR}$  (400 MHz,  $\text{CDCl}_3$ )  $\delta$  7.71 (d,  $J = 8.3$  Hz, 2H), 7.26 (d,  $J = 8.0$  Hz, 2H), 7.19 (d,  $J = 6.6$  Hz, 1H), 7.09 (t,  $J = 7.7$  Hz, 1H), 6.81 (d,  $J = 6.7$  Hz, 1H),

4.76 (dt,  $J = 17.9, 1.7$  Hz, 1H), 4.19 – 4.07 (m, 3H), 2.48 (s, 3H), 2.42 (s, 3H), 0.83 (s, 9H), -0.01 (d,  $J = 4.6$  Hz, 6H).  $^{13}\text{C-NMR}$  (100 MHz,  $\text{CDCl}_3$ )  $\delta$  144.32, 143.65, 141.12, 136.85, 129.98, 129.29, 128.33, 127.92, 127.79, 110.05, 84.37, 78.47, 51.48, 41.09, 25.72, 21.59, 18.18, -5.31, -5.33. *LC-MS*: 570.2 ( $\text{M}+\text{H}^+$ ) 609.2 ( $\text{M}+\text{K}^+$ ).

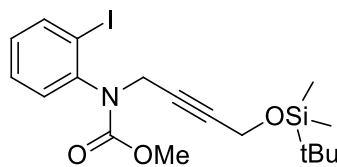


**7g.** Yellow oil. Yield = 51% (not optimized), (cHex:EtOAc = 95:5).  $^1\text{H-NMR}$  (400 MHz,  $\text{CDCl}_3$ )  $\delta$  7.75 (d,  $J = 8.2$  Hz, 2H), 7.51 (s, 1H), 7.29 (d,  $J = 8.2$  Hz, 2H), 7.03 (s, 1H), 4.69 (dt,  $J = 17.7, 1.8$  Hz, 1H), 4.36 (dt,  $J = 17.7, 1.8$  Hz, 1H), 4.21 (t,  $J = 1.9$  Hz, 2H), 2.43 (s, 3H), 2.36 (s, 3H), 2.25 (s, 3H), 0.86 (s, 9H), 0.03 (s, 6H).  $^{13}\text{C-NMR}$  (100 MHz,  $\text{CDCl}_3$ )  $\delta$  143.51, 142.40, 140.23, 138.64, 138.43, 137.58, 132.29, 129.45, 128.03, 100.90, 83.99, 78.91, 51.61, 40.68, 25.74, 21.56, 20.65, 20.38, 18.21, -5.34. *LC-MS*: 601.4 ( $\text{M}+\text{H}_2\text{O}$ ).

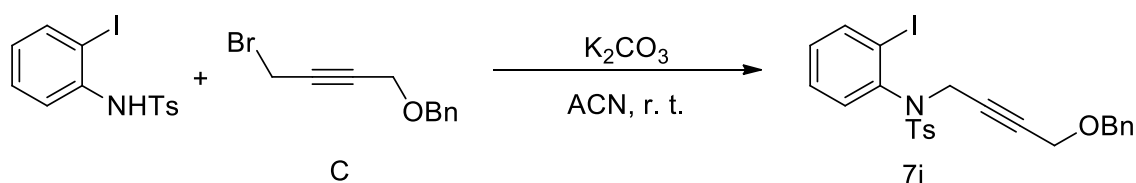
#### 4.4.3 Procedure for the synthesis of 7h



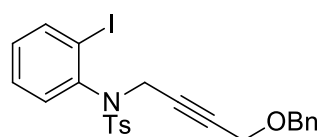
*N*-methyl 2-iodophenylcarbamate was prepared following reported procedures.<sup>[35]</sup> The product **7h** was synthesized following the procedure utilized for the synthesis of products **7a-g**.



**7h.** Yellow oil. Yield = 56% (not optimized), (cHex:EtOAc = 95:5).  $^1\text{H-NMR}$  (400 MHz,  $\text{CDCl}_3$ )  $\delta$  7.88 (d,  $J = 7.8$  Hz, 1H), 7.40 – 7.35 (m, 2H), 7.07 – 7.00 (m, 1H), 4.84 (d,  $J = 17.5$  Hz, 1H), 4.29 (s, 2H), 4.00 (d,  $J = 17.6$  Hz, 1H), 3.66 (s, 3H), 0.89 (s, 9H), 0.07 (d,  $J = 2.1$  Hz, 6H).  $^{13}\text{C-NMR}$  (100 MHz,  $\text{CDCl}_3$ )  $\delta$  155.06, 142.75, 139.47, 130.05, 129.48, 129.02, 100.03, 83.21, 79.61, 53.35, 51.70, 39.38, 25.77, 18.24, -5.21. *GC-MS*: 402 ( $\text{M}-\text{tBu}$ ).

4.4.4 Procedure for the synthesis of **7i**

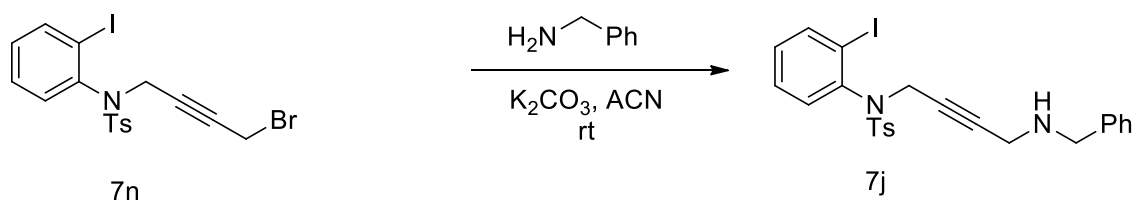
1-(Benzyloxy)-4-bromo-but-2-yne **C** was prepared following reported procedures.<sup>[36,37]</sup> The product **7i** was synthesized following the procedure utilized for the synthesis of products **7a-g**.



**7i**. Yellow oil. Yield = 94%, (*c*Hex:EtOAc = 9:1). <sup>1</sup>H-NMR (400 MHz, CDCl<sub>3</sub>) δ 7.90 (dd, *J* = 7.9, 1.4 Hz, 1H), 7.70 (d, *J* = 8.3 Hz, 2H), 7.37 – 7.17 (m, 7H),

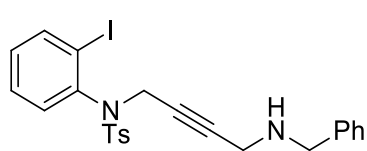
7.10 (dd, *J* = 7.9, 1.6 Hz, 1H), 7.07 – 6.98 (m, 1H), 4.76 (d, *J* = 18.1 Hz, 1H), 4.38 (s, 2H), 4.21 (d, *J* = 18.1 Hz, 1H), 4.02 (t, *J* = 1.9 Hz, 2H), 2.38 (s, 3H).

<sup>13</sup>C-NMR (100 MHz, CDCl<sub>3</sub>) δ 143.88, 140.82, 140.25, 137.24, 136.59, 130.92, 130.35, 129.39, 128.67, 128.37, 128.27, 127.90, 127.83, 102.75, 81.87, 80.33, 71.29, 57.11, 41.05, 21.53. LC-MS: 531.8 (M) 549 (M+H<sub>2</sub>O).

4.4.5 General procedure for the synthesis of **7j**:

To a solution of **7n** (0.5 mmol) in dry acetonitrile (3 mL) under nitrogen atmosphere, K<sub>2</sub>CO<sub>3</sub> (1.5 eq) was added, then the benzyl amine (1.2 eq) was added and the mixture was stirred at room temperature until TLC analysis indicates complete consumption of starting material. Subsequently, water (10 mL) was added and the aqueous layer was extracted with AcOEt (3 x 10 mL). The combined organic layers were dried with Na<sub>2</sub>SO<sub>4</sub>, filtered and concentrated under reduced pressure. The crude product was purified by column chromatography on silica gel to give the desired product.

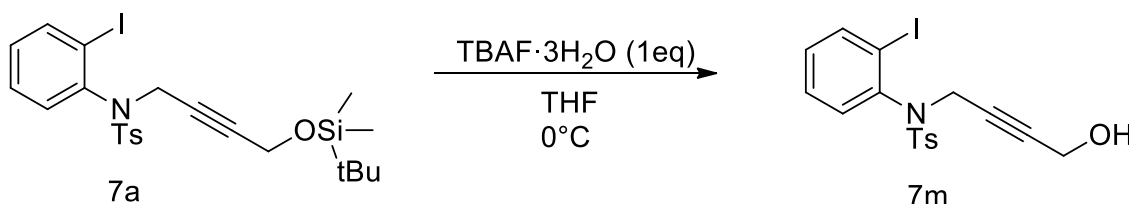




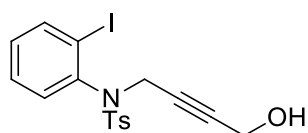
**7j.** Yellow oil. Yield = 73% (not optimized), (cHex:EtOAc = 8:2).  $^1\text{H-NMR}$  (400 MHz,  $\text{CDCl}_3$ )  $\delta$  7.90 (d,  $J = 7.9$  Hz, 1H), 7.70 (d,  $J = 8.2$  Hz, 2H),

7.38-7.17 (m, 8H), 7.12 (d,  $J = 7.9$  Hz, 1H), 7.03 (t,  $J = 7.6$  Hz, 1H), 4.71 (d,  $J = 17.9$  Hz, 1H), 4.19 (d,  $J = 17.9$  Hz, 1H), 3.65 (s, 2H), 3.26 (s, 2H), 2.37 (s, 3H).  $^{13}\text{C-NMR}$  (100 MHz,  $\text{CDCl}_3$ )  $\delta$  143.84, 140.96, 139.24, 136.66, 130.83, 130.29, 129.34, 128.61, 128.37, 128.31, 128.23, 127.12, 102.87, 84.12, 77.10, 52.15, 41.16, 37.40, 21.51. LC-MS: 531.2 (M).

#### 4.4.6 Procedure for the synthesis of 7m



To a solution of compound **7a** (0.5 mmol, 278 mg) in THF (5 mL) at 0 °C, TBAF·3H<sub>2</sub>O (1eq, 0.5 mmol, 158 mg) was added then the mixture was stirred until TLC analysis indicates complete consumption of starting material. Subsequently, water (10 mL) was added and the aqueous layer was extracted with AcOEt (3 x 10 mL). The combined organic layers were dried with Na<sub>2</sub>SO<sub>4</sub>, filtered and concentrated under reduced pressure. The crude product was purified by column chromatography on silica gel to give the desired product.

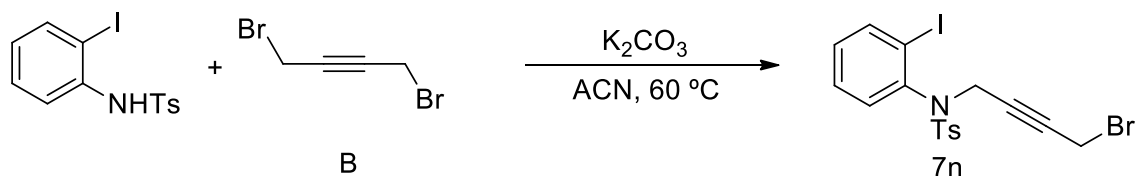


**7m.** Yellow oil. Yield = 67% (not optimized), (cHex:EtOAc = 9:1).  $^1\text{H-NMR}$  (400 MHz,  $\text{CDCl}_3$ )  $\delta$  7.92 (dd,  $J = 7.9, 1.5$  Hz, 1H), 7.73 (d,  $J = 8.3$  Hz, 2H),

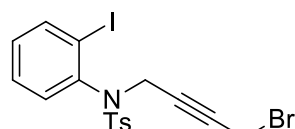
7.31 (m, 3H), 7.15 (dd,  $J = 7.9, 1.6$  Hz, 1H), 7.07 (m, 1H), 4.74 (d,  $J = 18.0$  Hz, 1H), 4.17 (d,  $J = 17.9$  Hz, 1H), 4.12 (s, 2H), 2.46 (s, 3H).  $^{13}\text{C-NMR}$  (100 MHz,  $\text{CDCl}_3$ )  $\delta$  143.99, 140.81, 140.21, 136.49, 130.97, 130.39, 129.36,

128.77, 128.34, 102.60, 84.08, 79.62, 50.82, 41.06, 21.57. *LC-MS*: 441.8 ( $M+H^+$ ), 459.0 ( $M+H_2O$ ) 463.8 ( $M+Na^+$ ).

#### 4.4.7 Procedure for the synthesis of **7n**

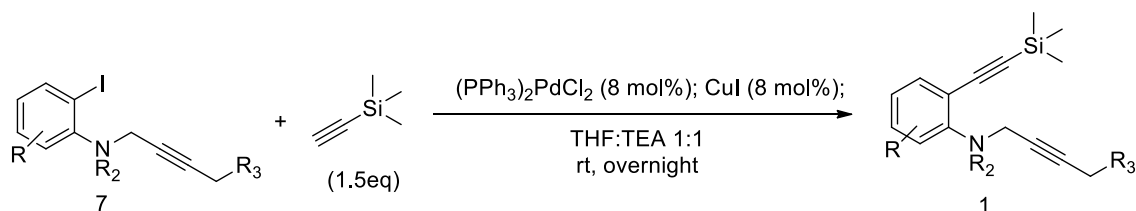


1,4-Dibromo-2-butyne was prepared following reported procedure.<sup>[38]</sup> The product **7n** was synthesized following a reported procedure for a similar product.<sup>[39]</sup>



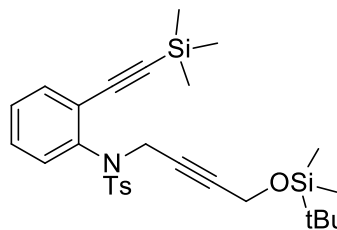
**7n**. Yellow oil. Yield = 75% (not optimized), (*c*Hex:EtOAc = 9:1). <sup>1</sup>H-NMR (400 MHz, CDCl<sub>3</sub>) δ 7.92 (d, *J* = 7.9 Hz, 1H), 7.72 (d, *J* = 8.3 Hz, 2H), 7.32–7.30 (m, 3H), 7.17 – 7.02 (m, 2H), 4.82 (d, *J* = 18.3 Hz, 1H), 4.14 (d, *J* = 18.3 Hz, 1H), 3.74 (t, *J* = 2.1 Hz, 2H), 2.46 (s, 3H). <sup>13</sup>C-NMR (100 MHz, CDCl<sub>3</sub>) δ 143.99, 140.74, 140.24, 136.58, 131.00, 130.46, 129.48, 128.79, 128.27, 102.71, 80.88, 80.62, 41.05, 21.63, 13.88. *LC-MS*: 505 ( $M+H^+$ ) 543.8 ( $M+K^+$ ).

#### 4.4.8 General procedure for the synthesis of **1**

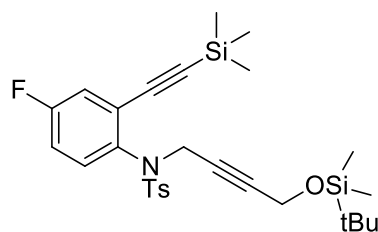


To a solution of **7** (0.5 mmol) in anhydrous THF (2 mL), freshly distilled TEA (2 mL), trimethylsilylacetylene (1.5 eq), (PPh<sub>3</sub>)<sub>2</sub>PdCl<sub>2</sub> (8 mol%) and CuI (8 mol%) were added. The mixture was stirring at room temperature and the reaction progress was monitored using TLC. After the consumption of starting material, the reaction mixture was extracted with ethyl acetate and

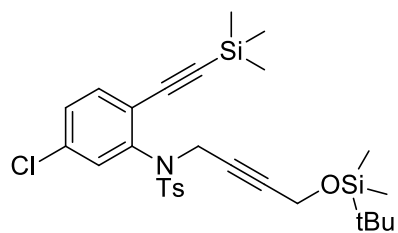
water. The organic layers were combined and dried with  $\text{Na}_2\text{SO}_4$ . After filtration, the solvent was removed under reduced pressure. The residue was purified by flash chromatography on silica gel.



**1a.** Pale yellow solid. Yield = 65% (*c*Hex:EtOAc = 95:5). Mp = 117-119 °C.  $^1\text{H-NMR}$  (400 MHz,  $\text{CDCl}_3$ )  $\delta$  8.40 (d,  $J = 7.3$  Hz, 1H), 7.79 (d,  $J = 8.2$  Hz, 1H), 7.69 (d,  $J = 8.3$  Hz, 2H), 7.32 (t,  $J = 7.2$  Hz, 1H), 7.22 (d,  $J = 8.0$  Hz, 2H), 7.04 (t,  $J = 7.2$  Hz, 1H), 4.67 (s, 2H), 4.23 (s, 2H), 2.37 (s, 3H), 0.94 (s, 9H), 0.26 (s, 9H), 0.12 (s, 6H).  $^{13}\text{C-NMR}$  (100 MHz,  $\text{CDCl}_3$ )  $\delta$  145.26, 144.38, 139.60, 133.70, 130.68, 129.76, 129.00, 127.10, 124.70, 123.20, 114.25, 111.84, 103.19, 64.51, 53.99, 25.89, 21.48, 18.33, -0.22, -5.28. LC-MS: 548.0 ( $\text{M}+\text{Na}^+$ ), 564.0 ( $\text{M}+\text{K}^+$ ).

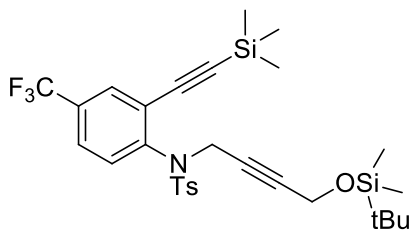


**1b.** Pale yellow solid. Yield = 43% (not optimized), (*c*Hex:EtOAc = 95:5). Mp = 94-96 °C.  $^1\text{H-NMR}$  (400 MHz,  $\text{CDCl}_3$ )  $\delta$  8.11 (dd,  $J = 9.5, 2.7$  Hz, 1H), 7.73 (dd,  $J = 8.9, 4.6$  Hz, 1H), 7.64 (d,  $J = 8.3$  Hz, 2H), 7.23 (d,  $J = 8.2$  Hz, 2H), 7.02 (t,  $J = 8.6$ , 1H), 4.67 (s, 2H), 4.21 (s, 2H), 2.38 (s, 3H), 0.93 (d,  $J = 2.9$  Hz, 9H), 0.31 – 0.21 (m, 9H), 0.15 – 0.08 (m, 6H).  $^{13}\text{C-NMR}$  (100 MHz,  $\text{CDCl}_3$ )  $\delta$  160.31, 157.92, 144.54, 141.30, 138.49, 138.46, 133.32, 130.80, 130.71, 129.81, 129.43, 127.85, 127.13, 117.42, 117.18, 115.29, 115.21, 113.36, 111.44, 111.18, 104.47, 103.31, 64.35, 54.46, 25.86, 25.71, 21.49, 18.32, -0.35, -5.32. LC-MS: 545 ( $\text{M}+\text{H}^+$ ), 562 ( $\text{M}+\text{H}_2\text{O}$ ).



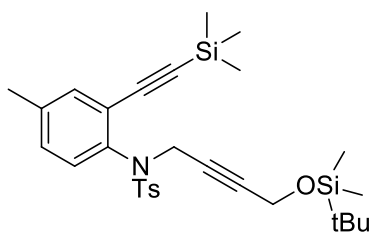
**1c.** White solid. Yield = 58% (not optimized), (*c*Hex:EtOAc = 98:2). Mp = 135-136 °C.  $^1\text{H-NMR}$  (400 MHz,  $\text{CDCl}_3$ )  $\delta$  8.27 (d,  $J = 8.5$  Hz, 2H), 7.76 (d,  $J = 1.9$  Hz, 1H), 7.66 (d,  $J = 8.4$  Hz, 2H), 7.23 (d,  $J = 8.0$  Hz, 2H), 6.97 (dd,  $J = 8.5, 1.9$  Hz, 1H), 4.65 (s, 2H), 4.18 (s, 2H), 2.36 (s, 3H), 0.90 (s, 9H), 0.21 (s, 9H), 0.08 (s, 6H).  $^{13}\text{C-NMR}$

*NMR* (100 MHz, CDCl<sub>3</sub>)  $\delta$  146.10, 144.73, 138.24, 136.37, 133.53, 129.93, 127.61, 127.07, 125.28, 123.40, 114.31, 112.37, 103.90, 103.69, 64.47, 54.33, 25.86, 21.52, 18.32, -0.27, -5.32. *LC-MS*: 559.0 (M), 597.4 (M+K<sup>+</sup>).



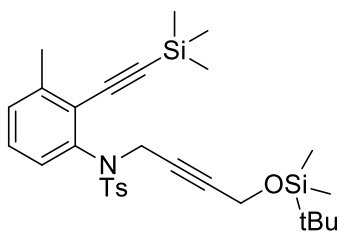
**1d.** Yellow wax. Yield = 44% (not optimized), (cHex:EtOAc = 95:5). <sup>1</sup>H-NMR (400 MHz, CDCl<sub>3</sub>)  $\delta$  8.70 (s, 1H), 7.83 (d, *J* = 8.6 Hz, 1H), 7.70 (d, *J* = 8.3 Hz, 2H), 7.55 (d, *J* = 8.6 Hz,

1H), 7.26 (d, *J* = 7.6 Hz, 3H), 4.75 (s, 2H), 4.24 (s, 2H), 2.39 (s, 3H), 0.94 (s, 9H), 0.25 (s, 9H), 0.12 (s, 6H). <sup>13</sup>C NMR (100 MHz, CDCl<sub>3</sub>)  $\delta$  144.92, 137.51, 133.62, 130.08, 130.01, 129.41, 127.61, 127.12, 127.05, 125.50, 121.95, 113.96, 113.67, 105.09, 102.88, 64.60, 54.40, 25.89, 21.55, 18.34, -0.40, -5.30. *LC-MS*: 593.2 (M).



**1e.** Pale yellow solid. Yield = 40% (not optimized), (cHex:EtOAc = 98:2). Mp = 118-120 °C. <sup>1</sup>H-NMR (400 MHz, CDCl<sub>3</sub>)  $\delta$  8.23 (s, 1H),

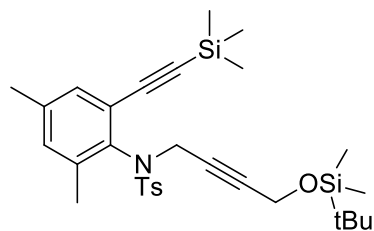
7.67 (m, 3H), 7.21 (d, *J* = 8.0 Hz, 2H), 7.13 (d, *J* = 7.1 Hz, 1H), 4.64 (s, 2H), 4.21 (s, 2H), 2.36 (s, 3H), 2.31 (s, 3H), 0.92 (s, 9H), 0.26 (s, 9H), 0.11 (s, 6H). <sup>13</sup>C-NMR (100 MHz, CDCl<sub>3</sub>)  $\delta$  144.25, 143.19, 139.80, 133.57, 132.95, 131.53, 129.71, 129.07, 127.13, 124.96, 114.12, 111.47, 104.08, 102.96, 64.44, 54.15, 31.36, 25.88, 21.46, 20.99, 18.32, 0.98, -0.15, -5.28. *LC-MS*: 539.0 (M<sup>+</sup>), 557.0 (M+H<sub>2</sub>O), 579.0 (M+K).



**1f.** Pale yellow wax. Yield = 58% (not optimized), (cHex:EtOAc = 9:1). <sup>1</sup>H-NMR (400 MHz, CDCl<sub>3</sub>)

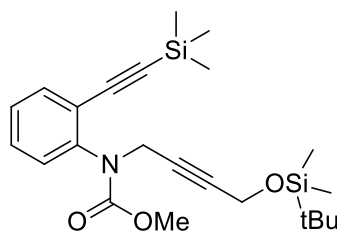
7.68 (d, *J* = 8.3 Hz, 2H), 7.59 (d, *J* = 8.1 Hz, 1H), 7.23- 7.19 (m, 3H), 6.85 (d, *J* = 7.6 Hz, 1H), 4.58 (s, 2H), 4.30 (s, 2H), 2.49 (s, 3H), 2.37 (s, 3H), 0.93 (s, 9H), 0.18 (s, 9H), 0.12 (s, 6H). <sup>13</sup>C-NMR (100 MHz, CDCl<sub>3</sub>) 144.92, 144.01, 141.00, 135.84, 133.21, 130.04, 129.43, 127.96, 127.21, 126.45, 115.83, 111.28, 105.58,

102.49, 66.24, 55.09, 25.69, 23.98, 21.31, 18.07, -0.33, -5.45. *LC-MS*: 539.4 ( $M^+$ ), 578.4 ( $M+K$ ).



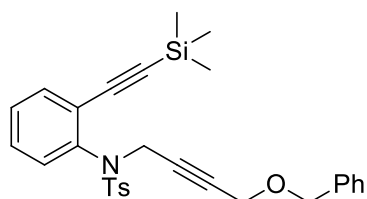
**1g.** Pale yellow solid. Yield = 44% (not optimized), (*c*Hex:EtOAc = 9:1). Mp = 132-134 °C.  $^1H$ -NMR (400 MHz,  $CDCl_3$ ) 7.84 (s, 1H), 7.22 (d,  $J = 8.3$  Hz, 2H), 7.08 (d,  $J = 8.0$  Hz, 2H),

7.04 (s, 1H), 4.50 (s, 2H), 3.99 (s, 2H), 2.57 (s, 3H), 2.35 (s, 3H), 2.32 (s, 3H), 0.92 (s, 9H), 0.24 (s, 9H), 0.09 (s, 6H).  $^{13}C$ -NMR (100 MHz,  $CDCl_3$ ) 144.03, 142.57, 141.40, 136.17, 134.80, 133.48, 131.87, 129.06, 128.03, 122.20, 112.71, 103.23, 101.53, 64.33, 56.58, 25.89, 21.45, 21.23, 19.55, 18.35, -0.09, -5.30. *LC-MS*: 575.4 ( $M+Na^+$ ), 625.8 ( $M+CH_3OH+CH_3CN$ ).



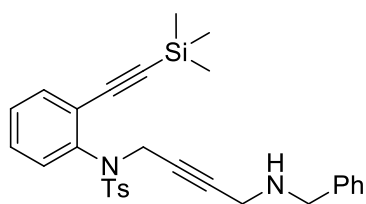
**1h.** Yellow oil. Yield = 46% (not optimized), (*c*Hex:EtOAc = 9:1).  $^1H$ -NMR (400 MHz,  $CDCl_3$ )  $\delta$  8.48 (d,  $J = 7.5$  Hz, 1H), 7.99 (d,  $J = 7.5$  Hz, 1H), 7.36 – 7.28 (m, 1H), 7.03 (t,  $J = 7.6$  Hz, 1H), 4.72

(s, 2H), 4.29 (s, 2H), 3.85 (s, 3H), 0.94 (s, 9H), 0.28 (s, 9H), 0.14 (s, 6H).  $^{13}C$ -NMR (100 MHz,  $CDCl_3$ )  $\delta$  210.46, 130.63, 124.52, 124.28, 122.59, 122.37, 120.62, 114.96, 114.70, 104.42, 102.84, 93.21, 86.99, 64.82, 64.46, 53.62, 52.66, 52.37, 25.90, -0.14, -5.22. *LC-MS*: 462.2 ( $M + MeOH + H^+$ ).



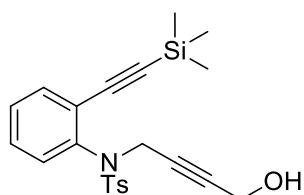
**1i.** Yellow wax. Yield = 48% (not optimized), (*c*Hex:EtOAc = 9:1).  $^1H$ -NMR (400 MHz,  $CDCl_3$ )  $\delta$  8.42 (d,  $J = 7.9$  Hz, 1H), 7.80 (d,  $J = 8.2$  Hz, 1H), 7.64 (d,  $J = 8.3$  Hz, 2H), 7.44 – 7.30 (m, 6H), 7.17

(d,  $J = 8.1$  Hz, 2H), 7.06 (t,  $J = 7.7$  Hz, 1H), 4.66 (s, 2H), 4.54 (s, 2H), 4.14 (s, 2H), 2.35 (s, 3H), 0.28 (s, 9H).  $^{13}C$ -NMR (100 MHz,  $CDCl_3$ )  $\delta$  145.52, 144.40, 141.73, 137.74, 133.56, 131.01, 129.76, 128.75, 128.40, 127.85, 127.79, 127.09, 124.83, 123.27, 114.38, 109.03, 104.27, 103.06, 72.03, 70.77, 54.08, 21.49, -0.18. *LC-MS*: 524.4 ( $M+Na^+$ ).



**1j.** Yellow oil. Yield = 59% (not optimized), (cHex:EtOAc = 8:2).  $^1\text{H-NMR}$  (400 MHz,  $\text{CDCl}_3$ )  $\delta$  8.34 (d,  $J = 7.8$  Hz, 1H), 7.75 (d,  $J = 8.2$  Hz, 1H), 7.64 (d,  $J = 8.3$  Hz, 2H), 7.36 – 7.26 (m, 5H), 7.19

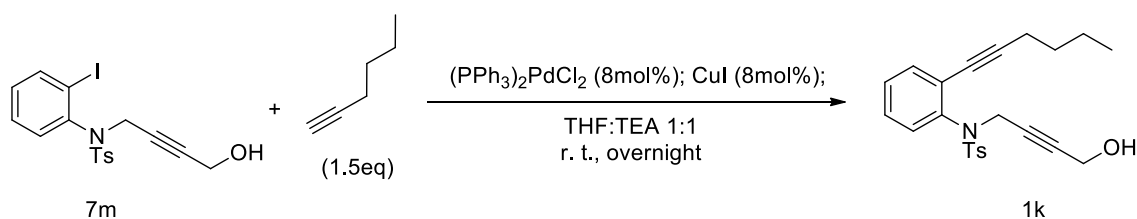
(d,  $J = 8.1$  Hz, 2H), 7.02 (t,  $J = 7.6$  Hz, 1H), 4.53 (s, 2H), 3.74 (s, 2H), 3.29 (s, 2H), 2.33 (s, 3H), 0.25 (s, 9H).  $^{13}\text{C-NMR}$  (100 MHz,  $\text{CDCl}_3$ )  $\delta$  145.42, 144.48, 133.65, 130.68, 129.80, 128.70, 128.46, 128.23, 127.21, 127.10, 124.51, 123.28, 114.36, 103.61, 54.03, 21.51, -0.12. *LC-MS*: 501.4 (M).



**1m.** White solid. Yield = 50% (not optimized), (cHex:EtOAc = 9:1).  $^1\text{H-NMR}$  (400 MHz,  $\text{CDCl}_3$ )  $\delta$  8.35 (d,  $J = 7.3$  Hz, 1H), 7.78 (d,  $J = 8.2$  Hz, 1H), 7.69 (d,  $J = 8.4$  Hz, 2H), 7.39 – 7.30 (m, 1H), 7.23 (d,  $J =$

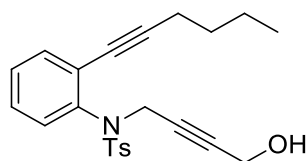
8.0 Hz, 2H), 7.11 – 6.98 (m, 1H), 4.64 (s, 2H), 4.17 (s, 2H), 2.37 (s, 3H), 0.27 (s, 8H).  $^{13}\text{C-NMR}$  (100 MHz,  $\text{CDCl}_3$ )  $\delta$  145.57, 144.54, 139.61, 133.71, 131.03, 129.85, 128.52, 127.12, 124.61, 123.30, 114.33, 111.37, 104.37, 63.09, 53.70, 21.51, -0.19. *LC-MS*: 412.0 ( $\text{M}^+$ ), 434.0 ( $\text{M}+\text{Na}^+$ ).

#### 4.4.9 General procedure for the synthesis of 1k



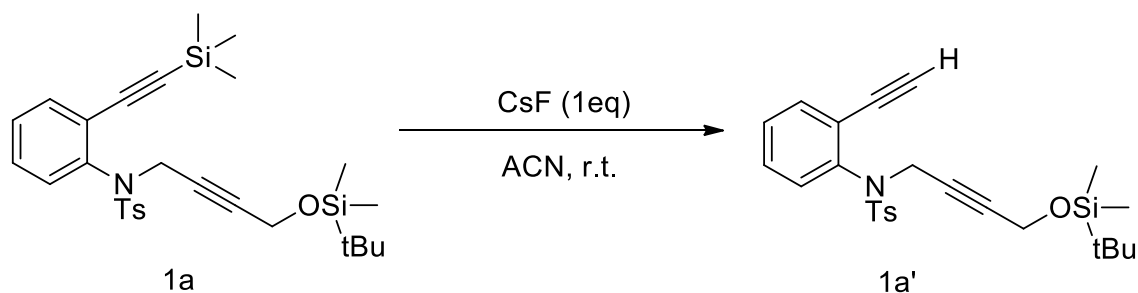
To a solution of **7m** (0.3 mmol) in anhydrous THF (2 mL) under nitrogen anhydrous TEA (2 mL), 1-hexyne (1.5 eq),  $(\text{PPh}_3)_2\text{PdCl}_2$  (0.08 eq) and CuI (0.08 eq) were added. The mixture was stirring at room temperature and the reaction progress was monitored using TLC. After the consumption of starting material, the reaction mixture was extracted with ethyl acetate and water. The organic layers were combined and dried with  $\text{Na}_2\text{SO}_4$ . After

filtration, the solvent was removed under reduced pressure. The residue was purified by flash chromatography on silica gel.

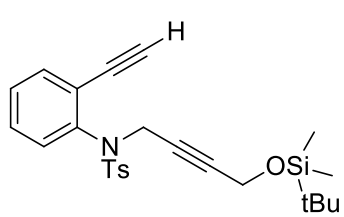


**1k.** Yellow oil. Yield = 44% (not optimized), (cHex:EtOAc = 9:1).  $^1\text{H-NMR}$  (400 MHz,  $\text{CDCl}_3$ )  $\delta$  8.27 (d,  $J = 7.7$  Hz, 1H), 7.75 (d,  $J = 8.2$  Hz, 1H), 7.69 (d,  $J = 8.3$  Hz, 2H), 7.35 – 7.27 (m, 1H), 7.23 (d,  $J = 8.3$  Hz, 2H), 7.03 (t,  $J = 7.7$ , 1H), 4.61 (s, 2H), 4.13 (s, 2H), 2.51 (t,  $J = 7.1$  Hz, 2H), 2.37 (s, 3H), 1.66 – 1.57 (m, 2H), 1.53 – 1.44 (m, 2H), 0.95 (t,  $J = 7.3$  Hz, 3H).  $^{13}\text{C-NMR}$  (100 MHz,  $\text{CDCl}_3$ )  $\delta$  145.09, 144.38, 136.42, 133.71, 130.40, 129.76, 128.82, 127.06, 123.96, 123.26, 114.16, 112.19, 100.07, 78.15, 63.32, 53.52, 30.61, 26.73, 22.01, 21.45, 19.53, 13.49. *LC-MS*: 396.2 ( $\text{M}^+ \text{H}^+$ ). Anal. Calc. for ( $\text{C}_{23}\text{H}_{25}\text{NO}_3\text{S}$ : 395.16): C, 69.85; H, 6.37; N, 3.54; found: C, 69.71, H, 6.49; N, 3.65.

#### 4.4.10 General procedure for the synthesis of 1a'



To a solution of compound **1a** (0.1 mmol, 53 mg) in ACN (3 mL) at room temperature, CsF (1 eq, 0.1 mmol, 15 mg) was added then the mixture was stirred until TLC analysis indicates complete consumption of starting material. Subsequently, water (10 mL) was added and the aqueous layer was extracted with AcOEt (3 x 10 mL). The combined organic layers were dried with  $\text{Na}_2\text{SO}_4$ , filtered and concentrated under reduced pressure. The crude product was purified by column chromatography on silica gel to give the desired product.



**1a'**. Brown oil. Yield = 85% (not optimized), (*c*Hex:EtOAc = 9:1). <sup>1</sup>H-NMR (400 MHz, CDCl<sub>3</sub>) δ

8.36 (d, *J* = 7.8 Hz, 1H), 7.79 (d, *J* = 8.2 Hz, 1H), 7.69 (d, *J* = 8.2 Hz, 2H), 7.32 (t, *J* = 7.8 Hz, 1H),

7.22 (d, *J* = 8.0 Hz, 2H), 7.04 (t, *J* = 7.7 Hz, 1H), 4.69 (s, 2H), 4.26 (s, 2H),

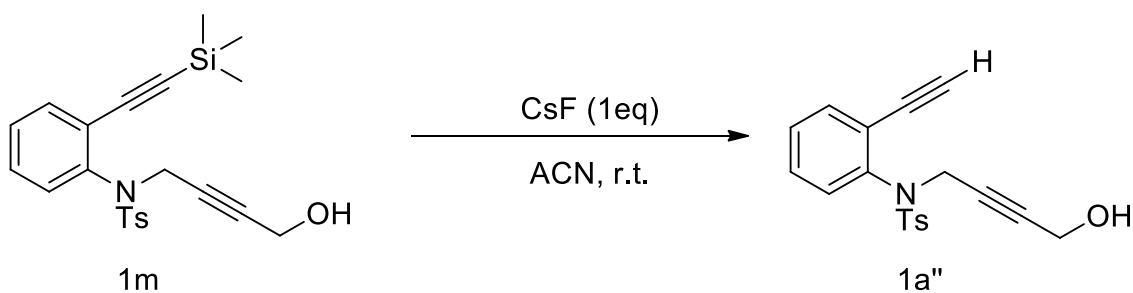
3.50 (s, 1H), 2.37 (s, 3H), 0.93 (s, 9H), 0.11 (s, 6H). <sup>13</sup>C-NMR (100 MHz,

CDCl<sub>3</sub>) δ 145.28, 144.42, 140.35, 133.81, 130.87, 129.80, 128.77, 127.15,

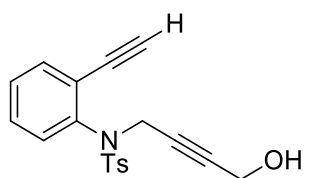
124.67, 123.40, 114.32, 110.70, 85.34, 82.62, 64.73, 54.02, 25.90, 21.51,

18.34, -5.30. LC-MS: 454.4 (M+H<sup>+</sup>), 476.4 (M+Na<sup>+</sup>).

#### 4.4.11 General procedure for the synthesis of 1a''



To a solution of compound **1m** (0.1 mmol, 41 mg) in ACN (3 mL) at room temperature, CsF (1eq, 0.1 mmol, 15 mg) was added then the mixture was stirred until TLC analysis indicates complete consumption of starting material. Subsequently, water (10 mL) was added and the aqueous layer was extracted with AcOEt (3 x 10 mL). The combined organic layers were dried with Na<sub>2</sub>SO<sub>4</sub>, filtered and concentrated under reduced pressure. The crude product was purified by column chromatography on silica gel to give the desired product.



**1a''**. Brown waxy solid. Yield = 71%, (*c*Hex:EtOAc = 9:1). <sup>1</sup>H-NMR (400 MHz, CDCl<sub>3</sub>) δ 8.34 (d, *J* = 7.4

Hz, 1H), 7.77 (d, *J* = 8.3 Hz, 1H), 7.70 (d, *J* = 8.3 Hz,

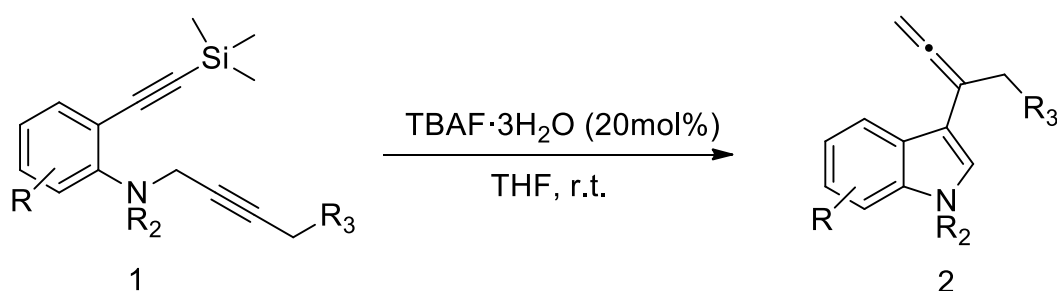
2H), 7.39 – 7.31 (m, 1H), 7.24 (d, *J* = 8.0 Hz, 2H), 7.10 – 7.02 (m, 1H), 4.65

(s, 2H), 4.20 (s, 2H), 3.56 (s, 1H), 2.38 (s, 3H). <sup>13</sup>C-NMR (100 MHz, CDCl<sub>3</sub>)

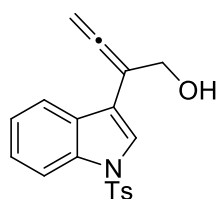


$\delta$  145.46, 144.52, 140.25, 133.64, 131.16, 129.82, 128.14, 127.07, 124.58, 123.43, 114.29, 110.08, 85.98, 81.51, 63.26, 53.61, 21.47. *LC-MS*: 340.2 ( $M+H^+$ ), 362.2 ( $M+Na^+$ ). Anal. Calc. for ( $C_{19}H_{17}NO_3S$ : 339.09): C, 67.24; H, 5.05; N, 4.13; found: C, 67.16, H, 5.11; N, 4.09.

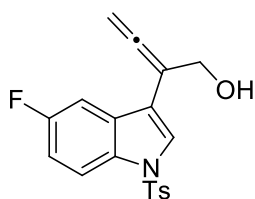
#### 4.4.12 General procedure for the one-pot synthesis of allenyl-indoles **2**



To a solution of **1** (0.05 mmol) in THF (800  $\mu$ L), a solution of TBAF·3H<sub>2</sub>O in THF (0.05 M, 0.2 eq) was added. The mixture was stirred at room temperature and the reaction progress was monitored using TLC. After the consumption of starting material, the reaction mixture was extracted with ethyl acetate and NH<sub>4</sub>Cl (sat.). The organic layers were combined and dried with Na<sub>2</sub>SO<sub>4</sub>. After filtration, the solvent was removed under reduced pressure. The residue was purified by flash chromatography on silica gel.



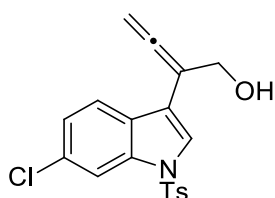
**2a**. Yellow waxy solid. (cHex:EtOAc = 8:2). <sup>1</sup>H-NMR (400 MHz, CDCl<sub>3</sub>)  $\delta$  7.99 (t,  $J$  = 7.3 Hz, 2H), 7.77 (d,  $J$  = 8.4 Hz, 2H), 7.65 (s, 1H), 7.37 – 7.31 (m, 1H), 7.26 – 7.17 (m, 3H), 5.35 (td,  $J$  = 2.5, 0.9 Hz, 2H), 4.53 (t,  $J$  = 2.5 Hz, 2H), 2.33 (s, 3H), 1.81 (s, 1H). <sup>13</sup>C-NMR (100 MHz, CDCl<sub>3</sub>)  $\delta$  208.41, 144.99, 135.34, 135.17, 130.01, 129.89, 127.81, 126.85, 125.02, 123.29, 122.69, 120.89, 113.59, 99.32, 80.59, 63.03, 21.54. *LC-MS*: 340.0 ( $M+H^+$ ), 357.0 ( $M + H_2O$ ), 362.0 ( $M+Na^+$ ). Anal. Calc. for ( $C_{19}H_{17}NO_3S$ : 339.09): C, 67.24; H, 5.05; N, 4.13; found: C, 67.01, H, 5.00; N, 4.01.



**2b.** Pale yellow solid. Yield = 84%, (cHex:EtOAc = 8:2).

Mp = 132-134 °C.  $^1\text{H-NMR}$  (400 MHz,  $\text{CDCl}_3$ )  $\delta$  7.93 (dd,  $J = 9.0, 4.5$  Hz, 1H), 7.75 (d,  $J = 8.4$  Hz, 2H), 7.69 (s, 1H), 7.64 (dd,  $J = 9.4, 2.4$  Hz, 1H), 7.23 (d,  $J = 8.0$  Hz,

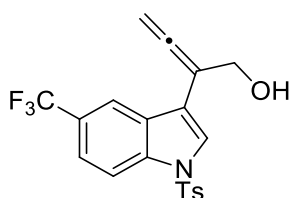
2H), 7.06 (td,  $J = 9.0, 2.6$  Hz, 1H), 5.36 (s, 2H), 4.52 (s, 2H), 2.35 (s, 3H).  $^{13}\text{C-NMR}$  (100 MHz,  $\text{CDCl}_3$ )  $\delta$  208.19, 160.67, 158.29, 145.24, 145.19, 134.80, 129.97, 129.93, 126.79, 126.77, 124.27, 114.60, 114.50, 113.14, 113.07, 112.88, 112.82, 106.81, 106.56, 99.00, 80.84, 63.06, 21.54. *LC-MS*: 358.0 ( $\text{M} + \text{H}^+$ ), 375.0 ( $\text{M} + \text{H}_2\text{O}$ ), 380.0 ( $\text{M} + \text{K}^+$ ). Anal. Calc. for ( $\text{C}_{19}\text{H}_{16}\text{FNO}_3\text{S}$ : 357.09): C, 63.85; H, 4.51; N, 3.92; found: C, 63.75, H, 4.66; N, 3.86.



**2c.** White solid. Yield = 93%, (cHex:EtOAc = 8:2). Mp

= 108-110 °C.  $^1\text{H-NMR}$  (400 MHz,  $\text{CDCl}_3$ )  $\delta$  7.98 (t,  $J = 2.4$  Hz, 1H), 7.86 (d,  $J = 8.6$  Hz, 1H), 7.75 (dd,  $J = 8.4, 3.6$  Hz, 2H), 7.61 (s, 1H), 7.23 (d,  $J = 7.9$  Hz, 3H), 7.20

– 7.14 (m, 1H), 5.32 (t,  $J = 2.4$  Hz, 2H), 4.49 (t,  $J = 2.4$  Hz, 2H), 2.34 (s, 3H).  $^{13}\text{C-NMR}$  (100 MHz,  $\text{CDCl}_3$ )  $\delta$  208.40, 145.35, 135.74, 134.85, 131.10, 130.07, 127.60, 126.86, 123.95, 123.13, 121.72, 115.04, 113.71, 99.00, 80.70, 63.09, 21.60. *LC-MS*: 374.2 ( $\text{M} + \text{H}^+$ ), 391.2 ( $\text{M} + \text{H}_2\text{O}$ ), 412.2 ( $\text{M} + \text{K}^+$ ). Anal. Calc. for ( $\text{C}_{19}\text{H}_{16}\text{ClNO}_3\text{S}$ : 373.05): C, 61.04; H, 4.31; N, 3.75; found: C, 61.20, H, 4.38; N, 3.66.

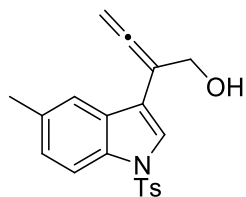


**2d.** Yellow solid. Yield = 38%, (cHex:EtOAc = 8:2).

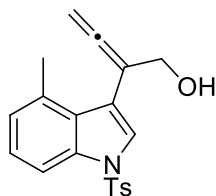
Mp = 137-139 °C  $^1\text{H-NMR}$  (400 MHz,  $\text{CDCl}_3$ )  $\delta$  8.38 – 8.20 (m, 1H), 8.09 (d,  $J = 8.7$  Hz, 1H), 7.78 (d,  $J = 8.6$  Hz, 3H), 7.57 (d,  $J = 8.8$  Hz, 1H), 7.27 – 7.24 (m, 2H),

5.40 (td,  $J = 2.4, 1.0$  Hz, 2H), 4.54 (t,  $J = 2.3$  Hz, 2H), 2.36 (s, 3H).  $^{13}\text{C-NMR}$  (100 MHz,  $\text{CDCl}_3$ )  $\delta$  208.49, 145.53, 136.67, 134.73, 130.08, 128.87, 126.86, 124.21, 123.12, 121.72, 118.51, 118.47, 115.32, 113.81, 98.71, 80.79, 63.22, 21.57. *LC-MS*: 408.0 ( $\text{M} + \text{H}^+$ ), 425.0 ( $\text{M} + \text{H}_2\text{O}$ ). Anal. Calc.

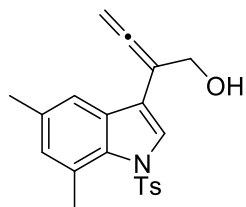
for (C<sub>20</sub>H<sub>16</sub>F<sub>3</sub>NO<sub>3</sub>S: 407.08): C, 58.96; H, 3.96; N, 3.44; found: C, 58.81, H, 3.85; N, 3.29.



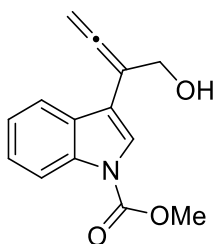
**2e.** Yellow solid. Yield = 86%, (cHex:EtOAc = 85:15). Mp = 95-97 °C. <sup>1</sup>H-NMR (400 MHz, CDCl<sub>3</sub>) δ 7.87 (d, *J* = 8.5 Hz, 1H), 7.75 (d, *J* = 8.2 Hz, 3H), 7.59 (s, 1H), 7.21 (d, *J* = 8.2 Hz, 2H), 7.15 (d, *J* = 8.5 Hz, 1H), 5.36 (t, *J* = 2.3 Hz, 2H), 4.52 (t, *J* = 2.3 Hz, 2H), 2.41 (s, 3H), 2.34 (s, 3H). <sup>13</sup>C-NMR (100 MHz, CDCl<sub>3</sub>) δ 208.24, 144.88, 135.09, 133.55, 132.99, 129.84, 126.80, 126.40, 124.68, 122.77, 120.69, 119.39, 113.27, 99.36, 80.69, 62.97, 21.54, 21.50. LC-MS: 371.4 (M + H<sub>2</sub>O). Anal. Calc. for (C<sub>20</sub>H<sub>19</sub>NO<sub>3</sub>S: 353.11): C, 67.97; H, 5.42; N, 3.96; found: C, 67.81, H, 5.31; N, 3.80.



**2f.** Pale yellow solid. Yield = 68%. (cHex:EtOAc = 85:15). Mp = 99-101 °C. <sup>1</sup>H-NMR (400 MHz, CDCl<sub>3</sub>) δ 7.86 – 7.81 (m, 1H), 7.78 (t, *J* = 8.5 Hz, 2H), 7.54 (s, 1H), 7.26 – 7.16 (m, 3H), 7.02 – 6.96 (m, 1H), 5.05 (t, *J* = 3.1 Hz, 2H), 4.33 (t, *J* = 3.1 Hz, 2H), 2.58 (s, 2H), 2.35 (s, 3H). <sup>13</sup>C-NMR (100 MHz, CDCl<sub>3</sub>) δ 207.00, 144.96, 135.12, 131.63, 129.90, 129.87, 126.93, 126.86, 125.54, 125.27, 124.77, 124.44, 111.62, 111.23, 78.17, 64.41, 21.56, 20.09. LC-MS: 371.2 (M + H<sub>2</sub>O). Anal. Calc. for (C<sub>20</sub>H<sub>19</sub>NO<sub>3</sub>S: 353.11): C, 67.97; H, 5.42; N, 3.96; found: C, 67.90, H, 5.32; N, 3.66.

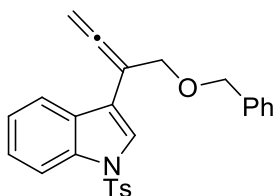


**2g.** Brown solid. Yield = 85%. (cHex:EtOAc = 85:15). Mp = 98-100 °C. <sup>1</sup>H-NMR (400 MHz, CDCl<sub>3</sub>) δ 7.78 (s, 1H), 7.64 (s, 1H), 7.54 (d, *J* = 8.4 Hz, 2H), 7.24 – 7.16 (m, 2H), 6.88 (s, 1H), 5.38 (t, *J* = 2.4 Hz, 2H), 4.54 (t, *J* = 2.4 Hz, 2H), 2.51 (s, 3H), 2.37 (s, 3H), 2.35 (s, 3H). <sup>13</sup>C-NMR (100 MHz, CDCl<sub>3</sub>) δ 208.10, 144.53, 136.63, 133.38, 130.13, 129.82, 128.37, 126.54, 126.43, 124.65, 118.40, 116.97, 114.43, 99.18, 80.77, 62.91, 21.66, 21.56, 21.12. LC-MS: 385.2 (M + H<sub>2</sub>O). Anal. Calc. for (C<sub>21</sub>H<sub>21</sub>NO<sub>3</sub>S: 367.12): C, 68.64; H, 5.76; N, 3.81; found: C, 68.51, H, 5.64; N, 3.64.



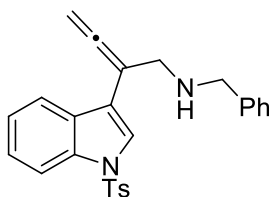
**2h.** Brown waxy solid. Yield = 45% (51% deprotected product 2h''), (*c*Hex:EtOAc = 85:15).  $^1\text{H-NMR}$  (400 MHz,  $\text{CDCl}_3$ )  $\delta$  8.21 (d,  $J = 8.1$  Hz, 1H), 8.04 (d,  $J = 8.1$  Hz, 1H), 7.68 (s, 1H), 7.41 – 7.33 (m, 1H), 7.29 – 7.24 (m, 1H), 5.38 (td,  $J = 2.5, 1.0$  Hz, 2H), 4.55 (s, 2H), 4.05 (s, 3H).  $^{13}\text{C-NMR}$

(100 MHz,  $\text{CDCl}_3$ )  $\delta$  208.46, 128.71, 125.03, 123.04, 121.92, 120.49, 115.05, 114.10, 99.48, 80.54, 63.05, 53.82. *LC-MS*: 244.2 ( $\text{M} + \text{H}^+$ ), 261.2 ( $\text{M} + \text{H}_2\text{O}$ ). Anal. Calc. for ( $\text{C}_{14}\text{H}_{13}\text{NO}_3$ : 243.09): C, 69.12; H, 5.39; N, 5.76; found: C, 69.30, H, 5.41; N, 5.85.



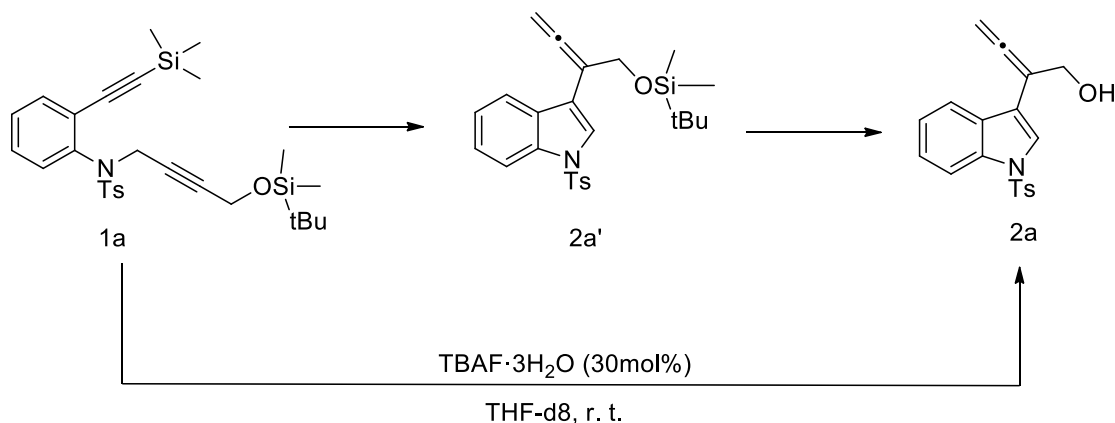
**2i.** Yellow oil. Yield = 70%. (*c*Hex:EtOAc = 9:1).  $^1\text{H-NMR}$  (400 MHz,  $\text{CDCl}_3$ )  $\delta$  8.01 (d,  $J = 8.4$  Hz, 2H), 7.78 (s, 1H), 7.71 (d,  $J = 8.1$  Hz, 2H), 7.46 – 7.28 (m, 6H), 7.22 (t,  $J = 7.6$  Hz, 1H), 7.12 (d,  $J = 8.3$  Hz, 2H), 5.27

(s, 2H), 4.59 (s, 2H), 4.49 (s, 2H), 2.31 (s, 3H).  $^{13}\text{C-NMR}$  (100 MHz,  $\text{CDCl}_3$ )  $\delta$  210.29, 144.79, 137.98, 135.27, 135.08, 129.78, 129.25, 128.42, 127.86, 127.68, 126.80, 124.82, 123.65, 123.20, 120.87, 115.47, 113.59, 95.70, 78.51, 77.20, 71.43, 29.67, 21.52. *LC-MS*: 447.4 ( $\text{M}^+ + \text{H}_2\text{O}$ ). Anal. Calc. for ( $\text{C}_{26}\text{H}_{23}\text{NO}_3\text{S}$ : 429.14): C, 72.70; H, 5.40; N, 3.26; found: C, 72.65, H, 5.28; N, 3.15.



**2j.** Yellow oil. Yield = 45%, (*c*Hex:EtOAc = 8:2).  $^1\text{H-NMR}$  (400 MHz,  $\text{CDCl}_3$ )  $\delta$  8.04 – 7.93 (t, 1H), 7.74 (d,  $J = 8.3$  Hz, 2H), 7.60 (s, 1H), 7.40 – 7.28 (m, 6H), 7.25 – 7.16 (m, 3H), 5.31 (s, 2H), 3.90 (s, 2H), 3.69 (s, 2H),

2.33 (s, 3H).  $^{13}\text{C-NMR}$  (100 MHz,  $\text{CDCl}_3$ )  $\delta$  208.91, 144.91, 135.37, 135.08, 129.84, 128.43, 128.27, 128.00, 127.05, 126.80, 124.93, 123.23, 122.56, 121.00, 119.72, 116.51, 113.57, 97.33, 79.87, 71.57, 53.07, 49.93, 21.54. *LC-MS*: 429.4 ( $\text{M} + \text{H}^+$ ). Anal. Calc. for ( $\text{C}_{26}\text{H}_{24}\text{N}_2\text{O}_2\text{S}$ : 428.16): C, 72.87; H, 5.65; N, 6.54; found: C, 72.75, H, 5.51; N, 6.38.

4.4.13  $^1\text{H-NMR}$  experiment

To a solution of **1a** (0.05 mmol, 26 mg) in THF-d<sub>8</sub> (500  $\mu\text{L}$ ), a solution of TBAF·3H<sub>2</sub>O (30 mol%, 4.7 mg, 0.3 eq) in THF-d<sub>8</sub> (200  $\mu\text{L}$ ) was added. The reaction was monitored by  $^1\text{H-NMR}$ .

**Table 4.3** Calculation of the relative conversions of product **2a**, intermediate **2a'** and unknown compound and starting material **1a**, at different reaction times by  $^1\text{H-NMR}$  spectroscopy.

Reaction time (min)	Conversion (%)			
	2a	2a'	Unknown	1a
2	49.5	17.3	18.8	14.3
4	54.5	17.4	19.3	8.7
6	60.0	15.6	16.5	7.8
8	64.9	17.2	17.8	n.d.
10	67.1	16.1	16.8	n.d.
20	73.8	12.1	14.0	n.d.
30	78.4	11.0	10.6	n.d.
3 hours	>98%	n.d.	n.d.	n.d.

n.d. = not determined

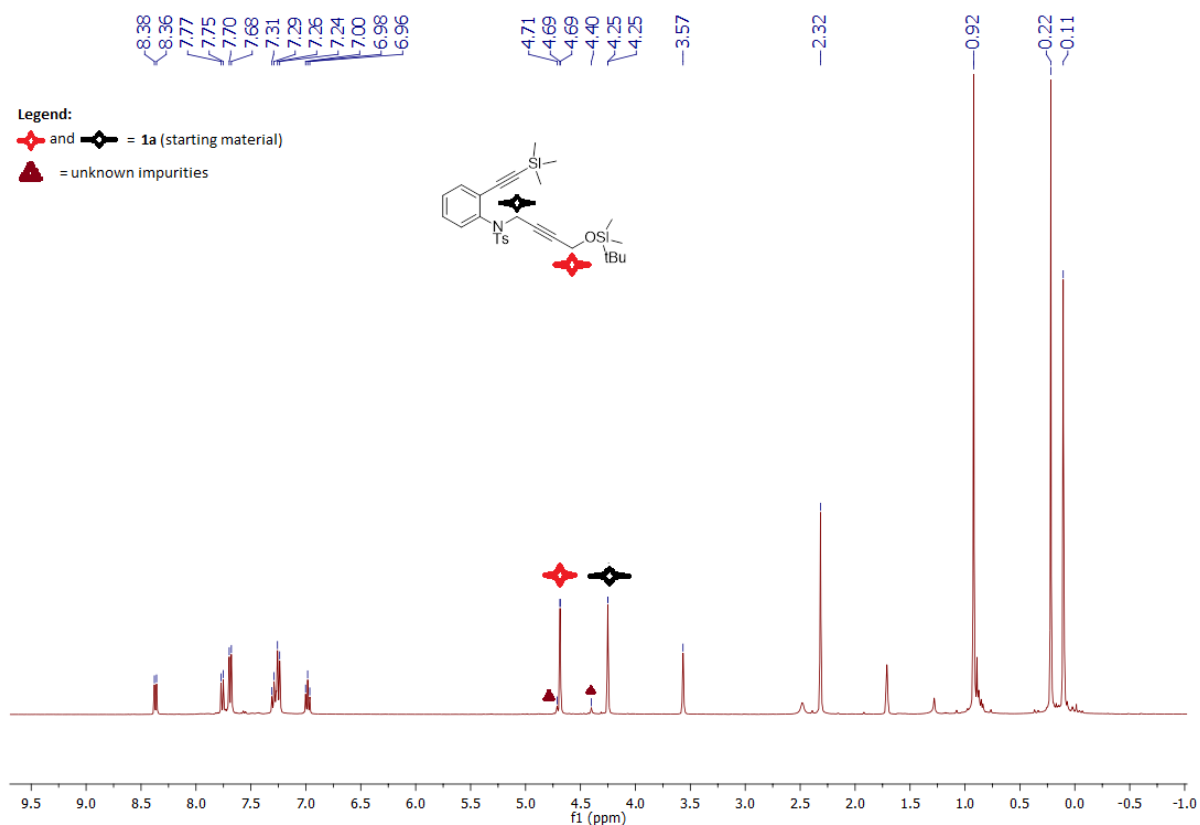


Figure 4.16  $^1\text{H-NMR}$  of compound 1a.

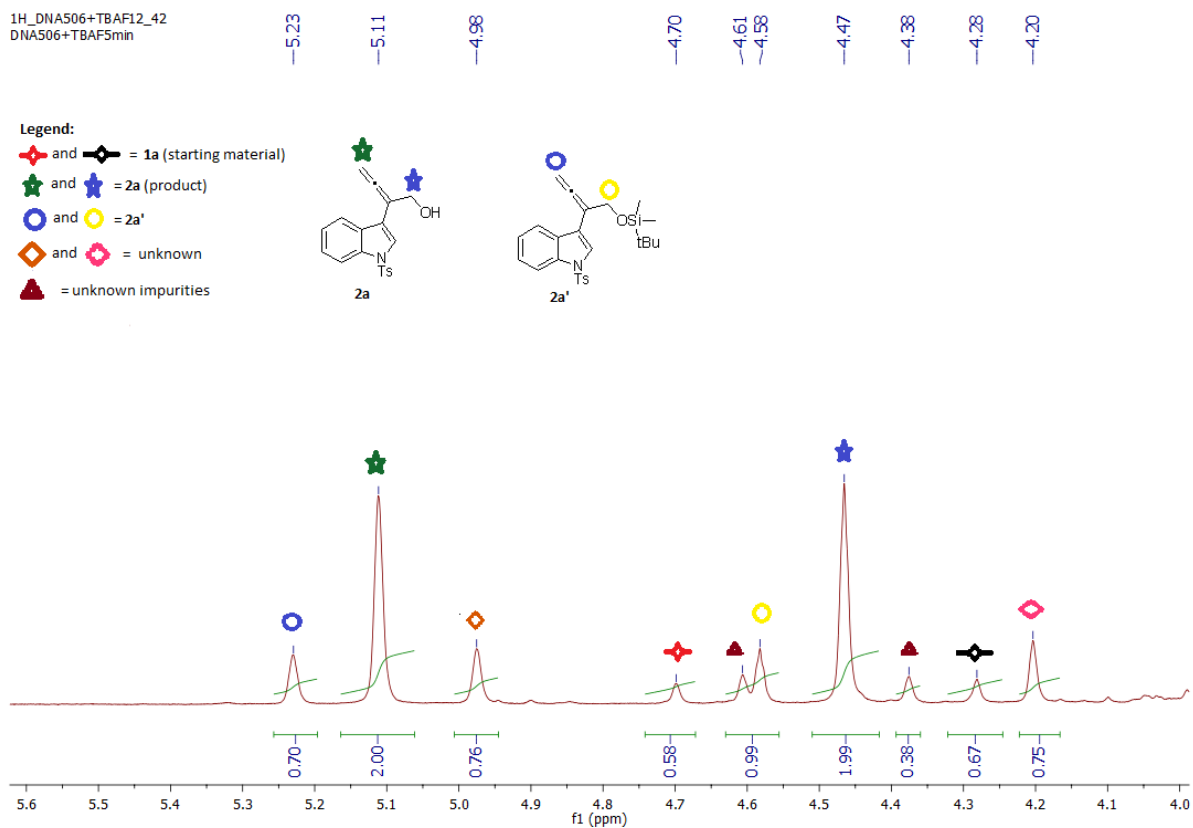


Figure 4.17  $^1\text{H-NMR}$  2 minutes after the addition of TBAF solution.

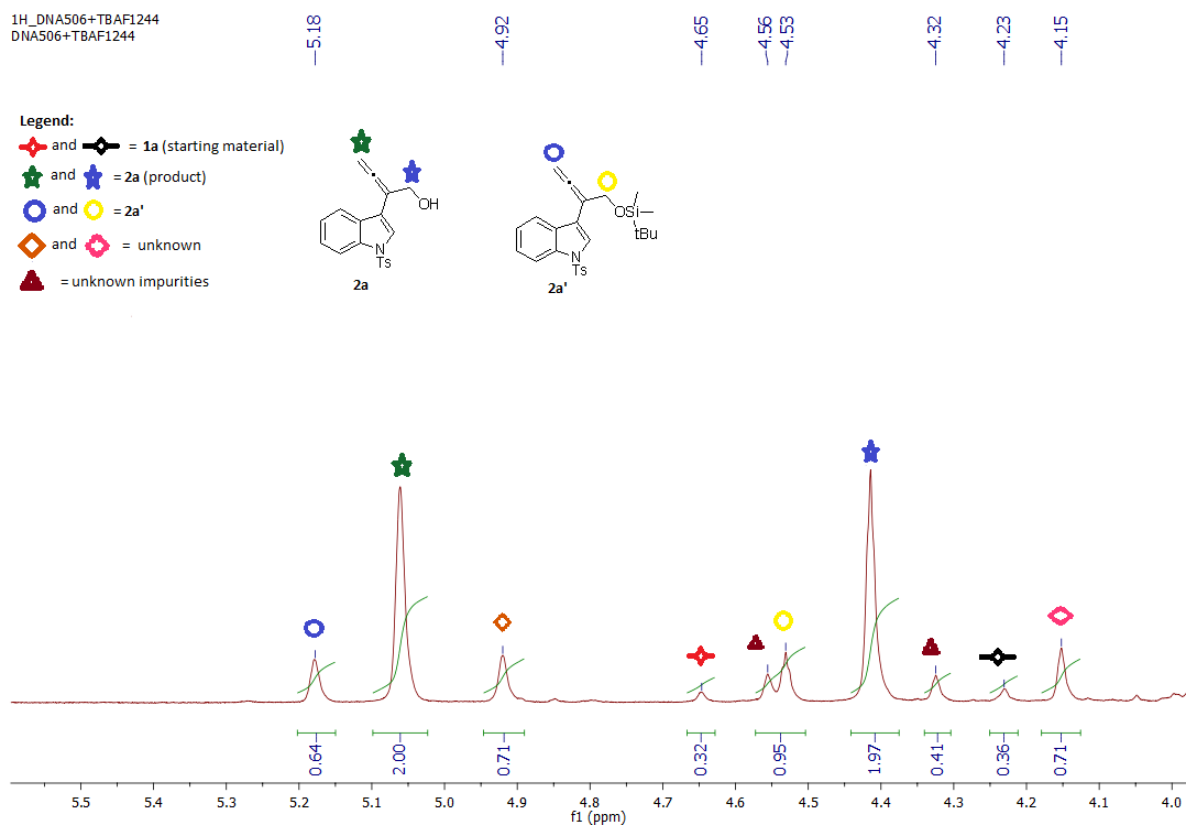


Figure 4.18  $^1\text{H-NMR}$  4 minutes after the addition of TBAF solution.

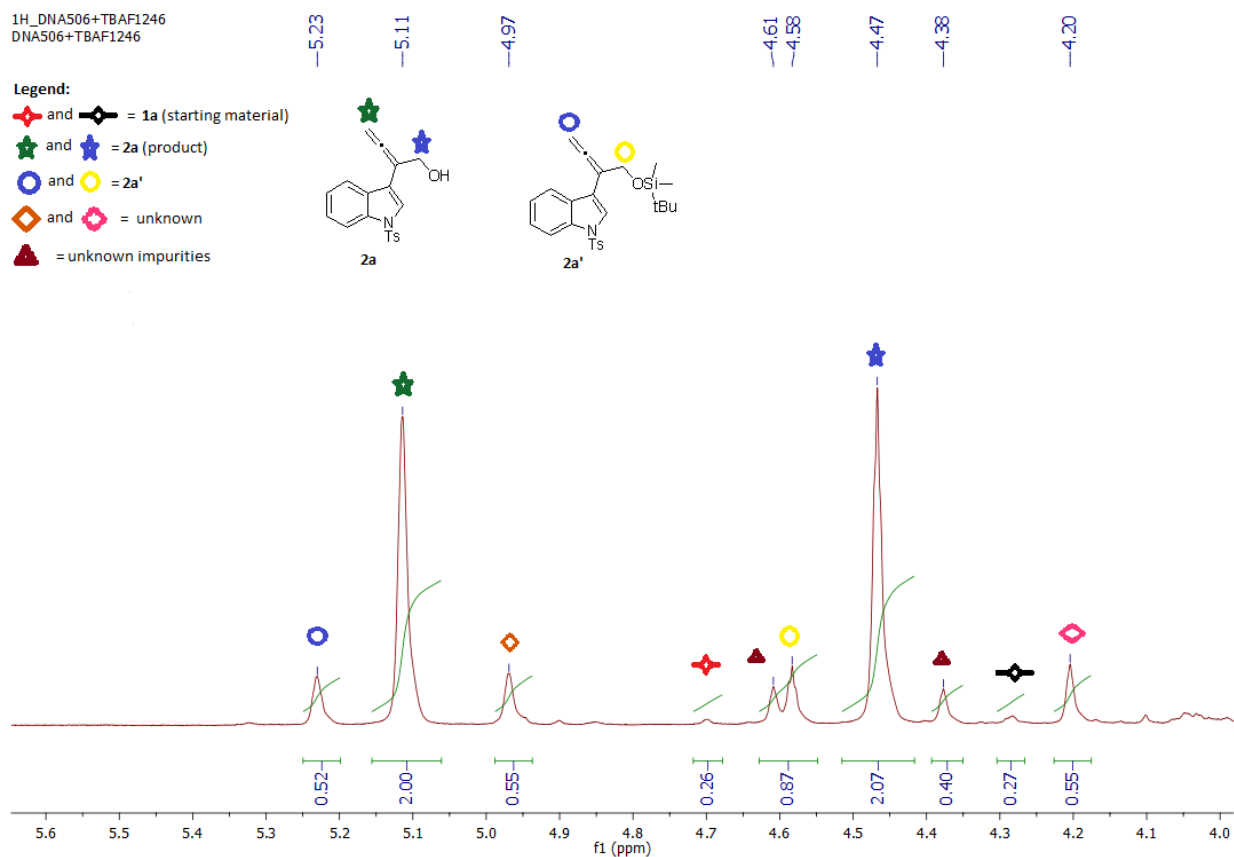


Figure 4.19  $^1\text{H-NMR}$  6 minutes after the addition of TBAF solution.

Chapter 4: I thought it was gold instead...TBAF catalysed one-pot synthesis of allenyl-indoles

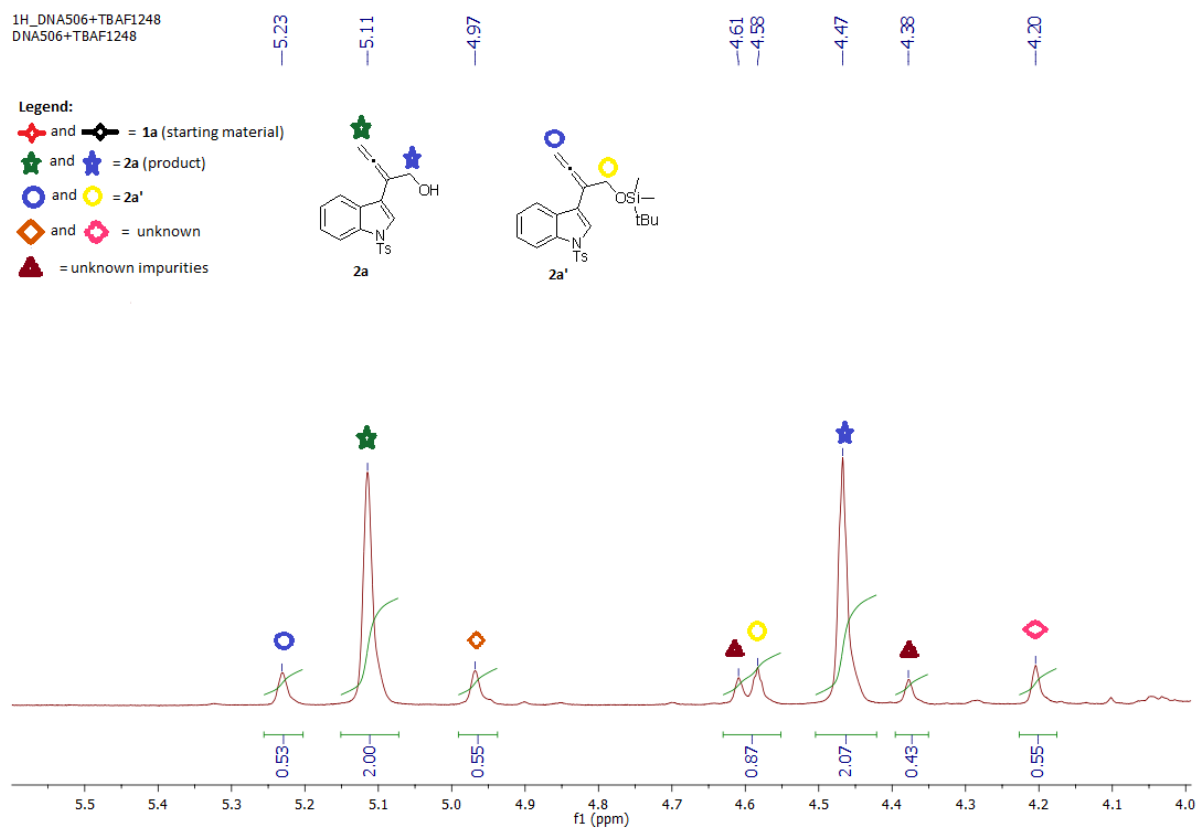


Figure 4.20  $^1\text{H-NMR}$  8 minutes after the addition of TBAF solution.

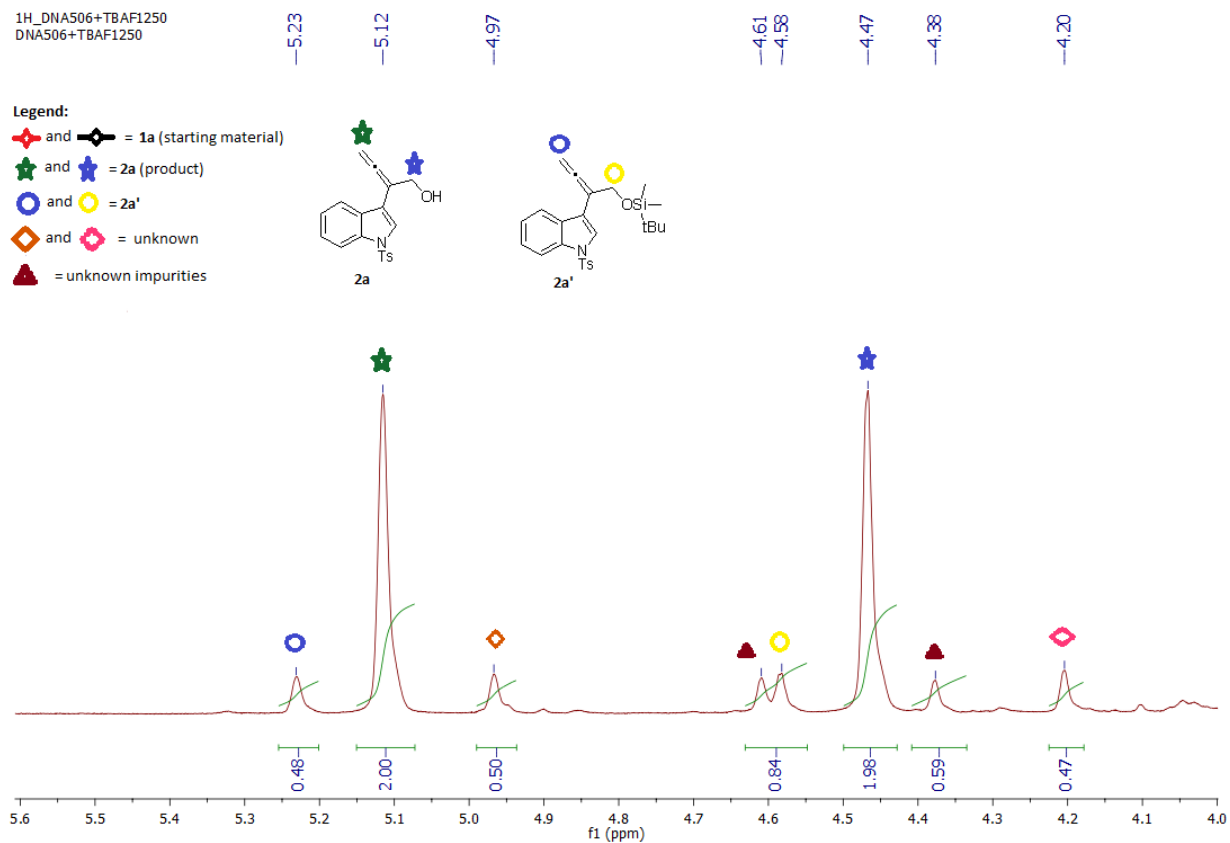


Figure 4.21  $^1\text{H-NMR}$  10 minutes after the addition of TBAF solution.



Chapter 4: I thought it was gold instead... TBAF catalysed one-pot synthesis of allenyl-indoles

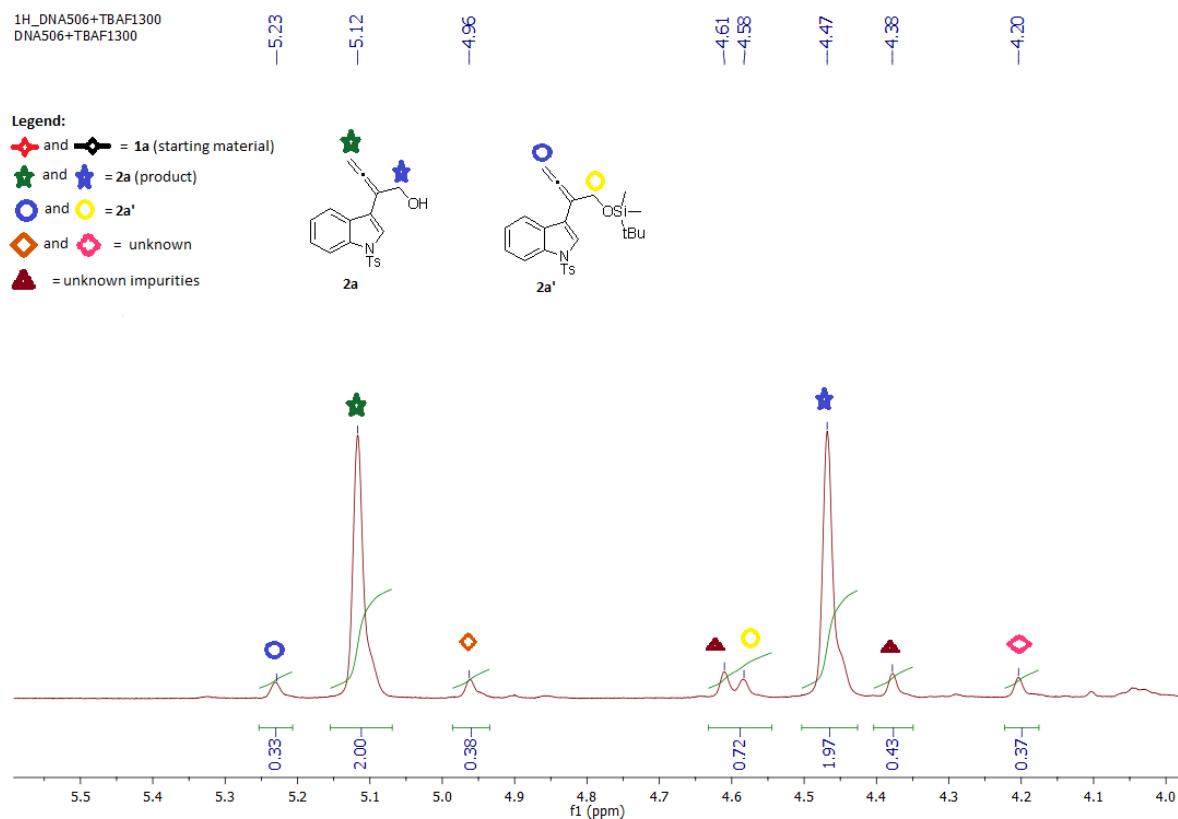


Figure 4.22 <sup>1</sup>H-NMR 20 minutes after the addition of TBAF solution.

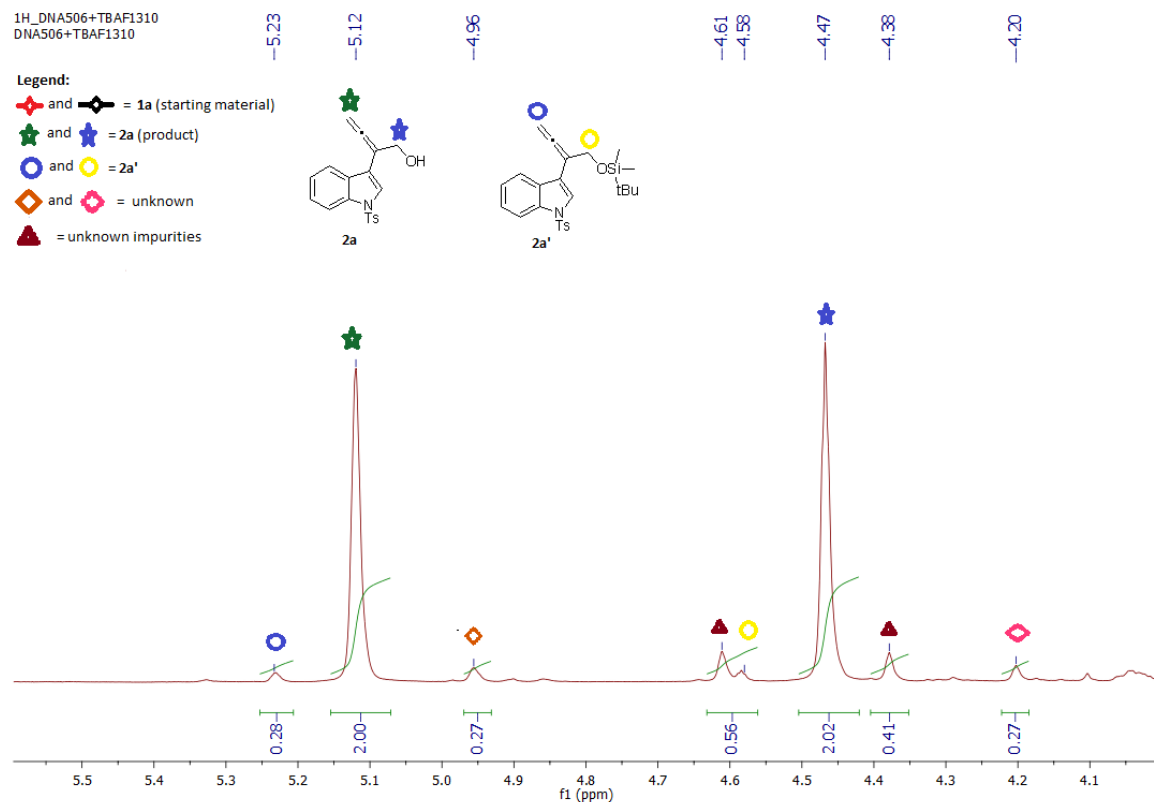
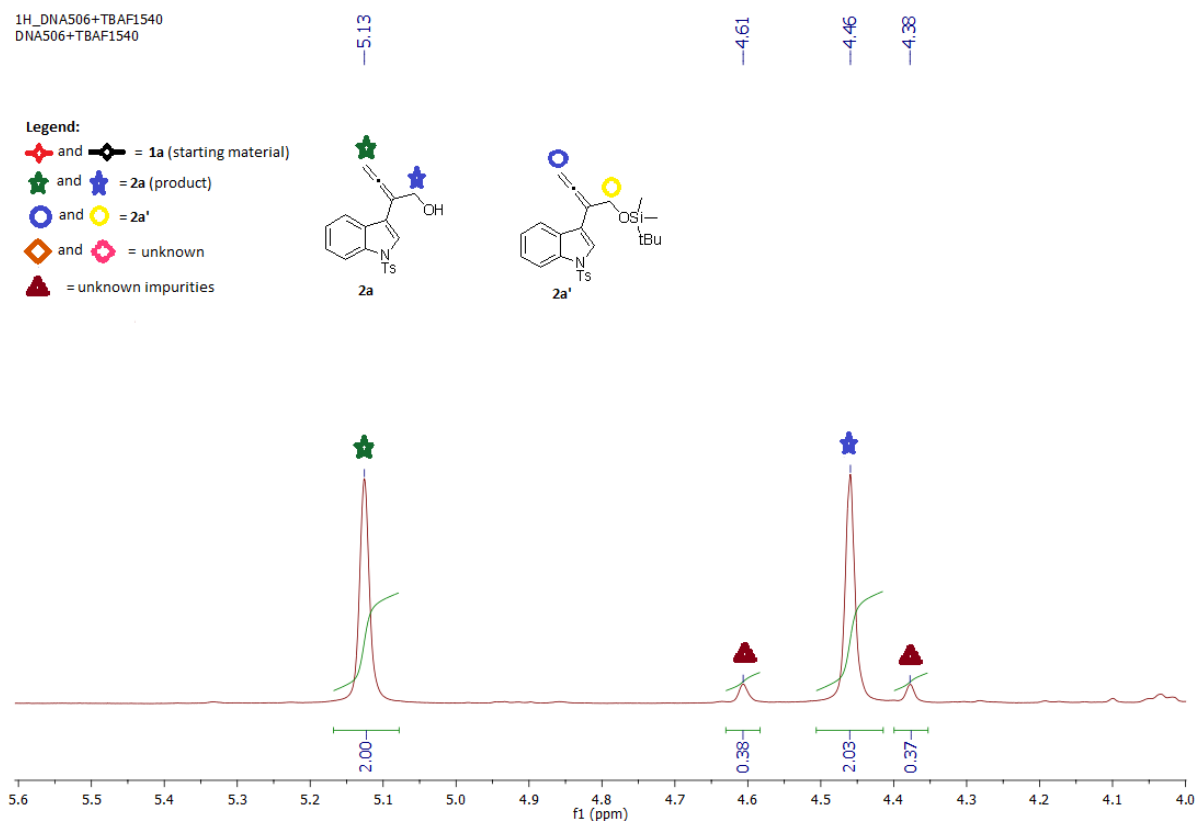
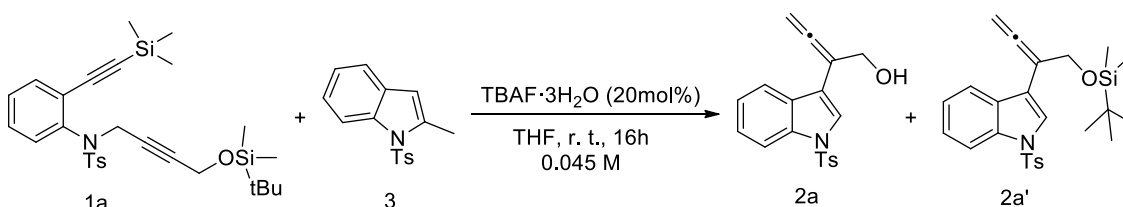


Figure 4.23 <sup>1</sup>H-NMR 30 minutes after the addition of TBAF solution.



**Figure 4.24**  $^1\text{H-NMR}$  3 hours after the addition of TBAF solution.

#### 4.4.14 Procedure for the scrambling reaction



2-Methyl-*N*-tosylindole was prepared following reported procedures.<sup>[40]</sup>

A screw vial was charged with 800  $\mu\text{L}$  of reagent grade THF, **1a** (34 mg, 0.065 mmol), indole **3** (28 mg, 0.098 mmol) and a solution of TBAF in THF (10 mg/mL, 330  $\mu\text{L}$ , 20 mol%). The mixture was stirred at room temperature and the reaction progress was monitored using TLC. After the consumption of starting material, the reaction mixture was extracted with ethyl acetate and  $\text{NH}_4\text{Cl}$  (sat.). The organic layers were combined and dried with  $\text{Na}_2\text{SO}_4$ .  $^1\text{H-}$

NMR of the reaction crude (see below) revealed a complete conversion of **1a** forming a mixture of **2a** and **2a'** in 2:1 ratio. Flash chromatographic purification allowed the quantitative recovering of unreacted **3**.

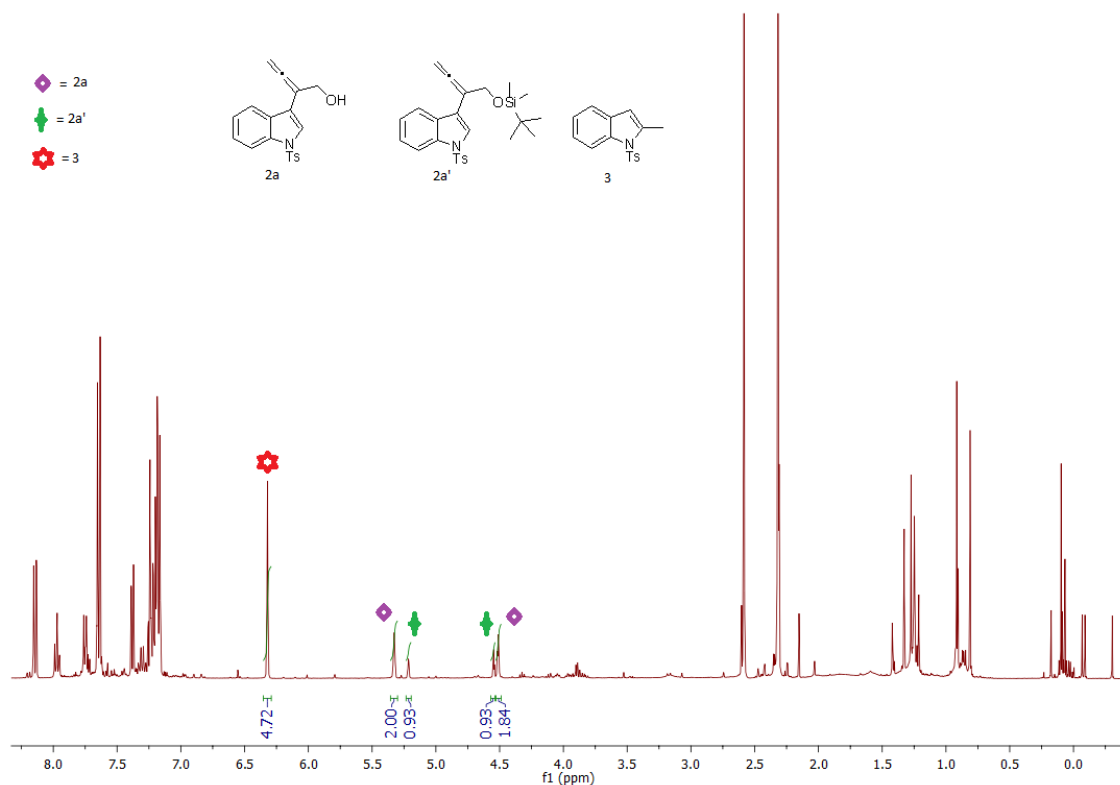
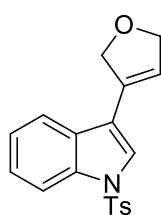


**Figure 4.25**  $^1\text{H-NMR}$  of the scrambling reaction crude.

#### 4.4.15 Optimization of the catalytic cyclization of **2a** to dihydrofuran **4a**

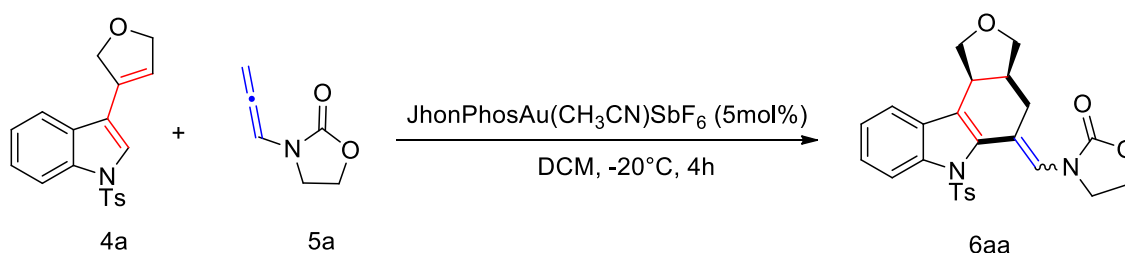
To a solution of  $\text{LAuCl}$  (5 mol%) in anhydrous toluene (1 mL), 5 mol% of  $\text{AgX}$  ( $\text{X} = \text{OTf}, \text{SbF}_6, \text{NTf}_2$ ) was added and the reaction mixture stirred for 15 min in the dark. Then **2a** (0.075 mmol, 25 mg) was added. The reaction was allowed to stir for 1 h, then directly charged into a column for the flash chromatography purification ( $c\text{Hex}:\text{EtOAc} = 9:1$ ).



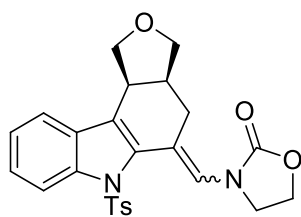
**4a.** White waxy solid.  $^1\text{H-NMR}$  (400 MHz,  $\text{CDCl}_3$ )  $\delta$  8.03 – 7.99 (m, 1H), 7.79 – 7.75 (m, 3H), 7.44 (s, 1H), 7.41 – 7.35 (m, 1H), 7.34 – 7.29 (m, 1H), 7.24 (d,  $J = 8.0$  Hz, 2H), 6.35 (s, 1H), 5.00 (td,  $J = 4.6, 2.0$  Hz, 2H), 4.89 (td,  $J = 4.8, 1.7$  Hz, 2H), 2.35 (s,

3H).  $^{13}\text{C-NMR}$  (100 MHz,  $\text{CDCl}_3$ )  $\delta$  145.16, 135.33, 134.98, 130.80, 129.93, 128.66, 126.81, 125.13, 123.71, 123.44, 121.23, 120.75, 115.18, 113.78, 76.86, 75.84, 21.52. *LC-MS*: 340.2 ( $\text{M} + \text{H}^+$ ), 362.0 ( $\text{M} + \text{Na}^+$ ), 378.2 ( $\text{M} + \text{K}^+$ ). Anal. Calc. for ( $\text{C}_{19}\text{H}_{17}\text{NO}_3\text{S}$ : 339.09): C, 67.24; H, 5.05; N, 4.13; found: C, 67.21, H, 5.00; N, 4.25.

#### 4.4.16 Gold-catalyzed synthesis of the tetrahydrocarbazole **6aa** through intermolecular cycloaddition of allenyl indoles and *N*-allenyl amides.



To a solution of **4a** (0.12 mmol, 40 mg) and allenamide **5a** (0.11 mmol, 13 mg) in dry DCM (1.5 mL) at  $-20^\circ\text{C}$ , [ $\text{JhonPhosAu}(\text{CH}_3\text{CN})\text{SbF}_6$ ] (5 mol%) was added. The resulting mixture was stirred at this temperature until disappearance of the starting reagents was confirmed by TLC analysis. The solvent was removed under reduced pressure and the resulting residue purified by column chromatography (*c*Hex:EtOAc = 6:4).



**6aa.** White waxy solid. Yield = 55%.  $^1\text{H-NMR}$  (400 MHz,  $\text{CDCl}_3$ )  $\delta$  7.79 (d,  $J = 8.2$  Hz, 1H), 7.47 (d,  $J = 8.3$  Hz, 2H), 7.28 (t,  $J = 7.3$  Hz, 1H), 7.11 (dd,  $J = 16.0, 7.9$  Hz, 3H), 6.97 (d,  $J = 7.4$  Hz, 1H), 6.26 (s, 1H), 5.14 (d,  $J = 2.3$  Hz, 1H), 4.60 (ddd,  $J = 14.1, 3.6, 1.8$  Hz, 1H), 4.49 (dd,  $J = 17.0, 8.3$  Hz, 1H), 4.44 – 4.32 (m, 2H), 4.26 (td,  $J = 8.6, 5.2$  Hz, 1H), 4.18 (t,  $J = 8.0$  Hz, 1H), 3.79 (dd,  $J = 16.9, 8.3$  Hz, 1H), 3.46 (q,  $J = 7.0$  Hz, 1H), 3.01 (dd,  $J = 10.1, 8.2$  Hz, 1H), 2.83 (s, 1H), 2.50 (dd,  $J = 14.4, 7.6$  Hz, 1H), 2.31 (s, 3H), 1.40 – 1.29 (m, 2H).  $^{13}\text{C-NMR}$  (100 MHz,  $\text{CDCl}_3$ )  $\delta$  157.19, 144.15, 144.02, 135.31, 134.86, 129.52, 129.18, 128.83, 127.34,

126.32, 124.89, 122.78, 122.16, 117.32, 72.63, 68.46, 63.55, 62.45, 46.07, 41.42, 31.04, 29.65, 21.45, 17.85. *LC-MS*: 465.2 (M+H<sup>+</sup>), 503.2 (M+K<sup>+</sup>).

#### 4.4.17 Single Crystal X-ray crystallography

A suitable crystal of **4a** was mounted on a goniometer head and cooled to 100 K in a stream of cold N<sub>2</sub> using Bruker Kryoflex low temperature device whereas the **2d** was mounted on a goniometer head and kept at room temperature. The X-ray intensity data for both structures were measured on a Bruker SMART Apex II CCD area detector diffractometer. Cell dimensions and the orientation matrix were initially determined from a least-squares refinement on reflections measured in three sets of 20 exposures, collected in three different  $\omega$  regions, and eventually refined against all data. A full sphere of reciprocal space was scanned by 0.3°  $\omega$  steps. The software SMART was used for collecting frames of data, indexing reflections, and determination of lattice parameters. The collected frames were then processed for integration by the SAINT program and an empirical absorption correction was applied using SADABS. The structures were solved by direct methods (SIR 2004) and subsequent Fourier syntheses and refined by full-matrix least-squares on F<sup>2</sup> (SHELXTL), using anisotropic thermal parameters for all non-hydrogen atoms. All hydrogen atoms were added in calculated positions, included in the final stage of refinement with isotropic thermal parameters,  $U(\text{H}) = 1.2 U_{\text{eq}}(\text{C})$  [ $U(\text{H}) = 1.5 U_{\text{eq}}(\text{C-Me})$ ], and allowed to ride on their carrier carbons.

Crystal data and details of the data collection for **2d** and **4a** are reported in Table 4.4.

**Table 4.4** Crystal data and structure refinement for **2d** and **4a**.

	<b>2d</b>	<b>4a</b>
<b>Empirical formula</b>	C <sub>20</sub> H <sub>16</sub> F <sub>3</sub> NO <sub>3</sub> S	C <sub>19</sub> H <sub>17</sub> NO <sub>3</sub> S
<b>Formula weight</b>	407.40	339.39
<b>Temperature/K</b>	293(2)	100(2)
<b>Crystal system</b>	Triclinic	<i>Monoclinic</i>
<b>Space group</b>	P1	<i>P 2<sub>1</sub>/n</i>
<b>a, Å</b>	8.5679(12)	7.8333(1)
<b>b, Å</b>	12.3701(14)	8.7742(2)
<b>c, Å</b>	18.181(3)	23.1441(4)
<b>α, °</b>	83.843(7)	90
<b>β, °</b>	89.595(12)	95.475(1)
<b>γ, °</b>	80.871(9)	90
<b>Cell volume, Å<sup>3</sup></b>	1891.4(5)	1583.46(5)
<b>Z</b>	4	4
<b>ρ<sub>c</sub>, Mg m<sup>-3</sup></b>	1.431	1.424
<b>μ(Mo-Kα), mm<sup>-1</sup></b>	0.221	0.222
<b>F(000)</b>	840	712
<b>Crystal size, mm</b>	0.20 x 0.10 x 0.05	0.30 x 0.20 x 0.10
<b>θ limits, °</b>	1.677 to 28.604	1.768 to 23.351
<b>Refl. collected, unique</b>	31491 / 17775 [R(int) = 0.1039]	19332 / 2296 [R(int) = 0.0528]
<b>Goodness-of-fit-on F<sup>2</sup></b>	0.892	1.235
<b>R<sub>1</sub>(F)<sup>a</sup>, wR<sub>2</sub>(F<sup>2</sup>) [I &gt; 2σ(I)]<sup>b</sup></b>	0.0738, 0.1707	0.0328, 0.0849
<b>Largest diff. peak and hole, e. Å<sup>-3</sup></b>	0.489, -0.278	0.185, -0.307

CCDC deposition number 1531577 1531578

<sup>a</sup>  $R_1 = \frac{\sum ||F_o| - |F_c||}{\sum |F_o|}$ , <sup>b</sup>  $wR_2 = \frac{[\sum w(F_o^2 - F_c^2)^2 / \sum w(F_o^2)^2]}{1}$  where  $w = 1/[\sigma^2(F_o^2) + (aP)^2 + bP]$  where  $P = (F_o^2 + F_c^2)/3$ .

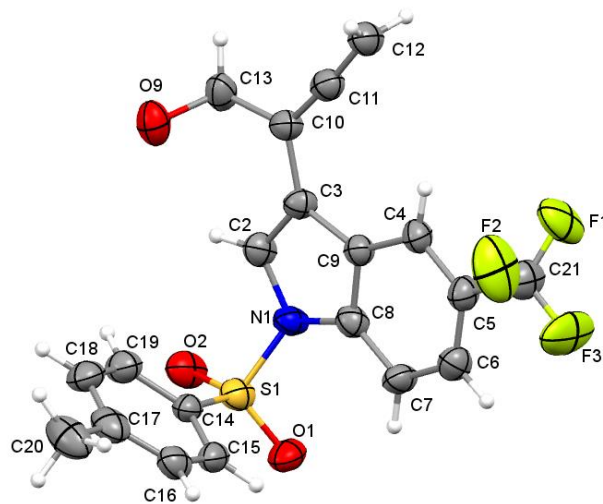


**Figure4.26** ORTEP drawing of one of the conformers of 2d (thermal ellipsoids at the 30% of the probability level). The alcoholic H atom was not located.

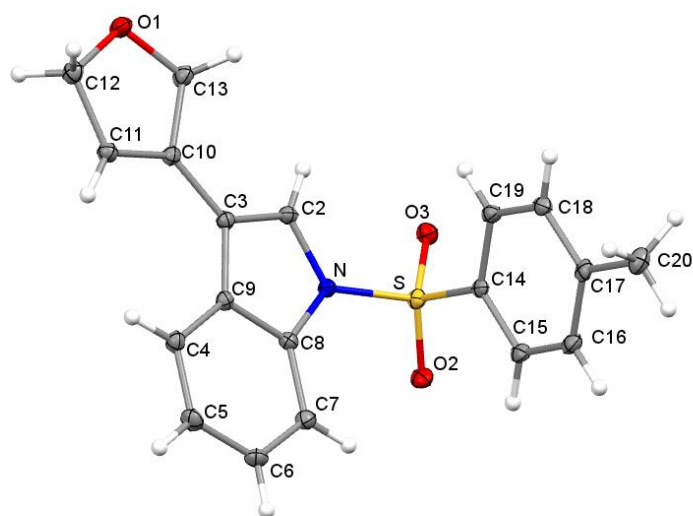


**Figure 4.27** ORTEP drawing of **4a** (thermal ellipsoids are at 50% of the probability level).



## 4.5 Bibliography

- [1] A. Y. Rulev, *New J. Chem.* **2017**, *41*, 4262–4268.
- [2] A. De Nisi, S. Sierra, M. Ferrara, M. Monari, M. Bandini, *Org. Chem. Front.* **2017**, *4*, 1849–1853.
- [3] A. Togni, H. Grützmacher, *Catalytic Heterofunctionalization*, Wiley-VCH Verlag GmbH, Weinheim, FRG, **2001**.
- [4] J. Hannedouche, E. Schulz, *Chem. - A Eur. J.* **2013**, *19*, 4972–4985.
- [5] C. Wang, J. Xiao, *Stereoselective Formation of Amines*, Springer Berlin Heidelberg, Berlin, Heidelberg, **2014**.
- [6] S. Cacchi, G. Fabrizi, *Chem. Rev.* **2005**, *105*, 2873–2920.
- [7] P. Reactions, S. Cacchi, G. Fabrizi, P. A. Moro, *Chem. Rev.* **2011**, *111*, 215–283.
- [8] R. Vicente, *Org. Biomol. Chem.* **2011**, *9*, 6469.
- [9] B. Alcaide, P. Almendros, J. M. Alonso, *Molecules* **2011**, *16*, 7815–7843.
- [10] M. Platon, R. Amardeil, L. Djakovitch, J.-C. Hierso, *Chem. Soc. Rev.* **2012**, *41*, 3929.
- [11] G. Abbiati, F. Marinelli, E. Rossi, A. Arcadi, *Isr. J. Chem.* **2013**, *53*, 856–868.
- [12] L. J. Gooßen, L. Huang, M. Arndt, K. Gooßen, H. Heydt, *Chem. Rev.* **2015**, *115*, 2596–2697.
- [13] N. Gupta, D. Goyal, *Chem. Heterocycl. Compd.* **2015**, *51*, 4–16.
- [14] H. Wang, L. Liu, Y. Wang, C. Peng, J. Zhang, Q. Zhu, *Tetrahedron Lett.* **2009**, *50*, 6841–6843.
- [15] M. Jacubert, O. Provot, J. F. Peyrat, A. Hamze, J. D. Brion, M. Alami, *Tetrahedron* **2010**, *66*, 3775–3787.
- [16] V. Prieur, N. Heindler, J. Rubio-Martínez, G. Guillaumet, M. D. Pujol, *Tetrahedron* **2015**, *71*, 1207–1214.
- [17] M. Patel, R. K. Saunthwal, D. K. Dhaked, P. V. Bharatam, A. K. Verma, *Asian J. Org. Chem.* **2016**, *5*, 213–221.
- [18] T. Aggarwal, S. Kumar, A. K. Verma, *Org. Biomol. Chem.* **2016**, *14*, 7639–7653.
- [19] T. Mahdi, D. W. Stephan, *Angew. Chemie - Int. Ed.* **2013**, *52*, 12418–12421.
- [20] P. A. Jacobi, H. L. Brielmann, S. I. Hauck, *Tetrahedron Lett.* **1995**, *36*, 1193–1196.

- [21] P. A. Jacobi, H. L. Briemann, S. I. Hauck, *J. Org. Chem.* **1996**, *61*, 5013–5023.
- [22] F. Huguenot, C. Delalande, M. Vidal, *Tetrahedron Lett.* **2014**, *55*, 4632–4635.
- [23] W. Chen, Y. Zhang, L. Zhang, M. Wang, L. Wang, *Chem. Commun.* **2011**, *47*, 10476.
- [24] C. Raji Reddy, G. Krishna, N. Kavitha, B. Latha, D. S. Shin, *European J. Org. Chem.* **2012**, *2012*, 5381–5388.
- [25] M. Wang, P. Li, W. Chen, L. Wang, *RSC Adv.* **2014**, *4*, 26918–26923.
- [26] R. Balderrama-Martínez-Sotomayor, M. Flores-Jarillo, A. Alvarez-Hernandez, *Arkivoc* **2015**, *2016*, 36–47.
- [27] K. Hiroya, R. Jouka, M. Kameda, A. Yasuhara, T. Sakamoto, *Tetrahedron* **2001**, *57*, 9697–9710.
- [28] N. Krause, C. Winter, *Chem. Rev.* **2011**, *111*, 1994–2009.
- [29] B. Alcaide, P. Almendros, *Acc. Chem. Res.* **2014**, *47*, 939–952.
- [30] V. Pirovano, L. Decataldo, E. Rossi, R. Vicente, *Chem. Commun.* **2013**, *49*, 3594.
- [31] V. Pirovano, E. Arpini, M. Dell’acqua, R. Vicente, G. Abbiati, E. Rossi, *Adv. Synth. Catal.* **2016**, *358*, 403–409.
- [32] V. Pirovano, M. Borri, G. Abbiati, S. Rizzato, E. Rossi, *Adv. Synth. Catal.* **2017**, *359*, 1912–1918.
- [33] A. K. Mailyan, I. M. Geraskin, V. N. Nemykin, V. V. Zhdankin, *J. Org. Chem.* **2009**, *74*, 8444–8447.
- [34] G. Cera, P. Crispino, M. Monari, M. Bandini, G. Cera, P. Crispino, P. Crispino, M. Monari, M. Monari, M. Bandini, et al., *Chem. Commun.* **2011**, *47*, 7803–7805.
- [35] C. Guissart, A. Dolbois, C. Tresse, S. Saint-Auret, G. Evano, N. Blanchard, *Synlett* **2016**, *27*, 2575–2580.
- [36] A. J. Cresswell, S. T.-C. Eey, S. E. Denmark, *Nat. Chem.* **2015**, *7*, 146–152.
- [37] N. Kern, A. Blanc, J.-M. Weibel, P. Pale, *Chem. Commun.* **2011**, *47*, 6665.
- [38] G. Blond, C. Bour, B. Salem, J. Suffert, *Org. Lett.* **2008**, *10*, 1075–1078.
- [39] R. Grigg, V. Loganathan, V. Sridharan, P. Stevenson, S. Sukirthalingam, T. Worakun, *Tetrahedron* **1996**, *52*, 11479–11502.
- [40] R. Kuwano, M. Kashiwabara, K. Sato, T. Ito, K. Kaneda, Y. Ito,

Chapter 4: I thought it was gold instead...TBAF catalysed one-pot synthesis of allenyl-indoles

*Tetrahedron Asymmetry* **2006**, *17*, 521–535.